POLYGENETIC OXISOLS ON TERTIARY SURFACES, MINAS GERAIS, BRAZIL

Soil genesis and landscape development

Cristine Carole Muggler

Promotor: Dr. N. van Breemen,
hoogleraar in de Bodemvorming en Ecopedologie

Co-promotor: Dr. ir. P. Buurman,
universitair hoofddocent, Departement Omgevingswetenschappen

POLYGENETIC OXISOLS ON TERTIARY SURFACES, MINAS GERAIS, BRAZIL

Soil genesis and landscape development

Cristine Carole Muggler

Proefschrift
ter verkrijging van de graad van doctor
op gezag van de rector magnificus
van de Landbouwuniversiteit Wageningen,
Dr. C.M. Karssen,
in het openbaar te verdedigen
op maandag 14 september 1998
des namiddags te vier uur in de Aula

CIP-GEGEVENS KONINKLIJKE BIBLIOTHEEK, DEN HAAG

Muggler, C.C.

Polygenetic Oxisols on Tertiary surfaces, Minas Gerais, Brazil. Soil genesis and landscape development / C. C. Muggler, - [S.1.: s.n.]. - III. PhD thesis Wageningen. - With ref. - With summary in Dutch and Portuguese.
Subject headings: Oxisols, soil genesis; polygenetic soils; soil-landscape; Brazil.

ISBN 90-5485-907-5

To all people committed to build a better world for everybody

The research reported in this thesis was sponsored by CAPES/Ministry of Education of Brazil and Federal University of Viçosa, Minas Gerais, Brazil, as a full Ph.D. training programme.

Cover layout by Celso Marcatto and Renato Roscoe
Drawing by Renato Roscoe

FOREWORD

By the time of my undergraduation, I was often struck by the impressive landscape around São João del Rei, along with its quartzitic chains, sets of convex hills and huge gullies. During my M.Sc. course in Lavras, I happened to make visits to this neighboring area, as a geological consultant, with my supervisor Prof. Nilton Curi and other students. On these field trips, we discussed the landscape, the parent materials and the resulting soils, which are sometimes much shallower than expected. From these discussions it became clear that the genesis of these soils and related landscapes deserved much more attention than they had had previously. This situation could be designed into an interesting problem for a Ph.D. research.

Since I had heard about the existence of a chair in tropical soils and about an international soil museum in Wageningen, I was already interested in going there to study. Wageningen also appeared to be very attractive because of the use of English as the working language in the university, and the presence of a Department of Ecological Agriculture, where my husband Celso could also pursue a M.Sc. degree. On a more personal basis, going to study in The Netherlands would fulfill my curiosity to experience my European roots. All of these factors proved to be only partially correct, and to come to Wageningen was not an easy task. But, since life sometimes turns out all right even after taking what seem to be "wrong" shortcuts, I am happy to have had the opportunity to study and live in Wageningen for some years. Some people were of great help in this: Nilton Curi, Mauricio Fontes, Liovando Marciano, José Machado, João Bertoldo, Rosivaldo. I thank them all for their share in this effort.

In Wageningen, at the Department of Soil Science and Geology (now Laboratory of Soil Science and Geology), Nico van Breemen accepted to be my promotor and Peter Buurman became my co-promotor and direct supervisor. Peter was always very interested in my research, pushing me forward and encouraging me to go on, even when sometimes I was about to clash with apparently unsolvable problems. His talent to make a synthesis of a wealth of information and to come out with simple and consistent concepts always amazed me. I thank him very much for his guidance and friendship during all these years. Due to the nature of my research, I had less contact with Nico van Breemen in the first three years. Even so, every now and then he pushed me to stick to my real problem through his valuable comments. I took some time to experience the meaning of "Breemenization" of a manuscript, which proved to be a great discovery: Nico's clear and consistent scientific reasoning contributed remarkably to improving my writing and gave me a strong confidence to go on. Thanks!

I also thank my co-authors Jan van Loef, Ed Meijer, Tom Pape, and Corine van Griethuysen for their contributions to this thesis. I am grateful to Toine Jongmans for his guidance in my early steps in micromorphology, his assistance whenever needed, and for the relaxed chats we had among the microscopes. In 1996, I met Prof. Georges Stoops for the first time during a training course in micromorphology in Gent, Belgium. His experience with tropical soils and his expertise in micromorphology are remarkable and opened my eyes to this new and fascinating micromorphological world. Georges Stoops gave valuable support to my

work, always ready to answer or discuss any of my questions and to help with the characterization of the intricate unfamiliar features I found at each new sequence. I thank him very much for his kindness to me and for the stimulating discussions we had in the last two years.

Most of my research was conducted at the Laboratory of Soil Science and Geology in Wageningen, apart from two field trips to Brazil. Of all the people working at the Laboratory, I have a special word of thanks for Jan van Doesburg, who helped me a great deal with XRD determinations and other laboratory routines. Ton Engelsma introduced me to the 'dry' laboratory in early times; Corine van Griethuysen and Tom Pape did most of the laser grain-sizing determinations; Bram Kuyper, and later Jan Huttink, took care of the XRF analyses; Arie van Dijk prepared the thin sections for micromorphology; and Barend, Eef, Frans, and Nieltje from the chemical ('wet') laboratory did the routine analyses and assisted me in other chemical analysis. Cláudio Brustolini from the Laboratory of Soil Physics at the Federal University of Viçosa took care of preparation and texture determination of part of the samples. Hetti Leferink from PCM was a great help in teaching me about the preparation of samples for TEM and the use of it -what a nightmare of work! I am grateful to all of them for their share and help during this research.

Field work in Brazil was made possible due to the organization and supportive work done by Luiz Fontes, Nilton Curi, and Luiz Marcelo Aguiar Sans. The synthesis of the geomorphological knowledge and its field aspects could not have been completed without the valuable contribution of Prof. Dr. Alaoua Saadi from the Institute of Geosciences at the Federal University of Minas Gerais. Alaoua kindly joined one of the field trips to show us the main neotectonic evidences in the area of São João del Rei, when he provided us with a very sound explanation of the Cenozoic evolution of the landscape. I am very pleased with all of these contributions.

My study for the Ph.D. has only been possible through the support offered by my department at the Federal University of Viçosa. I am deeply grateful to my colleagues and friends at the department who were always encouraging and helpful. Some of them were especially important: Luiz Fontes, who took care of all the red tape during my absence, facilitated things as much as he could every time it was needed, and above all for his unwavering friendship. Irene Maria Cardoso took the onus of taking on my former activities and classes during my absence, not to mention that her close friendship provided me with positive encouragement all the time. Maurício Fontes also assumed part of my activities, besides providing assistance every time I needed it. Furthermore, I acknowledge the assistance of Sônia do Carmo Almeida and the staff of the Assessoria de Assuntos Internacionais who took care of the administrative aspects of my leave. In Wageningen, the administration of the Laboratory of Soil Science and Geology as well as the Dean's Office for International Students were of great help in the administrative aspects of my research, bureaucratic procedures and practical arrangements of my stay.

Upon my arrival to the Department, I had the good fortune to share an office with Else Henneke: I learnt from her all about the department functioning and she helped me a great deal

with the translation of correspondence and messages sent to me in Dutch. Else was always available and willing to help me get through all sorts of difficulties. With Leo Tebbens I could share views of life, science, cultural differences and many more things during very pleasant, sometimes extended, coffee breaks. Other people were very willing to help me with all kinds of problems and difficulties when asked; I would like to mention Marcel Lubbers, Salle Kronenberg, Hans Huisman, Hugo van der Gon, Rienk Miedema, and Tini van Mensvoort. The foreign group in the department provided a pleasant interaction, funny moments and tasty international dinners during early times of my stay. Unfortunately it shrank very much in the last years and I missed quite a lot the presence of Jorge, Virginie, Ioulia, Gandah, Minh, among others. However, a former student of mine, Renato, started his Ph. D. recently and we have been able to enjoy very nice and motivating chats during coffee breaks and other times. The artistic skills of Renato that were previously unknown to me made a decisive contribution to the cover of this thesis. Renato spent many days together with Celso developing and taking care of the final layout. Also, Fayez who finished his thesis shortly before me was very helpful in providing me with all sort of tips about the final arrangements for the printing of my thesis.

Besides the research itself, a Ph. D. leave abroad is a lifelong experience and develops into a history where many people leave their marks. People come and go, but they will never leave alone: they will always carry a bit of you away with them and I am sure that they also left a bit of themselves in me. I would like to recall on this piece of paper some people who were not directly involved in my research but who helped me very much with exchanging experiences, personal feelings and sharing their joy of life. They were very important in keeping me on track in different ways and moments. Of course I will not be able to recall all people who were important during this time, but that does not mean that I am not indebted to them.

The arrival and adaptation to The Netherlands proved to be more difficult than expected. Culture shock was a reality which I had never experienced or even thought possible before my stay here. It was made smoother, and I could cope with it through the support provided by many people: Mariet Verstegen was able to immediately pick up the cultural differences that may have created many more red tape problems. Her performance at the municipality office in Arnhem was great! A special credit is to be given to the Brazilian community living here, providing us with warmth and attention, apart from the uncountable practical tips on how to live here. I would like to particularly mention the two Bernardes families, who surpassed the possible to help us. Ina van Hartog was our Dutch contact in Brazil before we came here, and to our good fortune she lived in Arnhem, where we went to live for the first three months. She helped a lot with our initial settling (cradle, blankets, baby buggy, etc, etc...) and was always a good friend. Through her, we got to meet Deborah, Dirk and Margreth with whom we shared many special occasions.

I could share many special moments, weekends, trips, excursions, outings and simply chats with good friends among whom I would like to mention Miriam, Ana and Jorge, Mundie, Maria Nomikou, Francesco, Fiona, Roberto, Angelo and Madelaine, Rianne and Johanniek, Vera Marcelino, André and Diva, and Taas. Ad van Oostrum and his family were of

unconditional support always available when needed, providing me with attention and even with a bike chair for Pedro (the back one; the front one we used earlier was provided by Marriet Verstegen). We had many visitors from Brazil during these years, who also provided us with the Brazilian flavour and warmth.

I want to express my gratitude to my family: my sisters Monica, Lena, and Hildinha two of whom came to visit me here; Elites a kind of second mother who has a special talent to find the definitive *knuffel* for a child, either me or Pedro; my mother who always encouraged me to pursue my initiatives; and my father who kindly received us in his home in Switzerland during these years. A special thanks is due to Iuja, my mother-in-law who came to The Netherlands to help with the care of my son Pedro and with other things, during my first field trip to Brazil; Iuja always gave words of encouragement to us when things looked too difficult.

Finally, I want to mention that motherhood was also a new experience for me, something which almost coincided with my stay abroad: what a fascinating one! I fear that Pedro is even more important to me than I am for him. Celso, had such a goodwill and a capacity to share things and life with me, that I do not have enough words to thank him for all his love and dedication. Both Pedro and Celso did a great job coping with my enormous absence, especially in the last six months of my thesis work!

CONTENTS

OUTLINE OF THIS THESIS

The objective of this research is to establish the main aspects of soil polygenesis and landscape development in geologically old tropical landscapes from the state of Minas Gerais, Brazil.

Chapter 1 describes the research problem, the objective, and the approach used to tackle the problem. It gives a general overview of the situation, physical environment, geology, and geomorphology of the studied areas. Furthermore, it discusses the evolution of the landscape, and introduces the relation between soil formation and geomorphic processes in geologically old landscapes. Also the characterization and identification of the soil-landscape units are presented in this chapter.

The subsequent chapters are grouped in two parts. **Part I** deals with the characterization and interpretation of pedogenetic processes by means of the study of chemical, mineralogical, and micromorphological properties of the soils; it contains chapters 2, 3, 4, and 5. **Part II** comprises studies of texture and aggregation of the soils by laser diffraction grain-sizing. Part II is composed by chapters 6, 7, and 8.

Chapter 2 describes the chemistry and mineralogy of all studied soil sequences. Chemical and mineralogical analysis consisted of determinations of major and trace elements, and general (clay) mineralogy. Mineral transformations were approached by micromorphology too. Differences between the soil sequences were assessed by mineralogical studies and statistical analysis. The integration of chemical data was done by factor analysis.

Chapter 3 describes the micromorphological aspects of a toposequence composed of red Oxisols and yellow (eroded) Oxisols developed on a continuously exposed (stable) surface apparently not influenced by tectonic activity. Recent and relict soil features were characterized and interpreted in terms of successive phases of soil formation.

Chapter 4 consists of a detailed characterization of micromorphological features of soils and buried soils found in a sedimentary sequence from a graben zone. The interpretation of past and present soil formation and erosion circumstances in distinct (pedo)sedimentary layers enabled the identification of various evolutionary phases undergone by the soils during their polygenetic history.

Chapter 5 contains the results of a detailed investigation on the mineralogy of iron oxides, as potential (paleo)environmental indicators. Variations in type, composition, morphology, and size of the iron oxides were interpreted in relation to weathering and pedogenic circumstances that affected the various soil sequences.

Chapter 6 describes the methodological adaptations undertaken to fit the laser diffraction grain-sizing method with the required type of analysis and samples. The laser diffraction method was chosen for its capacity to measure a large range of grain-size fractions

in the same suspension, giving detailed grain-size distributions, which are not obtained by other common methods.

Chapter 7 describes the results of laser diffraction grain-size determinations for three selected profiles. These studies aimed to identify and interpret changes in grain-size upon weathering and to assess the aggregation of the materials. With the obtained grain-size distribution curves, changes in clay formation and weathering with depth in the profiles could be accurately followed.

Chapter 8 presents laser diffraction grain-size distribution curves of all horizons of the studied soil sequences after three different pretreatments. The comparison of the distribution curves allowed the analyses of changes in aggregation within profiles and between the various soil sequences. The results showed the distinct role played by different iron forms in aggregation.

Chapter 9 presents the synthesis of the research and its main results. It discusses the polygenesis of the soils and the main associated features. The chemical, mineralogical, textural, and (micro)morphological properties of the soils, buried soils, and saprolites were integrated, and the main soil processes were characterized. Evolutionary phases found in relict and in buried soils are linked in an attempt to reconstruct the pedological history of the studied soils in relation to the evolution of the landscape.

1. GENERAL INTRODUCTION

The state of Minas Gerais is situated in the southeast of Brazil, bordering with the states of Rio de Janeiro and São Paulo. The state has an area of approximately 590000 km², and some 16 million inhabitants. The name Minas Gerais (general mines) refers to its richness in mineral resources, especially iron ores, gold, precious and semi-precious stones. At present, agroforestry is an important activity, fostered by the extension and geographical situation of the state, near the main markets of the country. Notwithstanding lasting economic crises the state experiences an increasing expansion of agriculture, with intensification of the use of agricultural land, and continuous conversion of new areas into agriculture.

Natural environments and associated soils vary widely in the state. Three of the six main morphoclimatic domains of Brazil (Ab'Saber, 1970) are recognized there: *Cerrado* (planated tropical highlands with savanna-type vegetation); *Mares de morros* ('sea of hills': tropical forested demi-orange hills); and *Caatingas* (semi-arid lowlands), in addition to many intergrades. At least two of the morphoclimatic domains and intergrades are related to geologically old landscapes that have been exposed since the Tertiary or longer.

A significant part of these long-time exposed landscapes is developed on fine- and medium-textured sedimentary and metamorphic rocks, which comprise about 30% of the state's area. The soils found in these areas are dominantly Oxisols (Ferralsols), which are very deep when situated on flat and gently undulating parts of the landscape. In slightly more energetic slope positions the Oxisols have been eroded and are shallower. Erosion is usually accompanied by a change in colour of the surface soils from red to yellow. Also, a degradation in the vegetation type from *cerrado* to *campo cerrado*, and to *campo limpo* follows the decrease in solum thickness (Almeida, 1979). The shallower soils frequently show surface sealing and have a poor vegetal cover (Almeida, 1979; Curi et al., 1993). This, combined with frequent burning, results in a high susceptibility to erosion. Soil erosion is indeed the main constraint of these soils (Brasil, 1983; Almeida and Resende, 1985). The formation of the common large and very deep gullies in these areas is facilitated by the deep weathered mantle, which is even more susceptible to erosion. Rills easily turn into gullies when incisions reach the saprolites, either under anthropic influence or in natural conditions (Resende et al., 1988).

The Oxisols are known to be polygenetic, but very little is known about their (poly)genesis. Especially the understanding of the relation between soil genesis and landscape development is very incomplete, certainly in relation to soils developed on fine- and medium-textured metamorphic and sedimentary rocks. Furthermore, an integrated study of soil properties coupled with the interpretation of soil and landscape forming processes will not only contribute to the general comprehension of soil genesis, but also to the understanding of environmental aspects of this kind of landscape and parent material in tropical areas. Basic studies on soil genesis are also essential to subsidize further studies that aim to reduce soil

degradation.

The objective of this research is to establish the main aspects of soil genesis in relation to landscape development in this type of tropical environment. It is achieved by the study of soil-landscape units developed on similar parent materials related to a Tertiary surface, which has been more or less affected by neotectonic movements. Study sites were selected on surfaces affected and not affected by neotectonism. The juxtaposition of stable areas and graben zones opens up new possibilities to tackle polygenetic soils. In the stable parts of the landscape, soils have been exposed to soil formation and erosion phases during millions of years, and all phases have been overprinted. Here, soil genetic studies may be able to identify many different phases of soil formation, but not their relative time frame. In adjacent graben zones, sedimentation alternated with soil formation. Although overprinting may still be present in some buried soils, the fact that various phases of soil formation are separated by sediments, enables to study the single phases and the comparison with the polygenetic soils of the stable areas. A sketch of this development is given in Figure 1.1. One should keep in mind, though, that even the oldest soils in the graben are younger than the oldest soils on stable surfaces.

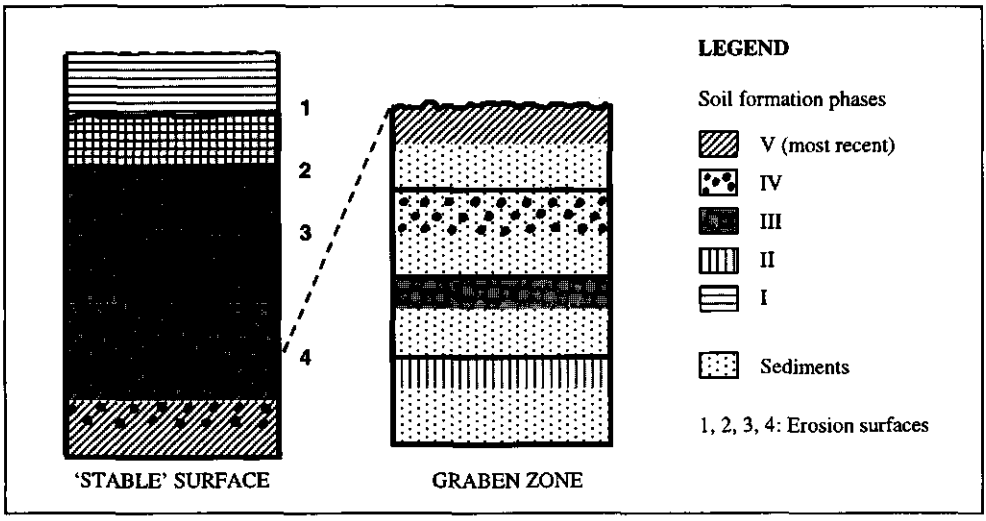

Figure 1.1: Schematic diagram of the hypothetical relation between soil genesis on continuously exposed (stable) surfaces and on sedimentary layers.

This research encompasses the understanding of the soil processes occurring in distinct and/or successive pedoenvironments between and within soil profiles. It involves the interpretation of features imprinted in soils, buried soils and saprolites throughout their evolution. These features consist mainly of textural, morphological, and mineralogical properties.

Continuously exposed landscapes on fine- and medium-textured sedimentary and

metamorphic rocks and sedimentary graben fillings were selected for the research. They are located in the central and central-southern part of the state of Minas Gerais, near the towns of Sete Lagoas and São João del Rei (Figure 1.2). In the following text, the areas will be identified as SL and SJR, respectively. Geographical coordinates are 19-20°S and 44-45°W for the SL area, and 21-22°S and 44-45°W for the SJR area.

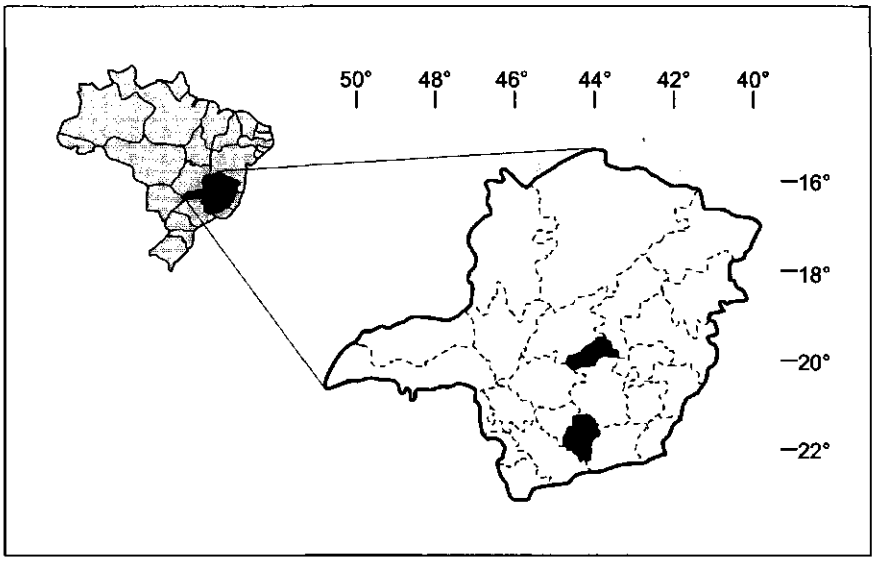

Figure 1.2: Location of the state of Minas Gerais within Brazil (left) and of the geographical regions that contain the study areas within Minas Gerais (right).

Soils and landscapes

> "Soil bodies and their parent materials, are not only characterized by their composition, but also by their shape; they are geomorphic units... In the intensity of transformation, the upland part resembles the topsoil and the lowland part the subsoil, the inter-pedon translocations resemble the inter-horizon translocations, and the leaching from soils resembles the discharge from the landscape"
>
> adapted from Jungerius, 1985

Soil formation in long time exposed landscapes is influenced by a complex geomorphic history, as usually observed in the humid tropics (Ollier, 1959; Lichte, 1990; Stoops et al., 1994). The geomorphic evolution is driven by exogenous and endogenous processes active on the Earth's surface, from which climatic changes and tectonism are especially relevant. Climatic changes are generally considered to be the main process intervening in the geomorphic evolution in humid tropical areas (Thomas, 1994). Climatic changes trigger pediplanation phases during drier periods, and sculpturation of convex reliefs during wetter periods.

Tectonic processes have received little attention in current mainstream geomorphological thinking, although they often have greatly influenced the morphogenesis of tropical landscapes. Evidence of tectonic, in particular neotectonic (defined as Cenozoic tectonic movements), influence on tropical morphogenesis from different areas is increasingly found (Riccomini et al., 1989; Magalhães and Saadi, 1994; Schwarz, 1994; Ollier, 1995; Zeese and Fodor, 1997). Such tectonic processes consist of epirogenic movements, reactivation of crustal fractures and discontinuities, and the movement of the lithospheric plate (King, 1976; Hasui, 1990; Saadi, 1991). Resulting morphotectonic features are positive and negative tectonic reliefs, stepped planation surfaces, and structurally controlled landforms (Clapperton, 1993).

The resulting landscapes are polycyclic, characterized by the overprinting of processes connected to successive geomorphological cycles. Soil formation on polycyclic landscapes comprises a number of unstable (erosion, truncation of soils and subsequent sedimentation), and stable (weathering, undisturbed soil formation) phases (Stoops, 1989). The erosional reprises caused either by climatic changes or tectonic movements, promote the rejuvenation of the landscape and trigger new soil formation cycles. The resulting soils are polygenetic, in the sense that they have multiple genetic linkages of exogenous and endogenous processes, factors, and conditions (Johnson et al., 1990). Moreover, the soils are commonly developed on pre-weathered parent material (Ollier, 1959), derived from earlier soil material or from very deep saprolites. The continuous reworking of such highly weathered material hardly affects its chemical and mineralogical nature, but does change its organization (Stoops, 1991).

During polygenetic evolution, different soil formation phases become mingled and thus are very difficult to separate, although evidence of their presence may be abundant. Geomorphic polycyclicity involves alternation of phases of erosion and deposition, with weathering and pedogenesis leaving their imprint during periods of greater stability. Sedimentary layers, especially those related to graben zones, in which soil formation took place, permit the separation of different phases in time and space. Buried soil horizons contained in such deposits have a great potential for assessing the nature of geomorphic and soil formation cycles.

PHYSICAL CHARACTERIZATION OF THE STUDY AREA

Climate, vegetation and topography

The SL area has a gently undulating to rolling topography, with altitudes ranging from 600 to 900 m asl. The climate of the area is a Tropical Savanna (*Aw* in the Köppen classification) climate, with an average annual temperature of 22°C, and average annual precipitation of 1300 mm. Rainfall is concentrated in the months of October to April (summer), and is less than 35 mm/month in the dry period (Sans, 1986). At higher altitudes, the climate type changes to a Tropical Highlands (*Cwa*) type.

The SJR area shows an undulating to rolling topography, with altitudes of 900 to 1100 m asl. The area has a Tropical Highlands (*Cwa*) climate, with an average annual temperature of 19-20°C, an average annual precipitation of 1400 mm, with rain concentrated from November to April (summer), and 4 to 6 dry months.

In both areas, the original vegetation is represented by *cerrado, campo cerrado,* and *campo limpo*, the particular vegetation type depending mainly on water availability. The greater the stress induced by water deficiency, the fewer forest species can survive. *Cerrado* is a low dense evergreen savanna forest composed of trees of 5 to 15 m height; it does not have a continuous canopy, but there are no large open spaces. *Campo cerrado* is a more open savanna with plentiful, but isolated trees of 2 to 5 m height that are scattered fairly evenly; grasses and shrubs occur in varying proportions. *Campo limpo* is an open grassland with very few trees. The typical trees of the cerrado areas are tortuous and often have a thick, fire resistant bark. Along water courses, the number of trees and species increases, leading to the growth of gallery forests.

Geology

The country of Brazil is situated on the South American Platform, a 'stable' part of the lithospheric South American plate. This platform reached its consolidation by the end of the Proterozoic and the beginning of the Paleozoic era, when the orogenic *Brasiliano* cycle (450-700 my) finished. The main tectonic elements of the platform are the crystalline basement, mobile belts, and Paleozoic/Mesozoic sedimentary basins. The crystalline basement consists of cratonized areas, one of which is the area known as the *São Francisco* craton. This craton accommodates sedimentary covers correlated to the Brasiliano cycle, and includes the *Bambuí* group. The SL area is situated in the domain of this Late Proterozoic group. The Bambuí group consists of sediments deposited on a stable epicontinental platform with low gradient and shallow waters (Schobbenhaus et al., 1984). The group has distinct clastic and chemical facies related to variations in the nature of the sedimentary episodes. At the studied site, the dominant lithologies are fine-textured sedimentary and slightly metamorphised rocks (shales, siltstones and corresponding slates).

The SJR area is situated in a mobile belt bordering the São Francisco craton to the south, known as the *Ribeira* mobile belt. The main geological units found in the area are the *Barbacena, São João del Rei,* and *Andrelândia* groups. The Barbacena group is of Archean age and consists of more or less migmatized gneisses and schists, and constitutes the crystalline basement of the São João del Rei and Andrelândia groups (Brasil, 1983; Schobbenhaus et al., 1984). These two groups are of Middle/Late Proterozoic age. They replace each other laterally, and appear to belong to the same sedimentary cycle (Karfunkel and Noce, 1983). The São João del Rei group is constituted of metasedimentary rocks (metasiltstones, phyllites, and fine textured schists) related to a green-schist metamorphic facies (Valeriano, 1986). The Andrelândia group shows a gradual increasing metamorphism to amphibolite facies (Heilbron, 1985), and consists mainly of phyllites, biotite schists, quartzites, and gneisses. In addition to the Proterozoic units, Tertiary and

Quaternary sediments (Santos and Ferreira, 1989) are scattered in the area, mostly related to sedimentary basins formed upon neo-Cenozoic tectonic reprises (Saadi, 1991).

Tectonic reprises consisted of an overall reactivation of pre-Cambrian crustal instabilities, following the Mesozoic breakup and movement of the South American tectonic plate (Hasui, 1990). These processes are indicated by sedimentary, morphological and geophysical evidence (Haralyi et al., 1985; Riccomini et al., 1989), with distinct expression depending on the type of previously existing structures (Saadi, 1993), and varying intensities in time and space (Magalhães and Saadi, 1994). The Cenozoic tectonism observed in the mobile belts of southeastern Brazil is usually marked by an initial deformation of extensional nature related to the reactivation of the pre-Cambrian crustal fractures (Haralyi et al., 1985). This gave origin to rift structures (Almeida, 1976, Saadi, 1993; Thomas, 1994), which triggered erosional reprises and yielded large amounts of sediments, subsequently deposited in the grabens (Saadi et al., 1989).

The older sediments found in the grabens are of Pliocenic age and consists of eroded soil materials, whose clay fraction indicates humid tropical conditions of soil formation in the late Miocene (Saadi and Valadão, 1990). Overlying coarser facies in the graben fillings suggest the deepening of the incision through the saprolites reaching remaining quartz veins of the weathered rocks. The dominance of alluvial fans of unsorted material among the sedimentary deposits indicates either a drier climate, or a climate with marked seasonality (Saadi and Valadão, 1990; Saadi, 1991). Associated lacustrine deposits are also found (Santos and Ferreira, 1989). The sedimentary layers were subsequently deformed by tectonic compression from the Early Quartenary (Pleistocene). This compression caused bending and faulting of the sediments, which gave origin to domes and uplifted structural units (Saadi, 1992). Cratonic areas have also been affected by the Cenozoic tectonism, either by reactivation of discontinuities, or by deformation related to accumulating intraplate tension (Saadi, 1993).

Geomorphology

The SL area is part of the geomorphological region known as *Depressões Interplanálticas do São Francisco* (interhighland lowlands), which is part of the São Francisco craton (Brasil, 1983). It consists of dissected, planated and dissolved landscapes influenced by present-day morphoclimatic conditions. The studied area does not show signs of significant tectonic influence on its morphogenesis; on the contrary, its homogeneous gently undulating relief with planated hilltops suggest a succession of dissection and planation cycles.

In the SJR area, two main geomorphological units are formally recognized: *Planalto de Campos das Vertentes* and *Planalto de Andrelândia* (Brasil, 1983). Both units are described as homogeneously dissected highlands, consisting of hills with convex to tabular tops, convex slopes, and some asymmetrical elongated crests. Distinction between the two units is hardly possible in the study area. In the field, however, two distinct landscapes that are not necessarily related to the above described ones were clearly distinguished. The first consists of a chain of homogeneously

dissected hills, known as the *Planalto de Madre de Deus de Minas*. The planalto is a remnant of the Sulamericana surface lying at altitudes of 1000 to 1100 m, which has been affected by regional epirogenetic uplift (King, 1976). The second landscape consists of lower hills with strong structural control (Ribeiro and Saadi, 1989), that was not recognized by Brasil (1983). This landscape is observed along the so-called *São João del Rei* rift (Figure 1.3), which consists of a stretch with 250 km length and 5 km width (Saadi, 1990). The dissection phases related to the neotectonic episodes are illustrated by different levels of stepped fluvial terraces and dislocations in alluvial sequences, which show abundant cut and filling structures (Saadi et al., 1989; Santos and Ferreira, 1989; Saadi, 1991). The continuation of the tectonic activity during the Quaternary is attested by the change of drainage axis and by dislocation of Holocene fluvial terraces (Saadi, 1991).

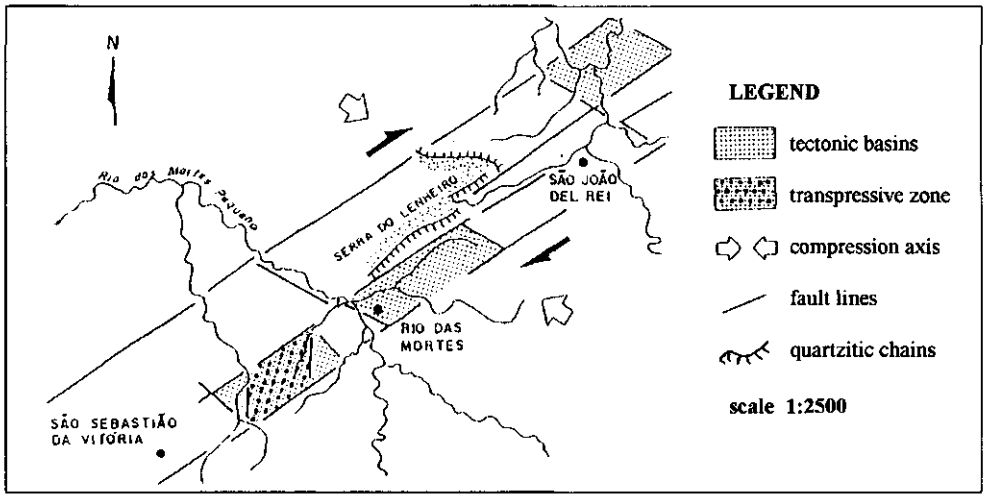

Figure 1.3: Simplified map of part of the SJR area, showing the São João del Rei rift and tectonically controlled sedimentary basins (Saadi and Valadão, 1990).

Landscape evolution

The geomorphic evolution of the southeastern Brazilian landscape has been postulated as a repetitive sequence of dissections and planations caused by climatic changes, superposed on different lithologies (Braun, 1971; Bigarella and Becker, 1975; Meis and Moura, 1984; Pedro and Volkoff, 1984; Lichte, 1990, Thomas, 1994). This morphoclimatic approach emphasizes denudacional processes acting on a deeply weathered crystalline basement, which may have been exposed since the Cretaceous period (Clapperton, 1993). This evolution is well illustrated by the occurrence of monotonous landscapes composed of convex hills, that are sporadically cut by quartzitic chains. Even if strongly dissected, these landscapes show typical remnants of planated areas, such as flat crests at the same altitude, or subhorizontal structures that do not follow the rock

structure (Saadi, 1991; Thomas, 1994). More recently, however, this morphoclimatic conceptual model has been challenged by evidence that the geomorphic processes in the humid tropics are only partially dependent on climate (Gupta, 1993; Olllier, 1995). In this view, the southeastern Brazilian landscape is the result of the interplay between climatic changes and tectonic processes (Melo, 1984; Saadi, 1991; Clapperton, 1993).

Two main Cenozoic erosional cycles and the associated surfaces are generally recognized at the regional scale: the *Sulamericana* and the *Velhas* surfaces (King, 1957; Volkoff, 1985). The Sulamericana surface formed throughout the Early Tertiary, and the Velhas surface is dated to Late Tertiary and Early Quaternary (Plio-Pleistocene), with palaeontological dating from Early Pleistocene (Braun, 1971). The Sulamericana surface is considered to be the most complete and largest planation that occurred in Brazil (King, 1957; Braun, 1971; Magalhães Jr and Saadi, 1994; Thomas, 1994), being the reference element of the southeastern Brazilian landscape. It started to dismantle from the Miocene, and in some areas it was largely destroyed by the onset of neo-Cenozoic tectonic reactivation and subsequent erosive episodes. At present, the Sulamericana surface is found on the Brazilian Central Plateau and on smaller plateaus scattered over the country (Pedro and Volkoff, 1984). The valley fillings that followed the erosion of the Sulamericana surface constitute the early phases of the Velhas cycle. The Velhas surface is related to an erosive cycle less extensive than the first, probably incomplete and still active, showing different intensities and ages in the various regions (King, 1957; Braun, 1971).

MATERIALS

The field areas were thoroughly studied for the identification, characterization, and selection of soil-landscape units. A striking difference between saprolites in the field led to the distinction of two main parent materials: rock-saprolites and Tertiary sediments. Rock-saprolites show pinkish or pallid colours, are coarse grained and very friable. Sediments have intense red and/or yellow colours and are very firm. The soils developed on rock-saprolites show red and/or yellow colours depending on their position in the landscape. The red soils are very deep and stable soils, found on the remnants of the Tertiary Sulamericana surface. They occur in both Sete Lagoas (SL) and São João del Rei (SJR) areas. The similarity of the saprolites of the otherwise distinct sedimentary (SL), and metamorphic (SJR) parent rocks, indicates that the soil evolution trend is akin, thus comparable. The soils overlying Tertiary sediments occur in the SJR area and usually show red colours. The combined field aspects of soils, saprolites, parent materials, and landforms, enabled the distinction of three main soil-landscape units, which are identified and characterized as follows:

SL-sap: red and yellow soils developed on fine-textured sedimentary and metasedimentary rocks from the SL area. They consist of deep and of eroded Oxisols, respectively located in more stable and in dissected parts of the landscape.

SJR-sap: red and yellow soils developed on fine and medium-textured metamorphic rocks from the SJR area. They consist of Oxisols developed on stable surfaces, which were or not eroded in relation to neotectonic activity (respectively proximal and distal areas). Eroded Oxisols on slopes formed in response to a (sub)recent overall rejuvenation of the landscape are also included in this unit.

SJR-sed: red soils developed on Tertiary sediments, which consist of reworked soils and saprolites deposited in grabens formed by neo-Cenozoic tectonic activity. These soils have variable depth and are commonly associated with soft or hardened iron enriched layers.

Red and yellow soils developed on rock-saprolites were not considered as separate units because they constitute toposequences. Red soils occur in the more stable parts of the landscape (flat tops or upper convex slopes), while yellow soils occur on the slopes, where the original red Oxisols were eroded. These yellow soils have developed on in-situ saprolites and former subsoil layers, and frequently show colluvial characteristics.

A collection of 14 sections consisting of vertical (weathering or sedimentary), and/or horizontal (topographic) sequences were described and sampled. Their identification and general situation is given in Table 1.

Table 1. Location, identification, geomorphologic and geologic aspects of the selected sections.

Area	Section	Soil-landscape unit and situation	Parent material	Type of sequence
SJR	P1	SJR-sap; red Oxisol on stable surface (distal areas); part of the P2-P5 toposequence	metamorphic rocks	vertical/toposequence
	P2-P5	SJR-sap; toposequence of yellow Oxisols on stable surface (distal areas)	metamorphic rocks	toposequence
	P6	SJR-sed; eroded Oxisol on sediments from graben zone	sediments	vertical
	P7	SJR-sap; eroded Oxisol on stable surface (proximal areas)	metamorphic rocks	vertical
	P8	SJR-sap; Oxisol on stable surface (distal areas)	metamorphic rocks	vertical
	VP	SJR-sed/sap; Oxisol on transition between graben zone and stable surface (proximal areas)	sediments; metamorphic rocks	vertical
SL	C1-C3	SL-sap; Oxisols on stable surface	sedimentary rocks	toposequence
	C4	SL-sap; eroded soil on dissected landscape	sedimentary rocks	vertical/toposequence
	C5	SL-sap; eroded soil on stable surface	sedimentary rocks	vertical

PART I

CHEMISTRY, MINERALOGY, AND MICROMORPHOLOGY OF POLYGENETIC OXISOL SEQUENCES

Chapter 2
Cristine C. Muggler, Edward L. Meijer, and Peter Buurman
Chemistry and mineralogy of polygenetic Oxisols developed on rock-saprolites and sediments in Minas Gerais, Brazil

Chapter 3
Cristine C. Muggler and Peter Buurman, 1997.
Micromorphological aspects of a catena of polygenetic soils on metamorphic rocks in Minas Gerais, Brazil
In: S. Shoba, M. Gerasimova and R. Miedema (Editors), Soil Micromorphology: Studies on Soil Diversity, Diagnostics, Dynamics. *Proceedings of the 10th International Working Meeting on Soil Micromorphology*, 1996, Moscow, Russia: 129-138.

Chapter 4
Cristine C. Muggler and Peter Buurman, 1998.
Erosion, sedimentation and pedogenesis in polygenetic Oxisol sequences from Minas Gerais, Brazil.
(submitted)

Chapter 5
Cristine C. Muggler, Jan J. van Loef and Peter Buurman
Mineralogical and (sub)microscopical aspects of iron oxides in polygenetic Oxisols from Minas Gerais, Brazil
(submitted)

2. CHEMISTRY AND MINERALOGY OF POLYGENETIC OXISOLS DEVELOPED ON ROCK-SAPROLITES AND SEDIMENTS IN MINAS GERAIS, BRAZIL

Cristine C. Muggler, Edward L. Meijer and Peter Buurman

Abstract

In tropical areas multiple climatic changes and geomorphic cycles give origin to polygenetic soils. Polygenesis involves new soil formation phases taking place on preweathered materials from previous phases, resulting in soils with rather similar chemical and mineralogical properties. Polygenetic soils from Minas Gerais, Brazil, were investigated with the purpose of distinguishing mineralogical and chemical trends in relation to parent rock, geomorphic evolution, degree of reworking of the materials, and landscape position. The soil materials were studied by micromorphology and electron microscope and analyzed by XRF and XRD. Data were processed using factor analysis. All soils are strongly weathered and even show weathered grains of ilmenite and quartz. Kaolinite and iron oxides are the main clay minerals found in the soils. Gibbsite is commonly present in A and B horizons, and micas are frequent in subsoils. Kaolinites formed differently in saprolites and in soils, resulting in smaller and less ordered crystals in soils than in saprolites. Factor analysis yielded four factors that explained 89% of the total variance of 14 elements. 32% of the total variance is explained by the ferralitic weathering status. A further 40% of the total variance is explained by factors mainly connected to differences in parent material and associated weathering. Scores of the last three factors highlighted the differences between the materials, apart from weathering, and resulted in a fair separation between 3 groups. The element-pairs Al/Ga, Zr/Nb, and Ce/Nd appear as the signature elements differentiating the parent materials. The integration of mineralogy, micromorphology, and factor analysis gave a good compromise between qualitative/semiquantitative and quantitative methods in explaining the differences in origin and soil formation circumstances between distinct polygenetic soil profiles.

Keywords: Brazil; Oxisols; polygenesis; soil mineralogy; factor analysis.

INTRODUCTION

In the humid tropics, soils have a complex evolutionary history caused by multiple climatic changes and geomorphic cycles. Because of that, they are polygenetic, and have different evolution phases overprinted on the profiles. Each following soil formation commonly took place in preweathered materials of the previous phase, and, therefore, the various phases yield soils with rather similar chemical and mineralogical properties. The chemical composition of the soils is marked by partial or complete loss of Si and basic cations, and by accumulation of less mobile elements, which is the common (ferr)allitic weathering trend (Krauskopf and Bird, 1995). This, however, does not completely rule out the effect of parent material differences (Chesworth, 1977). The assemblage of minerals formed in such environments consists usually of Fe and Al oxides and hydroxides, and kaolinite. Less commonly, 2:1 clay

minerals are also found, usually as transitional phases in the weathering.

Secondary minerals are formed in response to environmental changes produced by weathering and pedogenesis, and may store information about the conditions prevailing during their formation (Resende, 1976; Zeese et al., 1994). These conditions are not necessarily reflected in the type of minerals formed, but rather in the structure, morphology and composition of the minerals. Also the proportions of the various mineral components in each assemblage may be connected to the environmental conditions. Moreover, in very old and highly weathered materials, differences in parent material may still be recognized (Curi, 1983), even if the soils developed in preweathered parent materials. In this context, geological information is essential for the interpretation of associations of secondary minerals in soils and saprolites (Bühman, 1994).

The combined study of chemical and mineralogical aspects of polygenetic soils, if connected with micromorphology, provides an optimal insight into the processes and circumstances of soil formation (Stoops et al., 1990; Bronger et al., 1994). As a first step in this approach, polygenetic soils from Minas Gerais, Brazil, were studied with the purpose of distinguishing mineralogical and chemical trends in relation to parent rock, geomorphic evolution, degree of reworking of the materials (in situ, or redeposited), and landscape position.

MATERIALS

The studied areas are located in the central and southern part of the state of Minas Gerais, between 19 and 22°S and 44 and 45°W, near the towns of Sete Lagoas (SL) and São João del Rei (SJR). The dominant lithologies in the SL area are fine-textured sedimentary and slightly metamorphized rocks (shales, siltstones and corresponding slates) of the Late Proterozoic Bambuí group. In the SJR area, the main lithologies are low- and medium-grade metamorphic rocks belonging to the Archean Barbacena group and to the Middle/Late Proterozoic São João del Rei and Andrelândia groups, beside localized occurrences of neo-Cenozoic sediments.

The present climate in the SL area is a Tropical Savanna climate, with an average annual temperature of 22°C and average annual precipitation of 1300 mm. The SJR area has a Tropical Highland climate, with an average annual temperature of 19-20°C and an average annual precipitation of 1400 mm. The topography in the SL area is gently undulating to rolling (600-900 m asl), and in the SJR area it is undulating to rolling with altitudes of 900-1100 m asl. In both areas the original vegetation is represented by *cerrado* and *campo cerrado* (savanna-like and sparse savanna-like vegetation). Soils are Oxisols, with eroded equivalents on dissected slopes.

Based on their parent material the selected soil sequences are classified in 3 groups which are characterized and identified as follows:

SJR-sap: fine- and medium-textured metamorphic rocks and saprolites;

SJR-sed: neo-Cenozoic sediments;

SL-sap: fine-textured sedimentary and metasedimentary rocks.

The classification of the soils and some field aspects are presented in Table 2.1. Complete profile descriptions are given in Appendix 1. Group SJR-sap consists of one erosive catena of Oxisols (P1-P5) where consecutively deeper parts of the original profile are exposed downslope, and two Oxisol-saprolite-weathered rock sequences (P7 and P8). Group SJR-sed consists of two sequences, P6, and VP, which developed on sedimentary graben fillings. The P6 sequence has three layers of sediments (I,II,III), in each of which soil formation has taken place. These layers are overlaid by a well-sorted sediment, with an Oxisol, which has thin petroplinthite layers towards its base. The VP sequence consists of a deep Oxisol, developed in layered, probably lacustrine, sediments. The bottom part of VP, below the sedimentary layers, consists of saprolite developed from the same metamorphic rocks as Group SJR-sap. Group SL-sap consists of a catena of Oxisols (C1- C4), and one Inceptisol-weathered rock sequence (C5).

Table 2.1: Profiles, classification and general field aspects of the studied groups.

Group identification	Profile/ sequence	Profile position	depth (cm)	Soil classification	Colour[1]
SJR-sap	P1	crest	550+	Anionic Acrudox	10R 4/6
	P2	upper slope	200+	Anionic Acrudox	5YR 5/8
	P3	middle slope	170+	Inceptic Hapludox	7.5YR 5/8
	P4	lower slope	200+	Inceptic Hapludox	7.5YR 4/4
	P5	lower slope	200+	Udoxic Dystropept	7.5YR 5/6
	P7	upper slope	500+	Anionic Acrudox	10YR 5/8
	P8	crest	500+	Anionic Acrudox	2.5YR 4/6
SJR-sed	P6	middle slope	2300+	Petroferric Acrudox	2.5YR 4/6
	VP	upper slope	1560+	Anionic Acrudox	2.5YR 4/6
SL-sap	C1	crest	400+	Typic Haplustox	10R 4/6
	C2	upper slope/crest	210+	Typic Haplustox	2.5YR 4/8
	C3	middle slope	470+	Typic Haplustox	2.5YR 5/8
	C4	middle slope	540+	Inceptic Haplustox	10YR 7/8
	C5	upper slope	1070+	Ustoxic Dystropept	10YR 7/8

[1] Munsell colour of the moist B horizon of all profiles, except in profile C5, where the colour refers to horizon C1.

METHODS

Soils in the field were described according to the FAO guidelines (FAO, 1990). Soil bulk samples were collected, air dried and passed through a 2 mm sieve to obtain the fine earth fraction for subsequent laboratory determinations. Routine textural and chemical analyses were carried out in the fine earth samples, as described by Buurman et al., (1996). Removal of organic matter (and iron, if necessary), and separation of the clay fraction were done according to Buurman et al.

(1996). Mineralogical analyses of the clay fraction were done by X-ray diffraction, using a Philips PW 1710 diffractometer with a graphite monochromator, employing CoKα radiation at 30mA and 40kV. Semiquantitative determination of kaolinite and gibbsite in deferrated samples were done by thermogravimetric analyses, using a Dupont 951 Thermogravimetric Analyser (TGA). Evaluation of the intercalation capacity of kaolinites was done by exposing glycerol-saturated oriented clay to dimethyl sulphoxide (DMSO) vapour at 70°C for 72 hours in an exsiccator (Scholten et al., 1995a; Felix-Henningsen et al., 1997). Quantification of the intercalation was done by comparing peak intensities of the expanded and unexpanded component. Sand and silt fractions were studied by binocular microscope, and hand-picked grains were identified by X-ray diffraction. Mössbauer spectroscopy was done for selected bulk and iron concentrated samples. The Mössbauer spectra were taken at room temperature (295K) and at liquid nitrogen temperature (77K) with a constant acceleration spectrometer using a ^{57}Co in Rh source.

Thin sections of 7x7 cm, for micromorphological characterization were prepared from undisturbed samples. Selected areas of uncovered thin sections were separated, reimpregnated, and microtomed for observation by transmission electron microscope (TEM), using a JEOL 1200 EXII at 80kV. Clay fractions and soil aggregates were studied with a Scanning Electron Microscope (SEM) and analyzed with a 9900 Energy Dispersive X-Ray analyzer (EDAX). For X-ray fluorescence analyses, subsamples were ground in a sialon ball mill, ignited at 900°C, and subsequently mixed (1:10 w/w) and melted into lithium tetraborate disks. 28 Major and trace elements were measured using a Philips PW 1404 spectrometer.

Principal Component Analysis (PCA) was used on a set of 14 elements as an extraction method for the factors (Davis, 1986). The 14 elements were selected by analyzing the communalities of all 28 measured elements, in a reconnaissance factor analysis. Elements with low communality (variation independent from the other elements) have been omitted in further analysis. This includes Ca, which shows independent scattering, that may be caused by vegetation cycling. Factor analysis is used to derive the simplest model that yields a reasonable explanation of the chemical composition of the materials (Tidball et al., 1989). The most important orthogonal factors that explain the variance of the soils and subsoils from the 3 groups were so derived.

RESULTS AND DISCUSSION

Mineralogy and weathering

The semiquantitative mineralogical composition of the clay fraction as determined by XRD is given in Table 2.2. The molar ratio SiO_2/Al_2O_3 of the fine earth fraction is included in the table for an assessment of the degree of weathering.

Micas

Apart from some accessory minerals, micas are the only primary minerals found in the studied sequences. They are observed in the saprolites and BC horizons of profiles P7 and P8 (group SJR-sap); throughout the soils of group SL-sap, and occasionally in the P6 sequence (group SJR-sed). Micas are found either in the clay or in the silt and sand fractions. The micas in the coarse size-fractions, as observed in thin sections, consist of muscovite. In the clay fraction, the micas are most likely illites, since the kind of parent rocks (shales and slates derived from them) is usually rich in fine-grained illite-type micas (Fanning et al., 1989). This is substantiated by a strong 002 reflection in the X-ray diffractograms, which is ascribed to muscovite/illite type micas. The illites may also have formed by weathering of coarser muscovites with retention of K (Murray, 1988; Allen and Hajek, 1989).

In group SJR-sap, the presence of micas in the saprolites of profiles P7 and P8, and their absence in profiles P1-P5, may be due to differences in the metamorphic grade of the original rocks (lower for P7-P8 than for P1-P5), which can influence the nature and the particle size of the primary micas (Fanning et al., 1989). Micromorphological observations of the saprolites of P1-P5 and VP-sap showed pseudomorphic kaolinite booklets with accumulation of minute iron oxides crystallized along the former cleavage plans of micas. This suggests that the mica previously existing in the parent rock was biotite, which is now completely weathered.

Micas make way for mixed-layer clay minerals, (hydroxy-Al interlayered) vermiculite and kaolinite, as observed in the surface horizons of profiles P7, P8 (group SJR-sap), and in all profiles of group SL-sap (Table 2.2). The transformation mica→vermiculite→kaolinite, and the decreasing ratio of mica to their associated secondary minerals towards the surface, is reported by other authors (Rebertus et al., 1986; Douglas, 1989; Stolt et al., 1991; Aoudjit et al., 1996). Apparently, K-bearing micas have been transformed to expandable 2:1 minerals through replacement of K^+ by hydrated cations. This is termed 'simple transformation', because a considerable portion of the mica structure is retained (Fanning and Fanning, 1989). Under acid conditions, the expandable 2:1 minerals, vermiculite in this case, may be further transformed to hydroxy-interlayers or destroyed (Fanning et al., 1989), enabling kaolinite formation, as observed in the studied profiles. The simple transformation is replaced by the destruction of the parent crystalline lattice, in the direct transformation muscovite→kaolinite. In this case, the kaolinite may display obvious parental relationships with the associated muscovite (Brilha et al., 1991; Nahon, 1991).

Hand-picked sand-sized 'micas' from the saprolites of group SJR-sap were analyzed by X-ray diffraction, and found to be pure kaolinite, indicating that they are pseudomorphs, as reported previously for other saprolites in Southeastern Brazil (Pinto et al., 1972). Although the sand-sized kaolinites display a mica morphology, the complete absence of vermiculite or any other intermediate phases, even in the deepest saprolite of profiles P1-P5, points to a neoformation of kaolinite after biotite as also reported by other authors (Bisdom et al., 1982;

Ojanuga, 1990). Therefore, the absence of vermiculite in profiles P1-P5 indicates that this stage in the mica weathering was by-passed, and micas were directly transformed into kaolinites.

Table 2.2: Qualitative and semiquantitative mineralogical composition of selected samples from the studied soil sequences.

Group	Profile/ sequence	horizon	Clay %	clay mineralogy [1,2] Ka	Gb	Gt	Hm	Vm/Mxl	Mi	Ka/ (Ka+Gb)[3]	SiO_2/ Al_2O_3[4]
		A	73	++++	++	+	+	-	-	0.65	1.25
		Bw2	65	++++	++	+	+	-	-	0.55	1.03
	P1	BC1	51	++++	++	+	+	-	-	0.68	1.58
		C	6	++++	tr	+	-*	-	-	0.99	2.22
		A	73	++++	+	+	-	-	-	0.85	1.96
	P2	Bw	77	++++	+	+	-	-	-	0.84	1.72
		C	24	++++	+	+	tr	-	-	0.88	2.03
		AB	66	++++	+	+	-	-	-	0.88	2.37
	P3	Bw	62	++++	+	+	-	-	-	0.88	2.36
		C	22	++++	+	+	tr	-	-	0.91	2.24
S		AB	68	++++	+	+	-	-	-	0.88	2.08
J	P4	Bw	68	++++	+	+	-	-	-	0.87	2.05
R		C	29	++++	+	+	tr	-	-	0.90	2.33
-		Bw	59	++++	+	+	tr	-	-	0.89	2.39
s	P5	BC	23	++++	+	+	+	-	-	0.90	2.61
a		C1	15	++++	+	+	+	-	-	0.97	2.66
p		Bw	58	++++	++	+	-	+	-	nd	3.41
		BC1	48	++++	++	+	-	+	-	0.76	3.38
	P7	IIBC1	42	+++	+++	+	tr	-	-	0.61	2.74
		C2	2	++	tr	+	+	-	+	0.99	3.60
		rock	-	+	+	+	+	-	++	nd	2.57
		A1	55	+++	+++	+	tr	+	tr	0.38	1.87
		Bw1	47	++	+++	+	+	+	tr	0.33	1.83
	P8	BC1	36	++++	++	+	+	-	+	nd	2.36
		C	7	++++	+	++	tr	-	++	0.94	3.95
		rock	-	++++	++	++	nd	-	++	nd	2.91
	VP	sap	4	+++	-	+	+	-	-	nd	4.22
		sap	16	++	-	+	+	-	-	nd	3.28

Table 2.2: Continued

Group	Profile/ sequence	horizon	Clay %	clay mineralogy [1,2] Ka	Gb	Gt	Hm	Vm/Mxl	Mi	Ka/ (Ka+Gb)[3]	SiO_2/ Al_2O_3[4]
		Bw	81	++++	++	+	+	-	-	nd	1.89
		Bwm	-	++++	tr	+	+	-	tr	nd	2.17
S	P6	Bwv	51	++++	-	+	+	-	tr	nd	2.47
J		III	16	++++	-	+	+	-	+	nd	2.98
R		II	32	++++	-	+	+	-	+	nd	3.73
-		I	31	++++	-	+	+	-	++	nd	4.02
s		Bw1	66	+++	++	+	+	-	-	nd	1.74
e		BC1	55	++++	++	+	+	-	-	nd	2.04
d	VP	C1	59	++++	++	+	+	-	-	nd	1.68
		V	34	++++	+	+	+	-	-	nd	2.47
		IV	32	++++	-	+	+	-	-	nd	2.80
		A	73	++++	++	tr	+	++	+	nd	2.88
	C1	Bw	80	++++	++	-	+	++	+	nd	2.69
		BC4	78	++++	++	tr	+	+	+	nd	2.50
		A	69	++++	++	+	+	+	+	nd	2.71
S	C2	Bw1	72	++++	++	+	+	+	+	nd	2.66
L		BC	73	++++	++	+	+	+	+	nd	2.53
-		AB	72	++++	++	+	+	+	+	nd	2.79
s	C3	Bw2	69	++++	++	+	+	+	+	nd	2.70
a		IIBC1	60	++++	+	+	+	-	++	nd	3.32
p		C	36	+++	-	+	+	-	++	nd	4.14
		Bw	40	++++	++	+	-	+	+	nd	6.91
	C4	BC2	36	++++	+	+	tr	+	++	nd	6.14
		C2	27	+++	-	+	tr	-	+++	nd	6.33
	C5	C1	43	+++	-	++	tr	-	++	nd	4.31
		R	20	+	-	++	tr	-	+++	nd	4.95

[1] Mi: mica; Ka: kaolinite; Gb: gibbsite; Gt: goethite; Hm: hematite; Vm/Mxl: vermiculite/mixed layer clay mineral; [2] ++++: abundant; +++: common; ++: frequent: +: present; tr: trace; -: absent; nd: not determined; [3] mass ratio determined by TGA in the clay fraction, [4] molar ratio of oxides determined by XRF in the fine earth fraction.

Micas are still found in the topsoils of the Oxisols from groups SJR-sed and SL-sap. They were identified by X-ray diffraction, and their presence is also suggested by the moderate K_2O contents measured by XRF spectroscopy. However, they were rarely seen in thin sections. Investigation of iron concentrates by scanning electron microscopy and EDAX analyses, revealed that the micas are coated with a thin iron-oxide layer (Figure 2.1), which probably protected them against weathering. This is reported for Fe-bearing micas, where Fe is released as Fe^{2+} from the octahedral sheet, oxidized, and precipitated as a coating (Curmi, 1979). Such a protective film would further increase the stability of biotites (Eswaran and Heng, 1976; Nahon, 1991). However, we do not know previous reports of iron coatings protecting

muscovites and/or illites against weathering.

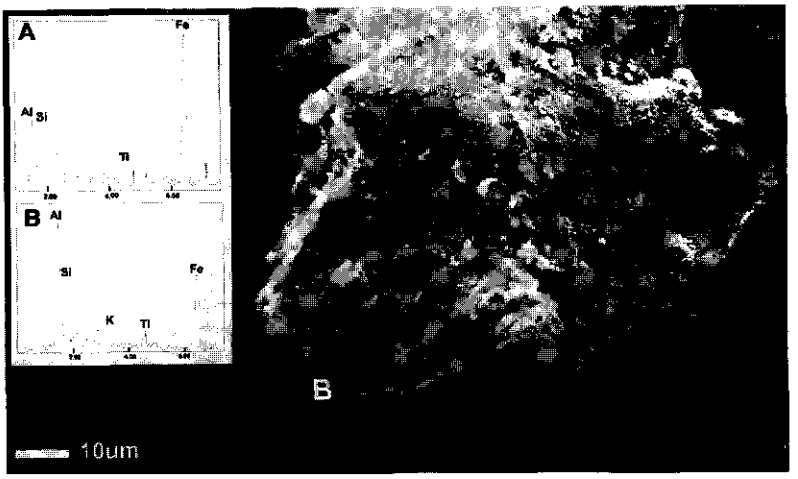

Figure 2.1: SEM photograph of a mica grain coated by iron oxides; EDAX profiles show chemical composition of coated surface (A) and of the grain edge (B).

Kaolinite

Kaolinite is the dominant clay mineral in all samples. It appears in two main forms: macrocrystalline booklets (Figure 2.2a) with sizes up to 2 mm, and submicron-sized particles. The booklets are found in the saprolites and weathered rocks, and the fine particles are found in the soils and sedimentary layers. The booklets have formed by weathering of micas, either biotite or muscovite/illite, through pseudomorphic transformation or dissolution and neoformation. The first process is characterized by a pseudomorphic replacement of the micas by secondary kaolinite (Rebertus et al., 1986; Fanning et al., 1989; Nahon, 1991; Tardy, 1993), where the original mica shape is fairly conserved. The kaolinite booklets formed this way are usually referred to as 'pseudomorphs after micas', although they may not result from simple transformation (degradation) alone, but also from (pseudomorphic) neoformation (Ambrosi et al., 1986; Nahon, 1991). On the other hand, an increasing influx of Si and Al in the solution leads to the growth of secondary kaolinite on primary mica, a typical neoformation (Nahon, 1991). In this case, the kaolinite booklets will have their sheets randomly oriented to those in the original micas (Stoops et al., 1990), while in pseudomorphic booklets they are parallel (Nahon, 1991). According to this distinction, most of the kaolinites from the saprolites are pseudomorphs after micas. In saprolites from profiles P1-P5 and VP-sap some domains of neoformed kaolinites were recognized. In these samples kaolinites that appear to have formed from biotite were also found, as shown the presence of minute crystals of hematite along the kaolinite flakes.

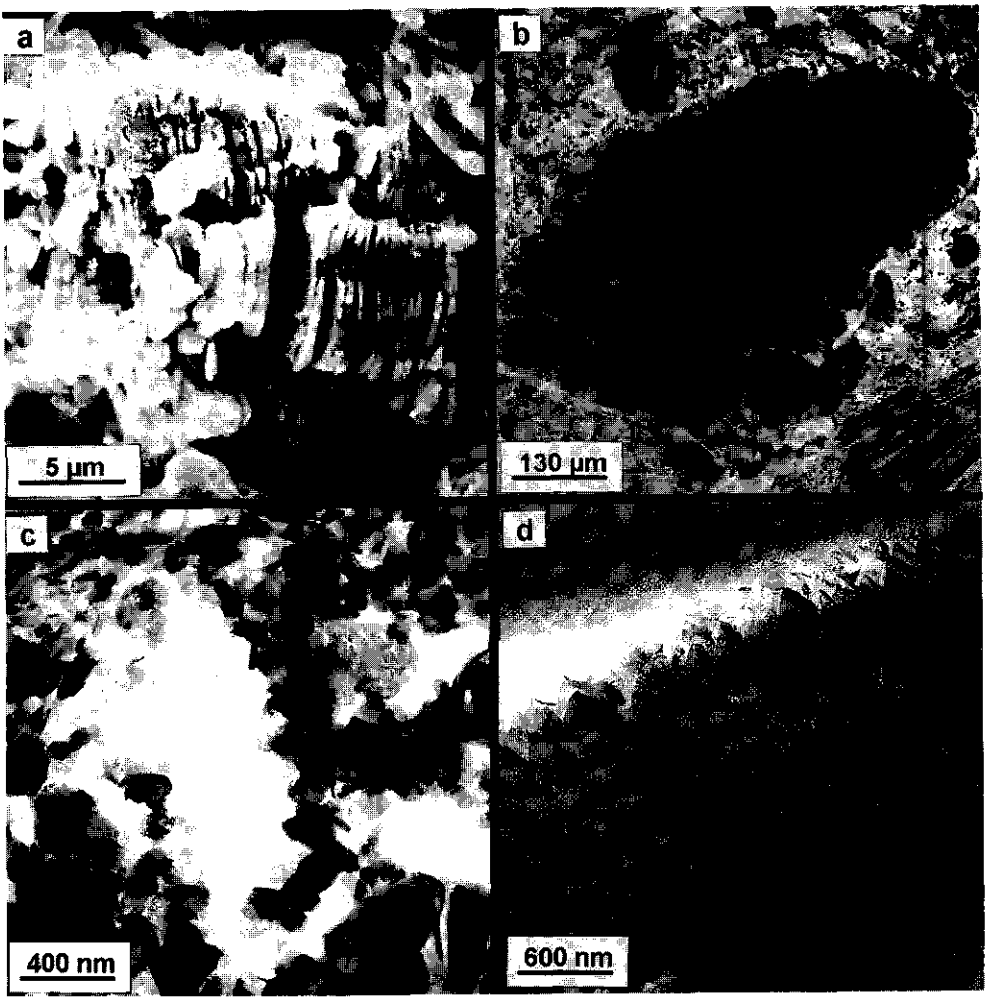

Figure 2.2: **(a)** SEM photograph of a kaolinite booklet showing loosened flakes; saprolite from profile C4, group SL-sap; **(b)** Microphotograph (PPL) of kaolinite booklets showing hematite inclusions (replacement) along flakes; saprolite from profile P1, group SJR-sap; **(c)** TEM photograph of kaolinite crystals from clay accumulations related to voids of layer I, sequence P6, group SJR-sed; **(d)** TEM photograph of gibbsite crystals grown on kaolinite surfaces in saprolites from group SJR-sap.

The kaolinite booklets disappear towards the surface, as a result of either particle comminution by pedoturbation or dissolution of the kaolinite booklets in response to a changing pedoenvironment. Particle comminution is considered by many authors as the main process in this transformation (Flach et al., 1968; O'Brien and Buol, 1984; Graham et al., 1989; Bakker et al., 1996). This appears unlikely in the present case, because the soil kaolinites have different crystallinity (see below). It appears that most of the kaolinite booklets are

dissolved, and eventually recrystallized to submicron-sized particles that constitute the homogenized groundmass. Dissolution and recrystallization of kaolinite from saprolites to soils under ferralitic weathering is reported for a wide range of circumstances (Ambrosi et al., 1986; Amouric et al., 1986; Muller and Bocquier, 1986; 1987; Lucas et al., 1987; Bilong, 1992; Felix-Henningsen, 1994; Zeese et al., 1994). Kaolinite dissolution is caused by the presence of iron, and is indicated by increasing ferruginisation of the kaolinite flakes and infilling of corroded booklets with ferruginous plasma (Ambrosi et al., 1986; Muller and Bocquier, 1986). These features are clearly observed in thin sections of saprolites from groups SJR-sap and SL-sap (Figure 2.2b). The reaction is described by Ambrosi et al. (1986), as an epigenetic replacement of kaolinite booklets by hematite crystals, following a mechanism analogous to ferrolysis. The dissolution of kaolinite is caused by the protons released during oxidation, hydrolysis and precipitation of iron oxides in conditions of low water activity, which is related to the small pore size of the kaolinite matrix (Tardy and Nahon, 1985; Ambrosi et al., 1986), The kaolinite is then precipitated further away, in microenvironments with higher water activity. Kaolinite formed in these conditions is submicron-sized (Cantinolle et al., 1984; Bilong, 1992), poorly crystalline (Rengasamy et al., 1975; Muller and Bocquier, 1987; Zeese et al., 1994), and usually accommodates some iron within its structure (Herbillon et al., 1976; Mestdagh et al., 1980).

In this context, the booklets and the submicron-sized soil kaolinites are designated respectively as 'primary' and 'secondary' kaolinites (Zeese et al., 1994). Primary kaolinites are the main component of the saprolites of groups SJR-sap and SL-sap. Primary kaolinites are usually well ordered, while secondary kaolinites are disordered, showing common stacking defects, which is reportedly related to the presence of iron in their structure (Tardy and Nahon, 1985; St. Pierre et al., 1992; Singh and Gilkes, 1992a; Scholten et al., 1995a). Indeed, the secondary kaolinites have isomorphic substitution of Fe for Al as shown by Mössbauer spectroscopy. Figure 2.3 shows the 77K Mössbauer spectra of the same sample, before and after concentration of iron oxides by 5M NaOH treatment. The spectrum of the untreated sample shows the presence of a large central doublet (arrow in Figure 2.3a) which disappears upon the removal of kaolinite and gibbsite (Figure 2.3b). This central doublet has Mössbauer parameters that are ascribed to kaolinite (Murad and Wagner, 1991), and indicate the presence of Fe^{3+} ions at octahedral positions (Taylor et al., 1968).

Properties of kaolinites are reportedly influenced by their environment of formation (e. g. Muller and Bocquier, 1986), but there is not much information about the relation between kaolinite properties, structural defects in special, and genetic conditions (Murray, 1988). The behaviour of kaolinites upon intercalation with organic substances may give an indication of the type of structural defects, and by way of this, of genetic conditions (Raussel-Colom and

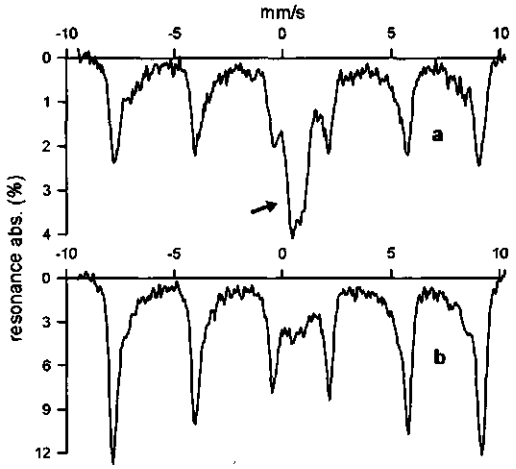

Figure 2.3: Mössbauer spectra at 77K of a clay sample from profile P8, group SJR-sap, before **(a)** and after **(b)** treatment with NaOH 5M for removal of kaolinite and gibbsite.

Serratosa, 1987). Intercalation of kaolinites with dimethyl sulphoxide (DMSO) is one of such techniques (Range et al., 1969). Figure 2.4 shows the results of intercalation of kaolinitic clays by DMSO of soils and saprolites from the three groups. The expansion of the kaolinite (001) basal spacing from 7.2 to 11.2 Å was usually lower in soils (secondary kaolinites), than in saprolites (primary kaolinites), although not complete in saprolites. Moreover, the intercalation behaviour of the kaolinites was different for the three groups: in group SJR-sed they did not intercalate at all; in group SL-sap they intercalated only in saprolites and less weathered horizons; in group SJR-sap they intercalated both in soils and saprolites, but to a lesser extent in soils. The incapacity of some kaolinites to expand upon exposing to DMSO and other organic substances, is explained by a higher disorder due to irregular isomorphic substitution of Al-for-Si in the tetrahedral sheet, and of Fe-for-Al in the octahedral sheet (Herbillon et al., 1976; Felix-Henningsen, 1997). This causes an increase in the cohesion energies bonding the kaolinite stackings (Raussel-Colom and Serratosa, 1987; Almeida et al., 1992). The results indicate that the type of weathering as well as the abundance of iron in the environment, play a definite role in the type of kaolinite formed. Thus, the sedimentary materials high in Fe, and presumably with a high Fe^{+2} activity due to periodical water saturation, showed the maximum intercalation disorder, while the soil kaolinites in group SJR-sap are partially intercalated, indicating that they may have been partly comminuted and not all dissolved and neoformed.

The disappearance of the coarser fractions and the fining up of the texture of the materials towards the soil surface shows that clay is being formed in soils of all groups. In groups SJR-sap and SL-sap, this is related to the breakdown of 'primary' to 'secondary' kaolinite, as indicated by the dominance of 'secondary' kaolinite in the topsoils and by the formation of gibbsite. Clay

precipitation features which accumulate as coatings and infillings also indicate neoformation of kaolinite. In group SJR-sed, pedofeatures related to formation and movement of clay are commonly observed. They consist of illuvial and chemically precipitated clay accumulations, essentially composed of kaolinite and iron oxides. Detailed characterization of these features is given in Chapter 4. The kaolinite crystals formed in such clay accumulation pedofeatures appear as plates with well developed hexagonal shapes, as shown by TEM (Figure 2.2c).

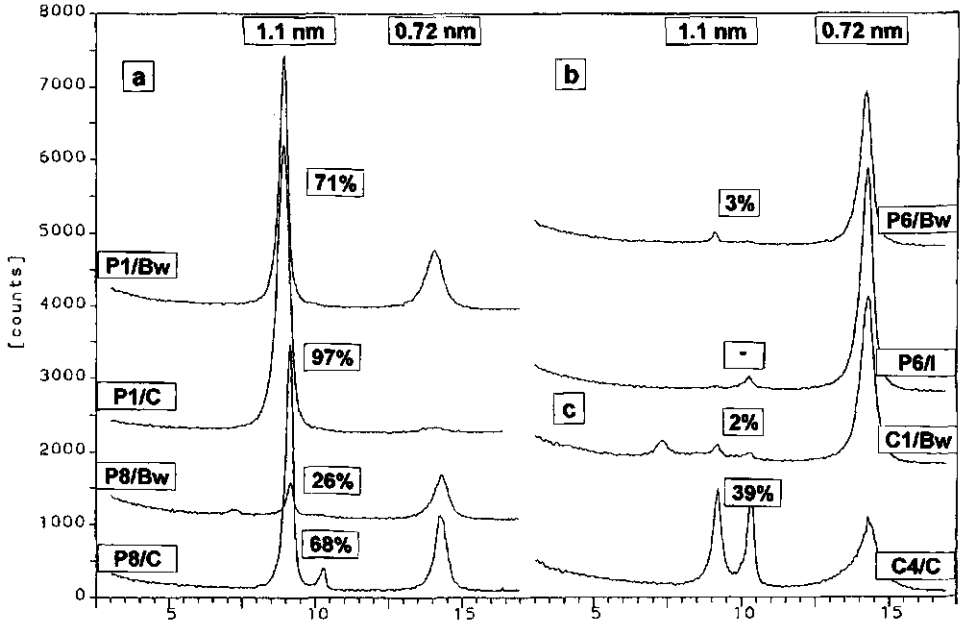

Figure 2.4: X-ray diffractograms of kaolinitic samples from groups SJR-sap (a); SJR-sed (b), and SL-sap (c), after intercalation with dimethyl sulphoxide (DMSO). The degree of intercalation given by the amount of expansion from a 7.1 Å to a 11.2 Å spacing is shown for each sample in the figure.

Gibbsite

Gibbsite is a common mineral in most of the profiles: it is absent only in the saprolites of group SL-sap, and in the sedimentary layers of sequence P6 (group SJR-sed). The amount of gibbsite usually increases towards the topsoils, as shown by XRD and TGA semiquantification (Table 2.2). In profiles P7 and P8, amounts of gibbsite equals, or even exceed, those of kaolinite, which indicates a strongly leaching environment, leading to allitization.

Micromorphological studies show that gibbsite is formed in two different ways (Eswaran et al., 1977; Nahon, 1991; Zeese et al., 1994): by replacement of kaolinite (relative accumulation) or by transfer of aluminium in soil solution (absolute accumulation). The first type is reported to take place in saprolites and C horizons, while the second type is associated

with upper soil horizons, which are already highly weathered (Calvert et al., 1980; Merino et al., 1993). The replacement of kaolinite by gibbsite is observed in thin sections of the saprolites from group SJR-sap, by the presence of gibbsitic domains in a kaolinitic matrix and of highly birefringent layers within the kaolinite booklets. The growth of euhedral gibbsite crystals on kaolinite platelets was also observed by TEM (Figure 2.2d). This transformation is described as a topotactic replacement of kaolinite (Nahon, 1991), related to microenvironments with in-situ desilicification (Stoops et al., 1990).

Absolute accumulation is clearly observed in the sedimentary layers from group SJR-sed, where gibbsite occurs as coatings and/or infillings related to voids and to quartz grains (see Figure 4.3b, Chapter 4). Gibbsite, in these accumulations is usually coarser than clay, and is, therefore, not identified by XRD in the clay fraction. The presence of gibbsite enclosing and infilling quartz grains was also reported by Dedecker and Stoops (1993), and may be explained as precipitation from Al-rich solutions, or as replacement of quartz (see *Quartz*).

Iron oxides

Goethite and hematite are the only iron oxides found in the clay and silt fractions. Goethite is present in all samples, even in the strongly red ones. Hematite is hardly found in the yellow topsoils of groups SJR-sap and SL-sap. Also, it is rarely found in the yellow clay fraction of some saprolites, although it is abundant in the silt fraction of these saprolites. Micromorphological analyses of the iron oxides forms showed that in the saprolites of groups SJR-sap and SL-sap, hematite has a typical 'droplet' morphology (see Chapter 3). A detailed characterization of the iron oxides is given in Chapter 5. Apart from their distinct morphology, and slight variations in crystal size, no other differences were found between hematites from the three groups. In contrast, goethite showed great variability in chemical and morphological aspects between and within the groups. These variations could be linked to differences in soil development, soil hydrology and polygenesis.

Quartz

Quartz is the dominant component of the silt and sand fractions of all soils, especially in groups SL-sap and SJR-sed. In group SL-sap, quartz is the dominant mineral in the silt fraction. Dominance of quartz in silt fractions of well drained soils formed on shales is reported as a common feature (Ojanuga, 1990). In group SJR-sap, quartz is more abundant in the topsoils and saprolites, where it also shows a higher variability in sizes, although it is predominantly silt- and fine sand-sized. In groups SJR-sap and SL-sap, the common (sub)angularity of the quartz grains indicates its derivation from quartz veins of the parent rock. This is supported by the fact that the grains are commonly polycrystalline and show undulating extinction. In group SJR-sed, quartz grains are commonly rounded, and related to the original sediment, although fractured fragments are common too.

Separation of polycrystalline quartz grains and fracturing of crystals start in saprolites

and increase considerably towards the surface. The grains are commonly infilled or separated into discrete subgrains by kaolinitic clay and/or iron oxides. In groups SJR-sap and SL-sap, the fractured quartz grains are frequently infilled with limpid red and/or dotted yellow clay related, respectively, to the hematite aggregates and to the surrounding soil groundmass. This kind of infilled quartz is common in tropical soils, and is termed 'runiquartz' (Eswaran et al., 1975). It consists of groundmass (plasma) infusion along the voids and fractures of quartz grains, which may either avoid further corrosion, or increase mechanical fragmentation (Eswaran and Stoops, 1979). Runiquartz with different types of infillings that are related or not to the present groundmass, point to in situ or relict weathering (Stoops, 1989). In this context, the quartz grains with red infillings found throughout the soils of the groups SJR-sap and SL-sap consist of relicts from former ferralitic weathering phases which gave origin to the present saprolites (see also Chapter 3). In group SJR-sed, runiquartz is only occasionally present, probably due to particle fragmentation during erosion and deposition.

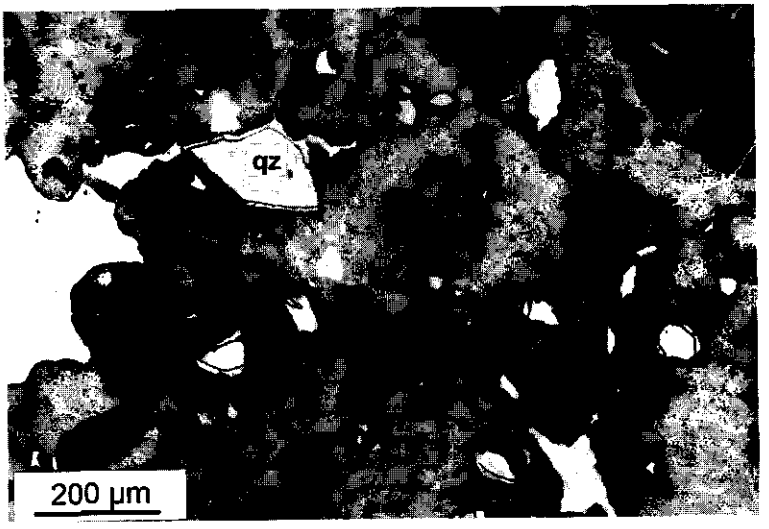

Figure 2.5: Microphotograph of quartz grains partially dissolved (layer I of sequence P6, group SJR-sed); plain polarized light (PPL).

In group SJR-sed, dissolution of quartz is indicated by the presence of grains that are smaller than the angular voids in which they are contained (Figure 2.5), as well as by the presence of concave boundaries, and coatings and infillings of gibbsite. An aureole of gibbsite crystals observed inside or around the quartz grains in some samples (see Figure 4.3b, Chapter 4), suggest that quartz was dissolved and replaced by gibbsite. This kind of transformation is described by Merino et al. (1993) as a pseudomorphic replacement, where the dissolution and crystal growth are simultaneous and have the same volumetric rate. Thus, the voids around

quartz grains may result from simple (congruent) dissolution, or from removal of an existing gibbsite aureole through dissolution or, artificially, during sample preparation.

Ilmenite and anatase

Ilmenite is occasionally found in group SL-sap, and is common in groups SJR-sap and SJR-sed. In group SJR-sap, ilmenite is more abundant in saprolites than in topsoils. Ilmenites present in saprolites and soils of group SJR-sap, as well as in group SJR-sed are weathered, whereas this is not clearly observed in group SL-sap. Weathering of ilmenite under oxidising conditions has been frequently reported (Anand and Gilkes, 1984a; Suresh-Babu, 1994; Ramakrishnan et al., 1997). In group SJR-sap, ilmenite grains show altered surfaces, characterized in thin section by a pellicular, dotted and/or complex alteration pattern (see Figure 3.2a, Chapter 3), similar to the pattern described by Anand and Gilkes (1984a) for a lateritic layer in Australia. In group SJR-sed, the weathering of ilmenite in thin section is shown by the presence of an external depletion hypocoating (see Figure 4.3c, Chapter 4). The presence of an isotropic weathering rind around the ilmenite grains in group SJR-sap suggests that the initial weathering results in a mixture of poorly crystallized mixture of Ti oxides (leucoxene). Leucoxene eventually recrystallizes to anatase, which is clearly identified in thin sections by its high birefringence, and occasionally to rutile. Anatase was found in almost all iron oxide concentrates examined by X-ray diffraction. Anatase is indeed reported as the most common Ti secondary phase, and is readily formed by weathering either of Ti oxides or Ti-bearing minerals (Milnes and Fitzpatrick, 1989).

Accessory minerals

Accessory minerals, which are sporadically found in all groups, are tourmaline, zircon and rutile. Tourmaline occurs as fine sand and occasional silt grains. The grains are limpid or very fractured (in some cases infilled with hematite); few occur as fibrous aggregates. Grains of tourmaline are usually fractured, but unweathered; however some show dissolved borders with partial replacement by iron oxides. Also some zircon grains show signs of weathering.

Chemistry

XRF major, minor and trace elements

Total concentrations of 28 elements were obtained by XRF analyses and are listed in Appendix 2. Rb, Sr and Th were below detection limits in all samples of profiles P1-P5 and VP, as well as Mg in most of them. Na and La were below the detection limit in more than 20% of the samples of the whole dataset.

The weathering state of the soils and saprolites can be assessed by the molar ratio SiO_2/Al_2O_3 of the fine earth samples (Table 2.2; Appendix 2). The most strongly weathered soil is P1, as shown by the low SiO_2/Al_2O_3 molar ratio and by the relatively high content of

gibbsite in the B horizon (Table 2.2). This ratio indicates a general highly weathered status of the soils from the SJR area, where redder soils are more weathered than the yellower ones, which have developed in deeper parts of the saprolite. Soils of the SL-sap group, although very deep and red, show a lower degree of weathering as given by the SiO_2/Al_2O_3 molar ratio, apart from the effect imprinted by the higher quartz contents in the silt fraction. Depth trends in the chemical composition of the studied soil sequences are consistent with the mineralogical trends discussed above. The chemical behaviour of the elements was investigated by statistics using factors extracted by principal component analysis. The results are discussed below.

Factor analysis

Factor analysis was applied to a set of fourteen elements, their correlation matrix is given in Table 2.3. From all mutual correlation coefficients, the thirteen coefficients having a value greater than 0.7 are underlined in the Table. Dimension reduction by PCA yielded four factors that explained 89% of the total variance of the fourteen elements in all samples. The remaining variance, explained by other factors, probably stands for experimental errors and random variation of the materials. Table 2.4 presents all factor loadings that are larger than 0.7, and the cumulative variance explained by the four factors.

Table 2.3: Correlation matrix of fourteen oxide components and trace elements used to extract four factors.

	SiO_2	Al_2O_3	Fe_2O_3	TiO_2	MgO	K_2O	Ba	Ce	Ga	Nb	Nd	Rb	Y	Zr
SiO_2	1.00	-0.92	-0.88	-0.81	0.67	0.58	0.36	0.17	-0.83	0.17	0.27	0.61	0.66	0.18
Al_2O_3	-0.92	1.00	0.65	0.83	-0.65	-0.59	-0.32	-0.05	0.86	-0.05	-0.15	-0.65	-0.65	-0.07
Fe_2O_3	-0.88	0.65	1.00	0.59	-0.67	-0.59	-0.42	-0.31	0.63	-0.31	-0.40	-0.58	-0.60	-0.31
TiO_2	-0.81	0.83	0.59	1.00	-0.54	-0.50	-0.48	-0.11	0.75	0.19	-0.10	-0.45	-0.37	0.21
MgO	0.67	-0.65	-0.67	-0.54	1.00	0.93	0.57	0.25	-0.61	0.22	0.34	0.92	0. 68	0.20
K_2O	0.58	-0.59	-0.59	-0.50	0.93	1.00	0.69	0.24	-0.53	0.17	0.27	0.92	0.64	0.16
Ba	0.36	-0.32	-0.42	-0.48	0.57	0.69	1.00	0.42	-0.36	-0.05	0.34	0.43	0.21	0.00
Ce	0.17	-0.05	-0.31	-0.11	0.25	0.24	0.42	1.00	-0.10	0.31	0.95	0.10	0.15	0.32
Ga	-0.83	0.86	0.63	0.75	-0.61	-0.53	-0.36	-0.10	1.00	0.08	-0.16	-0.56	-0.60	0.03
Nb	0.17	-0.05	-0.31	0.19	0.22	0.17	-0.05	0.31	0.08	1.00	0.54	0.24	0.38	0.94
Nd	0.27	-0.15	-0.40	-0.10	0.34	0.27	0.34	0.95	-0.16	0.54	1.00	0.21	0.32	0.56
Rb	0.61	-0.65	-0.58	-0.45	0.92	0.92	0.43	0.10	-0.56	0.24	0.21	1.00	0.73	0.22
Y	0.66	-0.65	-0.60	-0.37	0.68	0.64	0.21	0.15	-0.60	0. 38	0.32	0.73	1.00	0.40
Zr	0.18	-0.07	-0.31	0.21	0.20	0.16	-0.01	0.32	0.03	0.94	0.56	0.22	0.40	1.00

The first factor explains 32% of the variance and comprises mainly SiO_2, and Al_2O_3, Fe_2O_3, TiO_2 and Ga, which are negatively correlated with SiO_2. The scores on this factor are interpreted as related to the weathering state of the material. This general weathering trend is well known (e.g. Krauskopf and Bird, 1995), and is caused by leaching of basic cations, followed by Si, and relative accumulation of Al, Fe, Ti, and other less mobile minor and trace

elements, as for instance Ga. Ga is common in silicates, and upon weathering is incorporated by clay minerals and gibbsite, where it substitutes for Al (Anand and Gilkes, 1984).

Table 2.4: Loadings and cumulative explained variance of four factors (Varimax normalised; scores < 70% blanked out).

Variable	SiO_2	Al_2O_3	Fe_2O_3	TiO_2	MgO	K_2O	Ba	Ce	Ga	Nb	Nd	Rb	Y	Zr	Cumulative expl.var. (%)
Factor 1	0.93	-0.91	-0.72	-0.84					-0.87						32
Factor 2										0.93				0.93	50
Factor 3								0.95			0.86				65
Factor 4					0.83	0.92						0.85			89

The fact that elements commonly related to the weathering trends of leaching and accumulation, such as Mg and Zr (Ca is below detection limit), are not loaded in this factor must be attributed to an overriding 'parent material effect' (Chesworth, 1977). Chemical and mineralogical differences between parent materials were not obliterated by weathering and result in a deviation from the general weathering trend. This is illustrated by Figure 2.6, which shows the line plots of the experimental molar ratio SiO_2/Al_2O_3 given by the XRF measurements, and their fitted values given by the scores on factor 1. Details of the calculation are given by Meijer and Buurman (1997). The general correspondence between the experimental and fitted lines reflects the dominant influence of the weathering state on the relative amounts of the major oxides, which sum up to nearly 100%. The remaining deviation between the two lines is mainly related to the elements K and Mg, and is explained by factor 4. This separation of a parent material effect appears only after application of Varimax rotation. In fact, the present data clearly illustrate the effect of rotation. Originally, factor 1 described the variation due to a combination of weathering state and parent material (50% of the total variance), whereas the remaining parent material effect was described by factor 4 (8% of the total variance). After rotation, factor 1 (weathering state) describes 32% of the total variance (Table 2.4), whereas factor 4 (parent material) became the second most important factor, in describing 24% of the total variance.

The second factor includes Nb and Zr. Zr is a less mobile element, which usually accumulates during weathering. Its absence in factor 1, and its high loading in another factor is very surprising, and indicates a differentiation of Zr within the weathering residue. Zr is reported to be mostly present as zircon, an accessory mineral commonly found as minute inclusions in micas and other silicates (Murad, 1978; Anand and Gilkes, 1984; Milnes and Fitzpatrick, 1989). It is one of the most stable primary minerals (Allen and Hajek, 1989), unless it is metamictized i.e. altered by the presence of radiogenic elements in its structure (Erlanck et al., 1978). Upon weathering, zircon accumulates in the silt and sand fractions of soils and saprolites (Milnes and Fitzpatrick, 1989). Zircon is indeed observed in the silt and

sand fractions of the various groups as a residual mineral.

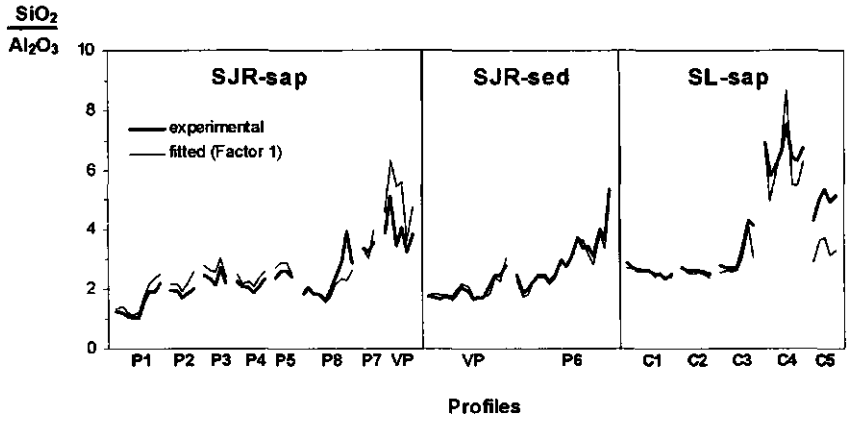

Figure 2.6: Line plots of experimental SiO_2/Al_2O_3 molar ratios of all samples, and of ratios calculated from fitted SiO_2 and Al_2O_3 using factor 1. The left to right sequence per profile refers to increasing soil depth.

Apart from the mineral zircon, Zr is also found in many minerals due to its ability to replace other elements with similar ionic radii, especially Ti oxides and ilmenite (Milnes and Fitzpatrick, 1989). Zr in Zr-bearing minerals (clinopyroxenes, amphiboles, micas and garnets) and in isomorphically substituted minerals (e.g. ilmenite) can be rather mobile (Melfi et al., 1996). Once released, Zr is partially leached or is incorporated in clay minerals, either by ion exchange or by substitution for Al (Erlanck et al., 1978; Melfi et al., 1996). Nevertheless, the mobility of Zr is very low, as shown by its low concentrations in natural waters, and Zr tends to accumulate in weathering profiles (Milnes and Fitzpatrick, 1989). Group SL-sap shows the highest contents of Zr, and a clear accumulation trend toward the topsoils. The higher Zr content in this group is likely related to the presence of mica throughout the soils of this group; its increase towards the topsoils is explained by residual accumulation of zircon due to weathering and soil development.

The fact that Ti and Zr are loaded in different factors suggests that, for the studied soils, the use of their ratio is not suitable for the assessment of parent material uniformity and degree of weathering. Moreover, the Ti and Zr minerals found in the soils are commonly weathered, implying that some net loss of these elements may have occurred, even if they were readily immobilized in secondary minerals.

The presence of Nb in factor 2 is explained by the fact that Nb isomorphically substitutes Zr in zircon (Heinrich, 1977), and probably accompanies Zr in other Zr-bearing minerals. The coupling of the two elements is clear in the XRF dataset ($r = 0.94$, Table 2.3), as well as by their common loading in the factor. Thus, the general assumption that Nb follows

the behaviour of Zr (Coughtrey and Thorne, 1983) is corroborated by our data. Insofar, it is concluded that Zr and Nb are governed by a combination of parent material and weathering effects. Factor 2, then, is interpreted as a subordinate weathering trend, distinctly expressed, because superposed on more important differences in parent material.

The third factor contains the light Rare Earth Elements Ce and Nd, which are well correlated ($r = 0.95$; Table 2.3), as expected, due to their similar chemical properties (Koppi et al., 1996). The light REEs are reported to be enriched in the weathering environment due to their overall low solubility (Braun et al, 1990). Ce is considered by some authors (Koppi et al., 1996) to be most strongly retained, although it can be removed by pedological processes that lead to leaching of iron compounds. Caggianelli et al. (1991) report that the REE distribution in pelitic sediments appears to be controlled by inherited illite, and secondarily by accessory minerals like as zircon, apatite, and Ti-oxides. In the studied profiles these elements may be related to the muscovite-illite type micas present in group SL-sap, which are likely inherited from the parent pelitic rocks. This cannot fully explain factor 3, because such an explanation would imply that factors 3 and 4 would form only one factor, (or that these elements would have a high loading in factor 4 and vice-versa). Thus, the factor may be interpreted as a combination of inherited illite and accessory minerals or another specific mineral (which however could not be identified).

The fourth factor is composed of MgO, K_2O and Rb and represents 24% of the total variance. The simultaneous presence of Rb and K is due to the strong tendency of Rb to be incorporated in K-minerals, and to the fact that it does not form minerals on its own. Moreover, Rb is more incorporated in micas than in K-feldspars (Heier, 1970). Factor 4 is interpreted as representing micas. Indeed, micas were identified in the clay (and coarser) fractions of all profiles from group SL-sap, in saprolites of profiles P7 and P8 (weathered phyllites and schists) from group SJR-sap, and in the deeper sedimentary layers of P6 (group SJR-sed).

Figure 2.7 shows the line plots of experimental data of K_2O and the communalities using three and four factors, respectively. The comparison between Figures 2.7 and 2.6 shows that the K/Mg factor explains the previously mentioned deviation from the general weathering trend. In addition, there are deviations which are not covered by the simple four-factor space model. As for instance, the excess contents of Fe are related to hydromorphic features, as shown by the line plot of experimental and fitted Fe contents in Figure 2.8. These deviations are mainly related to greater Fe accumulation or depletion in profiles VP-sed, P6 and P7. Micromorphological data show the presence of gley and pseudogley features in these samples (see Chapter 4), thus indicating sites of secondary Fe accumulations or depletion related to hydromorphic pedoenvironments.

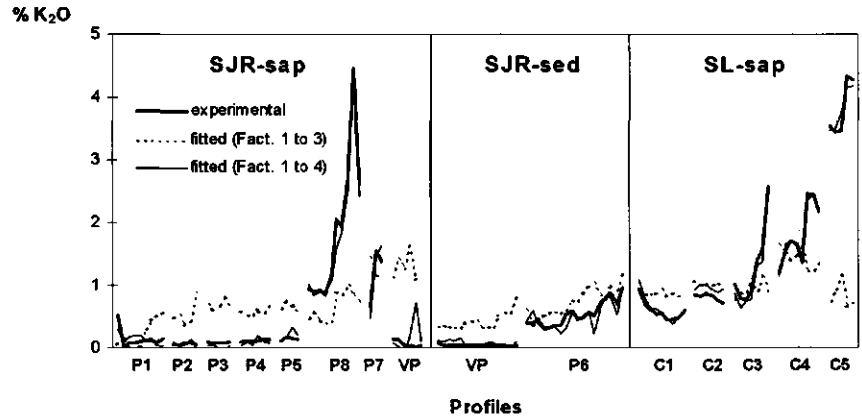

Figure 2.7: Line plots of experimental K_2O and fitted K_2O using factors 1 to 3 and factors 1 to 4 for all samples. The left to right sequence per profile refers to increasing soil depth.

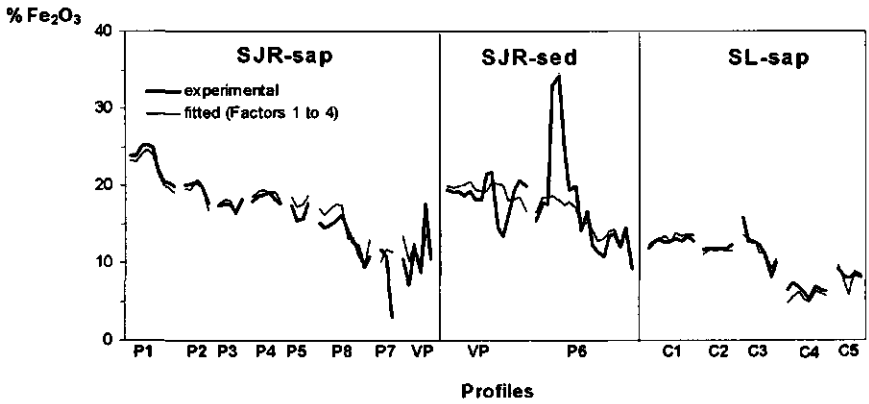

Figure 2.8: Line plots of experimental contents of Fe_2O_3 and fitted contents using factors 1 to 4 for all samples. The left to right sequence per profile refers to increasing soil depth.

Figure 2.9 shows scatterplots of trace elements that are specifically contained in the factors. It is possible to distinguish the three studied groups in the figures, indicating that these trace elements are effective signatures of the different origins of the materials.

The higher concentrations of some mobile minor and trace elements (e.g. Mg, K, Rb, Y) in the materials of group SL-sap compared to SJR, corroborates the lower degree of weathering of the SL materials, as also indicated by the SiO_2/Al_2O_3 molar ratio (Figure 2.6). A slight lasting effect of differences in the past climate, similar to the present difference (SL drier than SJR), over a prolonged period would account for a less intense weathering of the soils

from the SL area. Slower weathering would also favour the formation of Fe coatings on minerals, as in case of the micas. Inversely, the presence of protective Fe coatings on micas could hamper or decrease the weathering of the micas, to which Mg, K, and Rb are considered to be related.

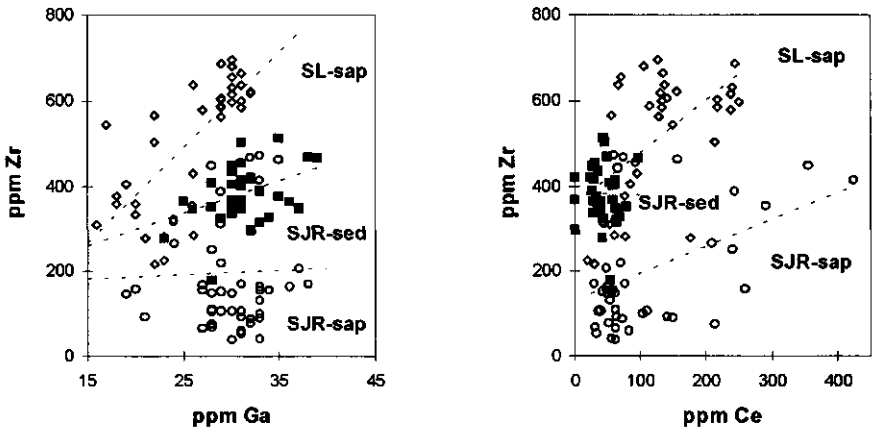

Figure 2.9: Scatterplots of trace elements that characterize almost uniquely one factor: **(a)** Zr (factor 2) versus Ga (factor 1), and **(b)** Zr (factor 2) versus Ce (factor 3).

CONCLUSIONS

By integrating mineralogy, micromorphology, and factor analysis a good compromise between qualitative/semiquantitative and quantitative methods in explaining the differences in origin and soil formation circumstances between the studied soil sequences was reached.

The mineralogical composition of all materials indicates a high degree of weathering and homogenization, which is characteristic for Oxisols in the humid tropics. Kaolinite and iron oxides are ubiquitous in all materials. They are usually accompanied by gibbsite in soils, and micas in subsoils. Kaolinites are formed by different processes in saprolites and soils, resulting in different morphology, size, degree of disorder, and chemical composition between the end-members. The presence of mica is restricted to soils of group SL-sap, and to a few sequences from groups SJR-sap and SJR-sed. The micas consist of muscovite-illite types and are altering to kaolinite, with an intermediate vermiculite/mixed layer clay mineral phase. In group SL-sap, the micas in the soils are protected against weathering by a thin iron oxide coating; also they contain relatively large amounts of Mg. Gibbsite in saprolites from group SJR-sap is early formed by relative accumulation, in a strongly leaching microenvironment. Absolute accumulation of gibbsite is observed in soils of groups SJR-sap and SL-sap, by the enrichment of the clay in gibbsite, and in soils and subsoils of group SJR-sed by the presence of crystalline

coatings and infillings. Ilmenite and tourmaline are accessory minerals found in all soils. Ilmenite is commonly altered to leucoxene, with anatase as a final product in the clay fraction. The mineralogical aspects together with the contents and proportions of major oxides found in the studied materials point to a general ferralitic weathering status. No further differences in major elements between the 3 groups were found.

Quantitative statistical (factor) analysis showed that 32% of the total variance of 14 elements is explained by one (ferralitic) weathering factor. A further 57% of the total variance was described by three factors mainly connected to differences in parent material and associated weathering processes. The analysis of element profiles and their explanation by each of the four factors, highlighted the differences between the materials, apart from weathering, and resulted in a fair separation between the 3 groups. The element pairs Al/Ga, Zr/Nb, and Ce/Nd are the most suitable elements to characterize differences between the materials.

3. MICROMORPHOLOGICAL ASPECTS OF A CATENA OF POLYGENETIC SOILS ON METAMORPHIC ROCKS IN MINAS GERAIS, BRAZIL

Cristine C. Muggler and Peter Buurman

Abstract

A representative catena of soils developed on metamorphic rocks in Minas Gerais, Brazil, was selected for the investigation on the genesis of yellow soils and red Oxisols in a rejuvenated landscape. Five profiles, starting from a red Oxisol at the summit and four yellow eroded Oxisols and Inceptisols downslope were studied. Besides chemical and mineralogical analyses, micromorphology was the most effective tool to unravel the polygenetic history of these soils. The actual parent material of the soils is saprolite which has undergone various phases of weathering. The preweathered saprolite consists essentially of kaolinite booklets and spherical micro-aggregates of hematite. The red Oxisol at the summit shows a complex granular microstructure which is more developed than the microstructure of the yellow slope soils. The red soil shows a circular striated b-fabric which is undifferentiated and random striated in the yellow soils. The microstructure, b-fabric and abundance of excremental infillings show that biological activity is the main process acting on the materials. The hematite 'droplets' are ubiquitously present, and are the main relicts of previous ferralitic weathering of the saprolites. Other main relicts are massive clayey granules and iron concretions. Most types of relicts are found in the red soils indicating that they do represent more than one evolutionary phase. The set of relicts present in the red and yellow soils point to the following evolution phases: 1) one (or more) soil formation phase(s) which produced yellow and/or red soils; 2) erosion and removal of the former soils, the relicts of them are embedded in the B horizon of the present red soil; 3) formation of red Oxisols; 4) landscape dissection and partial removal of the Oxisol cover, and; 5) new (subrecent) soil formation phase, forming the yellow soils observed downslope in the catena.

Keywords: Brazil; soil catena; polygenesis; micromorphology; relict features.

INTRODUCTION

The state of Minas Gerais, southeastern Brazil, presents a large diversity of natural environments and soils, many of which are related to long time geologically stabilized landscapes. In these areas soil development is influenced by a complex geomorphic history. Like many other areas in the humid tropics (Ollier, 1959; Stoops, 1989; Lichte, 1990; Stoops et al., 1994) the geomorphic evolution of the area is considered as a sequence of dissections and planations due to climatic changes, superposed on differences in lithology (Volkoff, 1985). The evolution comprises a number of unstable phases (truncation of soils and subsequent sedimentation on lower slopes) and stable phases (undisturbed soil formation), which resulted in soils of polygenetic nature. Stone lines are usually the clearest evidence of a polygenetic origin, although they are not always observed. In the studied area, the dominant Oxisols were

formed on preweathered materials, which were affected by erosion and landscape rejuvenation to different degrees. The latest rejuvenation phase resulted in a landscape with (remnants of) older soils at the summits, and younger soils developed on saprolites at the eroded slopes. The present landscape suggests the presence of at least two phases of soil formation represented by the (relict) red and the (recent) yellow soils. In such environments, the continuous reworking of the materials does not change much their physico-chemical properties, but rather their organization (Stoops, 1991), granting soil (micro)morphology a key role in the interpretation of the past and present soil processes (Bouma et al., 1990; Stoops et al., 1990; Bronger et al., 1994; Pereira and Fitzpatrick, 1995). Also, the lack of a characteristic parent rock, because of extremely deep weathering and intense homogenization makes the genetic study of such soil-saprolite sequences very difficult, so that commonly used chemical mass balances and weathering indexes are not suitable. Aiming a better understanding of the past and present soil processes, a typical catena of soils developed on deeply weathered metamorphic rocks was studied, and micromorphology was used to unravel the evolution of the soils in this combination of rock type and landscape.

MATERIAL AND METHODS

The area selected for the study is located in the southern part of the state of Minas Gerais, between 21 and 22°S and 44 and 45°W, near the town of São João del Rei. The predominant lithologies are fine- and medium-textured metamorphic rocks (phyllites and schists). The climate is a Tropical Highland climate, with an annual average temperature of 19-20°C, an annual average precipitation of 1400 mm, and 4 to 6 dry months. The topography is undulating to rolling with altitudes of 900-1100 m. The original vegetation is *cerrado* and *campo cerrado* (savanna-like and sparse savanna-like vegetation). The soils have an oxic character, and are classified as Oxisols or Inceptisols depending mainly on the thickness of the solum. One representative catena was selected and five profiles were sampled and described, starting from a deep red soil at the summit and four yellow shallower soils downslope. The profile descriptions, made according to FAO (1990), are summarized in Table 3.1. Undisturbed samples of the soils were collected and thin sections of 7x7 cm were prepared for micromorphological analyses. Micromorphological descriptions were made according the guidelines and terminology of Bullock et al., 1985. Selected features were studied with a Scanning Electron Microscope (SEM) equipped with a 9900 Energy Dispersive X-ray analyzer (EDAX).

RESULTS

General field aspects

The situation of the described profiles along the catena is given in Figure 3.1. The local land use is native pasture and occasional maize crops. At the time of sampling, the area around profiles P2, P4 and P5 was cultivated with maize. The pasture shows an increasing degradation downslope, due to soil erosion. Sheet erosion is moderate in P1, and severe in the other profiles; surface sealing was observed in P2 and P3. Based on the field descriptions and routine chemical data (Table 3.1; Appendix 1) the soils were classified as Anionic Acrudox (P1 and P2), Inceptic Hapludox (P3 and P4), and Udoxic Dystropept (P5) (Soil Survey Staff, 1994). Profiles P1 and P2, which have a similar chemistry, but are very different in terms of colour, structure and depth of the pedon, ended up in the same classification subgroup. This seems illogical, showing that the subdivision criteria are not yet fully adequate for description of the diversity of oxic materials. Profiles P2, P3, P4 and P5 are very similar, but differ in thickness of the solum, which decreases from P2 to P5, making them transitional between Oxisols and Inceptisols. Profile P1, situated at the top of the slope, is the deepest soil of the sequence and has red colours with slight yellowing at surface. Downslope, the soils become yellower and shallower. In the following text, the soils will be considered as two groups which are different in colour, structure and other properties: the group of *red* soils (here containing only profile P1), and the group of *yellow* soils (profiles P2, P3, P4 and P5).

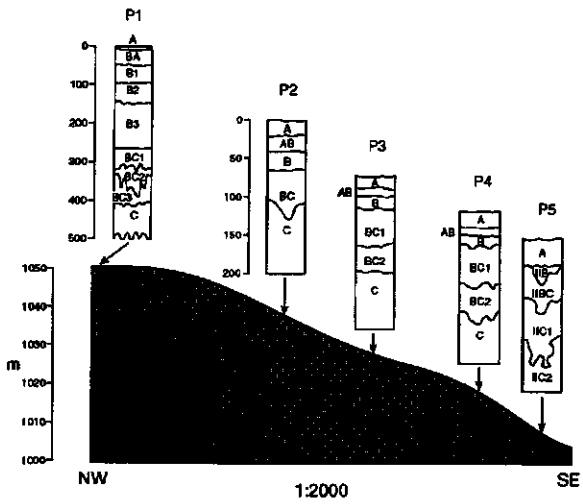

Figure 3.1: Situation and schematic representation of the sampled profiles in the studied toposequence.

Table 3.1: Summarized profile descriptions of the catena soils.

Profile	horizon	depth (cm)	colour	texture[1]	structure[2]		
Soil class					type	grade	size
	Ap	0-10	5YR 4/6	c	gra	mod	co
	BA	10-50	2.5YR 3/6	c	sblo→gra	we/st	med/vf
	Bw1	50-95	2.5YR 4/8	c	sblo→gra	we/st	med/vf
P1	Bw2	95-150	10R 4/6	c	sblo→gra	we/st	med/vf
Anionic	Bw3	150-265	10R 4/6	c	sblo→gra	we/st	med/vf
Acrudox	BC1	265-320	2.5YR 4/6	sc	sblo	we	med/fi
	BC2	320-330/390	2.5YR 4/4	scl	sblo	we	med/fi
	BC3	330/390-410	2.5YR 4/6	scl	sblo/sap	we	med
	C	410-550+	-	s	sap	-	-
	Ap	0-20	7.5YR 4/4	c	sblo→gra	mod/we	med/vf
P2	AB	20-40	5YR 5/6	scl	sblo	mod	med
Anionic	Bw	40-65	5YR 5/8	sl	sblo	mod	med
Acrudox	BC	65-105/130	5YR 5/6	s	sblo	mod	med
	C	105/130-200+	5YR 5/8	s	sblo	we	med
	A	0-15	10YR 3/4	c	gra	st	co
P3	AB	15-25	7.5YR 4/4	c	sblo	mod	fi/med
Inceptic	Bw	25-42	7.5YR 5/8	c	sblo	mod	fi/med
Hapludox	BC1	42-90	5YR 5/8	scl	sblo	we	med
	BC2	90-125	2.5YR 4/6	s	sap	-	-
	C	125-170+	2.5YR 5/8	s	sap	-	-
	Ap	0-20	10YR 4/4	c	sblo→gra	mod/we	med/vf
P4	AB	20-30	7.5YR 4/4	c	sblo	st	med
Inceptic	Bw	30-42/50	7.5YR 4/4	c	sblo	we	med
Hapludox	BC1	42/50-90/100	5YR 5/8	scl	sap	-	-
	BC2	90/100-130/150	2.5YR 4/8	sl	sap	-	-
	C	130/150-200+	5YR 4/6	s	sap	-	-
	A	0-35	5YR 4/6	-	apedal	-	-
P5	Bw	35-35/65	7.5YR 5/6	c	sblo	we	med
Udoxic	BC	35/65-75/100	5YR 4/6	sl	sap/sblo	we	med
Dystropept	C1	75/100-130/170	2.5YR 3/6	s	sap	-	-
	C2	130/170-200+	5YR 4/6	s	sap	-	-

[1] c: clay; sc: silty clay; scl: silty clay loam; s: silt; sl: silt loam; [2] gra: granular; sblo: subangular blocky; sap: saprolitic; → breaking into; we: weak; mod: moderate; st: strong; co: coarse; med: medium; fi: fine; vf: very fine.

Macro and microstructure

The main aspects of the macrostructure are presented in Table 3.1. The complete profile descriptions and routine chemical data are given in Appendices 1 and 2. The B horizon of the red soil (P1) show a subangular blocky structure breaking into very fine granules. With

increasing amount of saprolitic material the structure becomes more massive in the BC and C horizons. The yellow soils show granular structures in the topsoils, subangular blocky structure in the B horizons, and are massive and apedal in the lower BC and C horizons. They show yellow and brown colours in the solum, reddening at depth with the increasing influence of saprolitic materials. Iron concretions occur in the AB, B and BC horizons of profiles P2 and P3. Profile P5 shows a colluvial apedal cover as topsoil.

Table 3.2: Micromorphological aspects of the catena soils.

Prof.	horiz.	microstructure[1]	coarse	c/f RDP	groundmass	
			%	porph. type[2]	nature [3]	b-fabric
	BA	complex/gra	5	open	bR dotted clay	random/circular striated
	Bw1	complex/gra, sblo	5	open	bR dotted clay	random/circular striated
	Bw2	complex/gra, sblo	5	open	R dotted clay	circular/grano striated
	Bw3	complex/gra, sblo	5	open	yR dotted clay	circular/grano striated
P1	BC1	complex/sblo, gra	5-10	double spaced	bR dotted clay/ silty clay	random/circular striated
	BC2	complex/sap, gra	40	close	silty clay	random striated
	BC3	complex/mas, gra and sap	50	close	silt	striated/ crystallitic
	C	sap	50/100	close/ enaulic	silt	crystallitic
	AB	complex/ sblo	8	open	bY dotted clay	random striated, undifferentiated,
P2	Bw	complex/sblo, cra, mas	6	open	bY dotted clay	random striated, undifferentiated
	C	intergrain channel, sap	>90	close/enaulic	silt	crystallitic
	Bw	complex/sblo, cha	8-10	open	bY dotted clay	random striated, undifferentiated
P3	BC1	complex/sblo, cra	8-10	open	bY dotted clay	random striated, undifferentiated
	BC2	complex/gra (pellets), sblo, cra/cha, mas	12	open/double spaced	bY dotted clay	random striated, stipple speckled
	Bw/	complex/sblo, gra	6	open	bY dotted clay	random striated,
P4	BC1	(pellets)				undifferentiated
	BC2	complex/sap cha, mas	50	single spaced	b silt	stipple speckled
	C	intergrain channel	>80	close	b silt	crystallitic
	Bw/BC	complex/gra, mas	10-12	open	bY dotted clay	random striated
P5	BC	intergrain channel	>80	close	b silt	stipple speckled
	C1	sap; intergrain channel	>80	close/enaulic	b silt	stipple speckled, crystallitic
	C2	intergrain channel; sap	>80	close/enaulic	b silt	stipple speckled, crystallitic

[1] gra: granular; sblo: subangular blocky; sap: saprolitic; mas: massive; cra: crack; cha: channel; [2] coarse/fine related distribution pattern of porphyric type; [3] b: brownish; y: yellowish; R: red; Y: yellow.

The red soil shows a complex microstructure (Table 3.2) composed of granules, subangular blocks (mainly consisting of welded granules), and channels with infillings in the solum. The lower BC and C horizons have a more massive, saprolitic structure, with fragments of overlying solum commonly mixed in the BC horizons, and frequent fissures and biopores. The yellow soils too, have a complex microstructure, composed mainly of subangular blocks and secondarily massive domains and channels with infillings, in the solum. The BC horizons show a transitional character with dominance of massive homogenized saprolitic material (microheterogeneous) and few subangular blocks, channels, chambers and cracks. The C horizons are saprolitic showing an intergrain channel microstructure. Saprolitic material with some preserved rock fabric is observed in deeper horizons of P1, P2 and P5. They are very similar in composition and structure, although the rock fabric is better preserved in P5.

Groundmass

The coarse/fine limit was chosen at 20 μm to allow a useful distinction of features in the groundmass. The related distribution pattern in the A and B and in some BC horizons of all profiles is of an open porphyric type (Table 3.2). In the BC and C horizons, it shifts from double spaced to close porphyric and enaulic types, depending on the amount of coarse kaolinite booklets in the groundmass. In the very homogeneous A and B horizons of all profiles the groundmass consists essentially of fine material characterized as dotted clay. The colour is red with common yellow and redder spots in P1, and yellow in the other soils. In the BC and C horizons of all soils the groundmass turns into an heterogeneous brownish silty network of kaolinite booklets, the fine material consisting only of brown flecks between the kaolinites. The b-fabric of the groundmass reflects the degree of homogenization of the materials. Thus, predominantly fine and homogeneous material as seen in the A and B horizons of the soils results in a random striated to undifferentiated b-fabric, circular striated in P1. Coarsening and increasing heterogeneity of the groundmass result in speckled and crystallitic b-fabrics as observed in the deeper horizons of the soils (Table 3.2).

Coarse material

Quartz dominates the coarse fraction in all materials, representing less than 10% of the whole soil mass. Quartz is most abundant in topsoils and saprolites, where it also shows a higher variability in sizes, although it is predominantly fine sand-sized. The grains are dominantly angular and subangular, with few subrounded grains observed in the top horizons. Most of the grains do not seem chemically weathered, but they are commonly fractured. The fractured grains are frequently infilled with limpid red and/or dotted yellow clay, so-called 'runiquartz', formed by plasma infusion (Eswaran et al., 1975). The red infillings are similar to the hematite spherical aggregates found in the saprolites and red soils, and the dotted yellow infillings are similar to the soil groundmass. Such a feature points to relict (Stoops, 1989) or in

situ weathering. Both types occur together in all materials with small differences in relative abundance.

Opaque minerals: Ilmenite is the most common opaque component (1-3%) in all materials, and is more abundant in the red soil. The sand-sized grains are subangular to subrounded, have smooth boundaries, and are frequently surrounded by oriented clay. In the yellow soils and deeper horizons of the red soil, the grains show a pellicular and dotted alteration to leucoxene (Figure 3.2a), an alteration product of Ti minerals. The leucoxene aggregates consist mainly of anatase, similar to the observation reported by Anand and Gilkes (1984a) for a lateritic layer in Australia. *Magnetite* and other magnetic minerals are present in very low amounts in all materials, but they are slightly more common in the red soil.

Kaolinite neoformed booklets and pseudomorphs after mica are usually silt-, sometimes sand-sized, with scattered or banded red and (more rarely) yellow iron droplets. They are the main components of the saprolitic materials (BC and C horizons of all soils) and sporadically appear in the A and B horizons.

Saprolite fragments occur in all A, B and BC horizons as moderate to strongly iron impregnated subrounded sand-sized grains (relicts similar to those described by Faure, 1987). They also appear as isolated spots of in situ saprolite with diffuse boundaries, or as excrements brought up from deeper layers due to biological activity. Saprolite fragments commonly fall apart into silt-sized kaolinite booklets.

Tourmaline is accessorily present in all profiles as fine sand- and few silt-sized grains. The grains appear unweathered, or very fractured (in some cases filled with hematite), and few consist of fibrous aggregates.

Relicts

Relicts appear as coarse and fine material in the groundmass. They do not have relation with the present soil processes, and are inherited from the parent material or previous existing soils (Stoops, 1989; Bronger et al., 1994). They may belong to the original parent rock or may have been formed in one of the various polygenetic phases. Six types of relicts were recognized; they are labelled A to F and are described below.

A- *Iron (hematite) spherical aggregates or 'droplets'* (Hamilton, 1964): They are a prominent feature ubiquitously present in the studied catena. They appear as tiny clay- and silt-sized droplets, black under plane polarized light, and bright red under cross polarized light (Figure 5.1a, chapter 5). They are much more abundant in the saprolite and saprolitized materials than in the overlying horizons of the soils. In the saprolites the droplets occur both in bands related to the original rock fabric and scattered in ghosts of weathered minerals. With the reddening of the material, as observed in the red topsoil, their amount decreases. In the yellow topsoils they are few and are randomly mixed in the fine material of the groundmass. The decrease of the amount of droplets towards the topsoils is due to one or more of the following processes: gradual mixing and size reduction, dissolution and neoformation, and

coalescence into aggregates or strongly impregnated nodules.

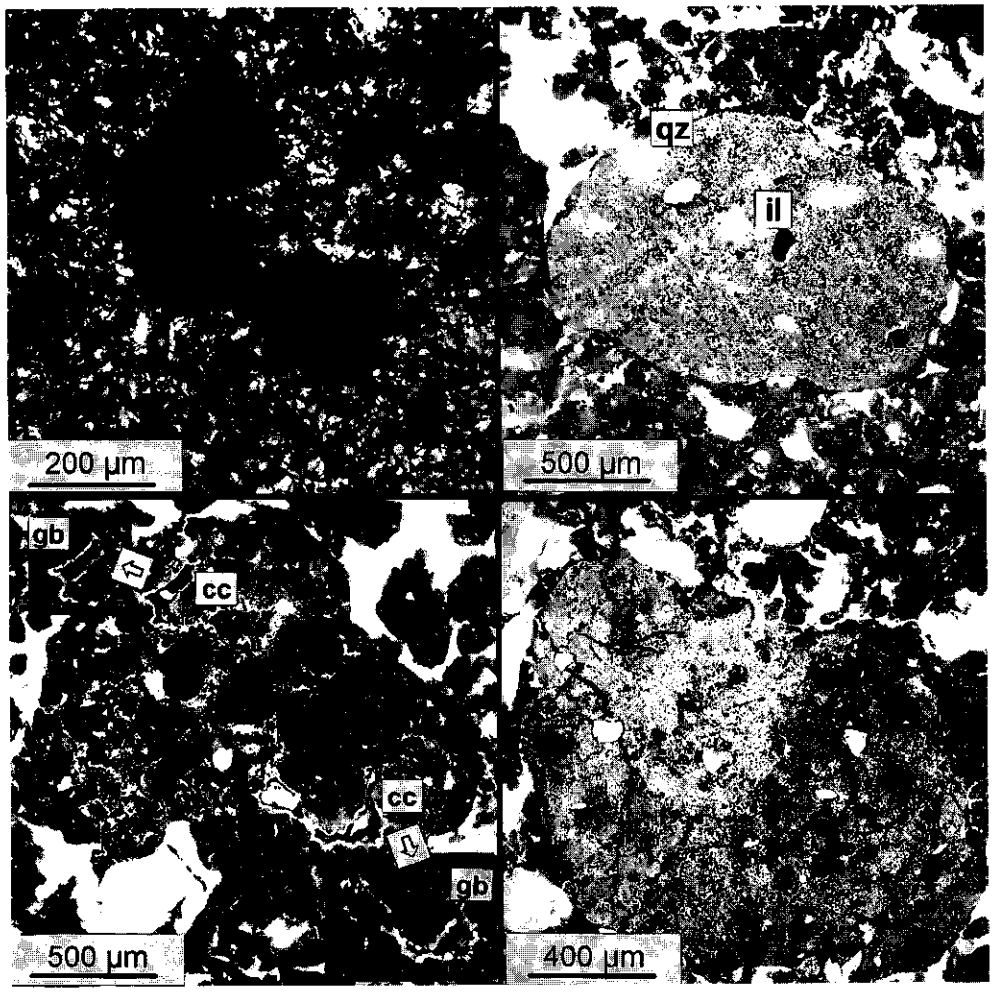

Figure 3.2: (**a**) weathered grain of ilmenite showing pellicular and dotted alteration to anatase (XPL); relicts observed in the soils (PPL): (**b**) B-type; qz: quartz, il: ilmenite; (**c**) C-type with details (XPL) of juxtaposed red clay (cc) and gibbsite (gb) coatings; (**d**) E-type.

B- *Brownish yellow massive clayey granules:* Subrounded to well rounded sand-sized grains, they are relicts of a former homogeneous groundmass. They are massive, have smooth boundaries and a groundmass consisting of dotted yellow clay with inclusions of quartz and ilmenite, showing an undifferentiated b-fabric (Figures 3.2b and 3.3). Phytoliths are observed in some granules, indicating they were part of a topsoil. The granules are usually surrounded by oriented clay, and sometimes by a redder clay accumulation. The general aspect of their groundmass is very similar to that of the present soil, especially to that of the yellow soils.

However, the clear smooth boundaries, the differences in colour, porosity, b-fabric, and their lower content of hematite droplets allow to distinguish them as individual units. They are very common in the B horizon of the red soil (P1) and scarce in the B horizon of P2.

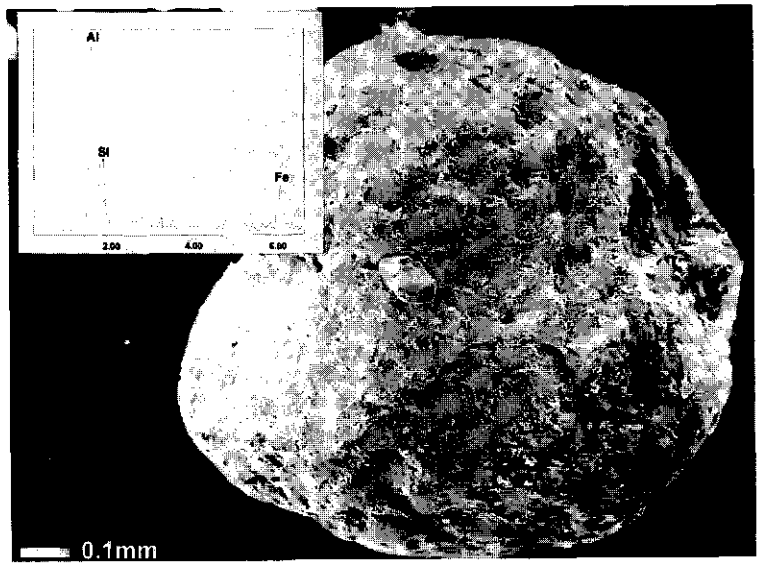

Figure 3.3: Scanning electron microphotograph and EDAX analyses of a hand-picked grain of B-type relict; qz: quartz grains.

C- *Pale red heterogeneous clayey granules* (Figure 3.2c): They consist of subrounded or irregular sand-sized grains with smooth boundaries. They are fragments of a groundmass composed of welded granules with inter- and intra-granule coatings and infillings of red dusty moderately oriented clay, and coatings of crystalline gibbsite. The two kinds of coatings occur occasionally juxtaposed. When juxtaposed, the gibbsite is covered by the red clay coatings. Also inclusions of quartz, ilmenite and hematite spherical aggregates are present. They are similar to the material commonly seen in the upper part of the pedoplasmation zone of oxic materials (Stoops, 1996; pers. com.). These features are observed in the A, B (more abundant) and BC1 horizons of the red soil.

D- *Red massive clayey units:* Usually rounded/subrounded, they appear as a weak to strong impregnation of the groundmass, showing smooth boundaries and a more undifferentiated b-fabric. They are commonly surrounded by oriented clay, and some are redder near the borders. Although their groundmass is very similar to that of the soil, they are clearly distinct and are considered relicts of a former homogenized soil material. This type is observed in the A, B and BC horizons of the red soil.

E- *Yellow and yellowish red limpid granules and fragments:* The granules are subrounded, sand-sized, rather massive and homogeneous in composition, showing quartz and

opaque inclusions, but not spherical aggregates of hematite, which result in a limpid yellow fine material (Figure 3.2d). Hematite hypocoatings are observed related to cracks and pores in the granule. The fragments are irregular and sand- or silt-sized. They consist of goethite and appear to be pseudomorphs after an unidentified former mineral, and/or remnants of pore infillings from the former saprolite. They are observed in all materials, more commonly in the A and B horizons of the yellow soils.

F- *Iron concretions*: Very coarse rounded or fragmented red units of hardened impregnated saprolitic materials. They may be remnants of petroplinthite layers. They are observed in the B horizons of the yellow soils P2 and P3.

Pedofeatures

Infillings of excremental type are very common in all soils and saprolitic materials. They reflect the intense biological activity in these soils. Usually they are loose continuous in soils, and dense in saprolitic materials, appearing as bow-like (striotubules) and crescentic features. Passage features (compacted zones around voids and channels) are also very common, although not always clear, due to loss of contrast with the groundmass. The mixing of the infillings in the groundmass by intense bioturbation results in a granular microstructure which is actually of excremental origin.

Very few *clay coatings* related to grains and nodules are observed. These are unlikely due to illuviation or precipitation, but due to stronger orientation of clay caused by pedoturbation, resulting in a circular and granostriated b-fabric. Such features have been observed in Oxisols elsewhere too (Embrechts and Stoops, 1987; Faure, 1987). *Fragments* of clay coatings are observed in the red topsoil. *Iron-impregnated hypocoatings and coatings* related to voids and fissures are occasionally observed in saprolitic layers of all soils. *Depletion hypocoatings* more or less related to voids (actually bleached areas) are observed in the surface horizons of the red soil.

Discussion

Macro- and micromophologically the soil profiles can be separated in two groups based on the colour and structure of the B horizon. The red soil of the summit (P1) constitute one group, and the yellow shallower soils on the slope (P2 to P5), all rather similar, constitute the other group. The parent material of all profiles is the same preweathered and ferralitized saprolite characterised by a network of booklets of neoformed and pseudomorphic kaolinite after mica, dotted by hematite 'droplets'.

The structure development together with the type, composition (colour) and homogeneity (b-fabric) of the groundmass can be used for a general characterization of the evolution stage of the soil and saprolitic materials. The development grade of the structural

elements and amount of pore space is clearly higher in the B horizon of the red soil, which shows a strong granular microstructure, locally coalescing into blocks by welding. In the yellow soils, the groundmass of the B and BC is homogeneously yellow, contrasting with the red spotted groundmass of the A, B, and BC1 horizons in the red soil. The different colours are ascribed to the dominance of goethite in the yellow soils, or to hematite in the red soils. The dominance of either goethite or hematite among the iron oxides present in the soils, is related to the different evolution undergone by the red and yellow soils. The red soils appear to have been continuously exposed and less eroded than the yellow soils. The yellow soils, on the other hand, developed from the saprolites or subsoil layers from eroded soils under (sub)recent pedogenesis.

The microstructure shows that biological mixing is the main process acting on the materials, most intensively in top horizons (regardless of composition and weathering stage) but also in saprolites. The micromorphological aspects that point to increasing soil development from the preweathered saprolite are: (a) clay formation (comminution and dissolution of the silt- and sand-sized kaolinite booklets, as well as neoformation of clay minerals); (b) increase of individualized structural elements (with decrease of their size) and porosity; (c) weakening of the b-fabric from crystallitic towards random striated and undifferentiated; and (d) uniform reddish or yellowish colouring of the materials, which is typical of oxic materials (Stoops et al., 1994). The higher amount and smaller size of the structural units and the moderate to strongly developed circular b-fabric suggest a longer evolution of the red soil. The circular striated b-fabric results from successive welding and separation of granules caused by bioturbation over long time. Excremental infillings, frequently mixed in the groundmass by pedoturbation, are very common in all soils, stressing the intense biological activity in recent and previous soil formation phases.

Different types of relicts are present in the soil. Types B, C and D are observed almost exclusively in the red soil. The B and D relict types are very homogeneous and might be remnants of former yellow and red topsoils. Despite their similar groundmass, no gradation between them was observed, indicating different soils or soil formation phases. Since the yellow soils presently observed in the area are situated on slopes, the B-type relicts are part of a former very homogenized soil, that was eroded and mostly removed by landscape processes. The same might be valid for the D-type relicts. The C-type relicts are remnants of a former pedoplasmation process in the P1 sequence probably related to the Oxisol formation phase.

In the literature about micromorphology of tropical soils, two features are repeatedly mentioned as evidence of preweathered and polygenetic materials: runiquartz (Eswaran et al., 1975) and plinthitic hematite (Schmidt-Lorenz, 1980). The latter corresponds to the hematite spherical aggregates here observed. These features have been observed in Oxisols from Africa, where they are usually related to plinthite formation (Ollier, 1959; Miedema et al., 1987; Muller and Bocquier, 1987; Stoops, 1989; Stoops et al., 1994). In the studied catena, however, no evidence of (petro)plinthite was observed. Few concretions (F-type relicts) are

found in the B horizons of profiles P2 and P3. Their presence in the yellow soils indicate that (petro)plinthitization in the saprolite may have occurred in the part of the saprolite exposed between P1 and the lower profiles, or after the Oxisol formation phase. The hematite, showing a 'droplet' morphology, seems to have been crystallized in this form already in the deepest saprolite. The red infillings of some runiquartz consists of the same kind of hematite, suggesting that both features have the same origin, and result from former ferralitic weathering phases which gave origin to the present saprolite, and are not necessarily related to plinthite formation.

CONCLUSIONS

The yellow and shallow soils occurring downslope have developed on in-situ saprolite and former subsoil layers of eroded soils. They have been formed under recent soil forming conditions, which are also affecting the red soils as shown by the yellowing of their topsoil. The yellow soils lack most of the relict features that are found in the red soil. The red soils, which dominate the remnants of the present landscape, do represent more than one pedogenetic phase. The relicts found in these soils point to the following phases of formation:

1. One (or more) soil formation phase(s) which produced yellow and/or red soils;
2. Dismantling of the landscape, erosion and removal of the former soils, the relicts of them are embedded in the B horizon of the present red soils;
3. A ferralitization phase, which originated the red Oxisols;
4. Landscape dissection and erosion of part of the Oxisol cover;
5. Subrecent pedogenesis giving origin to the yellow soils observed downslope in the catena.

The evolutionary history interpreted for the studied catena can be assumed for other catenas of red and yellow soils that are commonly observed in the area.

4. EROSION, SEDIMENTATION AND PEDOGENESIS IN POLYGENETIC OXISOL SEQUENCES FROM MINAS GERAIS, BRAZIL

Cristine C. Muggler and Peter Buurman

Abstract

The geomorphic evolution of the southeastern Brazilian landscape is influenced by climatic changes and tectonic activity. Soils developed on the resulting surfaces are mainly deep polygenetic Oxisols. The combination of stable landscapes (with continuously exposed soils), and neo-Cenozoic graben zones (filled with sediments that may have undergone soil formation), offers the possibility to unravel the history of the soils that are found at the present day surface. Soil-sediment sequences in the southern part of the state of Minas Gerais, Brazil were investigated by micromorphology and mineralogy in order to understand the polygenesis of the soils. Weathering, biological activity, clay accumulation and iron translocation are the main soil formation processes imprinted in the various pedosedimentary layers. Strong weathering is shown by dissolution of quartz and weathering of ilmenite. Bioturbation is ubiquitous even in older and deeper buried layers. Clay accumulation is observed as illuviation and precipitation features which were micromorphologically differentiated. Accumulation and movement of iron are represented by gley and pseudogley features, related to groundwater and surface-water saturation processes. These features combined with the layering of sediments and soils allowed the interpretation of the evolution undergone by the soils and sediments. As main soil formation phases, the graben fillings show two phases of clay formation and illuviation, separated by a phase of ferralitization. The whole was eventually overprinted by a phase of ferralitization and plinthite formation. These processes also acted on the soils of the stable areas (not affected by tectonic activity), but overprinting and erosion does not allow recognition of the separate evolution phases.

Keywords: Brazil; Oxisols; paleosols; polygenetic soils; micromorphology.

INTRODUCTION

The geomorphic evolution of the southeastern Brazilian landscape, is considered to be due to climatic changes (Volkoff, 1985) coupled with tectonic activity (Saadi, 1993), superposed on differences in lithology. Two main erosional cycles and the resulting surfaces are recognized: *Sulamericana* and *Velhas* (King, 1957; Braun, 1970). The large Tertiary *Sulamericana* surface was considerably dismantled by subsequent erosive cycles, presently remaining in the Brazilian Central Plateau and in smaller plateaus all over the country (Pedro and Volkoff, 1984). The *Velhas* surface is related to an erosive cycle less extensive than the first, dated to Late Tertiary and Early Quaternary (Plio-Pleistocene; Braun, 1970). Besides these morphoclimatic features, localized tectonic activity throughout Tertiary and Quaternary produced morphotectonic features by disruption and rebuilding of the landscape (Hasui, 1990).

Soils occurring on this landscape are mainly deep Oxisols (Ferralsols). Because of the extremely long periods of soil formation, and the different climates that have been operative in the past, such soils are polygenetic. Separation of the various phases of soil formation is hardly possible, although evidence of such phases may be abundant in the soil profile. The combination of stable surfaces -with continuously exposed soils-, and neo-Cenozoic graben zones -episodically filled with sediments (during periods of reactivation and increased erosion) and affected by soil formation (in tectonically stable periods)- may help to unravel the condensed history of the soils that are found at the present day surface. Therefore, a representative soil-sediment sequence from a neo-Cenozoic graben zone was investigated with the objective of reconstruct the evolution of the polygenetic soils related to a Tertiary landscape, in Minas Gerais, Brazil.

MATERIAL AND METHODS

The study area is depicted in Figure 4.1. It is located in the southern part of the state of Minas Gerais, near the town of São João del Rei. The area has an undulating to rolling topography (900-1100 m asl) with levelled small plateaus, that are remnants of the *Sulamericana* surface. Recent studies showed the influence of neo-Cenozoic tectonic processes in the morphogenesis of the area (Saadi, 1991). These processes resulted in the formation of rift systems, tectonically controlled (graben) fillings, and uplifts (Saadi, 1990). They are comprised between the Pliocene and the whole Quaternary (Saadi, pers. com., 1994). The landscape is dominated by more or less eroded Oxisols, developed on fine- and medium-textured metamorphic rocks (phyllites and fine schists) of Archean and Proterozoic age.

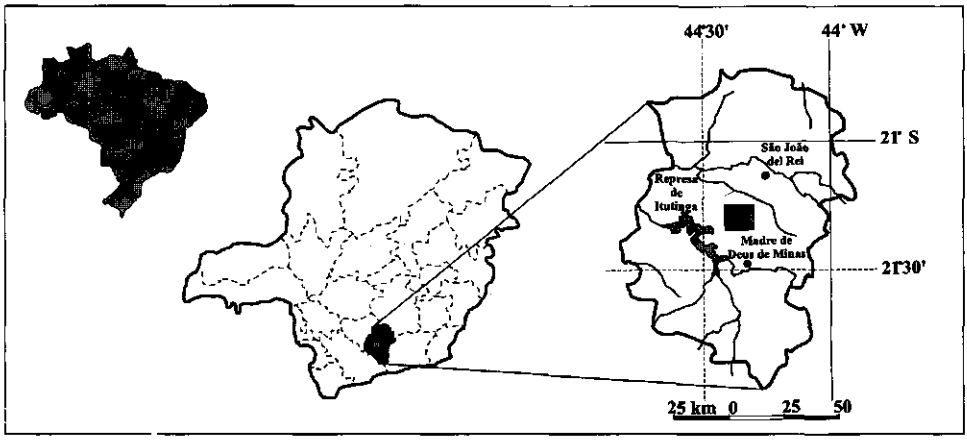

Figure 4.1: Location of the studied area in the state of Minas Gerais, Brazil.

In the field, areas affected and not affected by neo-Cenozoic tectonics, here called 'unstable' and 'stable' areas, were distinguished. 'Stable' areas usually present deep and red soils at the

summits, and yellow and shallower eroded soils on the slopes. 'Unstable' areas, which consist of graben fillings, show entirely red soil-sedimentary sequences. The sediments consist of remobilized soil and saprolite materials from higher landscape positions. After deposition, the layers were more or less affected by pedogenesis and tectonic activity. Despite their inherent variability, such graben fillings have many common characteristics, and a representative section was sampled for this study (Figure 4.2).

The soils were described in the field according to FAO guidelines (FAO, 1990). Routine textural and chemical analyses, XRF analyses of major oxides and trace elements, and mineralogy of the clay fraction were carried out according to Buurman et al. (1996). Thin sections of 7x7 cm of undisturbed soil samples were prepared for micromorphological analyses. This paper focuses on the micromorphological and mineralogical aspects of the studied materials.

RESULTS

The main macromorphological aspects of the sequence are illustrated in Figure 4.2. The sequence consists of a predominantly red to dark red material, with abundant signs of pedoturbation: it is intensely spotted by yellow to white mottles in the layers I, III and the top of II. The mottles, likely related to burrowing, show sizes up to 12 cm Ø, and consist of irregularly shaped patches, partially to completely devoid of iron compounds. The top of the sequence consists of remnants of an eroded Oxisol.

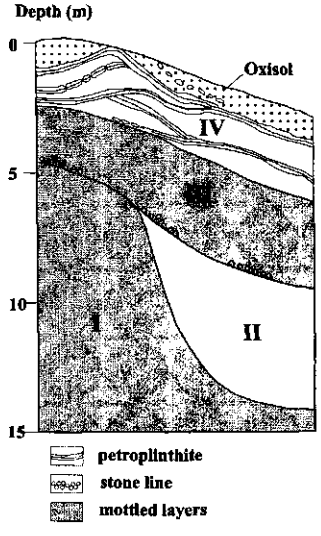

Oxisol: 0-0/80 cm; Yellowish red (5YR 4/6) to red (2.5YR 4/6; 10R 4/6) clay; strong very fine to fine granular structure; many fine and very fine pores; friable; many medium and fine roots; abrupt and wavy boundary;
layer IV: 0/80-175/380 cm; Red (7.5R 4/6; 10R 4/6) clay, strong medium angular blocky to massive structure; many fine and very fine pores; hard to very hard and firm; few to common rounded bleached root channels up to 2 cm Ø; abrupt and wavy boundary; presence of many red (10R 4/6) and dusky red (10R 3/2) petroplinthite layers 1 to 20 cm thick commonly layered and discontinuous;
layer III: 175/380-550/800 cm; 60-70% of yellow (2.5Y 7/6) to brownish yellow (10YR 6/6) burrows up to 5 cm Ø in a dark red (2.5YR 3/6) to red (10R 4/6) clay matrix in the top layer; the bottom layer has about 30% of pale yellow (5Y 8/4) burrows in a red (10R 4/6) clay matrix; stone line at the lower boundary up to 10 cm thick, consisting mostly of coarse (up to 7 cm) quartz gravels;
layer II: 550/800-550/1290 cm; Dark red (10R 3/6) to red (10R 4/6) clay with few burrows penetrating from the overlying layer up to 1-2 m depth; randomly distributed gravels, mostly of quartz, and some yellow 'ocre' and greyish nodules; the layer shows a cross linear fracture pattern and slickensides;
layer I: 550/1290-2300+ cm; Red (10R 4/6) to dark red (10R 3/6) and dusty red (10R 3/4) clay, intensely burrowed to the top (up to 90%); the burrows are brownish yellow (10YR 6/6), yellow (10YR 7/6), and pale yellow (2.5Y 7/4) to light gray (5Y 7/1) in the outer part; commonly they are red (2.5YR 5/8) in the inner part, and superimpose and obliterate almost all the yellow/grey ones.

Figure 4.2: Schematic sketch and field description of the studied graben filling (width of the section: 20m).

Characterization of the materials

General mineralogical and micromorphological aspects of the materials are summarized in Table 4.1. Layer IV consists of plinthite with hardened layers (petroplinthite), showing a massive homogeneous microstructure. Layer III shows a fragmentary microstructure with rounded clayey granules and various types of fragments of reworked soil material. Layers I and II show a massive channel and cracky microstructure with planar voids, and some recent and fossil channels. Fossil packing voids have cross linear section patterns that are likely related to tectonic activity. Layer II appears to have a compacted former granular structure, illustrated by a strong circular b-fabric. Coarse subrounded sand-sized fragments of the groundmass of layer I, embedded in the groundmass of the lower part of layer II, indicate an erosional reprise before deposition of layer II. Fragments of the underlying layers are also observed in the Oxisol and in layer III.

The groundmass of all layers consists of clay, which is moderately to highly birefringent, and shows an open porphyric related distribution pattern. The clay fraction in the whole sequence consists of kaolinite (dominant; >90%), hematite, and goethite. Gibbsite is found in the Oxisol; micas occur in layer I, and rarely in layers II and III. Coarse material consists of quartz (abundant), opaques (occasional), accessory minerals, and coarse fragments (rare). Quartz grains are mostly fine sand-sized, usually subangular and subrounded, occasionally rounded, indicating transport. Ilmenite is the dominant opaque mineral. Tourmaline and zircon are the main accessory minerals. Mica and/or kaolinite pseudomorphs after micas occur in the silt and fine sand fractions as lath shaped crystals and aggregates. Fragments of parent material, consisting mostly of an ilmenite phyllite, and iron impregnated saprolite are more or less frequent in the whole sequence.

Table 4.1: Main micromorphological and mineralogical aspects of the studied sequence.

Layer	Microstructure	Fine material			Coarse material[1]
		Nature	Composition[1]	B-fabric	
Oxisol	granular	dotted clay	Ka, Gt, Hm, Gb	undifferentiated, circular striated	3-7% Qz, Ilm, rare Mi/Ka pseudomorphs
IV	massive	limpid clay	Ka, Gt. Hm, Mi	random striated	10-20% Qz, Ilm, Ka, rock and saprolite fragments
III	massive, fragmentary	speckled clay	Ka, Gt, Hm, Mi	random and circular striated	10-15% Qz, Ilm, Ka, rock and saprolite fragments
II	massive, channel, cracky	dotted clay	Ka, Gt, Hm	circular and random striated	10-15% Qz, Ilm, Gb, Ka, rock fragments
I	massive, channel, cracky	dotted clay	Ka, Gt, Hm, Mi	random and granostriated	10-15% Qz, Ilm, Mi(Ka), rock fragments

[1] Ka: kaolinite; Gt: goethite; Hm: hematite; Gb: gibbsite; Mi: mica; Qz: quartz; Ilm: ilmenite.

Rounded and subrounded ferruginous coarse grains (up to 1 cm) and fragments, with a groundmass composed of predominantly yellow and red limpid to dusty clay, are observed in all materials (Figure 4.3a). They show abundant quartz inclusions, frequent oriented clay in situ and in fragments, common iron impregnation, and occasional kaolinitic saprolite fragments. These ferruginous fragments appear to be allochtonous, unrelated to any layer of the described sequence, thus considered as pedorelicts. In the following text, such fragments will be called "ferruginous pedorelicts".

Mineral weathering

In the studied materials, quartz grains commonly show signs of dissolution at their margins. They are smaller than the angular space in which they are contained, suggesting the voids surrounding them were produced by mineral dissolution. In some samples, an aureole of gibbsite crystals is observed around the quartz grains (Figure 4.3b), indicating that quartz may have been pseudomorphically replaced by gibbsite (Merino et al., 1993). Usually this gibbsite aureole is not observed, suggesting that it was removed by further dissolution and/or during sample preparation. No such signs of quartz dissolution were observed in the Oxisol, although quartz grains may show corroded borders. Occasionally, infillings of limpid or dusty yellow and red clay in internal fractures ('runiquartz' after Eswaran et al., 1975), as well as internal weathering are observed in coarser quartz grains of layers III and IV.

Ilmenite shows a dotted and/or complex alteration pattern to leucoxene and anatase, and is commonly surrounded by an external depletion hypocoating (Figure 4.3c). Tourmaline grains appear fractured, and some show dissolved borders with partial replacement by iron oxides. Zircon grains also show signs of weathering, although they are usually unweathered.

Bioturbation

Biological pedofeatures related to burrowing, consist of excremental loose infillings, passage, and crescentic features. They are more or less commonly observed in all samples, indicating active bioturbation on all layers. Small (up to 50 μm Ø and 200 μm length) fabric crescentic features are commonly observed in layer IV, and occasionally in bleached parts in top of layer III (Figure 4.3d). The moderate to high birefringence of the clayey groundmass of layers I, II and III indicates considerable reworking of the material, likely due to bioturbation. The abundant iron-depleted mottles observed in layer I, top of II, and III, are related to previous burrowing and/or rooting that allowed preferential water movement.

In layer I, many red unsorted heterogeneous infillings are observed, mostly found in bleached parts. Some of the bleached parts were almost completely destroyed and infilled by reworked material. The infillings show strong granostriated b-fabric, and consist mainly of quartz (18-20% of total mass), fragments of undisturbed and bleached groundmass, and ferruginous

pedorelicts. Localized clay infillings and bleaching are often observed in the fragmentary infillings. These unsorted infillings are also observed in layer II, although less common and not necessarily related to bleached parts.

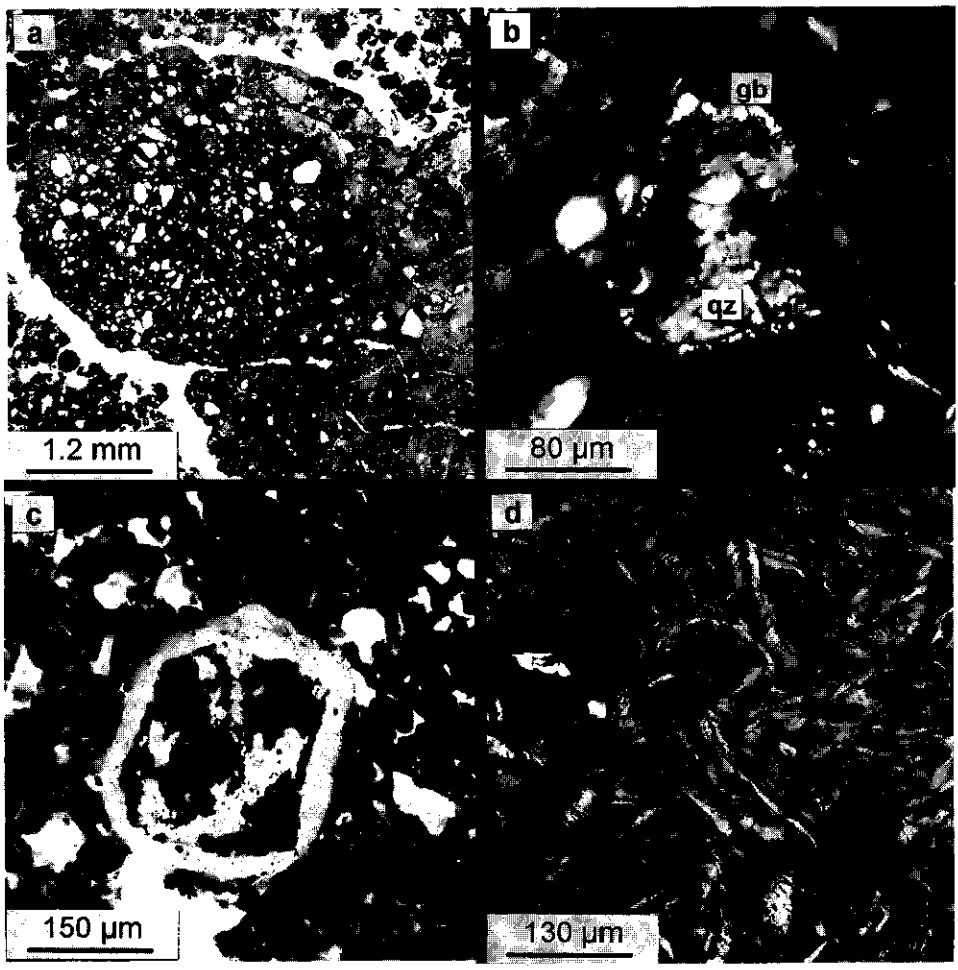

Figure 4.3: (**a**) Ferruginous pedorelict in the Oxisol, PPL; (**b**) Gibbsite (gb) aureole around quartz (qz) grain, layer III, XPL; (**c**) Weathered ilmenite grain with depletion external hypocoating, layer IV, PPL; (**d**) Fabric crescentic features in groundmass of layer IV, XPL.

Clay formation and movement

Pedofeatures related to formation and movement of clay occur with various aspects and abundance. Illuvial (I) and chemically precipitated (P) clay accumulations were distinguished on basis of the following main criteria: presence of textural layering (I); absence of textural

variations and general higher uniformity of the clay (P); and presence of gel-like surface if pores are not completely filled (P). Layering and/or microlamination were also the main criteria used by Feijtel et al. (1988) to distinguish illuvial from neoformed clay coatings. The main types are described below in chronological order. Figure 4.4 illustrates their occurrence and frequency.

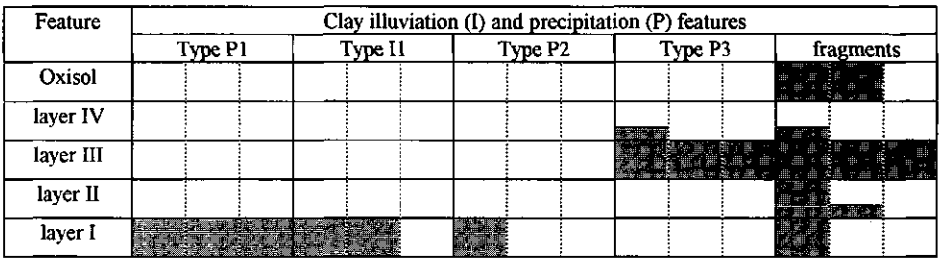

Figure 4.4: Occurrence and frequency of features (for description of types see text) related to clay formation and movement; (□) rare, (□□) occasional, and (□□□) many, as used in Bullock et al, 1985; abundant and very abundant are not included. Partial filling of a cell refers to the presence of a feature in the bottom, middle, or top of the layer.

Type P1: Brownish red microlaminated oriented clay coatings (Figure 4.5a). They are characteristic of layer I. Commonly they show a cross linear section pattern following the void's shape. The inner parts of these coatings are sometimes grainy, indicative of weathering.

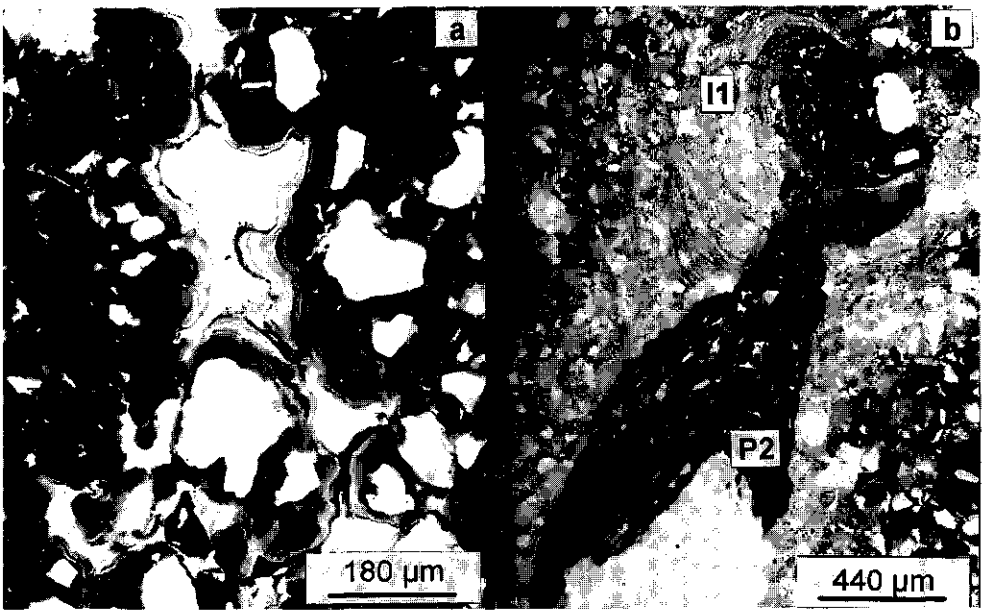

Figure 4.5. (**a**) Clay accumulation of type P1, layer I, PPL; (**b**) Clay accumulations of type P2 juxtaposed to type I1 in iron-depleted part of layer I, PPL.

Type I1: Brownish, reddish, and yellowish red, partially oriented impure clay infillings and coatings (Figure 4.5b). They are observed in layer I, mostly in the unsorted infillings, but thin ones also occur in the red matrix, juxtaposed to coatings of type P1. They occur mainly as infillings of variable thickness (up to 8 mm) and have different kinds of impurities (silt, small fragments of groundmass, and quartz grains). The thicker ones are frequently broken and reinfilled with reddish precipitated clay of type P2.

Type P2: Yellowish red and red, partially to poorly oriented dusty and limpid clay infillings. They are observed in layer I, related to channels present in unsorted heterogeneous infillings, and have irregular shapes and thickness. They follow localized bleaching in the fragmentary infillings, since they fill voids with bleached coatings of type I1 (Figure 4.5b).

Type P3: Brownish red, poorly and not oriented, dusty clay coatings and infillings (Figure 4.6a). They occur in layer III and bottom of layer IV, as well as fragments of them mixed in the groundmass. They are irregular and discontinuous, and thicken to dense discontinuous infillings; frequently they are broken and/or weathered (are grainy and show low birefringence).

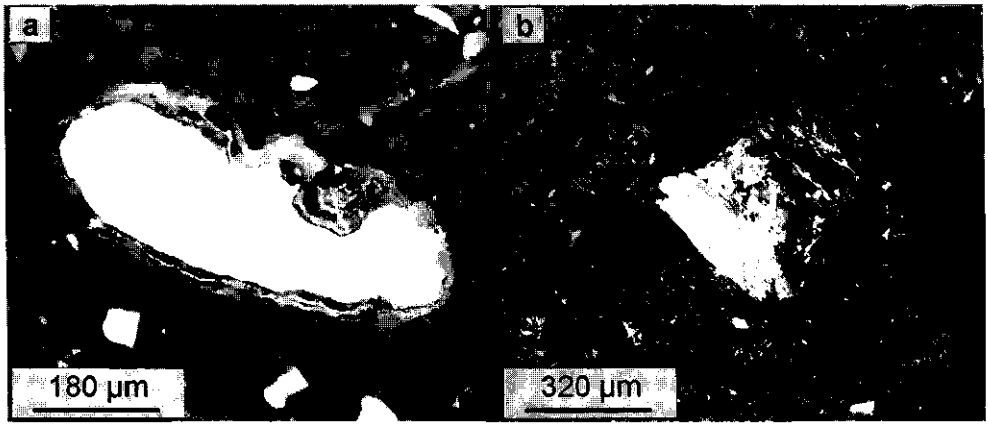

Figure 4.6: (**a**) Clay accumulation of type P3 in layer III, PPL; (**b**) Fragment of yellow precipitated clay accumulation in Oxisol, XPL.

Fragments of oriented clay are of two types: a) unrelated to the sequence, and b) products of reworking of the materials from the sequence. The first comprise yellow dusty and limpid oriented clay fragments (Figure 4.6b), which are ubiquituously present, although more abundant in layer III. They have a distinct yellow colour, bright yellow under cross polarizers. The fragments are subrounded or rounded and can be very coarse (up to 1 mm). Some appear in the ferruginous pedorelicts. They appear to be remnants of precipitated clay accumulations. The second type occurs sporadically above layer I. In layer II, they are brownish red and partially weathered, and oriented clay domains are observed. These oriented clay domains look like assimilation of clay

coatings and/or fragments of them into the matrix (Fitzpatrick, 1984).

Iron translocation features

Pedofeatures related to redistribution of iron are a major aspect in the whole sequence. They consist of overprinted gley and pseudogley features representing episodes of groundwater and surface water saturation as described by Bouma et al. (1990). They are related to a climate with contrasting dry and wet seasons. Figure 4.7 depicts the occurrence and frequency of the main types of iron accumulation (A) and depletion features which are described and interpreted in terms of gley and pseudogley processes, according to the criteria used by PiPujol and Buurman (1994). Gley features appear as iron accumulations (precipitation) in bleached and not bleached parts. Pseudogley features are mainly related to channels and/or burrows and consist mostly of bleaching, although some iron accumulations in the transition zone are also of pseudogley origin.

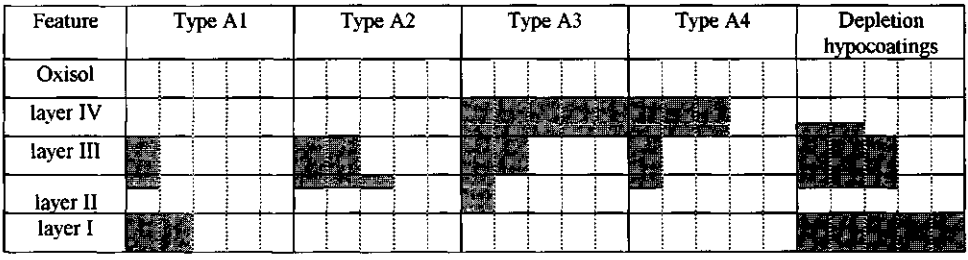

Figure 4.7: Occurrence and frequency of features (for description of types see text) related to iron mobilization and translocation; (□) rare, (□□) occasional, (□□□) many, (□□□□) abundant, and (□□□□□) very abundant, as used in Bullock et al, 1985. Partial filling of a cell refers to the presence of a feature in the bottom, middle, or top of the layer.

Type A1: Yellowish red hypo- and quasicoatings superimposed on clay coatings related to voids. They are observed in layers I, III, and top of II, mainly in iron depleted parts (Figure 4.8a). They appear to be related to the finer texture of the clay coatings, either iron was protected from removal, or dissolved iron present in water more strongly retained by the clay precipitated after further desiccation.

Type A2: Dotted red hypocoatings and impregnations, and yellow coatings and hypocoatings. They are observed in the strongest bleached parts in the top of layer II and layer III. The dotted red impregnations consist of discrete tiny (< 2 μm) hematite grains, and occur related to voids, aggregates, and grains, and impregnating large domains of the matrix as well (Figure 4.8b). The yellow coatings consist of goethite and occur related to voids and grains, sometimes covering the dotted red hypocoatings. Presence of either red and yellow colours are attributed to slight differences in water activity between microenvironments.

Type A3: Impregnative red hypocoatings with diffuse boundaries (Figure 4.8c). They are observed occasionally in the red matrix of layer II, in layer III, and are very common in layer IV. They are related to voids, cracks, and quartz grains, apparently to anything that interrupts the continuity of the groundmass. In layer IV they are frequently covered by yellow crystalline goethite coatings, and in the hardened part they appear as intercalations in the groundmass.

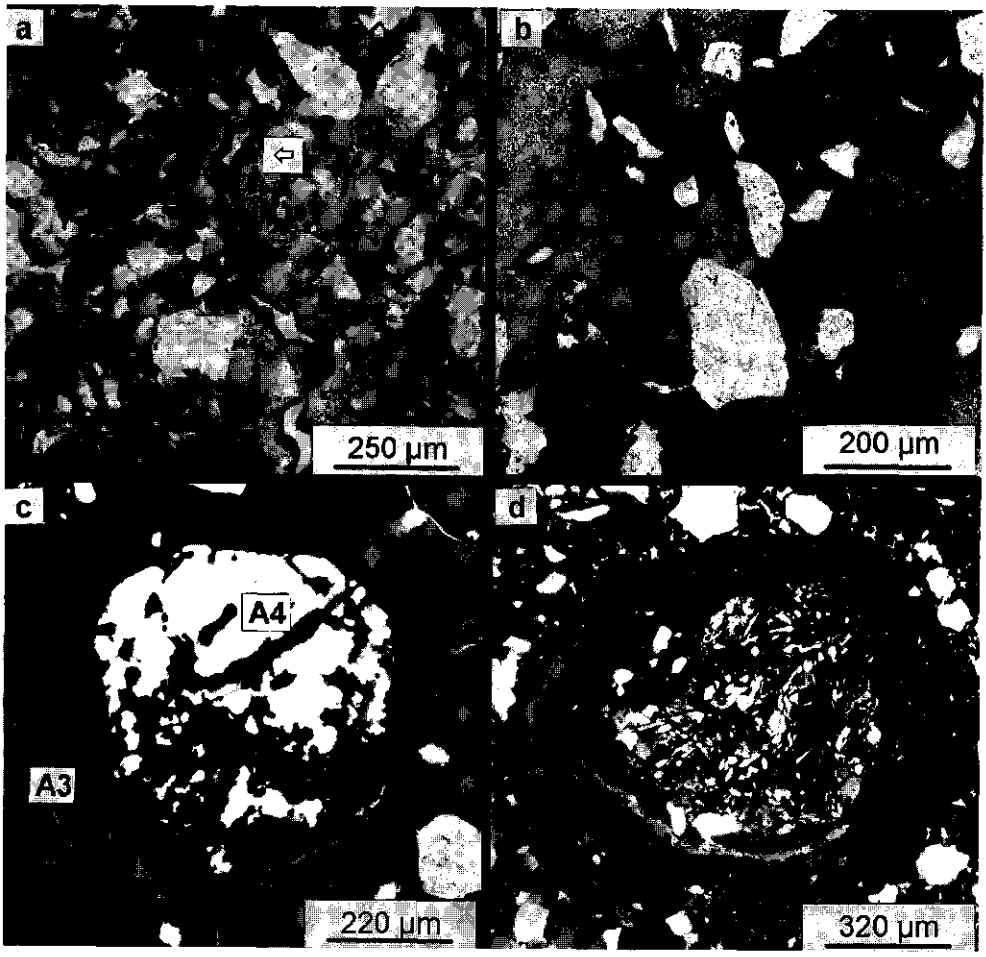

Figure 4.8: (a) Iron accumulation of type A1, layer I, PPL; (b) Iron accumulation of type A2 in iron depleted groundmass, top of layer II, PPL; (c) Iron accumulation of types A3 and A4, layer IV, PPL; (d) Nucleic concentric ferruginous nodule found in a fragment of layer I embedded in layer II, PPL.

Type A4: - Crystalline goethite coatings and infillings. They are common in layer IV (Figure 4.8c) where they frequently grow to fill a void, They are usually juxtaposed to A3

hypocoatings, and sometimes show juxtaposed thin gibbsite coatings. In layers II and III they are scarcely observed and are mostly related to larger channels in bleached parts.

Depletion pedofeatures consist of iron depletion hypocoatings *(albans)* related to recent or fossil voids, and are characteristic of pseudogley processes. They are common in layers I, II and III (Figures 4.3b, 4.5b, 4.8a, and 4.8b), being rather variable in thickness and colour, due to differences in intensity of iron removal related to stages of pseudogley development (PiPujol and Buurman, 1994). In layer I, they show diffuse boundaries, and are frequently disturbed by burrowing and related unsorted heterogeneous infillings. In layer II, they occur only at the top of the layer and have clear boundaries showing aureoles of tiny particles of hematite at the boundaries. There, they show a distinct colour zoning from the matrix towards the voids due to increasing removal of iron. In the grey parts, the b-fabric is much less differentiated (has lost its birefringence) than in the zones that are not iron-depleted, suggesting that it was affected by acid weathering related to ferrolysis (Brinkman, 1979). A new reddening is superimposed as particles of iron oxides are accumulating and coalescing in some parts (type A2 accumulations; Figure 4.8b), imparting a reddish grey colour to the matrix. In layer III, the depletion hypocoatings have diffuse boundaries, and contain red domains that were protected from bleaching. They also show an undifferentiated b-fabric, only speckled by occasional elongated silt-sized kaolinite crystals, indicating breakdown of clay.

Other iron accumulations consist of impregnative iron nodules, occasionally observed in the Oxisol, and of nucleic concentric ferruginous nodules (Figure 4.8d), observed in the top of layer I, and in related colluvial fragments at the bottom of layer II. This kind of nucleic concentric nodules is reported to occur in plinthite materials (Bullock et al, 1985). Both kinds of nodules are considered to be inherited from past pedogenetic processes.

Discussion: evolutionary history of the sequence

Source areas of the sediments are likely the same for all layers, because of the mineralogical similarity and weathering degree of the materials. This is suggested by the characteristics of the quartz grains and the assemblage of the accessory primary minerals present (ilmenite, turmaline and zircon). Ferruginous pedorelicts, fragments of precipitated clay, and ferruginous nodules found throughout the studied sequence, are relicts, since they are unrelated to any of the materials that compose the sequence. They indicate large erosional reprises as well as long soil formation periods. Their nature indicates that the former soils from which the graben filling was derived, were already strongly weathered (Stoops, 1989). Also the plinthitic nature of some of these fragments indicates previous existence of (petro)plinthites that were exposed by erosion in higher landscape positions, and completely eroded afterwards.

Weathering, biological activity, clay accumulation and iron translocation features are aspects that play key roles in the understanding of the processes undergone by sediments and soils in this kind of sequences (Buurman, 1980). Table 4.2 summarizes the processes

recognized in each layer of the studied sequence.

Table 4.2: Main processes and related features observed in the studied sequence.

LAYER	PROCESS	RELATED FEATURE
I	Clay accumulation (precipitation) phase I	Laminated oriented (compressed) dusty clay coatings
	Surface-water saturation	Depletion hypocoatings related to voids
	Burrowing of bleached channels	Matrix disruption and unsorted heterogeneous infillings
	Clay accumulation (illuviation) phase II	Poorly oriented impure (partially bleached and disturbed) clay infillings and coatings
	Groundwater saturation	Ferruginous hypo and quasicoatings related to voids
	Surface-water saturation	Localized depletion hypocoatings related to voids in burrowed parts
	Clay accumulation (precipitation) phase III	Limpid clay infillings juxtaposed to bleached phase II ones
II	Erosion and reworking of layer I	Fragments of layer I embedded in the groundmass of layer II
	Oxisol formation/ ferralitization	Circular striated b-fabric; compacted granular structure
	Rooting/burrowing	Matrix disruption and unsorted heterogeneous infillings
	Groundwater saturation processes	Ferruginous hypo and quasicoatings related to voids
	Surface-water saturation and clay weathering (ferrolysis)	Depletion hypocoatings and iron accumulation in the transition zone; undifferentiated b-fabric in grey parts
	Reprisal of tectonic activity; erosion and reworking of the materials	Voids with cross linear section shapes and bidirectional fracture system in layers I and II
III	Colluvium deposition	Fragmentary structure containing fragments from underlying layers
	Clay accumulation (precipitation) phase IV	Poorly and not oriented clay infillings and coatings
	Surface-water saturation and clay weathering (ferrolysis)	Depletion hypocoatings with undifferentiated b-fabric
IV	Deposition of a strongly weathered and well sorted sediment	Homogeneous and fine clayey groundmass (layer IV)
	Groundwater saturation; plinthite formation	Ferruginous hypocoatings and goethite accumulations related to voids (layers III and IV); plinthite and petroplinthite layers
	Biological activity (burrowing)	Fabric crescentic features (layers III and IV)
Oxisol	Pedo(bio)turbation/ Oxisol formation/ ferralitization	Strong fine granular structure; weathering of ilmenite
	Erosional reprise	Petroplinthite outcrops and shallow Oxisols

Layer I is a paleosol with illuvial and precipitated clay accumulations, where biological activity gave way to strong iron removal along channels (bleached areas up to 12 cm Ø) during surface-water saturation (pseudogley) episodes. Clay accumulations were also affected by iron depletion, although in some parts iron apparently was protected from removal, probably due to

the finer texture of the coatings. Next, burrowing produced unsorted heterogeneous infillings which contain also fragments of the previously bleached parts. Clay formation and illuviation resumed, since impure clay infillings are observed in the fragmentary infillings and in the matrix too. Localized iron removal and translocation, followed by clay precipitation is observed in the burrowed parts. The abundance of precipitated clay accumulations in this layer indicate a strong weathering environment in the upper part of the (eroded) soil.

Layer II appears to be a paleo-Oxisol, as shown by the remnants of a very fine granular structure and the complete absence of clay accumulations (Stoops and Buol, 1985). The bottom of the layer shows reworked material from the underlying layer indicating that the top of layer I is an eroded surface. Towards the top of the layer there is an increase of iron removal, clay weathering, and iron accumulation along voids, which indicate an overprinting of biological, pseudogley, and gley processes.

The discontinuous stone line that marks the boundary between layers III and II, indicates new erosion and deposition phases. The presence of a two-directional fracture system and compressed voids following a cross linear pattern, point to a tectonic overprint on layers I and II.

Layer III strongly retained the colluvial characteristics: it consists of unsorted fragmentary reworked material, including fragments of underlying layers. It shows much clay precipitation, which is attributed to a strong weathering environment. Removal, and translocation of iron is observed in two phases: a dominant removal (pseudogley) phase which may have affected also layer II, followed by a late (gley) phase of accumulation, probably related to the impregnation of layer IV.

Layer IV is a plinthitic layer with hardened parts overlaid by an eroded Oxisol. It has a groundmass composed of very homogeneous fine clay related to the colluvial deposition of a strongly weathered and well sorted material. It has distinct crescentic features of biological origin (which are also sporadically observed in the bleached parts in the top of layer III). In addition to the iron oxides already present in the clay groundmass, accumulation of hematite and goethite as (petro)plinthite indicate groundwater saturation (gley processes). The outcrops of petroplinthite testify that much of the overlying material was removed by erosion.

The remnants of the Oxisol at the top of the sequence, show very coarse granules of reworked colluvial material from the underlying layers and from nearby areas. Relicts of yellow and reddish clay granules, similar to those observed in summit Oxisols of the neighboring area (Muggler and Buurman, 1997; chapter 3) are also present, suggesting that this Oxisol formation phase was common to the whole area. Weathering of ilmenite observed in the whole sequence shows that the Oxisol formation overprinted all materials.

CONCLUSIONS

The studied graben filling show distinct evolutionary phases imprinted in its various layers, thus clearly separated in time, and allows the unraveling of the pedogenetic history undergone by the polygenetic soils of the area. The following phases of erosion, deposition and soil formation were recognized:

1. Deposition of reworked ferralitized soil material from nearby areas (layer I);
2. Formation of soils with illuvial and precipitated clay accumulations in layer I;
3. Erosion (with gully formation) followed by deposition of reworked soil material (layer II);
4. Formation of soils with a ferralitic character in layer II;
5. Tectonic activity, erosion and renewed colluvial deposition (layer III);
6. Formation of soils with gley and pseudogley features in the colluvium;
7. Deposition of a strongly weathered and well sorted sediment (layer IV);
8. Formation of Oxisols that overprinted the whole sequence, accompanied by groundwater saturation and development of plinthite and eventually petroplinthite;
9. Landscape inversion (by tectonic activity?), and erosion that removed most of the Oxisol cover and exposed petroplinthite layers;
10. (Sub)recent pedogenesis causing yellowing of the previously red soils.

These processes also took place on the soils of the stable landscapes (not affected by tectonic activity), but overprinting and erosion does not allow recognition of most of the distinct evolution phases.

5. MINERALOGICAL AND (SUB)MICROSCOPICAL ASPECTS OF IRON OXIDES IN POLYGENETIC OXISOLS FROM MINAS GERAIS, BRAZIL.

Cristine C. Muggler, Jan J. van Loef and Peter Buurman

Abstract

Iron oxides are known to be useful paleo-environmental indicators, and their properties may give information about past and present circumstances of weathering and soil formation. Iron oxides from polygenetic Oxisols from Minas Gerais, Brazil, were studied by mineralogical (X-ray diffraction, Mössbauer spectroscopy) and (sub)microscopical (micromorphology, transmission and scanning electron microscopy) techniques. The Oxisols developed either on rock-saprolites from stable Tertiary surfaces or on sediments that filled neo-Cenozoic graben zones. Hematite and goethite are the only iron oxides found in the clay and silt fractions. Micromorphology shows that during rock weathering hematite forms in the saprolites as 'droplets', which decrease in size by pedoturbation and eventually disappear in younger, yellow topsoils. In the graben zones, hematite was either inherited (from reworked soil material) or formed in situ as (hypo)coatings in response to periodic water saturation. The hematite of the soils on rock-saprolites has an uniform crystallite size and a low aluminium substitution. Crystallites of hematite in the soils on sediments are slightly larger, but Al-substitution is low too. The different forms of hematite could only be distinguished through micromorphology. Goethite is less commonly formed in the rock-saprolites and is mostly a 'secondary' product, that more closely reflects the soil forming environment. Aluminium substitution in goethites increases from the saprolites to the topsoils, in response to increasing Al activity. In environments of periodic water saturation, goethites occur evenly distributed in the groundmass and/or accumulated as coatings in bleached channels. Similarly to the hematite in such environments, this goethite has a low aluminium substitution and a slightly larger crystallite size than hematite. A large variation in goethite properties within the same horizon is found both in soils on rock-saprolite profiles and on sediments, which reflects the polygenetic nature of the soils.

Keywords: Brazil; iron oxides; Oxisols; micromorphology; XRD; Mössbauer; polygenesis.

INTRODUCTION

The state of Minas Gerais, southeastern Brazil, presents a large diversity of natural environments and soils, many of which are related to Tertiary or older landscapes. In these landscapes, as in several other areas in the humid tropics, soil development is influenced by a complex geomorphic history (Ollier, 1959; Stoops, 1989), with climatic and tectonic components. Soils resulting from such a long evolution are polygenetic. These soils are mainly deep Oxisols (Ferralsols), with kaolinite, gibbsite and iron oxides (hematite and/or goethite) as main mineral components, as is common in other Brazilian Oxisols (Schwertmann and Kämpf, 1985; Fontes and Weed, 1991).

In the studied area, a combination is found of remnants of old geomorphic surfaces in the stable parts of the landscape next to a variety of neo-Cenozoic graben fillings. Both, the old (stable) surfaces and the graben fillings, have undergone a number of clearly different soil formation phases

(see Chapters 3 and 4). In the stable parts of the landscape, the soils developed on fine- and medium-textured metamorphic rocks of Proterozoic age. The oldest geomorphic surfaces there are of Tertiary age. The graben fillings formed throughout the Tertiary and Quaternary. They consist of remobilized soils and saprolites of the adjacent areas, partly deposited as slope deposits, partly reworked in a presumably lacustrine environment (Saadi and Valadão, 1990). The most visible difference between the stable parts of the landscape and the graben fillings is the colour of the saprolites: pinkish on the stable parts of the landscape, and yellow and/or red in the graben fillings. The B horizons of the Oxisols are usually red. Shallow surface soils on more recently eroded slopes of the stable parts of the landscape are yellow.

Micromorphology indicated that soil genesis on the stable parts of the landscape and in the graben deposits has been different, especially with respect to hydrology. Hydrology is one of the main aspects affecting the mineralogy of iron compounds at a micro-scale (Schwertmann and Taylor, 1989; Cornell and Schwertmann, 1996). First, small changes in water activity result in formation of either goethite or hematite. Second, soil reduction associated with very wet conditions mobilize Fe, which can be translocated to oxic (micro)environments. Some soils in the graben fillings show signs of iron accumulation related to surface and groundwater saturation phenomena, which are virtually absent in the better-drained soils of the stable parts of the landscape.

Hematite and goethite can remain stable in aerobic environments over geological time, and may store information about the environment in which they formed, constituting useful (paleo)environmental indicators (Resende, 1976; Kämpf et al., 1988; Schwertmann and Fitzpatrick, 1992; Singh and Gilkes, 1992; Friedl and Schwertmann, 1996). Amount of substitution in Al-for-Fe in iron oxides is such an indicator (Fitzpatrick and Schwertmann, 1982; Anand and Gilkes, 1987). The various forms of hematite and goethite identified by micromorphology probably reflect different environmental conditions during their formation. This work is concerned with the characterization of the mineralogical aspects of the iron oxides in the various soil sequences. It is aimed to find differences between properties of the iron oxides, such as Al-substitution, crystal size and morphology of the various iron forms, and to relate them to conditions of formation. In this context, a large variation in amounts of substituting Al between goethites from the same horizon or profile may be due to mixture of soil materials, to a range of distinct pedoenvironments through time, or to the existence of simultaneous micro-environments with different Al-availability. Also, differences in weathering conditions between rock-saprolites and sediments should be reflected in the mineralogy and properties of the iron oxides. The characterization of the iron oxides, and the interpretation of the relation between their characteristics and circumstances of soil formation were approached by micromorphological studies, X-ray diffraction, electron microscopy, and Mössbauer spectroscopy.

MATERIALS

The study area is located in the southern part of the state of Minas Gerais between 21 and 22°S and 44 and 45°W, near the town of São João del Rei. The dominant lithologies are fine- and medium-textured metamorphic rocks belonging to the Barbacena and São João del Rei groups (Archean and Middle Proterozoic ages), with localized occurrence of neo-Cenozoic sediments. The present climate is a tropical highland climate with an annual average temperature of 19-20°C, and an annual average precipitation of 1400 mm. The topography is undulating to rolling with altitudes of 900-1100 m. The original vegetation is *cerrado* and *campo cerrado* (savanna-like and sparse savanna-like vegetation). Soils are mainly Oxisols, with oxic equivalents on eroded slopes.

Weathering and topographic sequences were selected and described according to FAO guidelines (1990). Table 5.1 summarizes the profile descriptions and main chemical data. Complete profile descriptions and routine chemical analyses are given in Appendix 1. The selected soil sequences, distinguished on the basis of their parent material are: (i) Oxisols developed on saprolites of metamorphic rocks from the stable parts of the landscape (P1, P2, P7, P8: Anionic Acrudox; P3, P4: Inceptic Hapludox; P5: Udoxic Dystropept); and (ii) Oxisols developed on sediments from the graben zones (P6: Petroferric Acrudox; VP: Anionic Acrudox). Profiles from the erosive catena P1-P5, where consecutively deeper parts of the original profile are exposed downslope, have been joined, and appear in the Tables as a composite profile. The cumulative depth of the profiles are about 14 m in P1-5, 5 m in P7, 5 m in P8, 16 m in VP and 23 m in P6.

Yellowing (or xanthization) of the topsoils is observed in most soils, and yellow *sola* occur on eroded slopes, apparently related to more recent pedogenesis. The Bw horizons of the profiles P2-P5 from the erosive catena (Table 5.1) are yellow horizons formed on exposed saprolite and subsoil layers from eroded Oxisols. The lower horizons are less changed by present soil formation. Their molar SiO_2/Al_2O_3 ratios indicate that they form a sequence of decreasing weathering with depth. Profile P7 is formed on saprolite; the upper two horizons are yellowed and show colluvial deposition; a stoneline is found between the second and the third horizon. Profile P8 is a relatively uneroded soil, with less yellowing in the topsoil than in the former profiles. Chemical analyses indicate that there is a gradual transition from C to AB horizon. The VP sequence consists of a deep Oxisol, developed in layered, probably lacustrine sediments. The lower layers, in which soil formation has not obliterated much the sedimentary structure, are coded with roman numerals. P6 consists of three layers of reworked soils and saprolites (I,II,III), in each of which soil formation has taken place. Layers I and III show abundant mottling due to periodical water saturation in the past. These layers are overlaid by a well-sorted sediment, in which an Oxisol has developed. This Oxisol has thin petroplinthite layers towards its base. Iron impregnation, linked to this petroplinthite, is also evident in layer III. The B horizon of P6 is developed in loosened petroplinthite and is slightly yellowed.

Table 5.1: Summarized profile descriptions, texture, chemistry of the fine earth fraction and clay mineralogy of the studied sequences.

Parent mat.	Profile seq.	horiz. layer	colour	text.[1]	structure[2]	pH H_2O	Fe_2O_3	Al_2O_3	SiO_2	TiO_2	SiO_2/Al_2O_3[3]	clay mineralogy[4]
							%					
	P1	Bw2	10R 4/6	c	gra	5.4	25.2	44.6	27.1	2.83	1.03	Ka, Gb
	P1	BC1	2.5YR 4/6	sc	sblo	5.5	22.2	38.9	36.2	2.48	1.58	Ka, Gb
r	P2	Bw	5YR 5/8	sl	sblo	5.1	20.3	38.3	38.7	2.24	1.72	Ka, Gb
o	P3	Bw	7.5YR 5/8	c	sblo	4.9	18.2	33.2	46.0	1.89	2.36	Ka, Gb
c	P4	Bw	7.5YR 4/4	c	sblo	4.7	18.8	35.6	43.0	2.24	2.05	Ka, Gb
k	P5	Bw	7.5YR 5/6	c	sblo	4.5	17.3	33.4	46.9	2.11	2.39	Ka, Gb
	P4	BC2	2.5YR 4/8	sl	mas	5.5	18.1	35.8	44.0	1.85	2.09	Ka, Gb
	P1	C	-	s	mas	5.3	19.8	33.8	44.1	1.9	2.22	Ka, Gb
s	P2	C	5YR 5/8	s	sblo	4.4	17.7	36.6	43.8	1.76	2.03	Ka, Gb
a	P3	C	2.5YR 5/8	s	mas	5.4	18.2	34.1	44.0	2.36	2.24	Ka, Gb
p	P5	C1	2.5YR 3/6	s	mas	5.0	15.8	32.0	50.0	1.6	2.66	Ka, Gb
r		Bw	10YR 5/8	c	ablo	4.6	11.7	28.5	57.2	1.61	3.41	Ka, Gb, Vm
o		BC2	5YR 5/6	c	sblo	5.1	12.4	30.6	54.4	1.6	3.03	Ka, Gb, Vm
l	P7	IIBw	2.5YR 4/8	c	ablo	5.0	11.9	34.0	51.2	1.51	2.56	Ka, Gb
i		IIBC2	2.5YR 5/6	cl	gra	5.3	10.7	29.4	56.8	1.11	3.29	Ka, Gb, Mi
t		C2	10R 5/4	sl	mas	5.4	2.9	30.5	64.5	0.39	3.60	Ka, Mi
e		AB	5YR 4/4	c	sblo	5.3	15.0	39.1	42.2	2.51	1.84	Ka, Gb, Vm
s	P8	Bw2	2.5YR 4/6	c	gra	5.6	16.1	40.9	38.9	2.55	1.62	Gb, Ka, Mi
		BC1	10R 4/6	scl	sblo	5.5	12.7	34.7	48.2	1.78	2.36	Ka, Gb, Mi
		C	10R 4/6	sal	mas	5.6	9.3	25.2	58.5	1.2	3.95	Ka, Mi, Gb
		Bw1	2.5YR 4/6	c	gra	5.0	19.0	38.4	39.3	2.97	1.74	Ka, Gb
		Bw5	10R 4/6	c	sblo	5.4	18.2	37.7	41.1	2.66	1.86	Ka, Gb
s	VP	C1	7.5YR 5/8	c	mas	5.4	21.7	37.9	37.5	2.74	1.68	Ka, Gb
e		C3	10YR 6/6	cl	mas	5.5	13.3	41.4	42.1	2.95	1.73	Ka, Gb
d		V	2.5YR 4/6	c	mas	5.1	20.6	31.2	45.4	2.47	2.47	Ka, Gb
i		IV	2.5YR 4/6	cl	mas	4.9	19.8	29.5	48.6	1.67	2.80	Ka, Gb
e		Bw	2.5YR 4/6	c	gra	5.1	17.7	37.4	41.6	2.67	1.89	Ka, Gb
n		Bwm	10R 4/6	sal	mas	5.0	59.9	17.1	21.8	1	2.17	Ka
t	P6	Bwv	7.5R 4/6	c	mas	5.0	34.2	26.0	37.8	1.64	2.47	Ka
s		III	2.5YR 3/6	sacl	mas	5.0	19.4	33.7	44.6	1.81	2.98	Ka, Mi
		II	10R 3/6	cl	mas	5.4	11.3	27.0	59.3	1.6	3.73	Ka, Mi
		I	10R 3/6	cl	mas	5.1	12.1	25.3	60.0	1.55	4.02	Ka, Mi

[1] c: clay; sc: silty clay; sl: silt loam; s: silt; cl: clay loam; scl: silty clay loam; sal: sandy loam; sacl: sandy clay loam; [2] gra: granular; sblo: subangular blocky; mas: massive; ablo: angular blocky; [3] molar ratio; [4] except iron oxides; in order of abundance; Ka: kaolinite; Gb: gibbsite; Vm: vermiculite and/or mixed layer clay minerals; Mi: mica; in order of abundance.

METHODS

Bulk samples were collected for textural (pipette) and chemical routine analyses, X-ray fluorescence analyses of major and trace elements, and mineralogy. Undisturbed samples were

collected for preparation of thin sections, in order to identify the distinct iron forms by micromorphology. Iron oxides for mineralogical and electron microscopical analyses were concentrated by treatment of the clay and clay+silt fraction with 5M NaOH (Kämpf and Schwertmann, 1982; Singh and Gilkes, 1991). Selected areas of thin sections were drilled out and ultramicrotomed for observation by transmission electron microscope (TEM). Samples of concentrated iron oxides and soil aggregates were studied by scanning electron microscope (SEM).

X-ray diffraction was performed on non-oriented powder samples, with a Philips PW 1710 diffractometer equipped with a graphite monochromator using CoKα radiation at 30mA and 40kV. The peaks were recorded from 22° to 78° 2θ at a speed of 0.6°2θ/min. XRD patterns were interpreted with the PC-APD Philips software that enabled calculation of accurate peak positions and line widths. The ratio Gt/(Gt+Hm) was obtained by integrating the peak intensities of the goethite (110) line and the hematite (012) line multiplied by 3.5 (Schwertmann and Murad, 1983). For calculation of the Al-substitution in goethite we used the *c* dimension (Schulze, 1984) in the relationship Al/(Al+Fe) = 1462 – 483c formulated by Schwertmann and Carlson (1994) for goethites from tropical soils. In hematite the *a* dimension derived from d(110) was used in the relationship Al/(Al+Fe) = 3141 – 623a (Schwertmann, 1988a) derived for hematites synthesized at 25°C. Mean coherence lengths (MCL) were calculated using the Scherrer formula, after correction for instrumental broadening (Schulze, 1984). For goethite, MCL's were calculated from the (110) and (111) line widths. For hematite they were calculated along the *a* and *c* crystallographic directions by projecting the MCL_{hkl} values on the respective crystallographic axes (Schwertmann and Kämpf, 1985). MCL_a was obtained from the average of the (110) and (300) lines and MCL_c from the average of the (012), (024), (104), and (113) lines.

Mössbauer spectra were obtained for selected untreated and 5M NaOH treated samples from the sequences P6 and P8. The spectra of the samples were taken at room temperature (295K) and at liquid nitrogen temperature (77K) with a constant acceleration spectrometer using a ^{57}Co in Rh source. Hyperfine fields were calibrated against the 51.5T hyperfine field of α-Fe_2O_3 at room temperature. Spectra obtained at intermediate temperatures, while slowly warming up the bath cryostat, were used for complementary information. Despite their lower resolution they give useful information, as the most obvious differences in the Mössbauer spectra occur in this temperature range, where superparamagnetic and magnetically ordered goethites may coexist (Van Loef, 1998). From the two distinct magnetic hyperfine splittings observed in the 77K spectra, the one characterized by sharp and narrow lines is attributed to hematite. The other, which is characterized by asymmetrically broadened lines, is ascribed to goethite. The relative intensity of the areas of the two distinct magnetic hyperfine fields in the spectra was used to calculate the hematite/goethite ratio. In this way proportions of hematite and goethite can be estimated within 10% accuracy or less, without correction for the free recoilless fraction, since the latter presents little variation at 80K and below (Amarasiriwardena et al., 1988). Because hyperfine lines of goethite at 77K are

asymmetrically broadened, the most dominant hyperfine field present, B', was determined from the positions of the steep outer edge of the lines. Mean dimensions (line widths) of the broadened goethite hyperfine fields were so determined and are given in Tesla (T). The total hyperfine fraction (h.f.s.) in each spectrum was determined by measuring the area of the magnetically ordered proportion of the spectra relative to that of the total spectrum.

RESULTS

Micromorphology of iron forms

The main modes of occurrence of iron compounds in the studied thin sections are described below and summarized in Table 5.2.

a. Uniform distribution of hematite or goethite in the groundmass. This results in homogeneous red and/or yellow colouring of the groundmass, where the separate particles cannot be distinguished at a magnification of 800X. It is typically observed in the A and B horizons of the soils developed on rock-saprolites;

b. Strong red or yellow impregnation of the groundmass. This secondary iron impregnation forms a clear red or yellow haze, which impregnates the clayey sedimentary materials, without cementation.

Table 5.2: Micromorphology of iron forms in the studied sequences.

Parent material	site of occurrence	micromorphological iron form[1]			
		a	b	c	d
rock saprolites	yellow soils	strong[2]	-	-	-
	red soils	strong	-	few[3]	-
	saprolite	-	-	abundant	-
sediments	topsoils	strong	weak	-	few
	sedim. layers	-	strong	-	abundant

[1] for description of types see text; [2] refer to intensity of impregnation; [3] refer to number of particles or features.

c. Hematite 'droplets' (Figure 5.1a). These 'droplets' consist of discrete spherical aggregates of hematite (*plinthitic hematite* after Schmidt-Lorenz, 1980; Stoops, 1989) which appear evenly distributed in homogenised groundmasses, or occur in accumulations in saprolites. In the saprolites, the droplets occur both in bands related to the original rock fabric and scattered in ghosts of weathered minerals. They are much more abundant in the saprolites and C horizons than in the overlying horizons. Hematite 'droplets' decrease towards the surface soils, and eventually disappear in the yellow eroded soils.

d. Localized gley and pseudogley iron accumulation features. Various secondary accumulations of iron oxides, related to surface- and groundwater saturation processes,

overprint the groundmass, mainly in the soil-sediment sequences. These secondary iron accumulations occur as infillings, and (hypo)coatings and their fragments, as well as diverse types of nodules. More details of these features and microphotographs are given in Chapter 4.

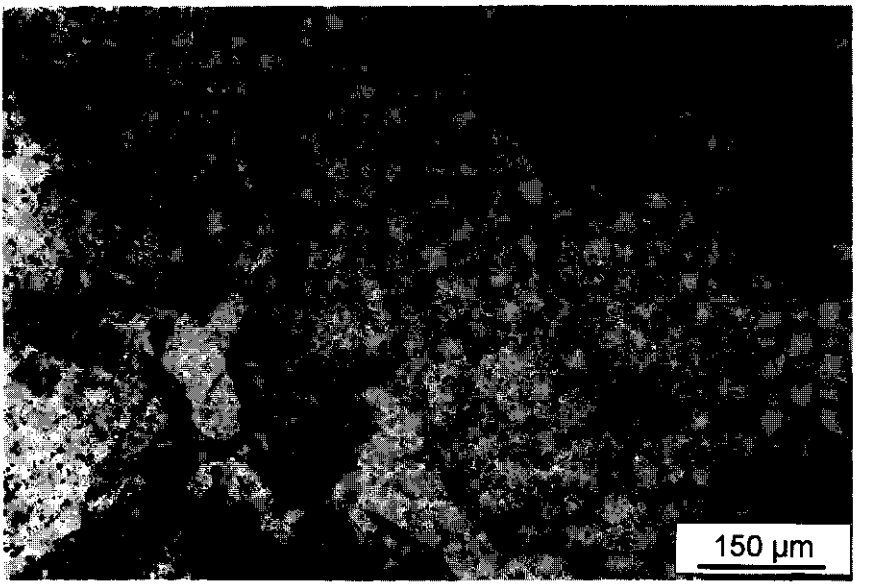

Figure 5.1: Microphotograph of hematite 'droplets' as observed in saprolites (C horizon, profile P1); PPL.

Mineralogy of iron oxides

The mineralogy of the iron oxides was determined by X-ray diffraction and Mössbauer spectroscopy of the samples treated with 5M NaOH. Mössbauer spectroscopy is very useful for distinguishing hematite from goethite in soils, since hematite is usually magnetically ordered at room temperature (295K) and goethite often is not. Even if some goethite is magnetically ordered at 295K, its much smaller hyperfine field allows distinction between the two minerals, and, therefore, the assessment of goethite/hematite ratios (Murad, 1990). Hematite and goethite were the only iron oxides identified in the samples. The ratios Gt/(Gt+Hm) calculated from the peak intensities obtained by XRD, are presented in Table 5.3. They are in good agreement with those derived from the proportions of hematite and goethite estimated by Mössbauer spectroscopy (Table 5.4). Mössbauer spectra of samples from sequences P6 and P8, measured at 77K and 295K, are shown in Figures 5.2a-d. It was assumed that the non-magnetic contribution in the central part of the spectra of P8/AB, P8/B and P6/B is due to goethite, because of the continuous increase of h.f.s. at 77K (see topic on Mössbauer spectroscopy). The presence of hematite in all samples is clear from the spectra measured at 295K (Figures 5.2a, b).

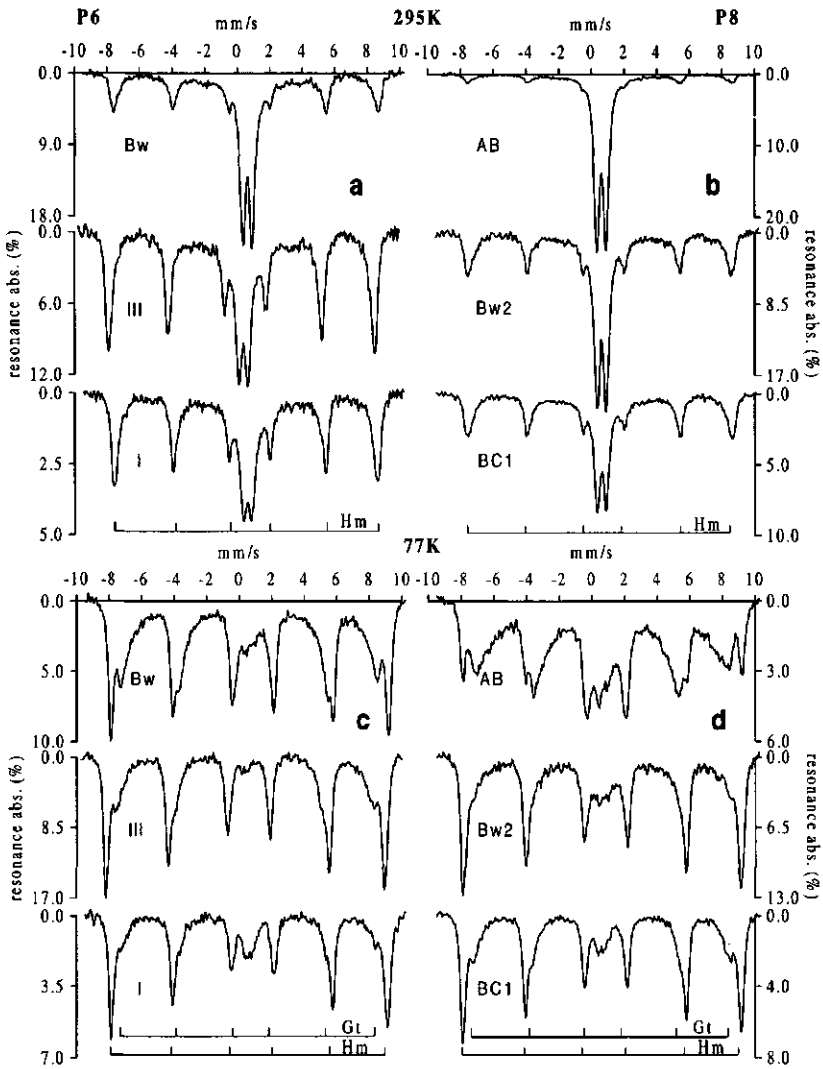

Figure 5.2: Mössbauer spectra of iron concentrated* samples from sequences P6: **(a, c)** and P8 **(b, d)**. * sample P6/I is not an iron concentrated sample.

Other minerals found in the concentrates were anatase (in all samples) and mica (in profiles P6, P7 and P8). Maghemite was not identified in any of the samples, even not in the petroplinthites, although it is commonly found in Brazilian Oxisols (Kämpf et al., 1988). The colour of the iron concentrates gives some indication about the presence of goethite and hematite. Very low contents of hematite impart a red hue to the soil matrix, but even dark red materials can contain considerable amounts of goethite (Resende, 1976; Schwertmann, 1993; Torrent et al., 1983). Indeed, goethite

was ubiquitously present, even in the dark red residues, but yellow materials were virtually free of hematite. Hematite is more abundant in the soil-sediment sequences than in the soil-rock-saprolite sequences.

In the subsoil of the P6 sequence, goethite, although less abundant than hematite, increases significantly in layers I and III, which show abundant mottling. BC and C horizons of the soil-saprolite sequences have more hematite than topsoils, and particularly in the saprolites this iron oxide is more concentrated in the silt fraction, as shown for samples C* and C1* (Table 5.3). This corroborates micromorphological observations which indicate the presence of droplets larger than 2 μm. Also, this explains the yellow colour and goethitic nature of the (clay) sample from horizon C of profile P8. Topsoils are yellower and richer in goethite, especially those developed on saprolites from eroded Oxisols (P2-P5 and P7).

Al-substitution calculated from XRD lines

Estimates of Al-substitution in goethites obtained from the shifts of the XRD lines (111) and (110), using the formula of Schwertmann and Carlson (1994) are presented in Table 5.3. This relationship gives figures that are up to 20% lower than those obtained with the widely used formula of Schulze (1984) for synthetic goethites. In case of very broad or double peaks of the goethite (111) line, a minimum and a maximum d-spacings were obtained through deconvolution of the peaks. The validity of this procedure was substantiated by the results obtained by Mössbauer spectroscopy (see below). Figure 5.3 illustrates the variation observed in the diffractograms from different samples. The highest Al-substitution (Al%>25) in goethites is observed in surface soils on both, rock-saprolites (P8) and sediments (VP sequence). Yellow topsoils of eroded Oxisols on rock-saprolites have a rather uniform high Al-substitution of 18-22%. Goethite in C horizons (saprolites) usually shows lower Al-substitution (10-15%). The pedosedimentary sequence P6 gives Al-substitution in goethite between 10 and 14%, while well-drained sequence VP has higher and more variable values.

Well defined and clear XRD peaks (Figure 5.3) indicate that there is little heterogeneity of hematite crystals in all materials. Indeed, Al-substitution in hematite of the soil saprolite sequences is rather uniform throughout each sequence. Hematites generally accommodate half as much aluminium as goethites (Schwertmann, 1985; 1988), and more than 10% of Al-substitution in hematites is most unusual (Anand and Gilkes, 1987). Among the soil-sediment sequences, P6 shows a slightly lower (4-7%), and VP a higher (9-12%) Al-substitution in hematites than the rock-saprolitic sequences. Considering that most of the studied hematites have formed in the saprolite, they have rather high Al-substitution. These high values may be partly due to the calculation procedure used. The relationship used here was derived for hematites synthesized at 25°C and pH 5.0 (Schwertmann, 1988a). It gives higher Al contents than the formula obtained from hematites synthesized at 70° C and pH 7.0 (Schwertmann et al., 1979) on which most publications are based.

Table 5.3: Mineralogical aspects of the iron oxides present in the iron concentrated clays of the studied sequences, determined by X-ray diffraction.

Parent material	Profile/ sequence	horizon/ layer	colour[2]	Gt/ (Gt+Hm)[3]	Al-substitution		MCL[4] Gt		MCL Hm	
					Gt	Hm	110	111	a	c
					%				nm	
	P1	Bw2	dR	0.49	14-26	9	18	20	29	11
	P1	BC1	yR	0.54	11-26	9	17	12	29	11
	P2	Bw	rY	0.89	18	10	16	11	30	10
	P3	Bw	Y	0.99	18	-	17	16	-	-
r	P4	Bw	Y	0.96	18	-	17	15	-	-
o	P5	Bw	rY	0.93	19	-	16	13	-	-
c	P4	BC2	yR	0.69	15	8	16	14	23	11
k	P1	C	Y	0.88	11	6	19	23	19	11
	P1	C*	dR	0.27	10	7	19	24	20	9
s	P2	C	yR	0.58	11	8	16	15	17	9
a	P3	C	dyR	0.77	15	8	15	18	23	16
p	P5	C1	dyR	0.65	14	6	17	19	21	9
r	P5	C1*	dR	0.25	14	7	16	23	18	8
o		Bw	Y	1.00	22	-	15	13	-	-
l		BC2	bY	1.00	20	-	14	11	-	-
i	P7	IIBw	R	0.48	19	8	18	15	38	15
t		*II*BC2	R-yR	0.63	16	7	17	14	31	14
e		C2	dR	0.23	13	5	23	14	32	15
s		AB	bY	0.86	16-31	6	18	11-25	30	16
	P8	Bw2	dR	0.39	16-31	7	16	11	29	13
		BC1	R	0.43	12-19	7	17	14	27	12
		C	Y	0.88	11	5	19	23	20	12
		Bw1	dR	0.68	31	10	19	14	30	12
		Bw5	dR	0.41	25	10	18	13	27	12
s	VP	C1	yR	0.72	17-32	9	15	11-17	18	12
e		C3	Y	0.77	13-28	-	15	11-20	-	11
d		V	yR	0.40	20-29	12	22	12	25	15
i		IV	dyR	0.52	17	9	25	27	27	14
m		Bw	yR	0.61	13-22	6	20	15	40	17
e	P6	Bwm	dR	0.19	12	6	23	19	37	14
n	P6	Bwv	dR	0.14	13	7	24	24	37	16
t		III	dyR	0.37	13	5	24	22	38	18
s		II	dR	0.11	13	5	24	20	40	16
		I	R	0.38	11	4	24	33	36	14

*: *silt* + clay sample; [2] descriptive general colour of the XRD tablet: R: red; Y: yellow; b: brownish; d: dark; r: reddish; y: yellowish; [3] Gt: goethite; Hm: hematite; [4] mean coherence length.

Crystal size and morphology

Mean coherence lengths (MCL) along the (110) and (111) directions of goethite, and along the *a* and *c* crystallographic directions of hematite are given in Table 5.3. Ranges of goethite $MCL_{(111)}$'s were obtained from the deconvolution of double peaks in the (111) goethite lines. Differential broadening of the various lines of goethite and hematite are interpreted in terms of crystal morphology, as they reflect differences in the various directions of crystal growth (Schulze and Schwertmann, 1984; Schwertmann and Taylor, 1989; Strauss et al., 1997). Hematite crystals are usually larger than coexisting goethite crystals, as generally observed in other tropical soils (Curi and Franzmeier, 1984; Anand and Gilkes, 1987; Schwertmann, 1988), with the exception of some C horizons of the soil rock-saprolite sequences, where they have similar sizes.

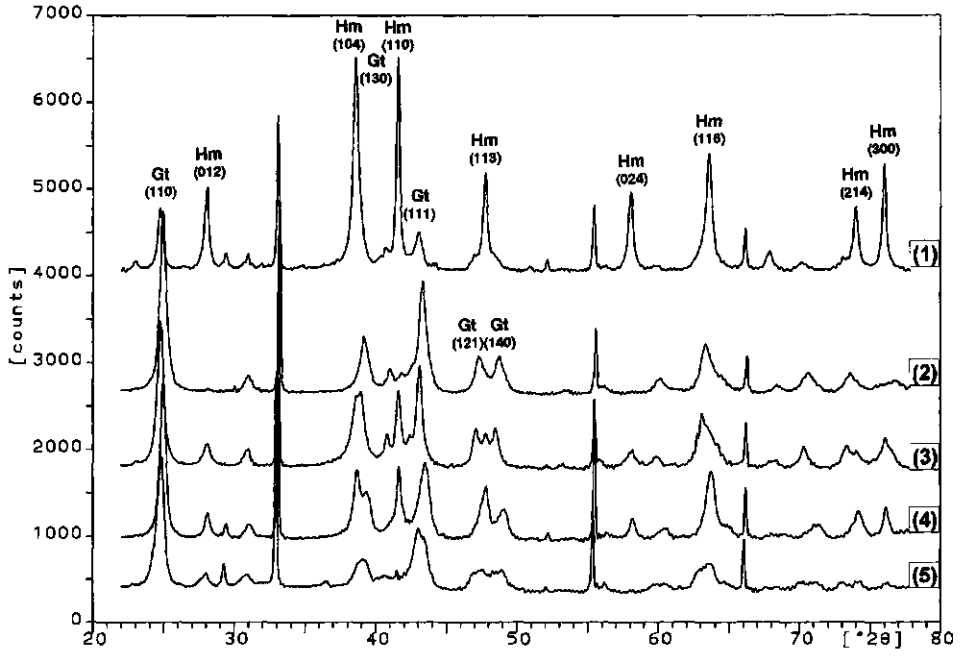

Figure 5.3: X-ray diffractograms of the iron concentrated clay samples: (1): dominant hematite, Bwm/P6; (2): dominant goethite, Bw/P3; (3) and (4): hematite and goethite; observe that the line (130) of goethite is shifted and distinct from the line (104) of hematite, due to Al-substitution, C1/P5 and Bw1/VP; (5): dominant goethite with low crystallinity, C3/VP.

In general, the rock-saprolite sequences show smaller MCL's for goethites than the sedimentary sequences, especially P6. In the soil-sediment sequences, the MCL's along the

two directions decrease towards the topsoil, and $MCL_{(111)}$ is usually smaller than $MCL_{(110)}$. This shows that the goethite crystals are isodimensional, instead of showing the typical lath or acicular shape of better crystallized goethites (Taylor and Schwertmann, 1989). The disruption of the lath/acicular morphology of goethite in soils is attributed to the presence of Al, which causes a preferential reduction in the *c* or needle axis direction by retarding the crystal growth in this direction (Fey and Dixon, 1981; Schwertmann, 1985; Strauss et al., 1997). In the saprolite samples a reverse tendency, $MCL_{(111)}$ being larger than $MCL_{(110)}$, is indicative of some acicularity, which was indeed observed in some star-like goethite crystals depicted by TEM (Figure 5.4a).

In the studied hematites, MCL_c showed values smaller than 20 nm, while MCL_a was usually larger than 20 nm, indicating platy crystals. Platiness of hematite crystals is also indicated by a (104) line width larger than the (110) one (Campbell and Schwertmann, 1984; Kämpf, 1988), which was observed in all analyzed samples. Platy crystals result from a slower growth along the c direction (Schwertmann and Kämpf, 1985; Amouric et al., 1986; Cornell and Schwertmann, 1996), which is also ascribed to the presence of aluminium (Schwertmann et al., 1977; Barron et al., 1987). The samples from the composite profile P1-P5 show smaller MCL_c's than the other profiles/sequences, indicating the hematites have thinner domains along the c direction. The general larger variation of MCL_a values, compared to MCL_c indicates the dominance of thin hematite crystals with variable width. The largest hematite crystals are found in sequence P6 (soil-sediment), where the crystals are also more uniform throughout the profile.

Morphological distinction between hematite and goethite under the electron microscope was impossible in most cases, due to the similarity and equidimensionality of the crystals. This is frequently reported for strongly weathered soils from tropical areas (Schwertmann and Kämpf, 1985; Schwertmann and Taylor, 1989). Scanning electron microscopy of iron concentrates from saprolites showed the spherical hematite aggregates already referred as 'droplets' (Figure 5.4b). In the concentrates containing mica the iron compounds are commonly present as thin coatings on unweathered micas (Figure 2.1; chapter 2). These coatings do not exhibit clear crystal morphology at the range of magnification used. Non-coating iron oxides have irregular, anhedric crystals and frequent aggregates as shown by transmission electron microscopy (Figure 5.4c). Crystals are larger and show a better developed morphology in the profiles from the soil-sediment sequences (Figure 5.4d). These crystals are likely hematites because they appear as equidimensional subhedric crystals that sporadically show hexagonal-type sections. The presence of granular aggregates of hematites (grainy structures), observed by TEM (Figure 5.4c), appears to be related to previous aggregates of ferrihydrite as precursors of hematite as described by Schwertmann and Fitzpatrick (1992).

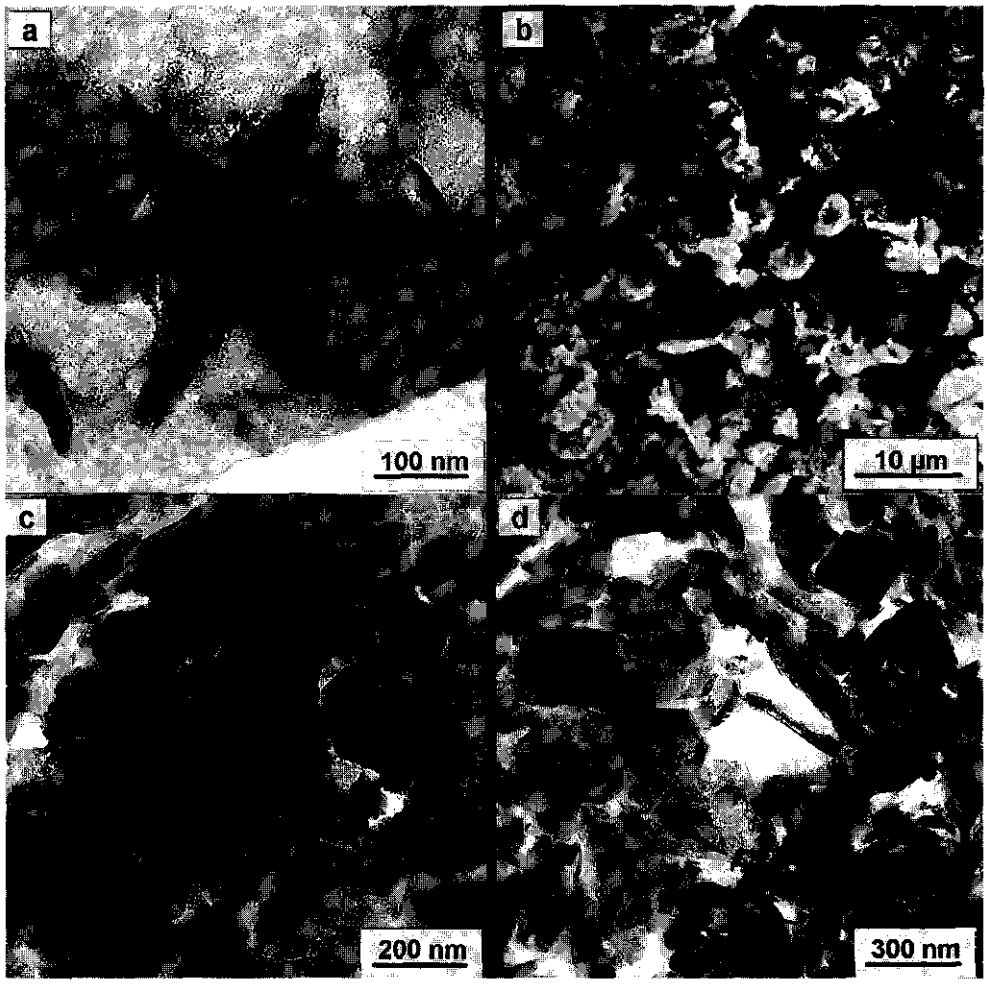

Figure 5.4: Electron microphotographs of iron oxides from the soil-rock-saprolite (a, b) and from the soil-sediment (c, d) sequences: **(a)** goethite star-like crystal in saprolite (TEM); **(b)** iron 'droplets' from silt+clay sample, profile P1 (SEM); **(c)** aggregated iron oxides, I/P6 (TEM); **(d)** crystals and aggregates of iron oxides in a kaolinitic matrix (kaolinite crystals were altered by the electron beam), I/P6 (TEM).

Mössbauer spectroscopy

The Mössbauer spectra of the 5M NaOH-concentrated samples showed a better resolution, a significantly higher resonance absorption, and an increased contribution of hyperfine-split subspectra than those of the untreated samples (not shown here). The latter contained iron-substituted kaolinite, which has a Mössbauer spectrum that consists of a doublet with parameters that are not significantly different from those of (super)paramagnetic goethite at 295K (Murad and

Wagner, 1991). The spectra of concentrated samples at 295K (Figures 5.1a, b) show a single magnetic hyperfine subspectrum due to hematite. The hematite subspectrum is superimposed on a central doublet, attributed mainly to goethite, because it practically disappears at 77K for most samples.

Goethite

The temperature dependence of the magnetic hyperfine fields (B') and the total hyperfine fraction (h.f.s) of goethite in the various samples in the temperature range 77-295K are illustrated in Figure 5.5. These parameters were determined from Mössbauer spectra taken at 77 and 295K, and at temperatures between 295K and 77K. With decreasing temperature, the total hyperfine fraction (h.f.s) in each spectrum increases approaching 100% when magnetic ordering of goethite is complete. In P6/I, P6/III and P8/BC1 complete magnetic ordering of goethite is attained at about 200K, below which h.f.s. remains constant (Figures 5.5b, d). In the other samples (P6/Bw, P8/AB, and P8/Bw2), h.f.s. keeps increasing down to 77K and below (Figures 5.5a, c). The curves show that the h.f.s. varies with the temperature in a very distinct way in the samples, suggesting distinct sets of Al-substitution and crystallinity. The much lower temperature of complete magnetic ordering of goethite in samples P6/Bw, P8/AB, and P8/Bw2 indicates both, paramagnetism as a result of Al-substitution, and superparamagnetism due to small crystal size (Murad, 1990; Cornell and Schwertmann, 1996; Murad, 1996). A reference curve of the temperature dependence of the hyperfine field in a powdered goethite sample from Cornwall, UK is added in the graphs for comparison. Synthetic pure nanocrystals of goethites give curves with a similar shape and lower hyperfine fields, B, (Van der Kraan and Van Loef, 1966). Thus, the large shape deviation of the curves of samples P6/Bw, P8/AB and P8/Bw2 is an indication that Al-substitution plays an important role in the magnetic behaviour of goethite in these samples.

Both B' and h.f.s. due to goethite should extrapolate to zero at approximately the same temperature, which is reasonably accomplished in all samples except P8/AB (Figure 5.5c). In the latter it was not possible to determine B' at temperatures above 200K, due to the strong smearing out of broadened hyperfine lines. The hyperfine fields in the subspectra of goethite at 77K have a significantly wider distribution in samples P6/Bw, P8/AB, and P8/Bw2 than in samples P6/I, P6/III and P8/BC1, as shown by the mean line widths (Table 5.4). This suggests that samples P6/Bw, P8/AB, and P8/Bw2 differ from the others not only with respect to the Al-substitution in goethite, but also in crystal size. Another indication of it is the area ratio of the total Mössbauer spectra at 295K and 77K (Table 5.4), which is significantly lower in P6/Bw, P8/AB, and P8/Bw2. The lower that ratio the smaller the recoilless fraction as a result of small crystallite size (Schroeer, 1970, Murad, 1996).

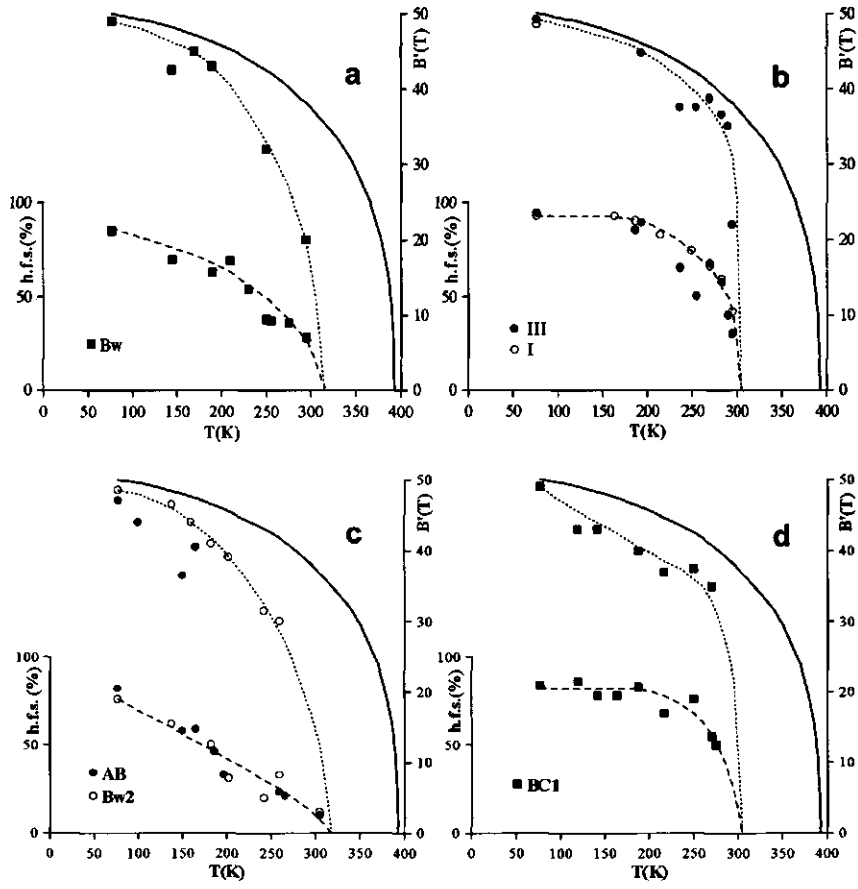

Figure 5.5: Temperature dependence of the hyperfine fraction (h.f.s., dashed line) and of the magnetic hyperfine field of goethite (B', dotted line) of samples from sequences P6 (**a**, **b**) and P8 (**c**, **d**) in the range 77-295K. The full line represents the hyperfine field of a goethite mineral (Cornwall, UK).

The temperature of the onset of magnetic order in goethite in the six samples is within an approximate range of 305 to 320K, which is considerably below the Néel temperature of 393K for well crystallized, pure goethite. On basis of the data reported by Pollard et al. (1991) it may be assumed that the onset of magnetic ordering in the various samples corresponds with a substitution of 8 to 10 mole% of Al, if only the effect of Al-substitution is accounted for. According to Pollard et al. (1991), an Al-substitution of 30% lowers the Néel temperature (T_N) to 218K, which is about the temperature at which magnetic ordering of goethite is complete for samples P6/I, P6/III and P8/BC1. This would suggest that goethite in these samples has an Al-substitution varying between 8 and 30 mole% Al, if crystal size effects are ignored. However, the ΔB' (B pure crystal - B' sample) at 77K of a 30 mole% Al goethite is 5.3T (Golden et al., 1979), while a ΔB' of only 1 to 1.5T is

observed in the studied samples. This fact, together with the mean value of the line widths of 1.7T (Table 5.4), contradicts such a high Al-substitution. Therefore, the observed magnetic behaviour must be attributed to an effect of small particle size. Indeed, relatively high hyperfine fields together with broadened lines may indicate a wide crystal size distribution (Vandenberghe et al., 1986). This is corroborated by the observation by Murad and Schwertmann (1983) that a particle size reduction from bulk to a $MCD_{(111)}$ of 21 nm results in a similar hyperfine field reduction as an Al-substitution of 10%. In P8/AB, on the other hand, ΔB' is 2.8T and the mean line width is 5.2T, indicating a substantially higher Al-substitution.

Hematite

The hyperfine fields and the mean widths of the symmetrical hyperfine lines of hematite at 77K are given in Table 5.4. The hyperfine field subspectra of hematite show less broadening and variation than those of goethite in the range 77-295K. In general, the hematite spectrum is less sensitive to effects of Al-substitution and small crystal size effects (Murad, 1990). Furthermore, hematites are often better crystallized (Cornell and Schwertmann, 1996), and accommodate less Al in their structures than goethites (Schwertmann, 1985; 1988). The small variation of the Mössbauer parameters among the samples (Table 5.4) shows that the hematites have a rather uniform Al-substitution and crystal size throughout the sequences, as was also indicated by XRD.

Table 5.4: Mössbauer parameters determined from spectra at 77K* of iron concentrates of profiles P6 and P8.

Prof.	horizon layer	Gt/ (Gt+Hm)	area[295K]/ area[77K]	B	B'	ΔB'[1]	line width[2]	
				Hm	Gt		Hm	Gt
					T			
	Bw	0.65	0.81	53.1	49.0	1.0	1.3	3.0
P6	III	0.38	0.89	52.9	48.9	1.1	1.2	1.7
	I[3]	0.37	0.88	52.9	48.9	1.1	1.1	1.6
	AB	0.80	0.71	52.8	47.2	2.8	1.1	5.2
P8	Bw2	0.53	0.69	52.7	48.1	1.9	1.2	3.3
	BC1	0.46	0.85	52.8	48.5	1.5	1.0	1.8

* except for the total area at 295K; [1] ΔB'= B(pure crystal)-B'; [2] line width of the outer absorption; [3] not concentrated sample.

The temperature dependence of the magnetic hyperfine fields in hematite in the temperature range of 77-295K is rather similar in all samples, although the B values are lower than those in pure hematite. The B values are systematically lower in P8 than in P6 at 77K (Table 5.4), and at 295K (not shown), indicating higher Al-substitution and/or smaller crystal size in the P8 samples. In using the XRD results for Al-substitution and MCL_a (Table 5.3) in the relationship B[295K] = 51.7 - 7.6*Al% - 32/MCD_a (Murad and Schwertmann, 1986), values similar to those measured in the Mössbauer spectra were obtained for all samples, except P8/AB. These results show that the data are internally consistent and that both Al-substitution and crystal size, are influencing the magnetic

behaviour of hematite in the samples. Murad and Schwertmann (1986) report that it is hardly possible to distinguish among the two effects, since they appear to have a similar influence on the magnetic properties of hematite.

The fact that the Morin transition (i.e. the change from an antiferrromagnetic state to a weakly ferromagnetic one at 260K in pure, well crystallized hematite) has not been observed in the hyperfine spectra of any of the samples. This is consistent with data from other Brazilian Oxisols (Fontes et al., 1991). The Morin transition is reported to be completely suppressed for an Al-substitution higher than 9 mole% (Coey, 1988) and for crystal sizes smaller than 20 nm (Schwertmann and Murad, 1983). The above figures show that the magnetic behaviour of the studied hematites is indeed influenced by the combined effects of crystal size reduction and Al-substitution (Murad, 1990), otherwise the Morin transition would have been observed in P6 and even in P8, according to the data obtained by XRD (Table 5.3).

A distinction between the effects due to Al-substitution and crystal size in goethite and hematite by Mössbauer spectroscopy is rather difficult because of the inherent variations in both, especially in goethite. Many attempts were already made to disentangle these effects on the magnetic properties of goethite (Golden et al., 1979; Murad and Schwertmann, 1983; Murad and Bowen, 1987; Friedl and Schwertmann, 1996) and to a lesser extent in hematite (De Grave et al., 1982, Murad and Schwertmann, 1986). Friedl and Schwertmann (1996) found that goethites from tropical soils show a stronger effect of Al-substitution on the hyperfine field, B, than of crystal size. On the other hand, the broadening and smearing out of the hyperfine lines is commonly related to the effect of crystallinity (Murad, 1988; Fontes et al., 1991; Cornell and Schwertmann, 1996; Murad, 1996). The so-called effect of crystallinity is a combined effect of small particle size and structural disorder which are even more difficult to predict and assess (Murad, 1996). For hematite, Murad and Schwertmann (1986) reported that both crystallinity and Al-substitution affect the Mössbauer parameters in a similar manner.

The analysis of the Mössbauer spectra from Figure 5.2, and derived parameters (Table 5.4) shows that in the topsoils of P8 and P6 magnetic ordering of goethite is still incomplete at 77K, and hyperfine fields show broader distributions than in the subsoils. This indicates a stronger effect of Al-substitution and crystallinity on the magnetic behaviour of goethite in the topsoils. Furthermore, the data indicate that in profile P8 the crystallinity is systematically lower, and the Al-substitution is slightly higher than in sequence P6. The variations of B and h.f.s. as a function of temperature were used in order to present additional evidence for the relative contribution of each Al-substitution and/or crystallinity effects. Figure 5.5 indicates that besides higher Al-substitution and lower crystallinity, the goethites from the *sola* are also less homogeneous within the respective horizons; they appear to have a distribution of various crystal sizes and different amounts of Al-substitution among the crystals. This is reflected by the very wide temperature range (from 320K to below 77K) in which magnetically ordered and paramagnetic goethites coexist, especially in P8/AB. Murad and Bowen (1987) explained a similar behaviour observed in Al-rich synthetic goethites by

compositional inhomogeneities in their samples. In the subsoil samples the coexistence of paramagnetic and magnetically ordered phases extended between 305 and 180K, indicating less heterogeneity within the samples.

Iron oxides, parent materials and soil formation circumstances

Micromorphology indicated distinct appearance of iron oxides related to different circumstances of soil formation among the studied materials. The soil sequences developed on sediments present a distinctive strong iron impregnation of the groundmass, as well as abundant secondary accumulations of iron oxides, which are clearly related to preferential water or air movement in the soil. On the other hand, the soils developed on saprolites show an homogeneous red or yellow colouring of the groundmass of the *sola*. This even distribution of the iron oxides in the groundmass is due to strong pedo(bio)turbation, and is typical of Oxisols (Stoops and Buol, 1985; Stoops et al., 1994). In saprolites and less pedoturbated horizons, hematite 'droplets' appear conspicuoulsy. Through mixing, droplets diminish in size and become randomly distributed in the groundmass or dissolve, or may coalesce into larger aggregates or strongly impregnated nodules. The hematite droplets eventually disappear in yellow topsoils.

The soil-sediment sequences contain in general more hematite than the soil-saprolite sequences (Tables 5.3 and 5.4). Hematites from the soil-sediment sequences have the lowest substitution in Al-for-Fe and the largest crystal sizes. The iron oxides found in the soil-sediment sequences can be inherited from the sediments, as well as formed in situ. In sediments, hematite forms through slow transformation of original metastable goethite, and once formed does not rehydrate into goethite (Tardy and Nahon, 1985; Nahon, 1991a), becoming the dominant iron oxide component. Past hydromorphism, as observed in sequence P6 (see Chapter 4), gave rise to hematite formation through oxidation of ferrous iron from flowing ground water. This appears to have increased the crystallite size by favouring crystal growth instead of nucleation. The low Al contents in these hematites, and in goethites as well, are attributed to two factors. First, in hydromorphic conditions iron is oxidized in larger pores which are further away from solid Al sources that can supply Al for substitution (Fitzpatrick and Schwertmann, 1982; Kämpf et al., 1988; Schwertmann, 1988b; Cornell and Schwertmann, 1996). Second, in reduced conditions pH is relatively high and Al activity and mobility are low. Therefore, Al-substitution in hematite remains low. Goethite in the P6 sequence also has a relatively low Al-substitution, although it is higher than in hematite due to the fact that Al goes preferentially into goethite when both minerals coexist (Schwertmann, 1988; Cornell and Schwertmann, 1996). Crystallite size of goethites in P6 are the largest of the studied materials, apparently in relation to the fact that most of the goethite occurs as well-crystallized coatings related to voids. In these sites, it is more likely that crystal growth of goethites is unhampered by Si (Schwertmann, 1988a), and not decreased along the c direction by Al (Schulze, 1984; Schulze and Schwertmann, 1984).

Yellow subsoils and yellow mottled layers from the soil-sediment sequences show an increase in contents of goethite, which is not always reflected in the colour of the iron concentrates (Table 5.3). In these environments hematite appears to have been preferentially dissolved and removed over goethite during water saturation phenomena (Barron and Torrent, 1987; Torrent et al., 1987; Macedo and Bryant, 1989; Jeanroy et al., 1991). This is well illustrated in layers I and III of the P6 sequence, where the originally red matrix is intensively mottled. It has abundant yellow patches related to voids, that turn to white and become completely devoid of iron coumpounds next to the voids, showing a sequential removal of hematite followed by goethite.

In the rock-saprolite sequences on stable parts of the landscape, low Al-goethite and most of the hematite appear to have formed during saprolite formation. Weathering conditions during saprolite formation tend to be uniform through large volumes. Presumably, pH in early weathering stages is high enough to prevent substantial amounts of Al in solution, so that low Al-substituted iron oxides form (Schwertmann and Kämpf, 1985). Also, high activity of silica during rock weathering favours accommodation of Al into kaolinite (Schwertmann, 1985). However, Al-substitution in the iron oxides found in the C horizons is not very low, which may be due to the richness of the parent rocks ('metapelitic' rocks) in this element, thus influencing the chemistry of the weathering environment during saprolite formation.

In early stages of weathering goethite may be the most commonly formed iron oxide, because the slow release of iron from primary minerals favours the formation of goethite over hematite (Fitzpatrick, 1988; Kämpf and Schwertmann, 1995). As weathering proceeds, however, pH decreases and causes more dissolution of primary minerals, increasing the release and activity of Fe in the solution. At the same time water activity decreases in relation to microporosity enhancement (Trolard and Tardy, 1987; Schwertmann, 1988b). These conditions favour the formation of hematite, probably via a short-term ferrihydrite phase (Schwertmann and Taylor, 1989), suggested by the widespread presence of spherical hematite aggregates (droplets) in the saprolites. Dominance of hematite over goethite in saprolites was also reported in other studies of tropical soils (Fölster et al., 1970; Schmidt-Lorenz, 1980; Stoops et al., 1990; Zeese et al., 1994). In topsoils, hematite is extensively converted to goethite, and droplets practically disappear. The decrease in hematite content with decreasing depth is not accompanied by a change in crystallite size and/or Al-substitution. In general, goethite is less abundant in saprolites and therefore, most of the goethite in the *sola* should have formed from previously existing hematite and/or from weathering of Fe-bearing minerals. No correlation was found between the Al content in goethite and hematite, which strongly suggest that they have formed at different times and under different pedoenvironmental conditions.

Goethite in topsoils is more abundant and is richer in Al than goethite in subsoils, both in profiles on saprolites and on sediments. Xanthization (yellowing) of topsoils is a common process, which is usually explained as a transformation of hematite to goethite due to the presence of organic

matter and/or higher water activity (Bigham et al., 1978a; Muller and Bocquier, 1987; Cornell and Schwertmann, 1996; Peterschmitt et al., 1996). Formation of Al-rich goethite in topsoils is favoured by a set of pedoenvironmental conditions, which include higher Al activity caused by low pH, low activity of Si and more organic matter. These conditions are reported to favour goethite instead of hematite, as well as higher Al-substitution in goethites (Kämpf and Schwertmann, 1985; Tardy and Nahon, 1985; Schwertmann, 1988; Schwertmann and Taylor, 1989; Singh and Gilkes, 1992). The presence of considerable amounts of gibbsite in these surface soils corroborates it, indicating an environment of strong desilication and high Al-activity during the synthesis of goethite (Schwertmann, 1985; Anand and Gilkes, 1987). Furthermore, the higher substitution in Al of the goethites may be enhanced by the dissolution of more easily reducible low-Al goethites in (micro)environments periodically saturated with water (Couto et al., 1985; Jeanroy et al., 1991; Peterschmitt et al., 1996). Higher Al-substitution of iron oxides and xanthization of surface soils are common in tropical areas (Bigham et al., 1978; Fabris et al., 1986; Jeanroy et al., 1991). They are reportedly related to the present pedoclimate, and indicate that Al-rich goethite is the main product of contemporary pedogenesis (Kämpf et al., 1988)

Goethite, in contrast to hematite, is constantly forming throughout the soils during their evolution, which is well illustrated in the studied materials by its chemical and morphological variability. Properties of goethite are therefore more closely linked to the local soil forming environment than those of hematites (Fitzpatrick and Schwertmann, 1982; Fabris et al., 1985; Cornell and Schwertmann, 1996). The range of Al-substitution in goethites observed in the topsoils suggests either mixture of soil materials, change of pedoenvironments through time, or simultaneous micro-environments with different Al-availability. Therefore, the variability of goethite properties in profiles and within the same horizon (Table 5.3) reflects the polygenetic character of the soils. Variability in goethites within the same sample and horizon is indicated by other authors (Bigham et al., 1978; Friedl and Schwertmann, 1996), and is explained by non uniform environmental conditions or polygenesis ((Fitzpatrick, 1988; Kämpf et al., 1988; Motta and Kämpf, 1992). Polygenetic features in these soils were also indicated by micromorphology (see Chapters 3 and 4).

The differences found in the properties of hematites and goethites between the sequences on saprolites and on sediments, and within the profiles demonstrate that distinct environments have been operative in the past, either successively or simultaneously. Similar observations were also reported in studies carried out in other tropical areas (Kämpf and Schwertmann, 1995, Motta and Kämpf, 1992; Zeese et al., 1994).

CONCLUSIONS

Hematite and goethite are the sole iron oxides present in the studied materials. Micromorphology shows that during rock weathering on the stable parts of the landscape, hematite forms in the saprolites as 'droplets'. Gradual mixing with the other soil components

reduces the amount of droplets either by reducing their size or by dissolution, and results in the formation of an homogeneously red groundmass. Later (subrecent) pedogenesis caused preferential formation of goethite and transformation of hematite to goethite, which reached its maximum in younger topsoils formed on saprolites from eroded Oxisols in the stable parts of the landscape. This indicates that in these soils, hematite is not formed during the later stages of soil formation, but only reduced in size. The constancy of aluminium substitution and crystallite size in hematite from all samples corroborates this view. The aluminium substitution is low, because of the prevailing low aluminium availability during its formation.

Hematite in the sedimentary sequences appears to have two different origins. Part of it was present in the eroded soil materials that constitute the sediments. This inherited hematite has characteristics somewhat similar to those of the rock-saprolite sequences. In addition, hematite (and some goethite) accumulated from groundwater during (petro)plinthite formation. This second phase of iron oxide formation yielded larger crystallites with low aluminium substitution, because of its oxidation in larger pores where (i) pH is not low enough to supply Al, (ii) Al minerals are absent in the immediate vicinity, and (iii) other crystallization inhibitors are absent.

Goethite is less commonly formed in the saprolites and is therefore mostly a secondary product that more readily reflects the soil forming environment. In addition to oxidation from ferrous iron released from primary minerals, goethite in the studied materials apparently has two main modes of formation: (i) through oxidation of ferrous iron that accompanies hydromorphic processes, in water-conducting, bleached channels and; (ii) through conversion of hematite to goethite (xanthization) in soils, more conspicuously in recent topsoils. Al-substitution in goethite increases from the saprolites to the topsoils, in response to decreasing pH and Si-activity, increasing Al-activity, and presence of organic matter. In environments of periodic water saturation, as found in pseudogley channels in the soil-sediment sequences, goethite has a low Al-substitution and larger crystallite size.

The observed differences between amounts, mode of occurrence, physical, chemical and morphological properties of the iron oxides present in the studied soil sequences are good indicators of the distinct circumstances of weathering and soil formation in the polygenesis of these soils.

PART II

LASER DIFFRACTION GRAIN-SIZE STUDIES OF POLYGENETIC OXISOL SEQUENCES

Chapter 6
Peter Buurman, Tom Pape and Cristine C. Muggler, 1997.
Laser diffraction grain-size determination in soil genetic studies: 1.Practical problems.
Soil Science, 162(3): 211-218.

Chapter 7
Cristine C. Muggler, Tom Pape and Peter Buurman, 1997.
Laser diffraction grain-size determination in soil genetic studies: II.Clay content, clay formation, and aggregation in Oxisols from Minas Gerais, Brazil.
Soil Science, 162(3): 219-228.

Chapter 8
Cristine C. Muggler, Corine van Griethuysen, Peter Buurman and Thom Pape.
Aggregation, organic matter and iron-oxides' morphology in Oxisols from Minas Gerais, Brazil.
(submitted)

6. LASER DIFFRACTION GRAIN-SIZE DETERMINATION IN SOIL GENETIC STUDIES: I. PRACTICAL PROBLEMS

Peter Buurman, Tom Pape and Cristine C. Muggler

Abstract

Grain-sizing by laser diffraction cannot replace the classical combination of sieving and sedimentation, as long as correlations between the methods have not been established for many populations of samples. Nevertheless, grain-size determination by laser diffraction has a great potential for use in soil science, e.g., for detailed comparison of samples from the same origin to establish homogeneity of parent materials; for the study of textural changes caused by weathering; and for changes in aggregation. In particular, the amount of information relating to fine fractions, and the continuous distribution curves make the method very valuable. Correct determination of clay-size fractions depends on the choice of optical properties for the measured material: these have to be obtained for each kind of material, and change with pretreatment of the samples. Laser diffraction will always provide more detailed information than can be obtained by sieving and sedimentation. Practical problems are mainly sample homogeneity/sample size and flocculation. Ways to overcome such problems were tested and are discussed in this chapter.

Keywords: laser diffraction grain-sizing; clay formation; texture; optical model.

INTRODUCTION

Determination of grain-size distribution by laser diffraction analyses is widely used in industrial applications, for e.g. determination of homogeneity of powders, gels, etc. This method has already proven its usefulness in the study of sediments (McCave et al., 1986; De Boer et al., 1987; Singer et al., 1988; Agrawal et al., 1991; Loizeau et al., 1994), but soil scientists are slow to trade in the labour-intensive classical pipette method. This reluctance is mainly due to three factors: 1) insufficient confidence in the results of laser diffraction: studies on correlations of laser-clay with pipette clay are still very scarce; the correlations usually deviate from 1:1 and are then considered unsatisfactory, 2) in many countries, the pipette method has been accepted as an international norm for particle size analyses of soils, and 3) the high cost of laser diffraction equipment.

Nevertheless, laser diffraction analyses has a lot to offer to soil scientists, especially in those cases where the normative (i. e., pipette-method) clay percentage of a soil sample is not the issue. Most laser diffraction apparatuses nowadays offer a wide range of grain-size fractions that can be determined in one measurement without changing the suspension. The large range of fractions has the advantage that grain-size changes upon weathering, and changes in aggregation may be followed accurately. Such detailed studies can be done by sieving and pipette-method and have been carried out in the past, but are very time-consuming.

Results for the sieve method can be correlated with the laser diffraction method for sand-sized particles (Loizeau et al., 1994; Zonneveld, 1994), although the distributions obtained by laser diffraction usually have a slightly coarser median. Such a difference is usually explained by two factors: (i) the different number of fractions in the two methods precludes exact concurrence of medians, and (ii) particles that are not spherical are included in smaller sieve-fractions than their volume would indicate because the smallest diameter of a particle determines in which sieve fraction it is found.

Correlation of clay fractions determined by pipette method and by laser diffraction is usually unsatisfactory. This can be attributable to various factors: First, laser diffraction apparatuses have a lower detection limit, below which particles are not observed. This lower detection limit for the early generation instruments, which only use the Fraunhofer diffraction theory lies around 5 times the wavelength of the laser beam (in the case, 5 * 750nm = 3.75 μm). According to Bayvel and Jones (1981) the Faunhofer model is inaccurate below 5 μm. With the Mie theory, the limit is brought down to 0.4 μm. For still smaller particles, the Polarization Intensity Differential of Scattered Light (PIDS) is used. The PIDS system measured the light scattering intensity sequentially at two perpendicular optical polarization angles, at six angles of detection. The difference between the two intensities is proportional to the amount of particle material at one-third of the wavelength of the light. By using polarized beams of 450, 600, and 900 nm wavelength, information on particles approximately 0.15, 0.20, and 0.30 μm, respectively, is obtained. According to Coulter (1995), the PIDS can be used for particle sizes between 0.1 and 0.6 times the wavelength of the polarized beam, which extends the lower limit to 0.045 μm. The calculation method, however, has not been certified for non-globular particles. In the Coulter LS230 used in this research, and in various other newer models of other firms, the lower detection limit is 0.04 μm. Particles smaller than the lower detection limit are not seen. This may lead to an underestimate of the clay percentage in very fine clays (e.g. some montmorillonite clays). With instruments that use the Fraunhofer theory only, determination of the clay fraction is not possible.

Second, to properly use the Mie + PIDS calculation module, light absorption at four different wavelengths (the main laser beam and the three polarized beams) should be known for the sample that is measured. These characteristics are usually unknown, but they strongly affect the calculated grain-size distribution (Hoff and Bott, 1990), as will also be shown in this paper.

Third, both pipette method and laser diffraction theory are based on spherical particles. It is well-known that Stokes' law, which underlies the pipette method, is valid for spherical particles and that because "flat thin plates settle more slowly, ... the amount of such material may be overestimated" (Loveland and Whalley, 1991). Therefore, the clay fraction determined by pipette method is usually an overestimate, the extent of which will depend on the bulk of clay and, probably, on the size-distribution within the clay fraction.

In laser diffraction, platy particles are also considered equivalent to spheres, because circulation during the measurement results in random orientation (R. Xu, pers. com.). This would imply that the volume of such particles is overestimated.

In addition, there are a number of pitfalls in laser grain-size diffraction of soil samples, that have not been discussed in the published literature. The present paper is dedicated to the possibilities and pitfalls of laser diffraction grain-size analyses when applied to soil samples. In a second paper in this issue (Muggler et al., 1997; Chapter 7), some results of laser diffraction grain-size analyses in soil genetic studies are discussed.

MATERIAL AND METHODS

For the present study a sample of commercially available building sand and a number of peroxide and dithionite pretreated samples from Brazilian Oxisols were used. Details of the Oxisol samples are given in Chapter 7 and in Appendix 1.

Grain-size determinations were done with a Coulter LS230 laser diffraction grain-sizer with a 5mW, 750 nm laser beam. It has a range of 0.04-2000 μm, with 116 fractions. The channel (fraction-size) starts from 0.04 μm; each following channel is 1.098 times the size of the previous one. The software used in the calculations was version 2.05.

For calculation, the instrument uses optical models, which should contain the refractive index (r.i.) of the medium and the solids. Water was used as the medium (r.i. =1.33 at 20°C), and a refractive index in the range of that of kaolinite was used for the solid phase (r.i.=1.56). In addition, absorption values of light at the four different wavelengths must be entered (see below). The combination of refractive index of the medium, refractive index of the sample, and absorption of the laser beam and the polarized light, defines the optical model.

The laser grain-sizer works adequately only within a specific range of suspension density, defined as the 'obscuration index'. The machine indicates whether the obscuration index is in the correct range; usually around 10%. If the concentration of the suspension is too low, the results will become less reproducible and unreliable; if the concentration is too high, too much multiple-scattering occurs. Measurements of samples with low clay contents are usually carried out at an obscuration in the suspension of around 10%. In the measured samples, higher densities resulted in coarser median values. In clayey samples, the suspension density should be such that the PIDS obscuration is around 50%. In samples that have low contents of clay, the 50% PIDS obscuration *may* coincide with the 10% total obscuration. In some of the samples used in this study, however, which have very high clay contents, a 50% PIDS obscuration coincided with a 2-3% total obscuration, whereas a total obscuration of around 10% resulted in a PIDS obscuration of 90% or more. The effect of these differences in obscuration is also discussed below.

RESULTS

Sample size and sample homogeneity: adequate sample preparation

The suitable sample size for laser diffraction depends on the clay content of the sample because clay contributes strongly to obscuration. Coarse sands may require several grams of sample, whereas for fine clays, amounts as low as 100 mg may be adequate. Soil samples are notoriously inhomogeneous, and it is obvious that the representativeness of very small subsamples may be questionable. In samples that do not need pretreatment, e.g. clean sands or silts, this poses no problem because its is easy to repeat the analyses and determine a mean value. In soil samples, however, where an elaborate pretreatment is necessary to remove aggregation, replicates of subsamples are impractical.

As in the pipette/sieve method, samples for laser diffraction have to be pretreated to remove aggregation and dispersed to prevent flocculation; the effect of the latter is discussed in a separate section. For the combination of sieving and pipette method, samples of 20 to 50 g are required. If samples of this size are used for laser diffraction, a subsample must be taken from the pretreated sample. Such subsampling of wet samples or of suspensions that contain both a suspended and a non-suspended fraction is not feasible: it is virtually impossible to obtain a representative subsample, especially if the non-suspended fraction is coarse.

In the case of clayey samples, the best solution is the selection and pretreatment of small subsamples that are taken from dry or moist soil. With dry soil, care should be taken that sorting has not occurred in the storage vessel, and samples will have to be homogenized carefully before subsampling. Moist soil can be homogenized by kneading, either mechanically or by hand. In the present study, the use of an electric mixer to homogenize moist samples warranted a very good reproducibility of subsamples.

Subsampling of dry sands meets with the same problem as subsampling of dried soil. Moistening the sand and taking a subsample after careful mixing appears to be a good solution. This method was used on the sand samples reported later in this article. Because of the good reproducibility of subsamples from moist soil, it may be feasible to do subsampling for grain-size analyses before drying the samples.

Pretreatments such as peroxide and dithionite treatment work more rapidly with a small subsample, on the order of 1 g or less for clayey samples, than with larger samples. After pretreatment, the whole sample is transferred to the measuring vessel of the grain-sizer. Usually, obscuration will still be too high. A first dilution can be obtained by adding more water to the vessel until the maximum fluid level is reached. If the correct obscuration cannot be obtained this way, part of the suspension is removed from the vessel while the circulation pump is working at full speed. After partial removal of the suspension, more water can be added until the correct obscuration is obtained. Partial removal of the suspension can be repeated, if necessary. The possibility of loss of coarse material by this dilution method was

investigated and is discussed in the next section.

Loss of coarse fractions through sample dilution in the measuring vessel

The dilution method described above is not likely to affect fine fractions, because the fluid is circulating at high speed and fine fractions should be distributed homogeneously throughout the suspension. To test whether coarse fractions were affected, a number of experiments were carried out. A coarse sand sample with a range in grain-sizes of about 100 to 2500 µm was used for the experiments. First the sample was sieved through a 2000-µm sieve to bring it to grain-sizes within the measurable range of the Coulter LS230 grain-sizer. Apart from the bulk sample, sieve fractions were also prepared by passing the sample through a 600- and a 300-µm sieve. For each of the fractions, bulk, >600, 300-600, and <300 µm, two separate measurements were done:

1) adding sample to the measuring vessel until the correct obscuration was obtained, followed by measurement.

2) adding sample until an obscuration of 22% was obtained and then diluting, by the method described above, to the same obscuration as used in (1), after which the measurement was carried out.

Each of the measurements was repeated with new subsamples and fully overlapping distributions were obtained in all cases.

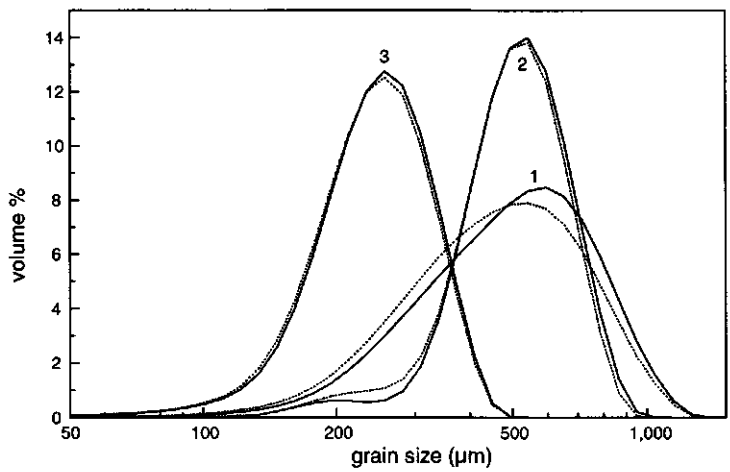

Figure 6.1: The effect of dilution in the sample measuring vessel for sandy samples. Sample pairs are: (1) total sample; (2) sieve fraction 300-600 µm; (3) sieve fraction <300 µm. Drawn lines: additive samples; dashed lines: diluted samples. Measurements were done at equal obscuration.

Figure 6.1 shows that the dilution procedure, compared to the addition procedure, caused virtually no change of grain-size distribution in the <300 and 300-600 μm fractions (curve pairs 3 and 2). In each of these cases, the curve obtained by dilution shows a negligible shift to smaller grain-sizes. The median values were 259 and 539 μm in the additive samples, versus 255 and 527 μm in the diluted samples (curve pairs 2 and 3). In the total sample (curve pair 1), there appears a slight loss of the coarsest fractions as a result of the dilution procedure and a shift of the median towards lower values (medians are 526 and 487 μm). A similar effect was found in the fraction >600 μm.

It means that the above described dilution can be used without changing the grain-size characteristics for samples with the coarsest components finer than about 800 to 1000 μm, whereas it may cause changes in coarser samples. The measurements were carried out with quartz-rich sands; therefore, the grain-size at which significant errors are introduced will be smaller for samples with high contents of heavy minerals and ores. High contents of clay may diminish the effect because this increases the viscosity of the fluid.

The optical model

The Coulter LS230 grain-sizer calculate the very fine fractions with the aid of Polarization Intensity Differential Scattering (PIDS). Two polarizations of three wavelengths (450, 600, and 900 nm) are used for the measurement. The optical model contains the following parameters: (i) refractive index of the medium (1.33 for water at 20°C), (ii) refractive index and light absorption by the sample, for the 750 nm laser beam, and for each of the polarized wavelengths.

In many soil samples, the suspended material is predominantly clay minerals and quartz. These minerals have refractive indexes in the same range: 1.48-1.61 for smectites, 1.54-1.57 for illites, 1.55-1.56 for kaolinites, 1.52-1.56 for vermiculites, and 1.54 for quartz (Deer et al., 1992). Within this range of refractive index, the differences have a negligible effect on the calculations. The chosen optical model was tailored for kaolinite and quartz-dominated samples, using a refractive index of 1.56.

Absorption coefficients for minerals, however, at the wavelengths of the laser beam and the three polarized wavelengths, are scarce. Absorption at various wavelengths are known for a number of pigments and refractory materials, such as kaolin, ochre, enamels and carbon black (Weast, 1974; Table E228). Values for absorption by soil samples are not available. Nevertheless, the influence of these absorption coefficients on the calculated grain-size distribution is very strong, as shown in Figure 6.2. Figure 6.2a shows the distribution curves of sample BR05 (67% pipette clay) at 10% PIDS obscuration, calculated with two different models. Figure 6.2b shows the curves of BR01 (78% pipette clay) at 50% PIDS obscuration, calculated with three different models. The parameters of the three models are given in Table 6.1.

Table 6.1: Parameters of the calcualtion models used in the distribution curves of Figure 6.2.

	Refractive	Absorption coefficients			
	Index	750 nm (laser)	450 nm	600 nm	900 nm
Curves 2,3	1.60	0.0	-	-	-
Curves 1,4	1.56	0.15	0.2	0.2	0.2
Curve 5	1.56	0.8	-	-	-

Figure 6.2b shows that a model without absorption (curve 3) results in a discontinuous grain-size distribution, with a minimum at 1 μm. If realistic parameters for kaolinite are entered, the curve has a maximum around 0.07 μm, from which it tails down to larger grain sizes, without major discontinuities. At an absorption value that is certainly too high (curve 5), the distribution has distinct maxima and minima and shifts towards coarser grain sizes. The effect in sample BR01 at 10% obscuration is less dramatic (Fig 6.2a), but increasing the absorption of the polarized beams from 0 (curve 2) to 0.2 (curve 1) also results in an increase in fractions below 1 μm.

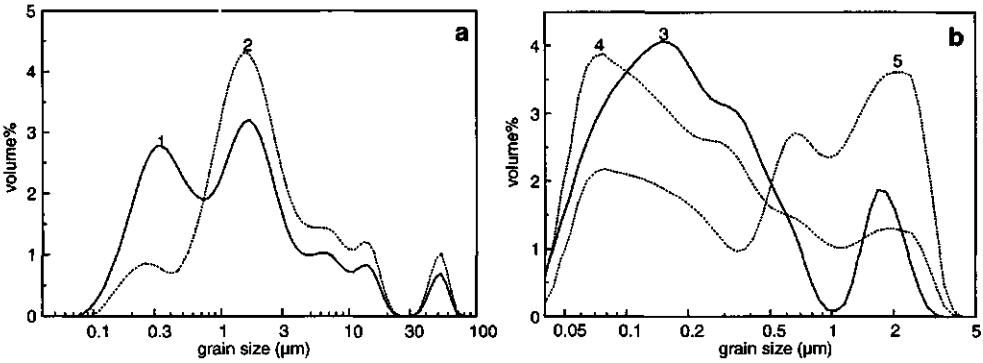

Figure 6.2: The effect of optical model on the calculated grain-size distribution: **(a)** Curves 1-2: Sample BR05, peroxide-dithionite treated, obscuration 10%; **(b)** Curves 3-5; Sample BR01, peroxide-dithionite treated, PIDS obscuration 50%. Optical model parameters are listed in Table 6.1.

Because the calculation model converts the polarization and foreward-diffraction intensities to isometrical particles, it is clear that a direct correlation with the size of clay platelets is not unity. Nevertheless, when the same optical model is used, comparison between samples of the same origin is feasible.

Soil samples that have not been deferrated do frequently have colors that are not white, but yellowish, brownish, or reddish. Such colors may influence the PIDS measurements because the absorption of each of the three wavelengths changes. The best way to measure absorption values for calculation models is to remove part of the suspension from the measuring vessel after the laser diffraction measurement and measure absorption directly in this

suspension (suspensions should be kept in a shaker until the adsorption is measured). Adsorption measurements are needed for both 10% obscuration and 50% PIDS-obscuration suspensions. The mean absorption values at four wavelengths (450, 600, 750, 900 nm) for a number of samples of the same origin and pretreated the same way, can be used to construct an optical model that is adequate for these samples. After obtaining the new optical model, the grain-size distributions of the pertinent samples have to be recalculated with the new model. The calculation model for the fine fractions may result in minor maxima and minima superimposed on an otherwise continuous grain-size distribution (see Fig. 6.2b, curve 4).

The problem of flocculation

Clays tend to flocculate at varying concentrations of cations. Such flocculation can be avoided when the samples have undergone complete pretreatment (peroxide, dithionite, washing, surfactant). In all other circumstances, there is always a risk of flocculation, especially when untreated samples are measured, and when the tap water is saturated with calcium bicarbonate. The presence of flocculation, even when suspected, is difficult to ascertain in samples with a wide range of grain sizes, because the flocs may have the same size range as that of primary particles. Flocculation can be eliminated by sonication, either with the internal sonication system, or through sonication before transfer of the sample into the measuring vessel.

Figure 6.3 illustrates the effect of flocculation by comparing the measurement of a sample with and without dispersant and sonication. When the sample from which organic carbon and iron had been removed is put into the measuring vessel, using tap water as a medium, and measured immediately, the distribution shows particles in the range of 100 to 400 μm (curve 2). When 50 ml sodium pyrophosphate 1% is added to 1 l of suspension, and sonication is used, this size fraction disappears (curve 1). Curve 1 does not change further with time, and it is safe to conclude that flocculation is absent because similar distributions were also found in related samples that were sonicated vigorously. In another kaolinitic sample, which had been sieved through a 50-μm sieve and dispersed in bicarbonate-rich water, flocs in the ranges of 60 to 350 μm and 500 to 800 μm were observed. They remained stable even at the high speed at which the suspension is pumped through the apparatus (16 l/min). These flocs also disappeared upon addition of pyrophosphate and sonication. Such stability of flocs was also reported by Gibbs (1982) for slightly different circumstances. An interesting fact is that in all observed cases, the ranges of floc sizes are discrete and not continuous.

The experiments illustrate that the application of a surfactant, sometimes in combination with sonication, is necessary for clayey samples. If sonication shifts the grain-size distribution to smaller sizes, flocculation is probably present.

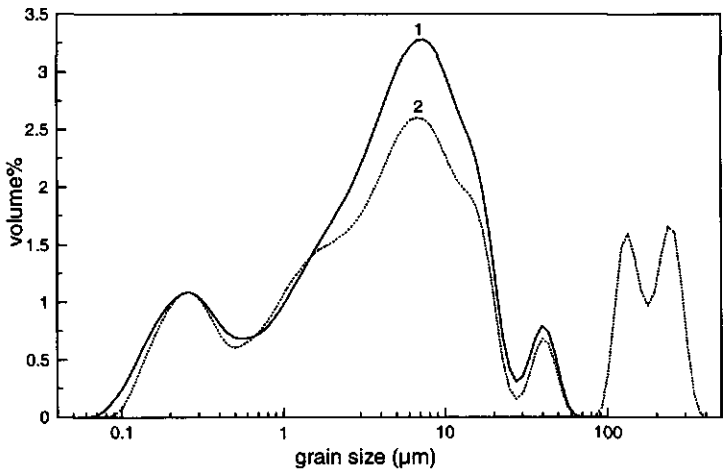

Figure 6.3: The effect of flocculation on the grain-size distribution curves (sample BR01, 10% obscuration); Curve 1: with sodium pyrophosphate and sonication; Curve 2: in water without further treatment.

The effect of suspension density

When samples with high clay contents are measured at 10% total obscuration, the PIDS obscuration, which must be around 50%, is usually far too high. This causes improper functioning, or even complete blocking, of the PIDS system. Therefore, when the PIDS system is used, as it will in all samples that contain an appreciable amount of clay, suspension concentrations usually have to be lowered. In high-clay samples, concentrations at which the PIDS measurement is adequate usually have about 3% obscuration (rather than the 10% used in coarser samples).

If soil samples that have a large clay fraction are measured at 50% PIDS-obscuration, fractions coarser than 5-10 µm may not be detected. The cutoff grain size depends on the clay content and distribution within the fine fraction. This 'disappearance' of coarse fractions is illustrated in Figure 6.4. The figure shows two curves of sample BR01, which is rich in fine clay, and two of sample BR06, which has more silt. The measurements were done at the obscurations given in Table 6.2.

If sample BR01 is measured at the correct PIDS obscuration (50%; curve 2), particles larger than 4 µm are not found in the distribution because the signal-to-noise ratio on the relevant detectors is too low. Measured at correct obscuration for the total sample (10%; curve 1), larger particles do appear, but information about the fine fractions is lost. Because these silt fractions have been measured by pipette method, they are surely present in the sample and are not artifacts caused by dense suspensions or flocculation. Sample BR06 has a much lower clay fraction, and here the two measurements (curves 3 and 4) are similar.

'Disappearance' of coarse fractions occurred both in the Brazilian samples reported on in this paper and in fine clay samples from other locations. It appears to be a problem in all samples with more than 50% pipette-clay. This means that neither of the measurements gives a complete picture of the grain-size distribution in very clayey samples. The measurements were carried out with software version 2.05. The new software version 2.09 has improved the detection of coarse fractions in predominantly fine materials but has not overcome the problem.

Table 6.2: Obscuration indexes of the measurements presented in Figure 6.4.

Sample	Obscuration	PIDS obscurations
BR 01a	9% (correct)	97%
BR 01b	2%	53% (correct)
BR 06a	10% (correct)	91%
BR 06b	2%	52% (correct)

In curve 2 of Figure 6.4, the grain-size distribution below 1 µm shows a maximum around 0.075 µm and two minor maxima at around 0.3 and 0.65 µm. The minor maxima should be attributable to the mathematical model, which makes optimal use of the polarization data in the range of 10% to 60% of the wavelength of each beam. It is already clear from Figure 6.2, that the optical model influences the location and the extent of maxima and minima.

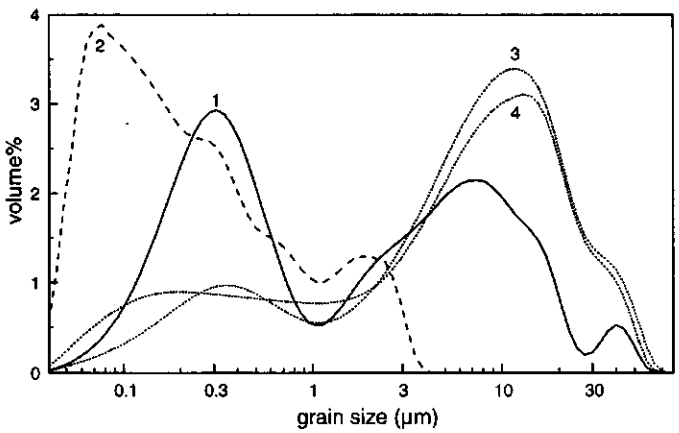

Figure 6.4: The effect of suspension density on calculated grain-size distribution: Curves 1,2: Sample BR01 at 10% obscuration and 50% PIDS, respectively; Curves 3,4: Sample BR06 at the same settings.

The correlation with pipette clay

Correlation between pipette-clay and laser diffraction-clay has been a main concern for various users of laser diffraction. The clay contents determined by laser diffraction are systematically lower than those determined by pipette method. According to Loizeau et al. (1994) the fraction that is detected by laser diffraction is proportional to the clay content determined by pipette-method. Various Dutch users of laser diffraction, both in the Free University of Amsterdam and in the State Geological Survey (pers. com.) have suggested that the fraction <8 μm of laser grain-size distributions (measured with the Fraunhofer model only) would show a good 1:1 correlation with the <2 μm fraction of the pipette method. Although such a correlation may hold true in some sets of samples, it is unlikely that it is universal.

Laser grain-sizers have a lower detection limit below which particles are simply not detected, irrespective of their abundance, and, therefore, are not measured. The grain-size distribution may hint at the existence of such small fractions when the lower end of the distribution curve does not tail to the baseline. For those grain-sizers that only use the Fraunhofer model for calculation, this lower boundary is around 3.5 μm. With the Coulter LS230, using the PIDS module, the detection limit is 0.04 μm. Therefore, any correspondence between the numerical fraction <8 μm (laser) with <2 μm (pipette) is not caused by ill-defined grain-sizes, either in laser diffraction or in the pipette method, but rather by the shape of the distribution curve on the clay and fine silt range. This 1:1 correlation will therefore be restricted to samples of a similar origin.

It is unlikely that a universal correlation between laser-clay and pipette-clay will be found, because aspect ratios of populations of particles vary according to their origin or genesis. Good correlations, however, have been reported for samples of similar origin (e.g. Loizeau et al., 1994). Very good correlations (r^2=0.98, n=50) were obtained between laser diffraction (10% obscuration) and pipette fractions <2, <4, <8, <16, <32, and <50 μm for Dutch fluviatile clays (unpublished data). Measured contents will be more similar in soils with coarse clays than in those with fine clays. It is logical that models that use only the main laser beam and the Fraunhofer scattering model will generally detect only a fraction of the clay, whereas extended models that use PIDS will detect a larger fraction. How much of the clay fraction is actually detected by the laser diffraction/PIDS method, will, however, depend on the grain-size distribution of the clay fraction itself.

CONCLUSIONS

Laser diffraction grain-size analyses have a high reproducibility, but the method contains a large number of pitfalls for clayey samples. Problems of sample homogeneity and subsample representativity can be solved by thorough mixing and, in some cases, by dilution of the suspension in the sample measuring vessel. Loss of coarse fractions by such dilution

appears to be negligible if the samples are finer than 1000 μm. For samples with coarser particles, this method should not be used without further verification.

An adequate optical model is the main issue for obtaining a correct distribution in the clay fractions. For refractive indexes and absorption coefficients, a 'kaolinite' model with absorption coefficients of approximately 0.2 shows good results on deferrated (white), kaolinitic samples. For coloured samples, adequate models can be constructed by light absorption measurements in suspensions at the concentrations that are used in the laser diffraction measurements.

In pretreated samples, flocculation can be avoided by ultrasonication and addition of dispersant. In untreated samples, where sonication should not be used, the amount of dispersant may need to be increased. Samples with large amounts of fine clay provide an extra challenge because upon measurement at the correct PIDS obscuration for clays, information on coarser fractions may be lost. On the other hand, measurement at correct total obscuration may result in complete blocking of the PIDS detectors and loss of information on the clay fraction. Correlations with pipette clay are best for the measurements at 10% obscuration, whereas maximum information on the distribution within the finest fractions is obtained by the measurement at 50% PIDS-obscuration.

When samples from a similar origin are measured with similar apparatus settings and calculated with the same optical model, the detailed grain-size distributions, especially in the fine fractions, give very valuable information for soil genetic studies (see Chapter 7). The amount of detail provided allows detection of small lithological discontinuities, which go unnoticed by less discriminative methods. Correlation between laser and sieve method of sand sized fractions do not pose a problem, but it is unlikely that a generally valid correlation between laser-clay and pipette-clay will be found. Such correlations have to be established for each population of samples separately.

Because of its reproducibility, the determination of the clay and silt-size particles as carried out by sedimentation methods, has become an international standard. The reproducibility, however, does not prove that the measured fractions agree with the predetermined grain-size intervals, and it is well known that interlaboratory variability of the method is considerable (Loveland and Whalley, 1991; Pleijsier, 1986). Sizes of colloidal, platy particles cannot be determined absolutely either by the pipette-method or by laser diffraction. Because correlations between pipette clay and laser diffraction clay are not 1:1, laser diffraction cannot replace the former method unless correlations for separate populations of samples are established. Nevertheless, when used carefully, and with proper sample pretreatment, laser diffraction gives reproducible results that can be used to compare samples and to gain insight into changes within the clay fraction and in coarser fractions.

7. LASER DIFFRACTION GRAIN-SIZE DETERMINATION IN SOIL GENETIC STUDIES: II. CLAY CONTENT, CLAY FORMATION, AND AGGREGATION IN OXISOLS FROM MINAS GERAIS, BRAZIL.

Cristine C. Muggler, Tom Pape and Peter Buurman

Abstract

Grain-size determination by laser diffraction can be a very useful tool in soil genetic studies. The laser diffraction grain-sizer provides much more detailed information than classical methods, which is very useful for identifying particle size shifts, especially in the smallest size fractions. In three deeply weathered soil profiles from Minas Gerais, Brazil, changes in clay content, grain-size distribution of the clay fraction, and disappearance of silt fractions as a result of weathering have been identified. Good correlations were found between pipette-clay and laser-clay, but never a 1:1 correlation. For very clayey samples, maximum information is obtained by measuring at two optical densities of the suspended material. The grain-sizer is also a useful tool in studies of soil aggregation. In the studied soils, a clear change of aggregation with depth could be followed. Sequential removal of organic matter and free iron indicated that the aggregation may be due to organic matter rather than to iron sesquioxides.

Keywords: Brazil, Oxisols, laser diffraction grain-sizing, clay formation, aggregation.

INTRODUCTION

Common settling velocity-based grain size analysis methods do not provide much information about the small-size end of the particle distribution range. The sedimentation-based methods are very time-consuming when dealing with particle-size ranges smaller than 2 μm, and for sizes smaller than 1 μm the results are increasingly unreliable because of Brownian motion (Allen, 1981; Loveland and Whalley, 1991). If further resolution is desired to get a better insight of changes in the smallest size fraction of a soil or sediment, other methods need to be used. Of the instrumental techniques and developments (Barth, 1984; Singer et al, 1988), the laser diffraction-based grain-sizers show great potential, especially if the issue is not a reference value of clay contents but, for example, particle size shifts in the clay and fine silt fractions. It is well known that the size distribution in the clay fraction of soils may vary considerably and can influence soil behaviour greatly.

The previous chapter discussed some of the problems related to the use of laser diffraction grain-size data in soil studies and the methodology adaptations for the proper use of the laser grain-sizer. This chapter illustrates some of the applications of laser diffraction in studies of soil genesis and investigates the correlation between pipette-clay and laser-clay for the studied samples. Formation and distribution of clay as a result of weathering, and aggregation are emphasized. Also, the detailed information on grain-size distribution within the silt and clay fractions provided by the laser diffraction technique is examined.

MATERIALS

Three deeply weathered Oxisol profiles from Brazil were selected for this study. The soils are classified according the Soil Taxonomy system (Soil Survey Staff, 1994), as Anionic Acrudox (P1); Typic Haplustox (C1), and Inceptic Haplustox (C4). Profile P1 is formed on metapelites and profiles C1 and C4 on pelites. P1 and C1 are fairly complete profiles. C1 and C4 are from the same catena and share the same parent material, but C4 represents a fairly recent soil, developed in the saprolite of the older soil. The parent materials are essentially fine- and medium-textured rocks consisting mainly of quartz and mica. The weathering products are rich in iron and predominantly kaolinitic in mineralogy. Clay contents in the topsoil of the uneroded Oxisols are very high. Some general properties of the soils are presented in Table 7.1. Complete profile descriptions and chemical routine analyses are provided in Appendices 1 and 2.

METHODS

After having been air-dried, crushed and passed through a 2 μm sieve, the samples were submitted to three pretreatments: (i) overnight shaking in deionized water (treatment for 'natural' clay); (ii) removal of organic matter through oxidation with hydrogen peroxide followed by overnight shaking with a dispersing agent (30 ml of 5% sodium pyrophosphate) and (iii) removal of organic matter and deferration by dithionite-citrate-bicarbonate (DCB) extraction also followed by overnight shaking with dispersing agent.

The grain-size distribution was determined by both sieving and pipette method (Van Reeuwijk, 1995) and by laser diffraction. A Coulter LS230 laser grain-sizer, software version 2.05, with a range of 0.04 to 2000 μm, in 116 fractions was used. The apparatus uses a 5-mW, 750 nm laser beam. The calculation model uses Fraunhofer and Mie theory, which is applicable down to grain-sizes of about 0.4 μm. For grain-sizes in the 0.04 to 0.5 μm range, the Coulter instrument uses the PIDS technology (Polarization Intensity Differential Scattering), with the Mie-theory for calculation. The calculation model used water as the medium (r.i.=1.33 at 20°C), a refractive index in the range of that of kaolinite for the solid phase (r.i.=1.56), and absorption coefficients of 0.15 for the 750 nm laser wavelength and 0.2 for the polarized wavelengths.

During the measurements, samples were diluted, if necessary, as described in Chapter 6 (Buurman et al. 1997), using normal tap water. For peroxide- and dithionite-treated samples, 10 ml of 5% sodium pyrophosphate were added to the suspension in the measuring vessel (approx. 1 l), and 50 ml to the water-dispersed samples to avoid flocculation. The measurements were done at 10% obscuration for all samples (laser10) and also at 50% PIDS obscuration (laser50) for all deferrated samples and for the peroxide-treated samples of profile C1.

Table 7.1: Main chemical properties and clay mineralogy of the studied soil materials.

Prof.	horizon	C	pH	pH	CEC	Base sat	Free Fe[1]	Fe_2O_3[2]	Qualitative clay mineralogy[3]			
		%	H_2O	KCl	cmol/kg	%	%	%	Ka	Gb	Gt/Hm	Vm/Mi
	A	2.3	4.8	4.7	5.6	15	6.2	24.1	++++	++	++	-
	BA	1.1	5	5.8	5.9	0	6.5	23.7	++++	++	++	-
	Bw1	0.9	5.2	6.2	6.0	0	6.4	24.8	++++	++	++	-
	Bw2	0.6	5.4	6.5	5.7	0	6.9	25.0	++++	++	++	-
P1	Bw3	0.4	5.6	6.6	5.2	0	7.3	24.8	++++	++	++	-
	BC1	0.2	5.5	6.0	4.6	0	7.4	22.1	++++	++	++	-
	BC2	0.3	5.5	5.0	4.3	1	7.6	20.2	++++	++	+	-
	BC3	0.2	5.5	4.8	3.8	0	8.6	20.2	++++	++	++	-
	C	0.0	5.3	4.6	4.8	0	7.4	19.6	++++	tr	++	-
	A	2.2	5.1	4.4	6.7	21	5.1	11.6	++++	++	+	++
	AB	1.2	4.6	4.3	6.6	2	5.4	12.3	++++	++	+	+
	Bw	0.4	4.6	4.5	5.3	0	5.4	12.6	++++	++	+	++
C1	BC1	0.6	5.0	4.7	5.9	0	5.4	12.4	++++	++	+	++
	BC2	0.6	5.1	4.8	5.7	0	5.5	12.5	++++	++	+	++
	BC3	0.5	5.0	5.3	6.2	2	5.3	12.9	++++	++	+	++
	BC4	0.4	5.2	5.1	5.9	0	5.7	12.5	++++	++	+	++
	BC5	0.4	5.2	4.6	5.3	0	6.2	12.6	++++	++	+	+
	Bw	1.0	4.8	4.2	5.1	1	2.4	6.3	++++	++	+	++
	BC1	0.6	5.2	4.4	6.3	0	3.0	7.2	++++	+	+	++
C4	BC2	0.3	4.4	4.2	7.2	0	3.0	6.6	++++	tr	+	++
	C1	0.2	4.7	4.2	7.6	0	2.7	5.9	++++	tr	+	++
	C2	0.2	4.7	4.2	7.3	5	3.3	6.8	+++	-	tr	+++
	C2	0.1	4.6	4.3	6.4	1	3.0	6.1	+++	-	tr	+++

[1] DCB extraction; [2] 900°C ignited, XRF; [3] Ka: kaolinite; Gb: gibbsite; Gt/Hm: goethite and/or hematite; Vm: vermiculite and/or mixed-layer clay mineral; Mi: mica.

RESULTS AND DISCUSSION

Comparison of pipette and laser clay contents

The clay contents obtained for the samples after pretreatments 2 and 3, by both methods are shown in Table 7.2. In all determinations, the 10% obscuration (laser10) measurements detected less clay than the 50% PIDS obscuration (laser50). The lower clay contents detected by laser10 are partially explained by improper functioning (too high absorption) of the PIDS system in concentrated suspensions, with a resulting loss of information in the range of 0.04 to 0.5 μm. Indeed, the difference between laser10 and laser50 results increases with clay content. Figures 7.1 and 7.2 show a comparison between the various measurements for the three profiles.

Table 7.2: Clay contents obtained by pipette and laser diffraction methods after three pretreatments, of three profiles from Minas Gerais, Brazil.

		Water dispersed		Peroxide treated			Peroxide+dithionite treated		
Prof	Horizon	Pipette	Laser10[1]	Pipette	Laser10	Laser50[2]	Pipette	Laser10	Laser50
					%				
	A	8.4	14.4	78.1	67.2	nd	79.7	53.4	93.7
	BA	1.7	10.8	78.4	60.9	nd	80.1	49.1	74.0
	Bw1	2.8	15.1	72.8	56.4	nd	78.9	50.5	82.9
	Bw2	20.6	38.4	68.0	48.3	nd	76.7	43.0	80.7
P1	Bw3	21.3	22.3	67.0	46.7	nd	72.5	39.0	69.6
	BC1	13.8	16.9	48.0	34.4	nd	51.4	23.9	30.5
	BC2	2.4	14.5	32.2	22.3	nd	33.8	13.3	19.7
	BC3	0.4	13.4	26.2	19.5	nd	28.6	12.7	17.0
	C	0.5	8.6	6.8	11.0	nd	8.6	8.8	10.7
	A	13.7	nd	69.6	54.6	84.9	72.1	45.2	78.6
	AB	4.4	nd	72.5	56.3	95.9	70.3	47.1	86.0
	Bw	0.2	nd	72.2	61.4	85.5	73.6	48.9	92.0
C1	BC1	0.3	nd	71.5	60.7	93.3	70.2	44.6	91.6
	BC2	0.3	nd	69.7	56.5	85.4	70.2	41.7	88.4
	BC3	3.1	nd	72.2	60.2	89.9	73.5	43.4	94.2
	BC4	0.5	nd	73.1	62.2	91.9	68.2	41.3	85.1
	BC5	0.3	nd	67.0	45.1	92.0	67.4	40.5	91.5
	Bw	7.3	nd	38.6	30.0	nd	36.7	19.7	24.1
	BC1	0.2	nd	39.3	27.6	nd	38.6	18.9	22.7
C4	BC2	0.3	nd	28.8	23.2	nd	28.7	17.2	20.3
	C1	0.3	nd	24.1	22.6	nd	22.9	15.9	17.3
	C2	0.2	nd	19.9	21.4	nd	21.8	16.9	17.1
	C2	0.2	nd	17.4	19.5	nd	19.4	16.1	17.8

[1] at 10% obscuration; [2] at 50% PIDS obscuration.

Profile P1 (Figure 7.1) shows a wide range of clay contents, as is expected for an Oxisol sampled from the surface down to the saprolite. Pipette clay decreases regularly from the top to the bottom, and clay contents increase slightly after deferration. Laser10 clay contents also decrease from the top to the bottom, but measured clay contents are lower. The laser10 clay contents are higher before (per/l10) than after (dit/l10) deferration, probably because the same optical model was used for both measurements and this model is not adjusted to the red colors of the peroxide-treated samples. This problem was already pointed out in Buurman et al., 1997 (Chapter 6).

Profile C1 (Figure 7.2a) is a very homogenous, deeply weathered profile, comparable to the top of profile P1. It has similar pipette-clay contents prior to and after deferration. Again, the laser10 clay contents are lower than pipette-clay figures. The very high clay contents measured at

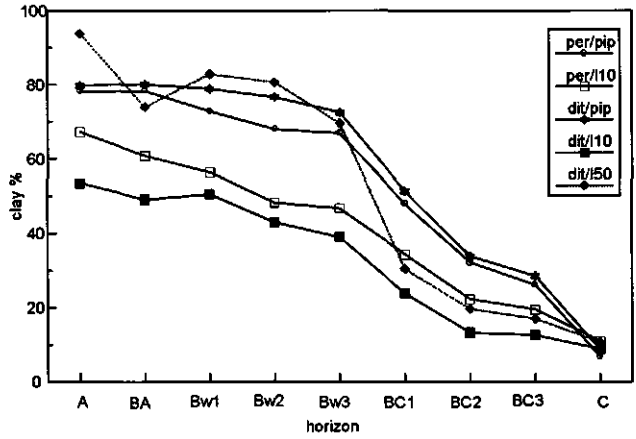

Figure 7.1: Clay content distribution curves of profile P1 samples obtained by pipette (pip), laser 10 (l10) and laser 50 (l50) methods after peroxide pretreatment (per) and peroxide+dithionite pretreatments (dit).

laser50 are probably due to the 'disappearance' or underestimate of the coarser fractions that was previously reported (see Chapter 6). As in profile P1, laser10 clay contents for peroxide-treated samples are higher than those for deferrated samples.

Profile C4 (Figure 7.2b) is a shallower soil, developed in the saprolite of an eroded Oxisol. Pipette clay contents are similar for peroxide-treated and deferrated samples, and show an increase towards the surface. Trends are similar to those of the BC2 to C horizons of P1.

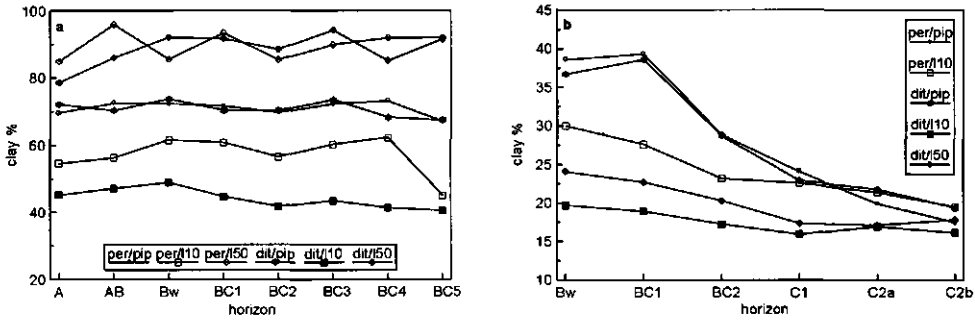

Figure 7.2: Clay content distribution curves obtained by pipette (pip), laser 10 (l10) and laser 50 (l50) methods after peroxide pretreatment (per) and peroxide+dithionite pretreatments (dit) of samples from (**a**) profile C1; (**b**) profile C4.

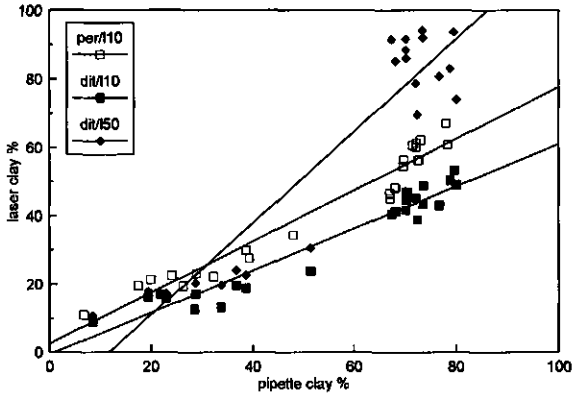

Figure 7.3: Correlations between pipette-clay and laser-clay for peroxide (per); and peroxide-dithionite treated samples (dit) at 10% total obscuration (l10) and at 50% PIDS obscuration (l50).

Figure 7.3 gives correlations between laser and pipette clay contents for all samples of the three profiles. The general correlations are good, especially for the laser10 measurements of peroxide and peroxide-dithionite treated samples (Table 7.3). The figure indicates that correlations for samples with high clay percentages alone will be unsatisfactory. This is due to both the relatively small range in clay contents in some cases and to increasing errors in the pipette method as a result of high suspension density. Errors in the laser50 measurement at high clay contents have already been mentioned. Correlations for the samples with clay contents less than 60% have r^2 values similar to those of the whole population, but have different slopes (Table 7.3).

Table 7.3: Correlations between pipette clay and laser clay (laser clay = a+b * pipette clay).

method	samples	a	b	r^2	n
peroxide/ laser10	all	2.46	0.75	0.91	23
	<60% clay	8.84	0.51	0.91	10
dithionite/ laser10	all	-0.61	0.62	0.94	23
	<60% clay	8.1	0.28	0.66	10
dithionite/ laser50	all	-15.67	1.34	0.89	23
	<60% clay	7.39	0.42	0.92	10

For peroxide/dithionite-treated samples, the correlation between pipette method and laser10 measurement has a lower r^2 value for the low-clay samples than for the total population, which is probably because of an outlier in this small number of samples. For samples with pipette-clay contents less than 60%, the correlations between laser- and pipette-clay contents are good and allow comparison of results, at least for samples from a similar origin, as was also reported by Loizeau et al. (1994). At higher clay contents, correlations between the methods are not satisfactory, both because of problems in the laser calculation module (underestimate of coarse

fractions at low suspension density and incorrect PIDS functioning at high suspension density) and errors in the pipette method (Singer et al., 1988; Loveland and Whalley, 1991).

Weathering effects: silt dissolution and clay formation

The changes in grain-size distributions of deferrated samples by profile give a good insight to the effects of weathering and soil formation. Figure 7.4 shows some of the distributions of profile P1, at 10% obscuration and 50% PIDS obscuration, for deferrated samples. The laser10 measurements (Fig. 7.4a) give information on the whole sample, and the laser50 graphs (Fig. 7.4b) give more details on the fine fractions. Figure 7.4a shows that from the C horizon (line 9) to the top of the profile there is a distinct increase in fraction <1 μm. Horizons BC3 and BC2 are similar to C, and significant formation of clay is first noticeable in the BC1 horizon (line 6). The effect of the fine clay fraction on the dit/laser50 measurements is clearly seen in Figure 7.4. Larger fractions (maximum at 100 μm in C horizon, line 9), which are probably compound particles, disappear, and elementary silt-sized particles (maximum at 40 μm) are set free so that the distribution in the silt fraction shifts to smaller sizes. The comparison of these trends with the shifts in the fine fractions (Figure 7.4b), shows that there is a distinct increase of fine clay towards the topsoil (maximum below 0.1 μm), at the expense of coarse clay.

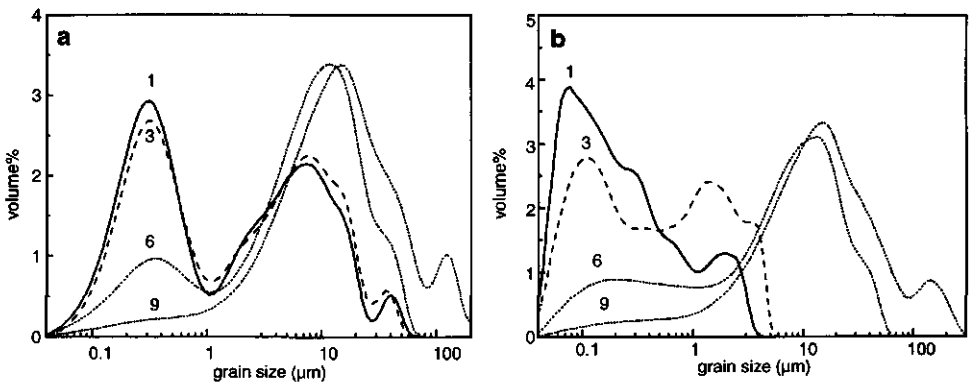

Figure 7.4: Laser 10 **(a)** and laser 50 **(b)** grain size distribution curves of some deferrated samples from profile P1; 1: A horizon; 3: Bw1 horizon; 6: BC1 horizon and 9: C horizon.

In both figures, the horizons that are not depicted have an intermediate position between the overlying and underlying horizons. The distribution observed for horizon Bw3 is closer to that of horizon Bw1 than to horizon BC1 (note the transition between horizons Bw3 and BC1 in Figure 7.1). Lines 1 and 3 in Figure 7.4b again demonstrate the 'disappearance' of coarse fractions in high-density suspensions when correct PIDS obscuration is used.

In profile C4, laser10 and laser50 curves show very little difference, and only the laser50

curves are shown (Figure 7.5). The horizons of this profile are not much mixed by burrowing, and, therefore, development trends are rather undisturbed. The distribution curves show formation of clay at the expense of fine silt, together with disappearance of the coarsest fraction (possibly disengagement of compound particles). The profile shows the early stages of weathering, rather similar to the transitional area between lines 6 and 9 (horizons BC1 and C) in profile P1. The coarse silt fraction shows a relative increase as a result of the disappearance of fine silt, but there is no shift in the size of the coarse silt fraction, which is dominated by quartz and probably not much affected by weathering.

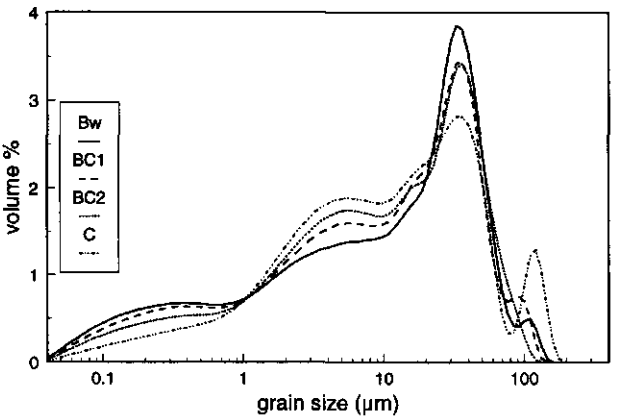

Figure 7.5: Laser50 grain-size distribution curves of some deferrated samples from the horizons Bw, BC1, BC2 and C of profile C4.

The grain-size distributions in profile C1 (Figure 7.6) are very similar for all horizons, and changes caused by weathering are not evident from the curves. This profile shows strong biological mixing over the sampled depth, and, therefore, development trends may be obscured. Both the laser10 and the laser50 curves indicate that the profile is intermediary between the topsoil and the subsoil of P1: it lacks both the shift towards very fine clay of the A horizon (line 1), and the very low clay contents found in the horizons BC1-C of P1 and in the whole of C4. Because of the high clay contents of the samples, all laser50 curves lack information on coarse fractions. The various maxima and minima that are found in the laser50 curves (Fig. 7.6b) are due to the calculation module (see Chapter 6). The fact that in all curves, the lower end does not tail to the baseline indicates that the samples contain finer fractions that are not measured because they are beyond the detection range of the apparatus.

Comparison of the three profiles indicates that profile P1 is a rather complete and continuous weathering sequence, whereas profiles C1 and C4 are more and less advanced stages of the same development. The deeper parts of profile C1 could not be sampled, but they are expected to have the characteristics of the much more eroded C4 profile, which is at a lower slope position in the same catena.

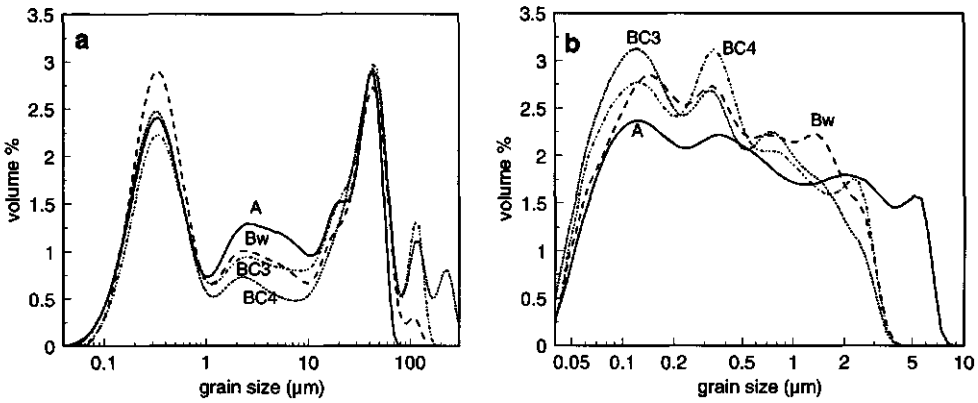

Figure 7.6: Laser10 **(a)** and laser50 **(b)** grain size distribution curves of deferrated samples from horizons A, Bw, BC3 and BC5 of profile C1.

Aggregation and water-dispersible clay

Aggregation in soils is usually studied by wet sieving, while a specific aspect of aggregation in Oxisols, the amount of water-dispersible clay, is determined by overnight shaking in water and determination of the clay fraction by pipette method. The question arises whether it would be possible to study both aggregation and water-dispersible clay through a combined measurement in the laser grain-sizer. The results of both classical methods depend strongly on experimental circumstances; therefore, inter-laboratory variation and even inter-operator variation may be considerable. Results of both methods are influenced by the water temperature, the moisture content of the soil at the moment of subsampling, and mechanical parameters such as the speed and amplitude of over-end shaking and the length of the sieve arm, and speed and frequency of movement in wet sieving (Jastrow and Miller, 1991)

Supposing that overnight shaking in distilled or deionized water has a similar effect to wet sieving (the similarity will depend on the parameters used in both methods), laser diffraction grain-sizing can be used to obtain detailed information on aggregate sizes as well as on dispersed fine fraction. However, if untreated samples are measured with laser diffraction, flocculation is likely to occur (see Chapter 6). Because flocculation may cause a discrete range of floc sizes and because it will decrease dispersed clay, its effect will interfere strongly with the interpretation of the measurements. Although, by definition, water dispersible clay by pipette method is determined without addition of dispersant (and the errors induced by this method are overlooked because they cannot be measured), the addition of dispersant during the measurement is necessary for laser grain-sizing because flocs form spontaneously, and ultrasonic treatment is, of course, out of the question. However, adding a dispersant to a sample that has been shaken overnight and that is being pumped around at high speed in the instrument should not make much difference. A clear advantage is that

the experimental conditions for which the measurements are made can be strictly controlled, and changes induced by different conditions can be accurately followed by laser diffraction grain-sizing.

Water-dispersible clay by pipette method was determined in all samples (Table 7.2). In profile P1, grain-size distributions by laser diffraction were determined for samples that had been shaken overnight with deionized water. 50 ml of a 5% Na-pyrophosphate solution were added to the sample in the measuring vessel before each measurement. Figure 7.7 shows the grain-size distributions of 'untreated' samples of profile P1, which illustrate differences in aggregation between horizons.

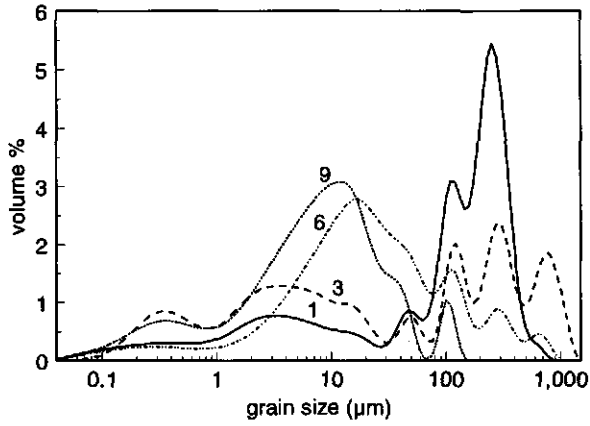

Figure 7.7: Laser10 grain-size distribution curves of some water-dispersed samples of profile P1; 1: A horizon; 3: Bw1 horizon; 6: BC1 horizon; 9: C horizon.

When comparing Figures 7.4a and 7.7, one has to disregard the effect of the difference in colour between the samples (white in Figure 7.4a, reddish in Figure 7.7). This is allowed, since the effect of color is smaller in laser10 than in laser50 measurements, and it is zero in the range coarser than 0.5 µm, which is not measured by the PIDS module. The figures show that aggregation is virtually absent in horizons BC1 and C (lines 6 and 9); the curves of the deferrated samples and the water-shaken samples are rather similar except for some aggregation above 200 µm in horizon BC1. In these samples there is hardly any reduction of clay-sized material because of aggregation. Aggregation is very strong in horizons A and Bw1 (lines 1 and 3), resulting in a strong reduction of clay-sized material and formation of aggregates that are much larger than the largest primary grains. Especially in the topsoil (line 1), where organic matter plays an essential role, the majority of particles is found in stable aggregates larger than 80 µm.

Comparison of results in Table 7.2 indicates that, in untreated samples, clay contents are higher when measured by laser diffraction (10% obscuration) than when obtained by pipette. This may be the result of strong flocculation in the water-dispersible clay determination or stronger dispersion in the grain-sizer caused by the high speed at which the suspension is pumped around.

Also the effect of dispersant cannot be ruled out completely. Flocculation was evident in laser diffraction when the samples were measured without addition of sodium pyrophosphate.

Comparison of pipette-clay percentages of peroxide- versus peroxide/dithionite-treated samples (Table 7.2) indicates that the increase in clay content upon deferration is negligible in most cases. This suggests that iron oxides are not a main aggregating agent in these soils.

CONCLUSIONS

Laser diffraction grain-sizing allows detailed study of small and larger shifts in grain-size distributions and aggregation that cannot be studied by classical grain-size methods. The addition of the PIDS technology provides detailed information on very fine fractions, which is of much interest in soil genetic studies. Even though correlations with pipette-clay can still be improved, the use of the PIDS technology has a positive effect on the detection of clay particles. On the other hand, to obtain maximum information on clayey samples, measurements at both 10% obscuration and 50% PIDS obscuration must be carried out.

In the studied Oxisols, formation of clay and decreasing of silt fraction due to weathering were clearly accompanied. Shifts in clay population/size are accurately followed by the laser method, and details of the size distribution in the clay fraction give further information on the development of this fraction.

Although experimental conditions at which aggregation can be optimally studied still have to be investigated, it is clear that the laser method can provide much new information in this field. At present, it should be mentioned that comparisons have to be made within a relatively homogeneous set of samples, such as a profile, a toposequence, or a specific provenance.

8. AGGREGATION, ORGANIC MATTER AND IRON OXIDES' MORPHOLOGY IN OXISOLS FROM MINAS GERAIS, BRAZIL

Cristine C. Muggler, Corine van Griethuysen, Peter Buurman and Tom Pape

Abstract

The characteristic strong aggregation observed in Oxisols is usually attributed to the presence of aluminium and iron compounds. Previous investigation of Oxisols from Minas Gerais, Brazil, suggested that iron compounds may not necessarily play a role in aggregation. Oxisol profiles developed on different parent materials (rock-saprolites and sediments), and with different degree of polygenesis were investigated in order to assess whether the form, rather than the content of iron determines aggregation. Oxisols were investigated by means of micromorphology and laser diffraction grain-sizing. Grain-size distribution curves were determined after three pre-treatments: shaking with water; removal of organic matter; and removal of organic matter followed by deferration. Micromorphology indicated that soils developed on rock-saprolites have hematite 'droplets' in the saprolite, while 'droplets' are not found in soils on Tertiary sediments. On the other hand, secondary iron accumulations related to periodic water saturation are encountered in the soils on sediments, and not in the soils on rock-saprolites. Grain-size distribution curves showed that the Oxisols on rock-saprolites do not have strong aggregation due to iron compounds alone. Conversely, aggregation by iron is evident in the Oxisols on sediments. This indicates that remobilization of iron during soil formation is essential for iron forms to play a role in aggregation. These findings suggest that the mode of formation and mineralogy of the iron compounds determines their eventual effect on aggregation.

Keywords: Brazil, Oxisols, laser diffraction grain-sizing, micromorphology, aggregation, iron forms.

INTRODUCTION

Oxisols tend to have very strong aggregation of primary particles, resulting in very low amounts of water-dispersible clay in B horizons (Deshpande et al., 1964; Russell, 1971; Soil Survey Staff, 1975). Most of the clay particles, predominantly consisting of kaolinite and/or gibbsite, are aggregated into secondary particles of 5-300 μm. Aggregation is usually attributed to the effect of (poorly crystalline) iron compounds, because removal of such compounds, either partial or complete, leads to dispersion (Michalet et al., 1993; Cornell and Schwertmann, 1996). Nevertheless, some authors found that iron compounds did not influence aggregation in Oxisols (Deshpande et al., 1968; Borggaard, 1982). Greenland et al. (1968) established that iron oxide particles in the clay fraction tend to be discrete particles that have little effect on aggregation.

Previous studies of Oxisols from Minas Gerais, Brazil (Muggler et al., 1997) indicated that iron compounds do not necessarily play a role in aggregation and led to a more detailed investigation presented in this chapter. The studied soils have undergone various phases of soil formation and erosion that are more or less superimposed in the profiles. During such an evolution, different circumstances of soil formation were active and resulted in distinct nature and morphology

of the iron oxides (see Chapter 5). Goethite and hematite are the sole iron oxides found in these soils. Goethite is found in all soils, although in very small amounts in very red soils. Hematite is also common, except in the yellow topsoils. Previous micromorphological and mineralogical studies (see Chapter 5) indicated that goethite is continuously forming and changing in response to the pedogenic environment, and that hematite may have at least two main modes of formation, in relation to the parent material of the soil.

In this context, it seems that different iron forms have different effects on soil aggregation. In order to investigate whether the form rather than the content of iron determines aggregation, laser diffraction grain-size distribution studies of Oxisols developed on both rock-saprolites and sediments were carried out. The laser diffraction technique was chosen because of its highly discriminative power, given by the 116 grain-size classes yielded between 0.04 and 2000 μm. This has the advantage of allowing a detailed tracking of the shifts in grain-size distributions.

MATERIALS

The studied material consists of fourteen deep and/or eroded Oxisol profiles from two areas in Minas Gerais, Brazil. The situation and physical aspects of the areas are described in Chapter 1, and the complete profile descriptions are given in Appendix 1. Some general characteristics of the soils are presented in Table 8.1. The soils are more or less polygenetic, and have developed on two main types of parent materials. Profiles P1-P5, P7, and P8 developed on fine- and medium-textured metamorphic rocks. They formed on the Early Tertiary *Sulamericana* surface, and have undergone various cycles of soil formation and erosion. P1 and P8 are the most complete profiles. P2-P5 were formed in the saprolite and/or subsoil layers of P1. They lack the red, oxic B horizon, but have a yellow topsoil due to recent soil formation. P7 is a younger shallow soil developed on deep layers of a saprolite with ferralitic characteristics exposed by erosion.

Profile P6 consists of superposed soils developed on Cenozoic sediments deposited in a graben zone formed by neo-Cenozoic tectonic activity. The sediments consist of remobilized soils and saprolites from the surrounding areas. Profile VP also formed on Tertiary sediments, which appear to be lacustrine deposits.

Profiles C1-C5 were formed on fine-textured sedimentary and slightly metamorphic rocks. Of these, C1 and C2 are the most complete profiles. C3 shows clear signs of erosion, but still has (part of) the red oxic B horizon. C4 and C5 formed in the saprolite of eroded Oxisols.

With the exception of the profiles P2-P5 and C4-C5, which have yellow surface soils, the other soils are dominantly red, although they present some yellowing in the topsoil, due to recent pedogenesis. Profiles P1-P8 and VP are now in an udic moisture regime; the C-sequence is in an ustic moisture regime.

The clay fractions of the soils are predominantly kaolinitic and gibbsitic. Profiles C4 and P6 have gibbsite in the top horizons alone, and C5 lacks gibbsite. Goethite is found in all soils, but in very low amounts in C1. Hematite is present in all horizons of the soils, except in the yellow topsoils of P2-P5, P7 and C4.

Table 8.1: Classification (Soil Survey Staff, 1994), field aspects, and chemical characteristics of the studied Oxisols

Profile	Soil class	soil depth (cm)	colour[1]	structure[1]	C[2] %	Fe_2O_3 (%) total[3]	Fe_2O_3 (%) free[4]
P1	Anionic Acrudox	550+	10R 4/6	gra	2.25	19.8-25.2	8.8-12.3
P2	Anionic Acrudox	200+	5YR 5/8	sblo	2.41	17.7-20.3	7.9-10.2
P3	Inceptic Hapludox	170+	7.5YR 5/8	sblo	2.76	16.4-18.2	5.2-8.7
P4	Inceptic Hapludox	200+	7.5YR 4/4	sblo	2.87	17.7-19.1	7.3-9.2
P5	Udoxic Dystropept	200+	7.5YR 5/6	sblo	1.68[6]	15.4-17.6	8.1-9.9
P6	Petroferric Acrudox	2300+	2.5YR 4/6	gra	2.11	9.2-59.9	7.1-30.0
P7	Anionic Acrudox	500+	10YR 5/8	ablo	2.01[6]	2.9-12.4	0.4-7.0
P8	Anionic Acrudox	500+	2.5YR 4/6	gra	2.85	9.3-16.1	7.1-9.7
VP	Anionic Acrudox	1560+	2.5YR 4/6	gra	2.44	13.3-21.7	4.7-13.4
C1	Typic Haplustox	400+	10R 4/6	gra	2.22	11.9-13.3	7.3-9.2
C2	Typic Haplustox	210+	2.5YR 4/8	gra	1.98	11.7-12.3	6.5-7.0
C3	Typic Haplustox	470+	2.5YR 5/8	gra	0.73	8.1-15.8	5.2-9.2
C4	Inceptic Haplustox	540+	10YR 7/8	sblo	0.95	5.2-7.4	3.4-4.8
C5	Ustoxic Dystropept	1070+	10YR 7/8[3]	mas[5]	0.74[5]	8.0-9.3	5.0-5.5

[1] Munsell moist colour and structure of the B horizon; [2] C content of the A and/or AB horizon; [3] XRF, 900°C ignited; [4] Na-dithionite extraction; [5] C horizon; [6] B horizon.

METHODS

The soil profiles were described according to the FAO guidelines (FAO, 1990). Soil bulk samples were collected, air dried and passed through a 2 mm sieve for laboratory analyses. Routine chemical analyses, XRF major and trace elements, and clay mineralogy were carried out as described by Buurman et al. (1996). Sand and silt fractions were studied by binocular microscope. Thin sections of 7x7 cm were prepared from undisturbed samples. They were studied by polarizing microscope, to obtain information on the morphology of iron forms.

For grain-size analyses subsamples of the different horizons of each profile underwent three pretreatments routinely used in texture determinations (Buurman, et al., 1996): 1) overnight shaking in deionized water according to the routine for determination of 'water-dispersible clay'; 2) with hydrogen peroxide (H_2O_2) to remove organic matter; 3) with H_2O_2 to remove organic matter, and subsequently with Na dithionite-citrate-bicarbonate (DCB) to remove (free) iron oxides.

Grain-size distributions were determined by means of laser diffraction, using a Coulter LS230 laser grain-sizer with software version LS 2.09. The results are given in 116 grain size

classes, between 0.04 and 2000 μm. Each class boundary is 1.098 times the size of the preceding one. The application of laser diffraction to soil studies was discussed in previous studies (Chapters 6 and 7). All measurements were carried out at 10% obscuration of the laser beam, so as to represent the whole 0.04-2000 μm grain-size range. Absorption settings were 0.30, 0.20, 0.18, and 0.075 for the 450, 600, 750, and 900 nm beams, respectively. These parameters were obtained by measuring absorption at these wavelengths in suspensions of the investigated soil materials, before removal of iron. Settings for dithionite-treated samples were the same, because absorption appeared to change less than 5% with respect to the previous values. The other parameters used in the optical models were a value of 1.33 for the refractive index of water, and a mean value of 1.56 for the refractive index of minerals.

Because of the high clay content of the soils, only 1 gram of an air-dried, well-homogenized subsample was sufficient, without putting at risk sample homogeneity and representativeness. The samples were diluted in the measuring vessel to the correct obscuration for laser diffraction measurement. In order to prevent flocculation because of the use of tap water, a dispersing agent (5% sodium pyrophosphate) was added to the measuring vessel (30 ml to pre-treated samples up to 150 ml to untreated samples). In some of the samples, flocculation occurred nevertheless. These have been omitted from the discussion.

RESULTS

Iron forms

Apart from an homogeneous red and/or yellow colouring (impregnation) of the groundmass, micromorphology indicated the occurrence of two main forms of iron compounds in the studied profiles: 1) discrete hematite 'droplets', and 2) secondary accumulation of iron as coatings and hypocoatings, especially around pores. Table 8.2 indicates the occurrence and abundance of these two forms in each of the profiles.

In soils on rock-saprolites, mainly hematite is formed in the saprolite, largely as discrete 'droplets' of one to several μm in diameter. Through pedoturbation, these 'droplets' are gradually mixed with the kaolinite matrix, during which their size diminishes, or they dissolve. In well-developed B horizons, size-reduction and mixing results in a pervading red colour. Saprolites of profiles P1-P5, P7-P8, and C1-C5 always have hematite 'droplets' as the dominant iron form. Towards the B horizon they are not discernible anymore. In the red B horizons of P1, P7, and P8, the 'droplets' have decreased in size and abundance but are still recognizable. They are virtually absent in the red B horizons of C1 and C2, where the red colour cannot be attributed to any microscopically visible feature. 'Droplets' are rare or absent in the yellow topsoils.

In Oxisols and buried soils formed on Tertiary sediments (P6 and VP), hematite 'droplets' are absent. These soils show features indicating that they have suffered effects of imperfect drainage or percolating groundwater in their evolution (see Chapter 4). Thin sections of the deeper horizons

(BC, V) of VP show iron accumulation along pores, while in the upper horizons, weak, diffusely bounded iron segregation that overly the much smaller silt-sized aggregates are clearly visible. In sequence P6, secondary accumulation of iron in the matrix and around pores is clear, and is attributed to surface- and groundwater saturation phenomena (see Chapter 4). Characterization of the iron oxides (see Chapter 5) indicated that their crystallite-size is slightly larger in sediments (groundwater-related hematite and goethite accumulations) than in the rock-saprolite materials.

Aggregation characteristics

When interpreting the results of laser grain-size distributions, one has to keep in mind that after each treatment, the sum of all fractions is 100%. This implies that, where treatments with H_2O_2 or Na-dithionite result in the disappearance of discrete grain-size fractions, the percentage of remaining fractions will automatically increase. So, 'increases' upon treatment are always relative, and should be judged in the light of removed fractions, but decreases are absolute. Small amounts of coarse fractions that may have not been detected in the untreated samples (background), may appear after removal of organic matter or iron compounds. Such fractions are also very sensitive to sample heterogeneity, because a few large grains constitute a relatively large volume fraction. These changes in amounts of size fractions are clearly visible in the grain-size distribution curves, although they have not been quantified. Finally, the dip at 1μm constantly found in all sample measurements is regarded as an artifact of the calculation procedure of the apparatus. Nevertheless, ongoing research indicates that the <1 μm fractions of many samples correlate well with pipette clay measurements.

The aggregation characteristics of profile P1 (Figure 8.1a-c) are representative for the P1-P5 sequence. The water-shaken samples (Figure 8.1a) show that the horizons differ considerably in the grain-size distribution of aggregates. The deepest horizons (BC2, BC3, C) have similar grain-size distributions, with very little clay and low contents of particles larger than 100 μm. The overlying BC1 horizon has slightly more clay, but is otherwise similar. The AB, Bw2, and Bw3 horizons show higher amounts of clay and diminished contents in the 2-30 μm size fractions region. Horizons AB and Bw3 show an increase in larger particles (>100 μm) compared to the lower horizons.

After removal of organic matter by treatment with hydrogen peroxide (Figure 8.1b), particles coarser than 100 μm have virtually disappeared, indicating that these were aggregates bound by organic matter. The C horizon remains unchanged, while the BC2 and BC3 horizons show a slight increase in clay content. The horizons AB-Bw3 do not change upon removal of organic matter. Removal of organic matter has strongly increased the clay content, especially in the upper two horizons, and has brought out a maximum around 2 μm. Removal of iron compounds with dithionite (Figure 8.1c) resulted in disappearance of the peak around 2 μm, while the clay contents of the upper four horizons increase slightly. This indicates that the 2 μm peak is attributable to iron oxide aggregates of discrete size, which probably correspond to

the hematite 'droplets' that are visible under the optical microscope. The 1-50 μm fraction becomes gradually finer towards the top of the profile, indicating an upward increase in weathering and clay formation, but there is no clear indication of further disaggregation as a result of iron removal.

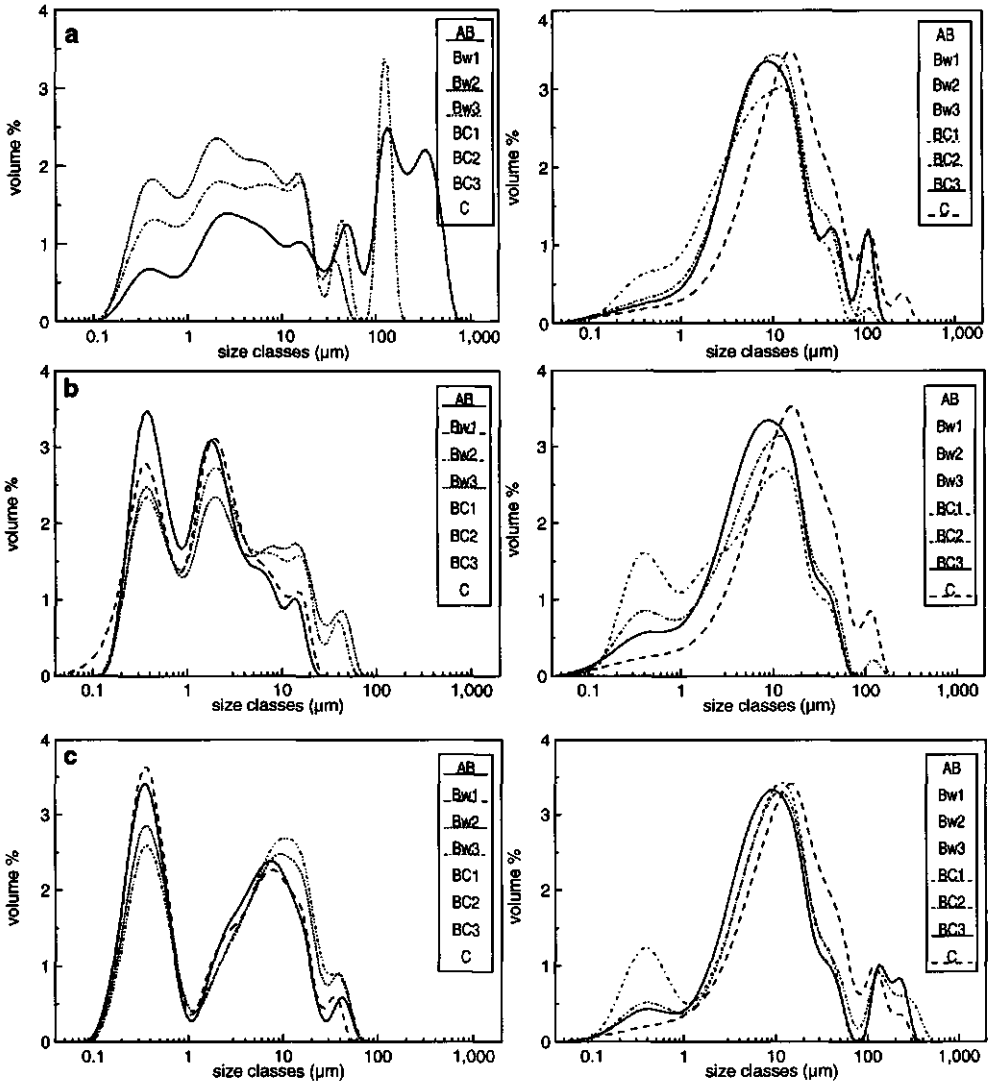

Figure 8.1: Grain-size distribution curves of profile P1 after treatments: **(a)** shaken with water; **(b)** removal of organic matter; **(c)** removal of organic matter and free iron.

Profiles P2-P5 and P7 (not shown here) also show an increase in clay fraction in the topsoils as a result of removal of organic matter, and further negligible effects of iron removal. The gradual fining of the silt fraction towards the soil surface is also found in these profiles. Profile P8 too is very similar to profile P1. Removal of organic matter of the upper five horizons also brings out a very distinct peak around 2 μm, which disappears deferration.

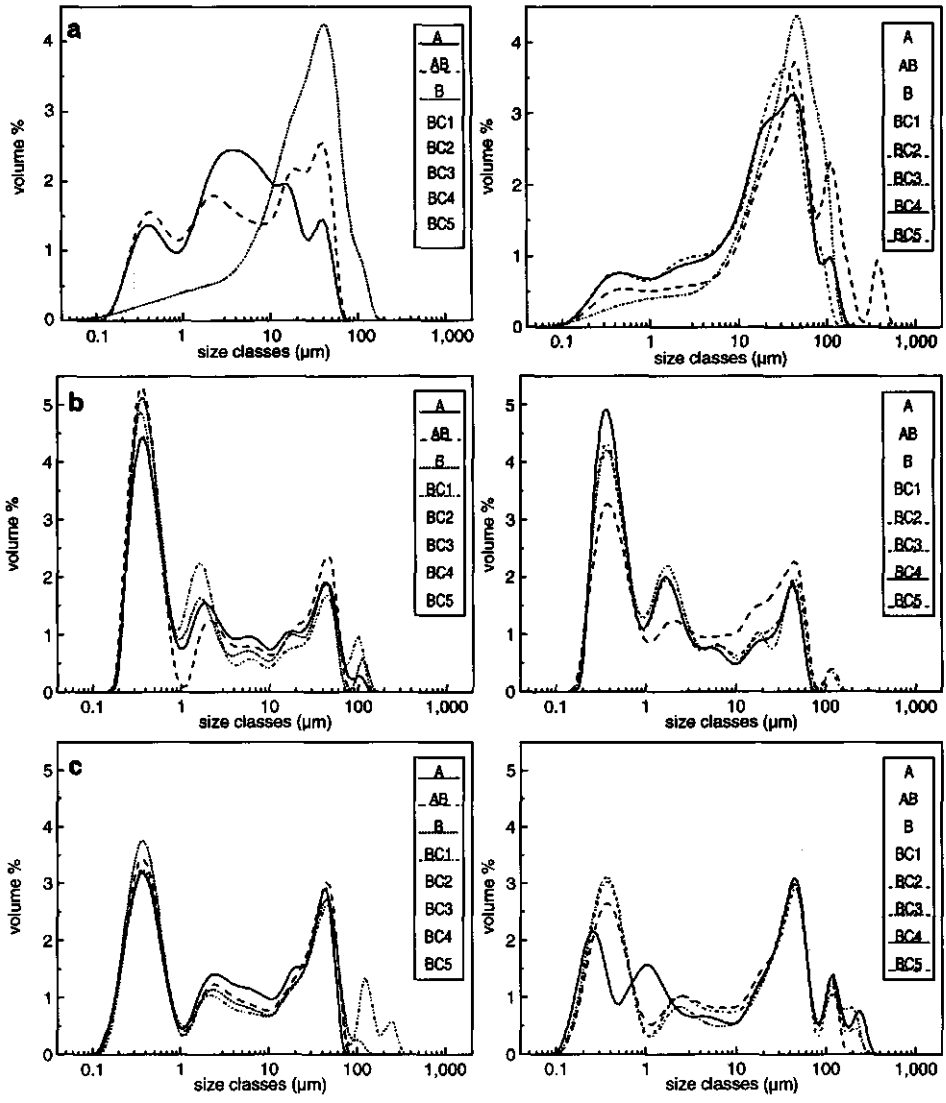

Figure 8.2: Grain-size distribution curves of profile C1 after treatments: **(a)** shaken with water; **(b)** removal of organic matter; **(c)** removal of organic matter and free iron.

The aggregation in sequence C1-C5 is best illustrated by profile C1 (Figure 8.2). Grain-size distributions of the water-shaken samples show relatively little clay; the highest clay contents occurring in the A and AB horizons. These two surface horizons do not show particles larger than about 80 μm and exhibit a rather continuous distribution, with maxima in the silt fraction around 5, 20, and 40 μm. Particles coarser than 200 μm are found only in the BC1 and BC5 horizons. All other samples have a maximum at about 40-60 μm. Removal of organic matter (Figure 8.2b) results in disappearance of all fractions above 200 μm and in a very strong reduction of the 40-60 μm peak. Maxima in the fine silt fraction, that were found in the A and AB horizons, have disappeared and all samples show a steep increase in clay content, accompanied by the appearance of a well-defined peak around 2 μm. Removal of iron results in a distinct decrease in the clay fraction of all samples and of the peak around 2 microns. As a result, coarse fractions increase and scarce particles larger than 200 μm become visible again (Figure 8.2c).

Grain-size distribution curves of profiles C2-C5 after the three treatments (not shown) have similar patterns, but organic matter aggregation is largely absent, probably because topsoils were more or less eroded. The dithionite-treated samples show the same effect of diminishing size of the fine silt fraction (<10 μm) with increasing of the clay content due to weathering (Figure 8.3) that was observed in P1 (Figure 8.1c).

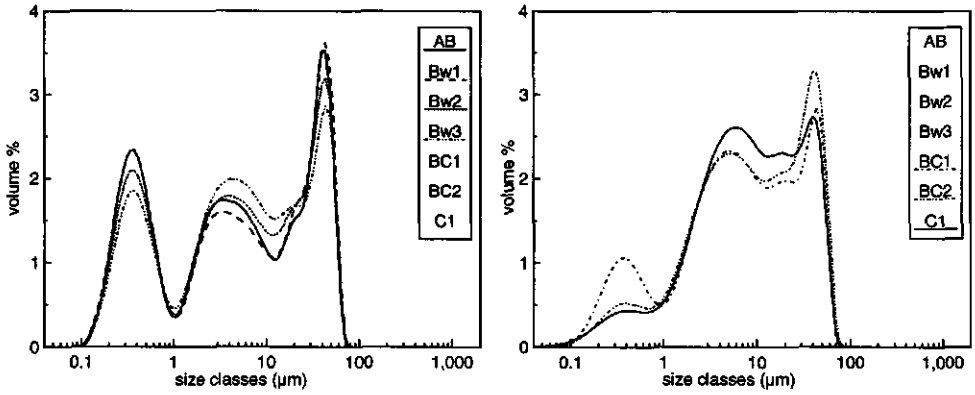

Figure 8.3: Grain size distribution curve of profile C3, after removal of organic matter and free iron, showing the effect of weathering on grain-size in the fine silt fraction.

A completely different picture is found in the Oxisols on sediments, P6 and VP. Water-shaken samples of P6 (Figure 8.4a) show a large range in particle sizes, with small peaks below 1 μm, and an abundance of peaks above 50 μm. The broad maximum in the fine silt fraction, which was observed in the A and AB horizons of profile C1 (Figure 8.2a) is also present in the AB horizon of P6. Removal of organic matter (Figure 8.4b) strongly increases the clay fraction in all samples, while fractions coarser than 500 μm disappear. The shift towards fine fractions

is most dramatic in horizons AB and B, where only particles smaller than 30 μm remain after the treatment. A peak around 2 μm becomes more clear in the samples from shallower horizons. The effect of removal of iron is very strong in all samples (Figure 8.4c): the clay fraction increases further, while all fractions coarser than 30 μm disappear. The maximum around 2 μm remains, indicating that it is not due to discrete iron particles.

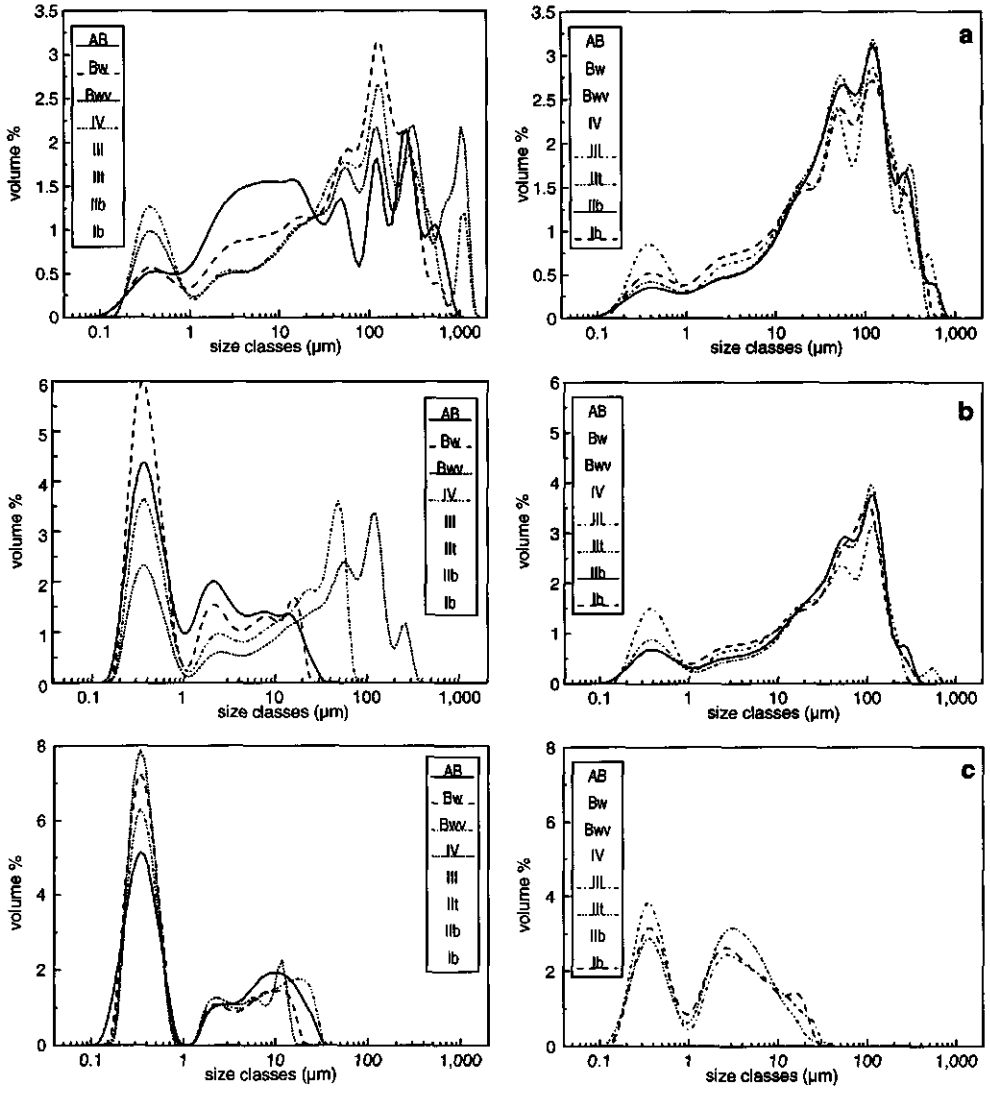

Figure 8.4: Grain-size distribution curves of profile sequence P6 after treatments: **(a)** shaken with water; **(b)** removal of organic matter; **(c)** removal of organic matter and free iron.

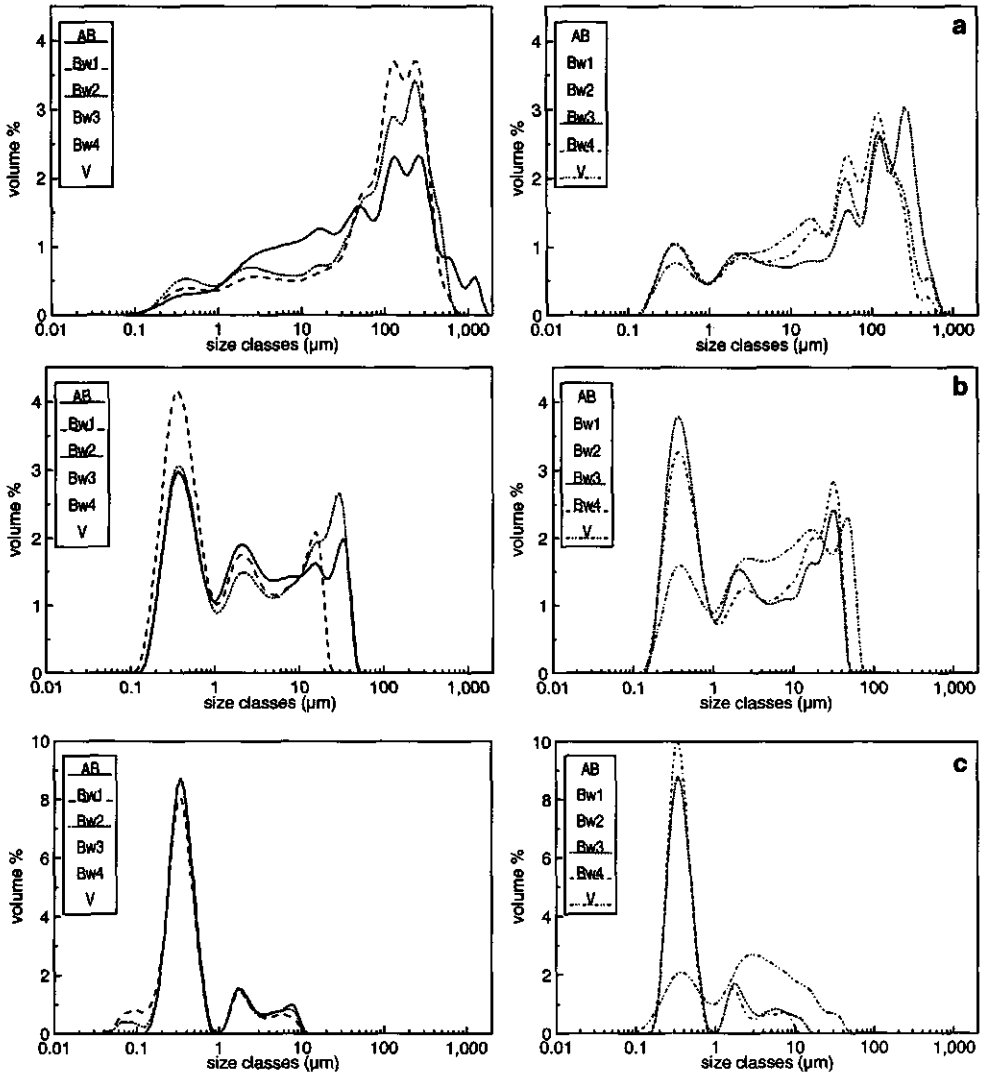

Figure 8.5: Grain-size distribution curves of profile VP after treatments: **(a)** shaken with water; **(b)** removal of organic matter; **(c)** removal of organic matter and free iron.

Similar effects, but superposed on a more homogeneous parent material, are observed in the Oxisol of sequence VP. Upon shaking with water, all samples show a broad range of grain sizes (Figure 8.5a), with a small peak below 1 µm and an array of peaks between 50 and 500 µm. The upper four horizons have a clear maximum around 250-300 µm, which is not found in the horizon B4 and layer V. This probably indicates a slight difference in sediment.

Clay contents are lowest in the topsoil and increase with depth. Upon organic matter removal (Figure 8.5b), all size fractions coarser than 70 μm disappear and clay-size fractions increase. The peak around 2 μm is here better-defined. The coarsest maximum in layer V does not shift, but all other samples have coarse maxima at grain-sizes where they were not found before removal of organic matter. Removal of iron (Figure 8.5c; note the difference in vertical scale) results in a further dramatic decrease in silt and sand fractions, accompanied by an increase in fractions below 1 μm. The grain-size distribution of layer V suggests that some geogenic aggregation remains, which has disappeared in the upper horizons, as indicated by the well separated peaks at 2 and 8 μm. As in P6, the peak around 2 μm does not disappear upon removal of iron. It increases slightly, indicating that this peak is not due to discrete iron particles.

DISCUSSION AND CONCLUSIONS

Data on micromorphology of iron compounds, effect of deferration treatment on amount of clay fraction, and type of aggregation are summarized in Table 8.2.

Hematite 'droplets' that form in the saprolite and, through coalescence have a range of sizes become a discrete and homogeneous population in the A and B horizons, as shown by the grain-size distributions. In these horizons, the discrete iron particles are visible as a maximum around 2 μm, which appears upon removal of organic matter, and disappears when iron is removed. In soils where pedogenesis may have caused strong diminution of 'droplets', as in the profiles P2-P4, P7 (top), and C1-C3, they are not visible in thin section. However, the decrease in fraction <1 μm upon iron removal suggests that there may still be discrete clay-sized particles of iron compounds. The decrease in size of the iron compounds has no effect on aggregation.

Aggregation in the Oxisols on sediments appears to be strongly influenced by iron compounds. The strong disappearance of coarse fractions upon peroxide and dithionite treatment in profiles P6 and VP is supported by micromorphological investigation. These profiles have a large amount of discrete, apparently non-porous, aggregates of sand and coarse-silt size. The size of aggregates encountered is in the same range as that reported in literature, but strong aggregation by iron is mainly found in silt-sized aggregates, which was also observed by Brito Galvão and Schulze (1996). Micromorphology of the profiles on sediments indicates that they are influenced by both surface- and groundwater saturation phenomena. During these processes, iron is reduced and reoxidized probably passing through a poorly crystalline phase (ferrihydrite), which causes a strong aggregation with clay. This was also observed in laboratory experiments (El-Swaify and Emerson, 1975; Chauvel et al., 1976; Bartoli et al., 1992) and suggested for natural conditions (Michalet et al., 1993). Ferrihydrite can then transform to hematite without intermediary dissolution phases (Cornell and Schwertmann, 1996).

Table 8.2: Aggregation and micromorphology of iron of the studied Oxisols.

Prof.	micromorphology of iron forms	gain (+) or loss (-) of clay upon iron removal		organic aggregation	iron aggregation
		<1 μm	2 μm		
P1	'droplets': abundant in saprolite; decreasing in solum	+ top = bot	-- top = bot	++ top	(+) top - bot
P2	'droplets': abundant in saprolite; decreasing and disappearing in yellow solum	- top	(-)top	++ top	none
P3	id.	--	(-)top	++ top	none
P4	id.	--	(-)top	++top	none
P5	'droplets': abundant in saprolite; decreasing in solum	=	-	+ top	none
P7	'droplets': abundant in saprolite; decreasing in yellow solum	-- top = bot	- top	++ top	none
P8	'droplets': abundant in saprolite; decreasing in solum	(+)top	-- top	++ top	none
C1	no visible 'droplets'	-- all	- all	++ all	none
C2	'droplets': common in subsoil; decreasing in solum	- all	(-)all	+ all	none
C3	'droplets': common in subsoil; disappearing in solum	- all	- top	++ top	none
C4	'droplets': abundant in saprolite; very few in yellow solum	(-)top	=	+ top	none
C5	'droplets': common in saprolite; decreasing in subsoil	=	=	(+) top	none
P6	no 'droplets'; impregnation along voids	++ all	=	++ top	++ all
VP	no 'droplets', some mottles in subsoil	++ all	=	++ all	++ all

++: strong; +: moderate; (+): minor; =: no change ; --: strong; -: moderate; (-): minor.

As reported in literature (e.g., Pinheiro-Dick and Schwertmann, 1996), shaking with water of this kind of soils does not result in a large clay fraction. Removal of organic matter by oxidation with H_2O_2 appears to have a disaggregating effect which is not always proportional to the organic matter content, and may be partially due to the effervescence caused by the oxidation process. Cambier and Picot (1988) and Pinheiro-Dick and Schwertmann (1996) indicated that the addition of anions may lead to increased dispersion. Although a phosphate anti-flocculant was added to all the studied samples during measurement, it is possible that anion adsorption was more efficient after removal of organic matter, because this removal exposes more of the positively-charged surfaces. This charge is reduced through surface adsorption of anions, resulting in some new aggregation, which cannot be assessed. This would mean that a weak aggregation due to iron is not measured in the present research.

Micromorphological investigation indicated that, in the studied sequences, all soils developed on rock-saprolites have hematite 'droplets' in the saprolite, whereas 'droplets' are not

found in the sequences on Tertiary sediments. On the other hand, secondary iron accumulations related to periodic water saturation are encountered in the sediments, and not in the soils on rock-saprolites. Parallel to this distinction, grain-size distribution curves obtained by laser diffraction technique showed that the Oxisols developed on rock-saprolites do not have strong aggregation due to iron compounds alone. In these soils the effect of iron on aggregation is probably indirect, through binding with organic matter (Emerson and Greenland, 1990). Conversely, aggregation by iron is evident in the Oxisols developed on Tertiary sediments. The obtained data suggest that remobilization of iron during soil formation is necessary for iron forms to play a role in aggregation. Such remobilization may also have occurred in the top of profile P1. These findings suggest that the mode of formation of the iron compounds determines their eventual effect on aggregation.

9. SYNTHESIS AND CONCLUSIONS

In geologically old landscapes of the humid tropics, soils usually have a very complex history. Because of extremely long periods of soil formation and different soil formation circumstances, these soils are polygenetic. The state of Minas Gerais has large areas of polygenetic soils developed on Tertiary surfaces. These soils, which are under growing pressure for various forms of use, are not well known, especially with regard to their genesis. Unraveling the genesis of polygenetic soils is a complex task because of the overprinting of various phases of soil formation. Such studies require the integrated characterization, interpretation, and separation in time of the many features imprinted on soils and subsoils throughout their evolution. In continuously exposed soil profiles, various phases of soil formation are superimposed, and thus very difficult to separate. The combination of continuously exposed (stable) landscapes and sedimentary deposits in graben zones offers the possibility of interpreting the history of the soils found at the present day surface. In graben zones, soil formation phases may be physically separated in time because of alternation of sedimentation and soil formation. Sediments were deposited during periods of tectonic activity, while soil formation on these sediments took place during periods of landscape stability. Therefore, studying the buried soil horizons in such deposits provides a means to understand the evolution of these polygenetic soils.

This research aimed to the understanding of the main aspects of soil genesis of polygenetic soils from Minas Gerais, Brazil, in relation to landscape development. It was attempted to reconstruct soil processes by studying differences in physical, chemical, mineralogical, and morphological properties of soils developed on continuously exposed surfaces and on sedimentary layers. In addition to field characterization, textural, chemical, mineralogical and (micro)morphological studies of topographic and weathering (continuous rock-saprolite-soil) sequences were undertaken.

Soil-landscape units

Field observation of soils, saprolites, parent materials and landforms led to the distinction of three main soil-landscape units related to two types of parent material. The first two units consist of red and/or yellow soils overlying deep reddish (purple) saprolites and weathered rocks on remnants of the Tertiary *Sulamericana* surface. They occur in the Sete Lagoas (SL) and São João del Rei (SJR) areas, on fine- to medium-textured sedimentary (SL), and metamorphic (SJR) parent rocks of pre-Cambrian age. The difference in rock type influenced some mineralogical and chemical trends, but the saprolites reacted similarly to soil formation holding this way the same general soil evolution trend, which makes comparison possible.

The third unit consists of red soils overlying red and/or yellow Tertiary sediments from graben zones. The three soil-landscape units are respectively identified and described as:

SL-sap: red and yellow soils developed on fine-textured sedimentary and metasedimentary rocks. The soils are Oxisols developed on continuously exposed surfaces that were more or less intensively dissected under (sub)recent climates.

SJR-sap: red and yellow soils developed on fine- and medium-textured metamorphic rocks. They are Oxisols developed on long-time exposed surfaces, which may have been eroded in relation to neotectonic activity and/or in response to a (sub)recent overall rejuvenation of the landscape.

SJR-sed: red soils developed on Tertiary sediments. The sediments consist of eroded soils and saprolites deposited in graben zones formed by neo-Cenozoic tectonic activity.

Red and yellow soils developed on rock saprolites were not considered as separate units because they constitute toposequences. Red soils occur in the more stable parts of the landscape (flat tops or upper convex slopes), while yellow soils occur on the slopes, where the original red Oxisols were eroded. The yellow and shallower soils on slopes have developed on in-situ saprolites and former subsoil layers of the eroded soils.

Erosion

Although erosion was not specifically studied in this research, field observation and laboratory results allow the drawing of some conclusions. As mentioned in the introduction, erosion is the main problem arising from the use of these soils, especially those developed on fine- to medium-textured sedimentary and metamorphic rocks. Sheet-like and linear erosion occur in both SL and SJR areas. Sheet-like erosion is more prominent on shallower soils where runoff exceeds the infiltration. When the incision reaches the saprolites the erosion increases dramatically and large and very deep gullies appear. The high friability of the saprolites, clearly observed in the field, facilitates removal of particles by water, especially when the amount and energy of water is increased by its concentration in rills and gully channels. Conversely, the red B horizons and the soils developed on Tertiary sediments have a lower susceptibility to erosion. A similar pattern of soil erosion was observed by Scholten et al. (1995) in areas of polygenetic soils and saprolites in Swaziland, Africa.

The difference in susceptibility to erosion between soils and saprolites is due to their structural stability, which is influenced by texture and aggregation. The saprolites have a coarser texture because of less particle comminution and clay neoformation at their present weathering stage. The saprolites show negligible aggregation caused by the absence of organic matter, and the relatively lower contents of Fe/Al. Furthermore, the iron forms present in saprolites play a minor role in aggregation, as shown by aggregation studies of the soils and saprolites (Chapter 8). On the other hand, iron forms found in the red B horizons and in soils

and subsoils on sediments show a strong binding with clay particles, which in the sediments may result in cementation.

Rills and gullies are impressive in the studied areas, and seem to be more numerous and larger in the SJR area. It appears that the higher geological instability of the area contributes to a higher erodibility of the soils either under anthropic use or in natural conditions. Furthermore, the abrupt change in consistence along the lithological contacts between rock-saprolites and sediments of tectonic origin in the SJR area, appears to play a role in the initialization of rills and gullies. This, however, requires further specific studies.

Polygenesis of the soils

Soils that have undergone more than one soil formation phase are considered to be polygenetic (Bronger and Catt, 1989). Because of the inherent uncertainties about the distinction between soil formation phases, all soils developed on geologically old landscapes in the tropics are considered polygenetic (Johnson et al., 1990). Polygenesis of soils is indicated by the presence in the soils of relicts, which are features inherited from previous soil formation phases, usually acquired under pedogenetic conditions different from the present ones. Micromorphology of soils is a very suitable tool to recognize and interpret this kind of features (Stoops, 1989; Bronger et al., 1994; Pereira and FitzPatrick, 1995).

The studied soils present a wide diversity of relict features, although the greatest diversity of relicts was found in the red soils of the SJR area. Ferruginous pedorelicts, such as iron nodules and concretions, are typical relict features found in all studied soils. The red colouring of the groundmass is also a relict feature, since it is not observed in the younger soils forming after (sub)recent landscape dissection. Indurated yellowish clay nodules found in the red soils from the SJR area on both sediments and saprolites, are also relicts, and show that these soils represent more than one evolutionary phase. Fragments of precipitated clay found throughout the SJR-sed sequences indicate the strong reworking of soils where clay illuviation and/or precipitation took place. The nature of all relicts suggests that the soils and saprolites from which they were derived were already strongly weathered. The ferralitic character of the yellow soils found in (sub)recent eroded slopes is inherited from their parent material, which was already ferralitized. This corroborates the idea that ferralitic characteristics are the most important relict features of most tropical soils, since the present pedogenic conditions would not lead to the formation of this type of weathered materials (Stoops, 1989; Ojanuga, 1990). Bronger et al. (1994) mention that an annual rainfall exceeding 2000 mm (6 humid months) would be necessary to form this type of strongly weathered materials, whereas the climate of the study areas is clearly dryer. The plinthitic nature of some of the relicts indicates previous existence of (petro)plinthites that were exposed by erosion in higher landscape positions, and completely eroded. Also, the large variation observed in goethite properties within the same horizon in soils on rock-saprolites and on sediments reflects the polygenetic nature of the soils.

Weathering, soil formation, and paleoenvironments

Weathering is a relatively slow process, but is one of the major soil forming processes in the tropics (Mohr et al., 1972). Due to the highly weathered nature of most tropical soils, it is hardly possible to distinguish actual weathering and soil formation from previous weathering processes. Effects of weathering and soil formation processes are well illustrated by micromorphological, chemical, mineralogical, and textural changes observed along the studied soil profiles and toposequences. The micromorphological aspects that point to increasing soil formation towards the surface are: clay formation (either by the destruction of silt- and sand-sized kaolinite booklets or by neoformation of clay minerals); increase of individualized structural elements (with decrease of their size) and porosity; weakening of the b-fabric of the groundmasses from crystallitic towards random striated and undifferentiated; and uniform reddish or yellowish colouring of the materials, which is typically observed in oxic materials (Stoops et al., 1994).

The microstructure of all the studied soils shows that biological mixing is the main process acting on the materials. Mixing is obviously most intense in top horizons, regardless of composition and weathering stage, but burrowing and rooting are also observed in saprolites. The circular striated b-fabric observed in some of the red B horizons is the result of successive welding and separation of granules caused by a prolonged bioturbation.

Changes in chemistry and mineral transformations

The mineralogical composition of all studied materials indicates a high degree of weathering and homogenization. Kaolinite and iron oxides (hematite and/or goethite) are ubiquitous in all materials, which is common to other Brazilian Oxisols in similar conditions (Melfi and Pedro, 1977; Kampf et al., 1988). These minerals are usually accompanied by gibbsite in *sola* and micas in saprolites. The high degree of weathering is illustrated by the dissolution of quartz and weathering of ilmenite, which is observed in all materials from the SJR area. Factor analysis indicated that 32% of the total variance of the chemical composition is explained by the weathering status, which is also reflected in the contents and proportions of major oxides.

Soils and saprolites from the SL area show a lower degree of weathering than those from the SJR area, apart from the fact that their parent materials are slightly different. The lower weathering is indicated by the higher SiO_2/Al_2O_3 molar ratios, and higher amounts of K, Mg, and other mobile trace elements in the SL soils (Appendix 3). Differences in parent material and associated weathering processes explain another 57% of the total variance of the chemical elements in the studied materials.

Clay formation and illuviation

Clay formation is one of the most conspicuous aspects of soil formation, especially in the tropics. Because in the studied materials clay minerals (e. g. kaolinite) also form as sand- and silt-sized particles, the expression 'clay formation' is here used to describe either the formation of clay-sized particles or the (neo)formation of clay minerals. This encompasses the processes of mineral comminution and/or dissolution, and (neo)formation of clay minerals. In terms of formation of clay-sized particles, the laser diffraction grain-size studies of the soils showed clearly the strong increase in clay contents and disappearance of silt fractions towards the soil surface, as a result of weathering and soil formation

Kaolinite is the main component of the clay fraction in the soils and of the silt and clay fractions in the saprolites. The occurrence of two types of kaolinite in the rock-saprolite sequences (SL-sap and SJR-sap) indicates different environments of formation during the evolution of the soils. Kaolinites formed in the saprolites are larger in size (silt and even sand-sized) and are well ordered, whereas the kaolinites found in soils and in the whole SJR-sed sequence are submicron-sized, disordered, and appear to have higher Fe-for-Al substitution, as indicated by Mössbauer spectroscopy and by intercalation with dymethil sulphoxide (DMSO). The coarser kaolinites from the saprolites are transformed into clay-sized particles either by comminution due to pedoplasmation (Graham et al., 1989), or by dissolution and neoformation caused by epigenetic replacement of kaolinite by hematite (Ambrosi et al, 1986). Kaolinites in the sediments were inherited as submicron-sized particles from eroded older soils.

Clay accumulation features are abundant in the buried soils of the sequence P6, developed on sediments. The clay accumulation features consist of coatings and infillings, which result either from precipitation or illuviation. Illuviation of clay is usually found in seasonal climates, where it takes place at the beginning of the rainy season. Clay illuviation does not usually occur in ferralitic soils, because of strong stabilization of aggregates by Fe/Al. Clay precipitation in subsoils is related to strong weathering higher up in the profile, and therefore not incompatible with ferralitization. The precipitation of clay from solution takes place upon saturation of the soil solution, e. g. as a result of desiccation of the profile. The fact that clay illuviation and precipitation are in close connection suggests that the eroded ferralitic materials might not have been strongly aggregated by Fe/Al, or that the aggregation was destroyed by reduction of Fe during deposition processes. This is in accordance with the findings that particulated/droplet iron forms that occur in saprolites do not stabilize soil aggregates.

The association of clay precipitation and illuviation in profile P6 indicates strong weathering and probably a climate with contrasting dry and wet seasons. Illuviation and precipitation of clay can coexist in the same soil profile as a result of seasonal fluctuations: in the beginning of the wet season, clay eluviation and illuviation take place. During the wet season weathering is most active; it is followed by desiccation and precipitation of clay at the end of the wet season. Both processes probably occurred over long periods of soil formation,

which were alternated with large erosional reprises, because clay formation and accumulation features are found in different buried layers of the sequence P6, and as relicts in the red soils found in the SJR area.

Iron oxides

Iron oxides are known to be useful paleo-environmental indicators, and their properties may give information about past and present circumstances of weathering and soil formation. Hematite and goethite are the only iron oxides found in the clay and silt fractions. Micromorphology suggests that during rock weathering, hematite forms in the saprolites as 'droplets' (spherical aggregates). Laser diffraction and micromorphology show that the hematite droplets have a discrete size of about 2 μm. The droplets diminish in size through pedoturbation and dissolution, and eventually disappear in younger, yellow topsoils, or occur in fractions smaller than 1 μm that are invisible under the optical microscope. Gradual mixing, size reduction, and partial dissolution of the droplets through pedoturbation results in the formation of an homogeneously red groundmass. In the sediments from the graben zones, hematite was either inherited (from reworked soil materials), or precipitated as (hypo)coatings as a result of periodic water saturation. The different forms of hematite could only be distinguished through micromorphology. This reinforces the usefulness of micromorphology in the identification and interpretation of features linked to present and past soil processes (Stoops, 1989; Bouma et al., 1990; Bronger et al., 1994).

Goethite is less commonly formed in the rock saprolites and is therefore mostly a 'secondary' product, that more closely reflects the soil forming environment. In addition to oxidation from ferrous iron released from primary minerals, goethite has two main modes of formation: (i) through oxidation of ferrous iron produced by pseudogley processes in water-conducting, bleached channels and; (ii) by conversion of hematite to goethite (xanthization), most conspicuously observed in younger topsoils. Recent pedogenesis causes the transformation of hematite to goethite. This transformation, known as 'xanthization' (Bisdom et al., 1978), reaches its maximum in topsoils that formed in saprolites of eroded Oxisols in the stable parts of the landscape. Xanthization also affects the red soils, as shown by a slight yellowing of the topsoils compared to the B horizons, in older (less eroded) Oxisols (Appendix 1).

Soil colours are mostly related to the type of iron oxide present in the groundmass, and mainly reflect differences in past and present hydrology of the soils due to distinct pedoclimates, whether or not caused by the overall climate. Differences are particularly well expressed in the profiles from group SJR-sed, which were exposed to relatively strong variations in surface- and groundwater saturation. These variations are likely related to the lower position of these sequences in the landscape, during sedimentation and subsequent soil formation. The soils from group SJR-sed show red colours, with more or less intense yellow mottling in the subsoils. Micromorphology of the sequences shows that the deeper horizons have iron accumulations related to the groundmass (pseudogley) and to larger pores (gley), indicating a

succession and/or alternation of surface- and groundwater saturation. Such accumulations are no longer visible in the B horizons, where they disappeared through pedoturbation.

Aggregation

A preliminary laser diffraction grain-size investigation of the soils after sequential removal of organic matter and free iron indicated that aggregation is due to organic matter rather than to sesquioxides (Chapter 7). Because this is at variance with the usual attribution of aggregation to iron, more detailed studies after various pre-treatments were undertaken (Chapter 8). The results, combined with micromorphological observations, showed that different iron forms have different influence on the aggregation of soils. Oxisols from both SL-sap and SJR-sap sequences do not have strong aggregation due to iron compounds alone. Hematite droplets that were formed in the saprolite do not appear to have an effect on aggregation. In such soils the effect of iron on aggregation is probably minor and indirect, through binding with organic matter (Emerson and Greenland, 1990). On the other hand, iron oxides that form through reduction, precipitation and recrystallization, as observed in the SJR-sed sequence, have a very strong aggregating effect. In this case, iron is reoxidized probably passing through a poorly crystalline phase (ferrihydrite), which causes a strong binding with clay (Michalet et al., 1993). This suggests that the mode of formation of the iron compounds determines their effect on aggregation. Apparently, iron needs to be remobilized during soil formation to play a major role in aggregation.

Unraveling the evolutionary history of the soils

The features related to the processes of weathering, biological activity, clay accumulation and iron translocation play key roles in the understanding of the processes undergone by saprolites, sediments and soils, in the studied sequences. The range of present and relict features indicates some of the evolution phases undergone by these polygenetic soils. It also gives clues about other phases that are obscured by overprinting on a sole profile.

Soils from group SL-sap have undergone a rather continuous evolution without evident major erosional and depositional events, indicating a minimal polycyclicity of the landscape. This is suggested by the few relicts found in these soils. With limited erosion, climatic changes apparently leave few imprints on deep Oxisol profiles: once formed, well developed Oxisols are not easily altered, because their chemistry, clay contents, and aggregation cannot be much changed from the status they reached. Furthermore, the climate in the SL area may have been slightly drier (and more constant?) than in the SJR area during the evolution of the soils, as it is at present. This is suggested by the lower degree of weathering of the materials, the redder colour of the soils, and the presence of iron-coated micas. Because of its lower complexity, the SL soil-landscape unit is taken as a reference situation for the studied area.

Conversely, the SJR area underwent a more complex evolution caused by the greater polycyclicity of the landscape and resulting higher polygenesis of the soils. Here, the stabilized

surface was disrupted by Cenozoic tectonic movements, which gave origin to rift structures. Such structures caused erosion both in the tectonically uplifted parts and in the proximal areas (by lowering of the base level). As a result, grabens and tectonically controlled basins were filled with colluvium derived from soils in the surroundings and sediments. Climatic changes may have triggered phases of more intense dissection and/or valley filling.

The relict features found in the oldest red soils formed on the Tertiary *Sulamericana* surface (group SJR-sap), suggest the following evolution phases (Chapter 3):

I. One (or more) soil formation phase(s) which produced yellow (and/or red) soils;
II. Removal of the former soils by erosion, with relicts of them being embedded in the B horizons of the present red soils;
III. A ferralitization phase that originated the red Oxisols;
IV. Landscape dissection and erosion of part of the Oxisol cover;
V. (Sub)recent pedogenesis on the dissected landscapes forming yellow soils either on saprolites or subsoil layers of eroded Oxisols.

In the soils developed on Tertiary sediments (group SJR-sed), the recognition of the different phases is greatly facilitated by soil formation in separate sedimentary layers. The following phases of erosion, deposition and soil formation were regognized in a representative soil sequence on sediments (P6):

1. Deposition of reworked ferralitized soil material from nearby areas (layer I);
2. Formation of soils with illuvial and precipitated clay accumulations in layer I;
3. Erosion and deposition of reworked soil material (layer II);
4. Formation of soils with a ferralitic character in layer II;
5. Tectonic activity, erosion and renewed colluvial deposition (layer III);
6. Formation of soils with gley and pseudogley features in the colluvium;
7. Deposition of a strongly weathered and well sorted sediment (layer IV);
8. Formation of Oxisols that overprinted the whole sequence, accompanied by groundwater saturation and development of plinthite and eventually petroplinthite;
9. Landscape inversion (by tectonic activity?), and erosion that removed most of the Oxisol cover and exposed petroplinthite layers;
10. (Sub)recent pedogenesis causing yellowing (xanthization) of the former red topsoils.

In correlating the two situations, one should keep in mind, that even the oldest soils in the graben are younger than the oldest soils in stable surfaces, and that the correlation is less uncertain for more recent processes than for ancient ones. Table 9.1 shows a tentative correspondence in time between evolutionary phases identified for the soils on continuously exposed ('stable') surfaces and on Tertiary sediments. The geological time frame encompassing this evolution extends from the Middle Tertiary (Late Paleogene) up to the Holocene (Quaternary), representing some 40 million years.

Table 9.1: Correspondence between evolution phases identified in soil sequences on continuously exposed ('stable') surfaces and on sediments.

Evolution phase in **SJR- sap** ('stable' surfaces)	Evolution phase in **SJR- sed** (sedimentary graben fillings)
I - soil formation	-
II - erosion	1 to 7
III - Oxisol formation	8
IV - erosion	9
V - formation of yellow soils	10

The correspondence presented in Table 9.1 illustrates well the masking effect caused by the superposition of erosion and soil formation phases on a sole profile, as in the soils formed on continuously exposed landscapes. Seven distinct phases are hidden in what appears as only two coupled phases. These coupled phases encompass at least three soil formation and subsequent erosional phases. Features indicating distinct soil formation phases in the buried soils, such as clay accumulation and illuviation features, will probably have also existed in the soils from the SJR-sap sequences, but were completely obliterated by pedoturbation during posterior soil formation phases. Because clay coatings are easily destroyed, very few fragments are found in the intensively reworked soils. Preservation of such features in the buried soils of the sedimentary sequences is possible due to the protection offered by overlying sedimentary covers.

The phases III, IV, and V are connected directly with phases 8, 9, and 10. Formation of yellow soils and xanthization of the red ones is the latest trend, so that phases V and 10 coincide. The stripping of both the saprolites and subsoil layers from SJR-sap and the petroplinthite layers from SJR-sed belong to the same erosional event (IV and 9 respectively). Finally, the latest Oxisol formation should have been common to the whole landscape. Plinthite formation and gley and pseudogley features are mainly observed in the SJR-sed soils because of their lower position in the landscape, which made them more prone to both surface- and groundwater saturation phenomena.

The listing and correspondence of the evolutionary phases presented above show that a fairly detailed history of the soils in a given area can be supplied by genetic studies of polygenetic soils developed on 'stable' landscape compartments in combination with such a study of buried soils in adjacent sedimentary deposits.

REFERENCES

Ab'Saber, A.N., 1970. Províncias geológicas e domínios morfoclimáticos no Brasil. IG/USP, Geomorfologia, 20, 26pp.

Agrawal, Y.C., McCave, I.N. and Riley, J.B., 1991. Laser diffraction size analysis. In: J.P.M. Syvitski (editor), Principles, methods and application of particle size analysis. Cambridge University Press, Cambridge, pp. 119-128.

Allen, T. 1981. Particle Size Measurement. 3rd edition. Chapman and Hall, London, 678 pp.

Allen, B.L. and Hajek. B.F., 1989. Mineral occurrence in soil environments. In: J.B. Dixon and S.B. Weed (editors), Minerals in soil environments, 2nd edition. Soil Science Society of America, Madison, pp. 199-278.

Almeida, F.F.M., 1976. The system of continental rifts bordering the Santos basin, Brazil. Anais da Academia Brasileira de Ciências, suplemento, 48: 15-26.

Almeida, J.R., 1979. Cromossequência de solos originários de rochas pelíticas do Grupo Bambuí. MS thesis. Universidade Federal de Viçosa, 150 pp.

Almeida, J.R. and Resende, M., 1985. Considerações sobre o manejo de solos rasos desenvolvidos de rochas pelíticas no Estado de Minas Gerais. Informe Agropecuário, 11: 19-26.

Almeida, J.A., Kampf, N., Klamt, E., 1992. Amidas e hidrazina na identificação de caulinita desordenada em solos brunos subtropicais do RS e SC. Revista Brasileira de Ciência do Solo, 16: 169-175.

Amarasiriwardena, D.D., Bowen, L.H. and Weed, S.B., 1988. Characterization and quantification of aluminum-substituted hematite-goethite mixtures by X-ray diffraction, infrared and Mössbauer spectroscopy. Soil Science Society of America Journal, 52: 1179-1186.

Ambrosi, J.P., Nahon, D. and Herbillon, A.J., 1986. The epigenetic replacement of kaolinite by hematite in laterite: Petrographic evidence and the mechanisms involved. Geoderma, 37: 283-294.

Amouric, M., Baronnet, A., Nahon, D. and Didier, P., 1986. Electron microscopic investigations of iron oxyhydroxides and accompanying phases in lateritic iron-crust pisolites. Clays and Clay Minerals, 34: 45-52.

Anand, R.R., and Gilkes, R.J., 1984. Weathering of hornblende, plagioclase and chlorite in meta-dolerite, Australia. Geoderma, 34: 261-280.

Anand, R.R. and Gilkes, R.J., 1984a. Weathering of ilmenite in a lateritic pallid zone. Clays and Clay Minerals, 32: 363-374.

Anand, R.R. and Gilkes, R.J., 1987. Iron oxides in lateritic soils from Western Australia. Journal of Soil Science, 38: 607-622.

Aoudjit, H., Elsass, F., Righi, D. and Robert, M., 1996. Mica weathering in acidic soils by analytical electron microscopy. Clay Minerals, 31: 319-332.

Bakker, L., Lowe, D.J. and Jongmans, A.G., 1996. A micromorphological study of pedogenic processes in an evolutionary soil sequence formed on late Quaternary rhyolitic tephra deposits, North Island, New Zealand. Quaternary International, 34: 249-261.

Barron, V. and Torrent, J., 1987. Origin of red-yellow mottling in a Ferric Acrisol of Southern Spain. Zeitschrift fur Pflanzenernahrüng und Bodenkunde, 150: 308-313.

Barth, H. G., 1984. Modern methods of particle size analysis. Wiley-Interscience, New York, 309 pp.

Bartoli, F., Burtin, G., and Guerif, J., 1992. Influence of organic matter on aggregation in Oxisols rich in gibbsite or in goethite. II. Clay dispersion, aggregate strength and water-stability. Geoderma, 54: 259-274.

Bayvel, L.P. and Jones, A.R., 1981. Electromagnetic scattering and its applications. Applied Science, London.

Bigarella, J.J. and Becker, R.D. (editors), 1975. International Symposium on the Quaternary (Southern Brazil). Boletim Paranaense de Geociências, 33 pp.

Bigham, J.M., Golden, D.C., Bowen, L.H., Buol, S.W. and Weed, S.B., 1978. Iron Oxide mineralogy of well-drained Ultisols and Oxisols: I. Characterization of iron oxides in soil clays by Mössbauer spectroscopy, X-ray diffractometry, and selected chemical techniques. Soil Science Society of America Journal, 42: 816-825.

Bigham, J.M., Golden, D.C., Bowen, L.H., Buol, S.W., Weed, S.B., 1978a. Mössbauer and X-ray evidence for the pedogenic transformation of hematite to goethite. Soil Science Society of America Journal, 42: 979-981.

Bilong, P., 1992. Caracteres des sols ferrallitiques a plinthite et a petroplinthite developpes sur roches acides dans la zone forestière du sud du Cameroun. Comparison avec les sols developpes sur roches basiques. Cahiers ORSTOM, série Pédologie, 27: 203-224.

Bisdom, E.B.A., Stoops, G., Delvigne, J., Curmi, P. and Altemuller, H.J., 1982. Micromorphology of weathering biotite and its secondary products. Pedologie, 32: 225-252.

Borggaard, O.K., 1982. Selective extraction of amorphous oxides by EDTA from selected silicates and mixtures of amorphous and crystalline iron oxides. Clay Minerals, 17: 365-368.

Bouma, J., Fax, C.A. and Miedema, R., 1990. Micromorphology of hydromorphic soils: Applications for soil genesis and land evaluation. Soil Micromorphology, pp. 257-278.

Brasil, Ministério das Minas e Energia, 1983. Projeto RADAMBRASIL: Folhas SF.23/24 Rio de Janeiro/ Vitória. MME/ Projeto RadamBrasil/Levantamento de recursos naturais, 32, 780 pp.

Braun, J.J., Pagel, M., Muller, J.P., Bilong, P., Michard, A. and Guillet, B., 1990. Cerium anomalies in lateritic profile. Geochimica et Cosmochimica Acta, 54: 781-795.

Braun, O.P.G., 1971. Contribuição à geomorfologia do Brasil Central. Revista Brasileira de Geografia, 33: 3-37.

Brilha, J.B., Sequeira-Braga, M.A. and Meunier, A., 1991. Muscovites and biotites kaolinization of the Campados kaolin deposit (Esposende, NW Portugal). In: Proceedings of the 7th Euroclay Conference, Dresden 1991, 1: 153-154.

Brinkman, R., 1979. Ferrolysis, a soil forming process in hydromorphic conditions. Agricultural Research Reports, 848. PUDOC, Wageningen, 106 pp.

Brito Galvão, T.C. and Schulze, D.G., 1996. Mineralogical properties of a collapsible lateritic soil from Minas Gerais, Brazil. Soil Science Society of America Journal, 60: 1969-1978.

Bronger, A. and Catt, J.A., 1989. Paleosols: Problems of definition, recognition and interpretation. In: A. Bronger and J.A. Catt (editors), Paleopedology: Nature and application of paleosols. Catena Supplement 16, Catena Verlag, Cremlingen, Germany.

Bronger, A., Bruhn-Lobin, N. and Heinkele, Th., 1994. Micromorphology of paleosols - genetic and paleoenvironmental deductions: Case studies from Central China, South India, NW Morocco and the Great Plains of the USA.. In: A.J. Ringrose-Voase and G.S. Humphreys (editors), Soil micromorphology: Studies in management and genesis. Proceedings IX International Working Meeeting on Soil Micromorphology, Townsville, Australia, 1992. Elsevier, Amsterdam, Developments in Soil Science, 22: pp. 187-206.

Bühmann, C., 1994. Parent material and pedogenic processes in South Africa. Clay Minerals, 29: 239-246.

Bullock, P., Fedoroff, N., Jongerius, A., Stoops, G. and Tursina, T., 1985. Handbook for soil thin section description. Waine Research Publishers, Wolverhalpton, 182 pp.

Buurman, P., 1980. Fossil soils in the Reading Beds (Palaeocene) of Alum Bay, Isle of Wight, U. K. Sedimentology, 27: 289-298.

Buurman, P., Van Lagen, B. and Velthorst, E.J. (Editors), 1996. Manual for soil and water analysis. Backhuys Publishers Leiden, 314 pp.

Buurman, P., Muggler, C.C. and Pape, T., 1997. Laser grain-size determination in soil genetic studies: 1. Practical problems. Soil Science, 162: 211-217.

Caggianeli, A., Fiore, S., Mongelli, G. and Salvemini, A., 1991. REE distribution in the clay fraction of pelites from southern Apennines (Italy). In: Proceedings of the 7th Euroclay Conference. Dresden, 1991, 1: 193-198.

Calvert, C.S., Buol, S.W. and Weed, S.B., 1980. Mineralogical characteristics and transformations of a vertical rock-saprolite-soil sequence in the North Carolina Piedmont: I. Profile morphology, chemical composition and mineralogy. Soil Science Society of America Journal, 44: 1096-1103.

Cambier, P. and Picot, C., 1988. Nature des liaisons kaolinite-oxyde de fer au sein des microaggregats d'un sol ferralitique. Science du Sol, 26: 223-238.

Campbell, A.S. and Schwertmann, U., 1984. Iron oxide mineralogy of placic horizons. Journal of Soil Science, 35: 569-582.

Cantinolle, P., Didier, P., Meunier, J.D., Parron, C., Guendon, J.L., Bocquier, G. and Nahon, D., 1984. Kaolinites ferrifères et oxyhydroxydes de fer et d'alumine dans les bauxites des Canonettes (S.E. de la France). Clay Minerals, 19: 125-135.

Chauvel, A., Pedro, G. and Tessier, D., 1976. Rôle du fer dans l'organisation des matériaux kaolinitiques. Science du Sol, 2: 101-112.

Chesworth, W., 1977. Weathering stages of the common igneous rocks, index minerals and mineral assemblages at the surface of the earth. Journal of Soil Science, 28: 490-497.

Clapperton, C., 1993. Quaternary geology and geomorphology of South America. Elsevier, Amsterdam, 779 pp.

Coey, J.M., 1988. Magnetic properties of iron in soil iron oxides and clay minerals. In: J.W. Stucki, B.A. Goodman and U. Schwertmann (editors), Iron in Soils and Clay Minerals. D. Riedel Publishing Company, Dordrecht, Holland, NATO ASI Ser. 217: 397-466.

Cornell, R.M. and Schwertmann, U., 1996. The iron oxides: structure, properties, reactions, occurrence and uses. Verlag Chemie, Weinheim, 573 pp.

Coughtrey, P.J. and Thorne, M.C., 1983. Radionuclide distribution and transport in terrestrial and aquatic ecosystems: A critical review of data, Vol. 1, A. A. Balkema, Rotterdam.

Coulter, 1995. Coulter short course Particle characterization by laser light scattering., Coulter Corporation, Hialeah, 80pp.

Couto, W., Sanzonowicz, C. and Barcellos, O., 1985. Factors affecting oxidation-reduction processes in an Oxisol with a seasonal water table. Soil Science Society of America Journal, 49: 1245-1248.

Curi, N., 1983. Lithosequence and toposequence of Oxisols from Goiás and Minas Gerais States, Brazil. PhD Thesis, Purdue University, West Lafayette, 158 pp.

Curi, N. and Franzmeier, D.P., 1984. Toposequence of Oxisols from the Central Plateau of Brazil. Soil Science Society of America Journal, 48: 341-346.

Curi, N., Chagas, C.S. and Giarola, N.F.B., 1993. Distinção de ambientes agrícolas e relação solo-pastagens nos Campos de Mantiqueira, MG. In: M.M. Carvalho, A.R. Evangelista and N. Curi (editors), Desenvolvimento de pastagens na zona fisiográfica Campos das Vertentes, MG. Anais da Reunião de Trabalho, 1992, ESAL, Lavras, pp. 22-43.

Curmi, P., 1979. Altération et différenciation pédologique sur granite en Bretagne. Etude d'une toposéquence. PhD Thesis, École Nationale Supérieure Agronomique de Rennes, 176 pp.

Davis, J.C., 1986. Statistics and data analysis in geology, 2nd edition. John Wiley and Sons, New York, 696 pp.

De Boer, G.B.J., De Weerd, C., Thoenes, D. and Goossens, H.W.J., 1987. Laser diffraction spectrometry: Fraunhofer diffraction versus Mie scattering. Particle Characterization, 4: 14-19.

Dedecker, D. and Stoops, G., 1993. Micromorphological and mineralogical study of a polygenetic laterite profile (Trombetas Area, Brazil). Pedologie, 3: 335-356.

Deer, W.A., Howie, R.A., and Zussman, J., 1992. An introduction to the rock-forming minerals, 2nd Harlow, Longman, London, 696 pp.

de Grave, E., Bowen, L.H. and Weed, S.B., 1982. Mössbauer study of aluminum substituted hematite. Journal Magnetism and Magnetic Materials, 27: 98-108.

Deshpande, T.L., Greenland, D.J. and Quirk, J.P., 1964. Role of iron oxides in the bonding of soil particles. Nature, 201: 107-108.

Deshpande, T.L., Greenland, D.J. and Quirk, J.P., 1968. Changes in soil properties associated with the removal of iron and aluminium oxides. Journal of Soil Science, 19: 108-122.

Douglas, L.A., 1989. Vermiculites. In: J.B. Dixon and S.B. Weed (editors), Minerals in soil environments, 2nd edition. Soil Science Society of America, Madison, pp. 635-674.

El-Swaify, S.A. and Emerson, S.S., 1975. Changes in the physical properties of soil clays due to precipitated aluminium and iron hydroxides: I. Swelling and aggregate stability after drying. Soil Science Society of America Journal, 39: 1056-1063.

Embrechts, J. and Stoops, G., 1987. Microscopic identification and quantitative determination of microstructure and potentially mobile clay in a soil catena in a humid tropical environment.. In: N. Fedororoff, L. M. Bresson and M. A. Courty, Proceedings 7th International Working Meeting on Soil Micromorphology, Paris, 1985. Association Française pour L'Étude du Sol, Plaisir, France, pp. 157-162.

Emerson, W.W. and Greenland, D.J, 1990. Soil aggregates - formation and stability. In: M.F. De Boodt, M.B. Hayes and A. Herbillon (Editors), Soil colloids and their associations in aggregates. Plenum Press, New York, pp. 485-511.

Erlank, A.J., Smith, H.S., Marchant, J.W., Cardoso, M.P. and Ahrens, L.H., 1978. Zirconium. In: K.H. Wedepohl (editor), Handbook of geochemistry. Vol. II-4, Sec. 40B-O. Springer-Verlag, Germany.

Eswaran, H., Sys, C. and Souza, E.C., 1975. Plasma infusion - A pedological process of significance in the humid tropics. Anales de Edafologia e Agrobiologia, 34: 665-674.

Eswaran, H. and Heng, Y.Y., 1976. The weathering of biotite in a profile on gneiss in Malaysia. Geoderma, 16: 9-20.

Eswaran, H., Stoops, G. and Heng, Y.Y., 1977. The micromorphology of gibbsite forms in soils. Journal of Soil Science, 28: 136-143.

Eswaran, H. and Stoops, G., 1979. Surface textures of quartz in tropical soils. Soil Science Society of America Journal, 43: 420-424.

Fabris, J.D., Resende, M., Galvão Silva, E. and Coey, J.M.D., 1985. Iron oxides in two Oxisols from the Brazilian coastal plain. Journal of Soil Science, 36: 543-550.

Fabris, J.D., Resende, M., Allan, J. and Coey, J.M.D., 1986. Mössbauer analysis of Brazilian Oxisols. Hyperfine Interactions, 29: 1093-1096.

Fanning, D.S. and Fanning, M.C.B., 1989. Soil: Morphology, genesis, and classification. John Wiley and Sons, New York, 395 pp.

Fanning, D.S., Keramidas, V.Z. and El-Desoky, M.A., 1989. Micas. In: J.B. Dixon and S.B. Weed (editors), Minerals in soil environments, 2nd edition. Soil Science Society of America, Madison, pp. 551-624.

Faure, P., 1987. Les héritages ferrallitiques dans les soils jaunes du Nord-Togo. Aspects micromorphologiques des elements figurés.. In: N. Fedororoff, L. M. Bresson and M. A. Courty, Proceedings 7th International Working Meeting on Soil Micromorphology, Paris, 1985. Association Française pour L'Étude du Sol, Plaisir, France, pp.. 111-118.

Feijtel, T.C., Jongmans, A.G. and van_Doesburg, J.D.J., 1989. Identification of clay coatings in an older quaternary terrace of the Allier, Limagne, France. Soil Science Society of America Journal, 53: 876-882.

Felix-Henningsen, P., 1994. Mesozoic-Tertiary weathering and soil formation on slates of the Rhenish Massif, Germany. Catena 21: 229-242.

Felix-Heningsen, P., Scholten, T. and Schotte, M., 1997. Characterization of disordered kaolinites from soil-saprolite complexes by DMSO intercalation. In: P. Felix-Henningsen and A. Bronger (editors), Recent

and paleo-pedogenesis as tools for modelling past and future global change. International Working Meeting of ISSS/Commission V and INQUA/Commission on Paleopedology, Book of Abstracts: 22-23.

Fey, M.V. and Dixon, J.B., 1981. Synthesis and properties of poorly crystalline hydrated aluminous goethites. Clays and Clay Minerals, 29: 91-100.

Fitzpatrick, R.W., and Schwertmann, U., 1982. Al-substituted goethite as an indicator of pedogenic and other weathering environments in South Africa. Geoderma, 27: 335-347.

Fitzpatrick, E. A., 1984. Micromorphology of Soils. Chapman and Hall, New York, 433 pp.

Fitzpatrick, R.W., 1988. Iron compounds as indicators of pedogenic processes: Examples from the southern hemisphere. In: J.W. Stucki, B.A. Goodman and U. Schwertmann (editors), Iron in Soils and Clay Minerals. D. Riedel Publishing Company, Dordrecht, Holland, NATO ASI Ser. 217: 351-396.

Flach, K.W., Cady, J.G. and Nettleton, W.D., 1968. Pedogenic alteration of highly weathered parent materials. Transactions International Congress of Soil Science, Adelaide, Australia, 4: 343-351.

Fontes, M.P.F. and Weed, S.B., 1991. Iron oxides in selected Brazilian Oxisols: I. Mineralogy. Soil Science Society of America Journal, 55: 1143-1149.

Fontes, M.P.F., Bowen, L.H. and Weed, S.B., 1991. Iron oxides in selected Brazilian Oxisols: II. Mössbauer studies. Soil Science Society of America Journal, 55: 1150-1155.

Friedl, J. and Schwertmann, U., 1996. Aluminium influence on iron oxides: The effect of Al substitution and crystal size on magnetic hyperfine fields of natural goethites. Clay Minerals, 31: 455-464.

Gibbs, R.J., 1982. Floc stability during Coulter size analysis. Journal of Sedimentary Petrology, 52: 657-660.

Golden, D.C., Bowen, L.H., Weed, S.B. and Bigham, J.M., 1979. Mössbauer studies of synthetic and soil-occurring aluminum-substituted goethites. Soil Science Society of America Journal, 43: 802-808.

Graham, R.C., Weed, S.B., Bowen, L.H. and Buol, S.W., 1989. Weathering of iron-bearing minerals in soil and saprolite on the North Carolina Blue Ridge Front: 1. Sand-size primary minerals. Clays and Clay Minerals, 37: 19-28.

Greenland, D.J., Oades, J.M. and Sherwin, T.W., 1968. Electron microscope observations of iron oxides in some red soils. Journal of Soil Science, 19: 123-126.

Gupta, A., 1993. The changing geomorphology of the humid tropics. Geomorphology, 7: 165-186.

Hamilton, R., 1964. A short note on droplet formation in ironcrusts. In: A. Jongerius (editor), Soil Micromorphology. Proceedings 2nd International Working Meeting on Soil Micromorphology, Arnhem, The Netherlands, 1964. Elsevier, Amsterdam, pp. 277-278.

Haralyi, N.L.E., 1985. Ensaio sobre a estruturação crustal pré-Cambriana do Estado de Minas Gerais com base na informação geofisica e geológica. Sociedade Brasileira de Geologia, Belo Horizonte, Boletim Especial, volume Djalma Guimarães, pp. 71-93.

Hasui, Y., 1990. Neotectônica e aspectos fundamentais da tectônica ressurgente no Brasil. Anais 1º Workshop sobre Neotectônica e Sedimentação Cenozóica Continental no Sudeste Brasileiro, SBG/MG, Belo Horizonte, Boletim n. 11: 1-31.

Heier, K.S., 1970. Rubidium. In: K.H. Wedepohl (editor), Handbook of geochemistry. Vol. 2-4, Sec. 37-G-1/2. Springer-Verlag, Germany.

Heilbron, M., 1985. O metamorfismo da área de Itutinga - Madre de Deus de Minas, MG. In: Anais do 3º Simpósio de Geologia de Minas Gerais, SBG/MG, Belo Horizonte, pp. 219-227.

Heinrich, E.W., 1977. Niobium. In: K.H. Wedepohl (editor), Handbook of geochemistry. Vol. 2-4, Sec. 41-G-1/2. Springer-Verlag, Germany.

Herbillon, A.J., Mestdagh, M.M., Vielvoye, L. and Derouane, E.G., 1976. Iron in kaolinite with special reference to kaolinite from tropical soils. Clay Minerals, 11: 201-220.

Hoff, E.V., and Bott, S. 1990. Optical theory and refractive index: Why it is important to particle size analysis. Coulter Technical Bulletin LS Series 1010, 8 pp.

Jastrow, J. D. and Miller, R. M., 1991. Methods for assessing the effects of biota on soil structure. Agricultural Ecosystems Environments, 34: 279-303.

Jeanroy, E., Rajot, J.L., Pillon, P. and Herbillon, A.J., 1991. Differential dissolution of hematite and goethite in dithionite and its implication on soil yellowing. Geoderma, 50: 79-94.

Johnson, D.L., Keller, E.A. and Rockwell, T.K., 1990. Dynamic pedogenesis: New views on some key concepts, and a model for interpreting Quaternary soils. Quaternary Reseach, 33: 306-319.

Jungerius, P.D., 1985. Soils and Geomorphology. In: P.D. Jungerius (editor), Soils and Geomorphology, Catena Supplement 6: 1-18.

Kämpf, N, and Schwertmann, U., 1982. The 5M NaOH concentration treatment for iron oxides in soils. Clays and Clay Minerals, 30: 401-408.

Kämpf, N., 1988. X-ray diffraction of iron oxides of selected samples from the 8th International Soil Classification Workshop pedons. In: F.H. Beinroth, M.N. Camargo and H. Eswaran (editors), Proceedings of the 8th International Soil Classification Workshop, SNLCS/EMBRAPA, USDA, Rio de Janeiro, 1: 139-144.

Kämpf, N., Resende, M., Curi, N., 1988. Iron oxides in Brazilian Oxisols. In: F. H. Beinroth, M.N. Camargo and H. Eswaran (editors), Proceedings of the 8th International Soil Classification Workshop, SNLCS/EMBRAPA, USDA, Rio de Janeiro, 1: 71-77.

Kämpf, N, and Schwertmann, U., 1995. Goethitas na interface solo-rocha em amostras do Rio Grande do Sul e Minas Gerais. Revista Brasileira de Ciência do Solo, 19: 359-366.

Karfunkel, J. and Noce, C.M., 1983. Desenvolvimento faciológico do Pré-Cambriano superior da Região de Carandaí - São João del Rei- Minas Gerais. In: Anais do II Simpósio de Geologia de Minas Gerais, SBG/MG, Belo Horizonte, pp. 16-29.

King, D.L., 1976. Planation remnants upon highlands. Zeitschrift für Geomorphologie, 20: 133-148.

King. L. C., 1957. A geomorfologia do Brasil Oriental. Revista Brasileira de Geografia, 18: 147-263.

Koppi, A.J. Edis, R., Field, D., Geering, H.R., Klessa, D.A. and Cockayne, D.J.H., 1996. Rare earth element trends and cerium-uranium-manganese associations in weathered rock from Koongarra, Northern Territory, Australia. Geochimica et Cosmochimica Acta, 60: 1695-1707.

Krauskopf, K.B. and Bird, D.K., 1995. Introduction to geochemistry, 3th edition. McGraw-Hill, New York, 647 pp.

Lichte, M., 1990. Stonelines as a definite cyclic feature in southeast Brazil: A geomorphological and pedological case study. Pedologie, 40: 101-109.

Loizeau, J.L., Arbouille, D., Santiago, S. and Vernet, J.P., 1994. Evaluation of a wide range laser diffraction grain size analyser for use with sediments. Sedimentology, 41: 353-361.

Loveland, P.G. and Whalley, W.R., 1991. Particle size analysis. In: K.A. Smith and C.E. Mullins (editors), Soil Analysis: Physical Methods. Marcel Dekker, New York, pp. 271-328.

Lucas, Y., Chauvel, A. and Ambrosi, J.P., 1987. Processes of Aluminium and Iron Accumulation in Latosols Developed on Quartz-Rich sediments from Central Amazonia (Manaus, Brazil). In: R. Rodriguez-Clemente and Y. Tardy (editors), Geochemistry and Mineral Formation in the Earth Surface, CSIC/CNRS, Madrid, pp. 289-299.

Macedo, J. and Bryant, R.B., 1989. Preferential microbial reduction of hematite over goethite in a Brazilian Oxisol. Soil Science Society of America Journal, 53: 1114-1118.

Magalhães Jr., A. and Saadi, A., 1994. Ritmos da dinâmica fluvial neo-Cenozóica controlados por soerguimento regional e falhamento: O Vale do Rio das Velhas na região de Belo Horizonte, Minas Gerais, Brasil. Geonomos, Revista de Geociências, 1: 42-54.

McCave, I.N., Bryant, R.J., Cook, H.F. and Coughanowr, C.A., 1986. Evaluation of a laser diffraction size analyser for use with natural sediments. Journal of Sedimtary Petrology, 56: 561-564.

Meijer, E.L. and Buurman, P., 1997. Factor analysis and direct optimization of the amounts and properties of volcanic soil constituents. Geoderma, 80: 129-151.

Meis, M.R.M. and Moura, J.R.S., 1984. Upper quaternary sedimentation and hillslope evolution: Southeastern Brazilian plateau. American Journal of Science, 284: 241-254.

Melfi, A.J. and Pedro, G., 1977. Estudo Geoquímico dos solos e formaçoes superficiais do Brasil. Parte 1: Caracterização e repartição dos principais tipos de evolução pedogeoquímica.. Revista Brasileira de Geociências, 7: 271-286.

Melfi, A.J., Subies, F., Nahon, D. and Formoso, M.L.L., 1996. Zirconium mobility in bauxites of Southern Brazil. Journal of South American Earth Sciences, 9: 161-170.

Melo, M.S., 1984. La tectonique méso-cénozoique et le paysage du SE Brésilien. Compte rendu du seminaire du laboratoire de geologie du quaternaire, CNRS-ORSTOM INQUA-PICG, Génèse de Paysages Brésiliens, Cahiers ORSTOM, sér. Géol., 9:173-174.

Merino, E., Nahon, D. and Wang, Y., 1993. Kinetics and mass transfer of pseudomorphic replacement: application to replacement of parent minerals and kaolinite by Al, Fe, and Mn oxides during weathering. American Journal of Science, 293: 135-155.

Mestdagh, M.M,. Vielvoye, L. and Herbillon, A.J., 1980. Iron in kaolinite: II. The relationship between kaolinite crystallinity and iron content. Clay Minerals, 15: 1-13.

Michalet, R., Guillet, B. and Souchier, B., 1993. Hematite identification in pseudoparticles of Moroccan rubified soils. Clay Minerals, 28: 233-242.

Miedema, R., Jongmans, A.G. and Brinkman, R., 1987. The micromorphology of a typical catena from Sierra Leone, West Africa.. In: N. Fedoroff, L. M. Bresson and M. A. Courty, Proceedings 7th International Working Meeting on Soil Micromorphology, Paris, 1985. Association Française pour L'Étude du Sol, Plaisir, France, pp. 137-144.

Milnes, A.R. and Fitzpatrick, R.W., 1989. Titanium and zirconium minerals. In: J. B. Dixon and S. B.Weed (editors), Minerals in soil environments, 2nd edition. Soil Science Society of America, Madison, pp. 1132-1205.

Mohr, E.C.J., van Baren, F.A. and van Schuylenborgh, J., 1972. Tropical Soils: A comprehensive study of their genesis, 3th edition. Mouton, The Hague, 481pp.

Motta, P.E.F. and Kämpf. N., 1992. Iron oxide properties as support to soil morphological features for prediction of moisture regimes in Oxisols of Central Brazil. Zeitschrift fur Pflanzenernahrüng und Bodenkunde, 155: 385-390.

Muggler, C. C. and Buurman, P., 1997. Micromorphological aspects of polygenetic soils developed on phyllitic rocks in Minas Gerais, Brazil. In: S. Shoba, M. Gerasimova, and R. Miedema, (Editors), Soil Micromorphology: Studies on Soil Diversity, Diagnostics, Dynamics. Proceedings 10th International Working Meeting on Soil Micromorphology, Moscow, Russia, 1996: pp. 129-138.

Muggler, C.C., Buurman, P. and Pape, Th., 1997. Laser grain-size determination in soil genetic studies 2. Clay content, clay formation, and aggregation in some Brazilian Oxisols. Soil Science, 162: 219-228.

Muller, J.P. and Bocquier, G., 1986. Dissolution of kaolinites and accumulation of iron oxides in lateritic-ferruginous nodules: mineralogical and microstructural transformations. Geoderma, 37: 113-136.

Muller, J.P. and Bocquier, G., 1987. Textural and mineralogical relationships between ferruginous nodules and surrounding clayey matrices in a laterite from Cameroon. In: L.G. Schultz (editor), Proceedings of the International Clay Conference. Denver, 1985, Clay Mineral Society, Bloomington, 186-194.

Murad, E., 1978. Yttrium and zirconium as geochemical guide elements in soil and stream sediment sequences. Journal of Soil Science, 29: 219-223.

Murad, E. and Schwertmann, U., 1983. The influence of aluminium substitution and crystallinity on the Mössbauer spectra of goethite. Clay Minerals, 18: 301-312.

Murad, E., Schwertmann, U., 1986. Influence of Al substitution and crystal size on the room-temperature Mössbauer spectrum of hematite. Clays and Clay Minerals, 34: 1-6.

Murad, E. and Bowen, L.H., 1987. Magnetic ordering in Al-rich goethites: influence of crystallinity. American Mineralogist, 72:194-200.

Murad, E., 1988. Properties and behavior of iron oxides as determined by Mössbauer spectroscopy. In: J.W. Stucki, B.A. Goodman and U. Schwertmann (editors), Iron in Soils and Clay Minerals. D. Riedel Publishing Company, Dordrecht, Holland, NATO ASI Ser. 217: 309-350.

Murad, E., 1990. Application of ^{57}Fe Mössbauer spectroscopy to problems in clay mineralogy and soil science: possibilities and limitations. Advances in Soil Science, 12: 125-157.

Murad, E. and Wagner, U., 1991. Mössbauer spectra of kaolinite, halloysite and the firing products of kaolinite: New results and a reappraisal of published work. Neues Jahrbüch Miner. Abh., 162: 281-309.

Murad, E., 1996. Magnetic properties of microcrystalline iron (III) oxides and related materials as reflected in their Mössbauer spectra. Physics and Chemistry of Minerals, 23 : 248-262.

Murray, H.H., 1988. Kaolin minerals: Their genesis and occurrences. In: S.W. Bailey (editor), Hydrous Phyllosilicates (exclusive of micas). Mineralogical Society of America, Reviews in Mineralogy, 19: 67-89.

Nahon, D.B., 1991. Introduction to the petrology of soils and chemical weathering. John Wiley and Sons, New York, 313 pp.

Nahon, D.B., 1991a. Self-organization in chemical lateritic weathering. Geoderma, 51: 5-13.

O'Brien, E.L. and Buol, S.W., 1984. Physical transformations in a vertical soil-saprolite sequence. Soil Science Society of America Journal, 48: 354-357.

Ojanuga, A.G., 1990. Minerals and mineral weathering in saprolites and soils of tropical humid to semi-arid West Africa. Transactions 14th International Congress of Soil Science, Kyoto, Japan, August 1990, 7: 106-111.

Ollier, C.D., 1959. A two-cycle theory of tropical pedology. Journal of Soil Science, 10: 137-148.

Ollier, C.D., 1995. Tectonics and landscape evolution in Southeast Australia. Geomorphology, 12: 37-44.

Pedro, G. and Volkoff, B., 1984. Grandes provinces pédologiques du Brésil. Cadre général de l'évolution pédologique. Compte rendu du seminaire du laboratoire de Geologie du quaternaire, CNRS - ORSTOM/INQUA - PICG, 1984: Génèse des Paysages Brésiliens, Cahiers ORSTOM, sér. Géol., 14: 169-188.

Pereira, V. and Fitzpatrick, E.A., 1995. Cambisols and related soils in North-central Portugal: their genesis and classification. Geoderma, 66: 185-212.

Peterschmitt, E., Fritsch, E., Rajot, J.L. and Herbillon, A.J., 1996. Yellowing, bleaching and ferritisation processes in soil mantle of the Western Ghats, South India. Geoderma, 74: 235-253.

Pinheiro-Dick, D. and Schwertmann, U., 1996. Microaggregates from Oxisols and Inceptisols: dispersion through selective dissolutions and physicochemical treatments. Geoderma, 74: 49-63.

Pinto, O.C.B., Yahner, J.E. and Roth, C.B., 1972. Natureza e formação de caolinita em forma de pseudomica, em solos de Viçosa, Minas Gerais. Experientiae, 13: 383-421.

PiPujol D. and Buurman, P., 1994. The distinction between ground-water gley and surface-water gley phenomena in Tertiary paleosols of the Ebro basin, NE Spain. Palaeogeography, Palaeoclimatology, Palaeoecology, 110: 103-113.

Pleijsier, L.K., 1986. The laboratory methods and data exchange programme: Interim report of the exchange round 86-I. Working paper 86/4. International Soil Information and Reference Centre, Wageningen, The Netherlands.

Pollard, R.J., Pankhurst, Q.A. and Zientek, P., 1991. Magnetism in aluminous goethite. Physics and Chemistry of Minerals, 18: 259-264.

Ramakrishnan, C., Mani, R. and Suresh-Babu, D.S., 1997. Ilmenite from the Chavara deposit, India: A critical evaluation. Mineralogical Magazine, 61: 233-242.

Range, K.J., Range, A. and Weiss, A., 1969. Fire-clay type kaolinite or fire-clay mineral? Experimental classification kaolinite-halloysite minerals. Proceedings of the International Clay Conference, 1969, Tokyo, Israel University Press, Jerusalem, 1: 3-13.

Rausell-Colom, J.A. and Serratosa, J.M., 1987. Reactions of clays with organic substances. In: A.C.D. Newman (editor), Chemistry of clays and clay minerals. Mineralogical Society, monograph 6: 371-422.

Rebertus, R.A., Weed, S.B. and Buol, S.W., 1986. Transformation of biotite to kaolinite during saprolite-soil weathering. Soil Science Society American Journal, 50: 810-819.

Rengasamy, P., Krishna Murti, G.S.R. and Sarma, V.A.K., 1975. Isomorphous substitution of iron for aluminium in some soil kaolinites. Clays and Clay Minerals, 23: 210-214.

Resende, M., 1976. Mineralogy, chemistry, morphology and geomorphology of some soils of the Central Plateau of Brazil. PhD Thesis. Purdue University, West Lafayette, 237 pp.

Resende, M., Curi, N., Santana, D.P., 1988. Pedologia e fertilidade do solo, interações e aplicações. MEC/ESAL/POTAFOS, Brasília, 81pp.

Ribeiro, F.S. and Saadi, A., 1989. Os terraços do Baixo Vale do Rio Carandaí (Minas Gerais): Possível significado. In: Anais do Simpósio de Geografia Física Aplicada, Nova Friburgo, Rio de Janeiro, 1: 131-148.

Riccomini, C., Peloggia, A.U.G., Saloni, J.C.L., Kohnke, M.W. and Figueira, R.M., 1989. Neotectonic activity in the Serra do Mar rift system (Southeastern Brazil). Journal of South American Earth Sciences, 2: 191-197.

Russel, E.W., 1971. Soil structure: Its mantenance and improvement. Soil Science, 22:137-151.

Saadi, A., Noce, C.M. and Quintão, N.H., 1989. Neotectônica na Região Sul de Minas Gerais. In: Anais do V Simpósio de Geologia, Núcleo Minas Gerais, I Simpósio de Geologia, Núcleo Brasília, SBG, pp. 115-119.

Saadi, A., 1990. Um "Rift" neo-Cenozóico na Região de São João del Rei, MG; borda sul do Cráton do São Francisco. Anais 1º Workshop sobre Neotectônica e Sedimentação Cenozóica Continental no Sudeste Brasileiro, SBG/MG, Belo Horizonte, Boletim 11: 63-79.

Saadi, A. and Valadão, R.C., 1990. Eventos tectono-sedimentares na bacia neo-cenozóica de Rio das Mortes (Região de São João del Rei-MG). In: 1º Workshop sobre Neotectônica e Sedimentacão Cenozóica Continental no Sudeste Brasileiro, SBG/MG, Belo Horizonte, Boletim 11: 81-100.

Saadi, A., 1991. Ensaio sobre a morfotectônica de Minas Gerais. IGC/UFMG, Belo Horizonte. (Tese para provimento de cargo de professor titular), 285pp.

Saadi, A., 1992. A zona transpressiva de São Sebastião da Vitória no rift Cenozóico de São João Del Rei (MG) e feições neotectônicas associadas. In: 37° Congresso Brasileiro de Geologia, São Paulo, SP, Boletim de Resumos Expandidos, 1: 603-604.

Saadi, A., 1993. Neotectônica e tectônica recorrente na porção sul do cráton do São Francisco. In: Anais do 3º Simpósio do Cráton do São Francisco, Salvador, Bahia, pp. 230-232.

Saadi, A., 1994. Neotectônica da Plataforma Brasileira: esboço e interpretação preliminares. Geonomos, Revista de Geociências, 1: 1-15.

Sans, L. M. A., 1986. Estimativa do regime de umidade, pelo método do Newhall, de um Latosssolo Vermelho-Escuro álico da região de Sete Lagoas, MG. PhD Thesis. Universidade Federal de Viçosa, Brazil, 190pp.

Santos, L.J.C. and Ferreira, A.M.M., 1989. Contribuição ao estudo de paleoambientes em depósitos coluviais no município de São João del Rei - MG. In: Anais do Simpósio de Geografia Física Aplicada, Nova Friburgo, Rio de Janeiro, 1: 117-129.

Schmidt Lorenz, R., 1980. Soil Reddening through Hematite from Plinthitized Saprolite. In: K.T. Joseph

(editor), Proceedings of the Conference on Classification and Management of Tropical Soils 1977, Kuala Lumpur, Malaysian Society of Soil Science, pp. 101-106.

Schobbenhaus, C., Campos, D.A., Derze, G.R. and Asmus, H.E., 1984. Geologia do Brasil. Texto explicativo do mapa geológico do Brasil e da área oceânica adjacente incluindo depósitos minerais. SNPMA/MME, Brasilia, 501 pp.

Scholten, T., Felix Henningsen, P. and Mushala, H.M., 1995a. Morphogenesis and erodibility of soil-saprolite complexes from magmatic rocks in Swaziland (Sothern Africa). Zeitschrift für Pflanzenernahrüng und Bodenkunde, 20: 169-176.

Scholten, T., Schotte, M. and Felix Henningsen, P., 1995. Bestimmung von kaolinit mit einlagerungsfehlordnung in einem boden-saprolit-komplex inter verwendung einer einfachen dimethylsulfoxid- bedampfungsmethode Miteilungen der Deutschen Bodenkundlichen Gesellshaft, 76: 1397-1400.

Schroeer, D., 1970. The Mössbauer effect in microcrystals. Mössbauer Effect Methodology, 5: 141-162.

Schulze, D.G., 1984. The influence of aluminum on iron oxides. VIII. Unit-cell dimensions of Al-substituted goethites and estimation of Al from them. Clays and Clay Minerals, 32: 36-44.

Schulze, D.G. and Schwertmann, U., 1984. The influence of aluminum on iron oxides. X. Properties of Al-substituted goethites. Clay Minerals, 19: 521-539.

Schwarz, T., 1994. Ferricrete formation and relief inversion: An example from Central Sudan. Catena, 21: 257-268.

Schwertmann, U., Fitzpatrick, R.W. and Roux, J., 1977. Al substitution and differential disorder in soil hematites. Clays and Clay Minerals, 25: 373-374.

Schwertmann, U., Fitzpatrick, R.W., Taylor, R.M. and Lewis, D.G., 1979. The influence of aluminum on iron oxides. Part II. Preparation and properties of Al-substituted hematites. Clays and Clay Minerals, 27: 105-112.

Schwertmann, U. and Murad, E., 1983. Effect of pH on the formation of goethite and hematite from ferrihydrite. Clays and Clay Minerals, 31: 277-284.

Schwertmann, U., 1985. The effect of pedogenic environments on iron oxide minerals. In: B.A. Stewart (editor), Advances in Soil Science, 1: 171-200.

Schwertmann, U. and Kämpf, N., 1985. Properties of goethite and hematite in kaolinitic soils of Southern and Central Brazil. Soil Science, 139: 344-350.

Schwertmann, U., 1988. Some properties of soil and synthetic iron oxides. In J. W. Stucki, B.A. Goodman and U. Schwertmann (editors), Iron in Soils and Clay Minerals. D. Riedel Publishing Company, Dordrecht, Holland, NATO ASI Ser. 217: 203-250.

Schwertmann, U., 1988a. Goethite and hematite formation in the presence of clay minerals and gibbsite at 25°C. Soil Science Society of America Journal, 52 : 288-291.

Schwertmann, U., 1988b. Ocurrence and formation of iron oxides in various pedoenvironments. In: J. W Stucki. B.A. Goodman. and U. Schwertmann (editors), Iron in Soils and Clay Minerals. D. Riedel Publishing Company, Dordrecht, Holland, NATO ASI Ser. 217: 251-266.

Schwertmann, U. and Taylor, R.M., 1989. Iron oxides. In: In: J.B. Dixon and S.B. Weed (editors), Minerals in soil environments, 2nd edition. Soil Science Society of America, Madison, pp. 379-438.

Schwertmann, U. and Fitzpatrick, R.W., 1992. Iron minerals in surface environments. In: H.C.W. Skinner and R.W. Fitzpatrick (editors), Biomineralization processes of iron and manganese. Catena Supplement 21, Catena Verlag, pp. 7-30.

Schwertmann, U., 1993. Relations between iron oxides, soil color, and soil formation. Soil Color, SSSA Special Publication n. 31: 51-69.

Schwertmann, U. and Carlson, L., 1994. Aluminum influence on iron oxides: XVII. Unit-cell parameters and

aluminum substitution of natural goethites. Soil Science Society of America Journal, 58: 256-261.

Singer, J.K., Anderson, J.B., Ledbetter, M.T., McCave, I.N., Jones, K.P.N. and Wright, R., 1988. An assessment of analytical techniques for the size analysis of fine-grained sediments. Journal of Sedimentary Petrology, 55: 590-593.

Singh, B., and R.J. Gilkes, 1991. Concentration of iron oxides from soil clays by 5M NaOH treatment: the complete removal of sodalite and kaolin. Clay Minerals, 26: 463-472.

Singh, B. and Gilkes, R.J.,1992. Properties and distribution of iron oxides and their association with minor elements in the soils from South-western Australia. Journal of Soil Science, 43: 77-98.

Singh, B. and Gilkes, R.J., 1992a. Properties of soil kaolinites from south-western Australia. Journal of Soil Science, 43: 645-667.

Soil Survey Staff, 1975. Soil Taxonomy: A basic system of soil classification for making and interpreting soil surveys. Agriculture Handbook 436. US Dept. of Agriculture, 754 pp.

Soil Survey Staff., 1994. Keys to Soil Taxonomy. 6th edition. United States Department of Agriculture, Soil Conservation Service, 306 pp.

Stolt, M.H., Baker, J.C. and Simpson, T.W., 1991. Micromorphology of the soil-saprolite transition zone in Hapludults of Virginia. Soil Science Society of America Journal, 55: 1067-1075.

Stoops, G. and Buol, S. W., 1985. Micromorphology of Oxisols. In: L. A. Douglas and M. L. Thompson (Editors), Soil Micromorphology and Soil Classification, Soil Science Society of America, Madison, pp. 105-119.

Stoops, G, 1989. Relict properties in soils of humid tropical regions with special reference to Central Africa. In: A. Bronger and J.A. Catt (editors), Paleopedology: Nature and Application of Paleosols. Catena Supplement 16: 95-106.

Stoops, G., Shi, G.C. and Zayuah, S., 1990. Combined micromorphological and mineralogical study of a laterite profile on graphite sericite phyllite from Malacca (Malaysia). Bulletin Societe Belge de Geologie, 99: 79-92.

Stoops, G., 1991. The influence of the fauna on soil formation in the tropics. Micropedological aspects. Académie Royale des Sciences D'outre-mer, Bulletin des Sèances, 36: 461-469.

Stoops, G., Marcelino, V., Zauyah, S. and Maas, A., 1994. Micromorphology of soils of the humid tropics. In: A.J. Ringrose-Voase and G.S. Humphreys (editors), Soil Micromorphology: Studies in Management and Genesis. Proceedings IX International Working Meeeting on Soil Micromorphology, Townsville, Australia, 1992. Developments in Soil Science 22, Elsevier, Amsterdam, pp. 1-15.

St-Pierre, T.G., Singh, B., Webb, J. and Gilkes, R.J., 1992. Mössbauer spectra of soil kaolins from South-western Australia. Clays and Clay Minerals, 40: 341-346.

Strauss, R., Brummer, G.W. and Barrow, N.J., 1997. Effects of cristallinity of goethite: I. Preparation and properties of goethites of differing crystallinity. European Journal of Soil Science, 48: 87-99.

Suresh-Babu, D.S., Thomas, K.A., Mohan Das, P.N. and Damodaran, A.D., 1994. Alteration of ilmenite in the Manavalakurichi deposit, India. Clays and Clay Minerals, 42: 567-571.

Tardy, Y. and Nahon, D., 1985. Geochemistry of laterites, stability of Al-goethite, Al-hematite and Fe^{3+}-kaolinite in bauxites and ferricretes: an approach to the mechanism of concretion formation. American Journal of Science, 285: 865-903.

Tardy, Y., 1993. Pétrologie de latérites et des sols tropicaux. Ed. Masson, Paris, 472 pp.

Taylor, G.L., Routsala, A.P. and Keeling, Jr. R.O., 1968. Analysis of iron in layer silicates by Mössbauer spectroscopy. Clays and Clay Minerals, 10: 381-391.

Thomas, M.F., 1994. Geomorphology in the Tropics. Wiley, Chichester, 460pp.

Tidball, R.R., Severson, R.C., Gent, C.A. and Riddle, G.O., 1989. Element associations in soil of the San Joaquin Valley of California. In: L.W. Jacobs, Selenium in Agriculture and the Environment, SSSA

Special Publication, Madison, 23: 179-193.

Torrent, J., Schwertmann, U. and Fechter, H. and Alferez, F., 1983. Quantitative relationships between soil color and hematite content. Soil Science, 136: 354-358.

Torrent, J., Schwertmann, U. and Barron, V., 1987. The reductive dissolution of synthetic goethite and hematite in dithionite. Clay Minerals, 22: 329-337.

Trolard, F. and Tardy, Y., 1987. The stabilities of gibbsite, boehmite, aluminous goethites and aluminous hematites in bauxites, ferricretes and laterites as a function of water activity, temperature and particle size. Geochimica et Cosmochimica Acta, 51: 945-957.

Valeriano, C.M., 1986. Geologia estrutural e estratigrafia do Grupo São João del Rei na região de São João del Rei, MG. In: Anais do XXXIV Congresso Brasileiro de Geologia, SBG, Goiânia, 1986, 2: 999-1018.

Van der Kraan, A.M. and Van Loef, J.J., 1966. Superparamagnetism in submicroscopic α-FeOOH particles observed by the Mössbauer effect. Physical Letters, 20: 614-616.

Van Loef, J.J., 1998. Mössbauer spectroscopic identification of iron oxides in rattle stones from North and South of the river Rhine (unpublished).

Vandenberghe, R.E., De Grave, E., De Geyter and Landuydt, C., 1986. Characterization of goethite and hematite in a Tunisian soil profile by Mössbauer spectroscopy. Clays and Clay Minerals, 34: 275-280.

Van Reeuwijk, L.P., 1995. Procedures for soil analysis, 5th edition, International Soil Reference and Information Centre, Technical Paper 9, Wageningen.

Volkoff, B., 1985. Organizations regionales de la couverture pedológique du Brésil. Chronologie des differenciations. Cahiers Orstom, sér. Pédol., 21: 225-236.

Weast, R.C. (editor), 1974. Handbook of chemistry and physics, 54 th Edition. CRC Press, Cleveland, 1624 pp.

Zeese, R., Schwertmann, U., Tietz, G.F. and Jux, U., 1994. Mineralogy and stratigraphy of three deep lateritic profiles of the Jos plateau (Central Nigeria). Catena, 21: 195-214.

Zeese, R. and Fodor, L., 1997. Dislocated ferricretes in central Nigeria as indicators of neogene crustal movement. In: P. Felix-Henningsen and A. Bronger (editors), Recent and paleo-pedogenesis as tools for modelling past and future global change. International Working Meeting of ISSS- Commission V and INQUA- Commission on Paleopedology, Book of Abstracts, pp. 54.

Zonneveld, P.C., 1994. Comparative investigation on grain-size determination (sieve/Malvern). Rept. No. OP 6500, State Geological Survey, Haarlem, The Netherlands.

APPENDICES

1. Profile descriptions
2. Routine chemical analyses
3. XRF analyses of major oxides and trace elements

1. PROFILE DESCRIPTIONS

Profile descriptions were made according to the FAO guidelines (FAO, 1990) and the soils were classified in conformity with the Soil Taxonomy system (Soil Survey Staff, 1994).

I - SÃO JOÃO DEL REI AREA

SJR catena - Profiles P1 - P5

Profile identification: P1
Classification: Anionic Acrudox
Location: Galeão Farm, São Sebastião da Vitória, Minas Gerais, Brazil
Geological unit: Barbacena (Archean) and São João del Rei (Proterozoic) groups
Parent material: saprolites of fine- and medium-textured metamorphic rocks
Soil-landscape unit: SJR-sap
Topography: almost flat to gently undulating
Elevation: 1050 m
Profile situation and position: roadcut, crest
Landuse and/or vegetation: extensive grazing (native pasture); annual field cropping (maize)
Erosion: sheet moderate
Drainage class: well drained

Description:

Ap (1)	*0-10cm*; Yellowish red (5YR 4/6) clay; coarse moderate granular structure; abundant fine and very fine pores; friable; abundant fine and very fine and few medium roots; clear and smooth boundary;
BA (2)	*10-50cm*; Dark red (2.5YR 3/6) clay; weak medium subangular blocky breaking into granular structure; abundant fine and very fine pores; very friable; common fine and very fine roots; gradual and smooth boundary;
Bw1 (3)	*50-95cm*; Red (2.5YR 4/8) clay; weak medium blocky breaking into very fine granular structure; abundant fine and very fine pores; friable; common fine and very fine roots; diffuse and smooth boundary;
Bw2 (4)	*95-150cm*; Red (10R 4/6) clay, weak medium blocky breaking into very fine granuluar structure; common fine and abundant very fine pores; firm; few fine and very fine roots; diffuse and smooth boundary;
Bw3 (5)	*150-265cm*; Red (10R 4/6) clay, weak medium blocky breaking into very fine granuluar structure; few fine and abundant very fine pores; friable; few fine and very fine roots; gradual and smooth boundary;
BC1 (6)	*265-320cm*; Red (2.5YR 4/6) silty clay; weak medium to fine subangular blocky structure; few fine and common very fine pores, friable, clear and smooth boundary; common angular quartz fragments;
BC2 (7)	*320-330/390cm*; Reddish brown (2.5YR 4/4) silty clay loam; weak medium to fine subangular blocky structure; few fine and common very fine pores, friable, clear and irregular (tongy) boundary; very few angular weathered rock fragments;
BC3 (8)	*330/390-410cm*; Red (2.5YR 4/6) silty clay loam; weak medium subangular blocky structure to structureless; few fine and very fine pores; friable; clear to gradual and smooth boundary; common angular weathered rock fragments;
C (9)	*410-550+cm*; silt; apedal; very few very fine pores; friable; abundant angular weathered rock fragments.

Profile identification: P2
Classification: Anionic Acrudox
Location: Galeão Farm, São Sebastião da Vitória, Minas Gerais, Brazil
Geological unit: Barbacena (Archean) and São João del Rei (Proterozoic) groups
Parent material: saprolites of fine- and medium-textured metamorphic rocks

Soil-landscape unit: SJR-sap
Topography: undulating to rolling
Elevation: 1035/1040 m
Profile situation and position: 2 m depth digged pit, upper (convex) slope
Landuse and/or vegetation: extensive grazing (native pasture); annual field cropping (maize)
Erosion: sheet severe, surface sealing
Drainage class: moderately well drained

Description:

Ap (11) *0-20cm*; Dark brown (7.5YR 4/4) clay; moderate to weak medium subangular blocky breaking into very fine granular structure; abundant fine and very fine pores; friable; common fine roots; clear and smooth boundary;

AB (12) *20-40cm*; Yellowish red (5YR 5/6) silty clay loam with dark brown (7.5YR 4/4) channels; moderate medium subangular blocky structure; abundant fine and very fine pores; firm; few fine roots; gradual and smooth boundary; few coarse (1cm) angular irregular hard nodules; presence of grey coloured burrows;

Bw (13) *40-65cm*; Yellowish red (5YR 5/8) silt loam; moderate medium subangular blocky structure; abundant fine and very fine pores; friable to firm; few fine roots; gradual and wavy boundary; few coarse (1cm) angular irregular hard nodules;

BC (14) *65-105/130cm*; Yellowish red (5YR 5/6) silt; moderate medium subangular blocky structure; abundant fine and very fine pores; friable to firm; very few fine roots; gradual and wavy boundary; few coarse (1cm) angular irregular hard nodules;

C (15) *105/130-200+cm*; Yellowish red (5YR 5/8) silt; weak subangular blocky structure; many fine and very fine pores; friable; abundant coarse angular irregular hard nodules, weathered rock fragments and quartz.

Profile identification: P3
Classification: Inceptic Hapludox
Location: Galeão Farm, São Sebastião da Vitória, Minas Gerais, Brazil
Geological unit: Barbacena (Archean) and São João del Rei (Proterozoic) groups
Parent material: saprolites of fine- and medium-textured metamorphic rocks
Soil-landscape unit: SJR-sap
Topography: rolling
Elevation: 1027 m
Profile situation and position: 2 m depth digged pit, middle (convex) slope
Landuse and/or vegetation: extensive grazing (native pasture); annual field cropping (maize); sparse savanna like vegetation (*campo cerrado*)
Erosion: sheet severe, surface sealing
Drainage class: moderately well drained

Description:

A (17) *0-15cm*; Dark yellowish brown (10YR 3/4) clay; strong coarse granular structure; abundant fine and very fine pores; firm; abundant fine and very fine roots; clear and wavy boundary;

AB (18) *15-25cm*; Dark brown (7.5YR 4/4) clay; moderate fine to medium subangular blocky structure; many fine and very fine pores; friable; many fine and very fine roots; clear and smooth boundary;

Bw (19) *25-42cm*; Strong brown (7.5YR 5/8) clay; moderate fine to medium subangular blocky structure; abundant very fine and common fine pores; friable; abundant very fine and common fine roots; clear and smooth boundary; pockets of angular quartz and iron concretions from 0.5 to 1 cm;

BC1 (20) *42-90cm*; Yellowish red (5YR 5/8) silty clay loam, weak medium subangular blocky structure; abundant very fine and few fine pores; friable; very few fine roots; gradual and smooth boundary; few angular quartz and iron concretions from 0.5 to 1 cm; (yellower in the top; the yellow red patterns are vertical)

BC2 (21) *90-125cm*; red (2.5YR 4/6) silt; massive; few very fine pores; friable; diffuse and wavy boundary;

C (22) *125-170+cm*; Dominant red (2.5YR 5/8) and strong brown (7.5YR 5/6) silt; massive; common very fine pores; very friable; common angular weathered rock fragments; no quartz.

Profile identification: P4
Classification: Inceptic Hapludox
Location: Galeão Farm, São Sebastião da Vitória, Minas Gerais, Brazil
Geological unit: Barbacena (Archean) and São João del Rei (Proterozoic) groups
Parent material: saprolites of fine- and medium-textured metamorphic rocks
Soil-landscape unit: SJR-sap
Topography: rolling
Elevation: 1018 m
Profile situation and position: 2 m digged pit, lower (convex) slope
Landuse and/or vegetation: annual field cropping (maize); sparse savanna-like vegetation *(campo cerrado)*
Erosion: sheet severe
Drainage class: moderately well drained

Description:

Ap (23) *0-20cm*; Dark yellowish brown (10YR 4/4) clay; moderate to weak medium subangular blocky breaking into very fine granular structure; few fine and many very fine pores; firm; clear and smooth boundary;

AB (24) *20-30cm*; Dark brown (7.5YR 4/4) clay; strong medium subangular blocky structure; few fine and many very fine pores; firm; clear and smooth boundary; common fine angular quartz grains; very coherent;

Bw (25) *30-42/50cm*; Dark brown (7.5YR 4/4) clay; weak medium subangular blocky structure; many very fine pores; friable; clear and wavy boundary; common fine angular quartz grains; less coherent;

BC1 (26) *42/50-90/100cm*; Yellowish red (5YR 5/8) silty clay loam with yellower channels protuding the horizon; massive; many very fine pores; very friable; clear and wavy boundary; common fine angular quartz grains; few large rounded weathered clay rock fragments (homogeneous no porous clay); less coherent;

BC2 (27) *90/100-130/150cm*; Red (2.5YR 4/8) silt loam (reddening to the bottom of the horizon); massive; many very fine pores; friable; clear and wavy boundary; very few medium angular quartz (it seems to be a vein); very coherent;

C (28) *130/150-200+cm*; Yellowish red (5YR 4/6) silt; massive; common very fine pores; very friable; medium (sharp) angular irregular dark yellowish brown (10YR 4/6) weathered rock fragments (clay concretions?); fine saprolite fragments at 1.75m and very clear ones at 2m.

Profile identification: P5
Classification: Udoxic Dystropept
Location: Galeão Farm, São Sebastião da Vitória, Minas Gerais, Brazil
Geological unit: Barbacena (Archean) and São João del Rei (Proterozoic) groups
Parent material: saprolites of fine- and medium-textured metamorphic rocks
Soil-landscape unit: SJR-sap
Topography: rolling
Elevation: 1007 m
Profile situation and position: 2 m digged pit, lower (convex to concave) slope
Landuse and/or vegetation: extensive (native) grazing
Rock outcrops and/or surface coarse fragments: gravel, stones and boulders of angular quartz
Erosion: sheet severe
Drainage class: moderately well drained

Description:

A *0-35cm*; Yellowish red (5YR 4/6) clay; clear and smooth boundary (colluvum);

Bw (29) *35-35/65cm*; Strong brown (7.5YR 5/6) clay; weak medium subangular blocky structure; abundant very fine pores; firm; few very fine roots; clear and wavy boundary;

BC (30) *35/65-75/100cm*; Yellowish red (5YR 4/6) silt loam; structureless to weak subangular blocky structure; many very fine pores; friable; very few fine roots; clear to abrupt irregular boundary; common fine to coarse angular weathered rock fragments locally with quartz;

C1(31) *75/100-130/170cm*; (B+C1); Dark red (2.5YR 3/6) silt; structureless; many very fine pores in B fragments, no pores in C1; friable; clear, wavy and tongy boundary; commonfine to very large angular weathered rock fragments locally with quartz; rock fractures surrounded by strong red hematite bands;

C2 (32) *130/170-200+cm*; Yellowish red (5YR 4/6) silt; structureless; very few fine pores; friable; common fine to very large angular weathered rock fragments locally with quartz; rock fractures surrounded by strong red hematite bands and very fine iron and manganese accumulations.

Profile P7

Profile identification: P7
Classification: Anionic Acrudox
Location: road BR 383 to Madre de Deus de Minas, 9 km from the crossroads with road BR 265.
Geological unit: Barbacena (Archean) and São João del Rei (Proterozoic) groups
Parent material: saprolites of fine textured metamorphic rocks (phyllites)
Soil-landscape unit: SJR-sap
Topography: undulating to rolling
Elevation: 1080 m
Profile situation and position: roadcut, upper (convex) slope
Landuse and/or vegetation: extensive grazing (native pasture); sparse savanna like vegetation *(campo cerrado)*
Erosion: sheet severe
Obs.: The sampling was done in two parts of the roadcut using a stone line (sl) as a correlation element.

Description:

A *0-5cm*; Yellowish brown (10YR 5/4) clay; strong fine granular and some fine subangular blocky structure; very friable; clear and smooth boundary;

Bw (41) *5-40cm*; Yellowish brown (10YR 5/8) clay; moderate fine angular blocky structure; many fine and very fine pores; very friable; common fine and very fine roots; clear and smooth boundary;

BC1 (42) *40-60cm*; Reddish yellow (7.5YR 6/8) clay; moderate medium angular blocky structure; common fine and very fine pores; firm; few fine and very fine roots; clear and smooth boundary; many quartz gravels up to 5mm;

BC2 (43) *60-85cm*; Yellowish red (5YR 5/6) clay; weak medium subangular blocky structure; common fine and many very fine pore; friable; very few fine roots; clear and smooth boundary; few quartz grains in the upper 5 cm and very few in the horizon;

st. line *85-95cm*; abundant angular coarse material up to 5 cm, white quartz dominating, some clay fragments;

IIBw (44) *95-125cm*; Red (2,5YR 4/8) clay; moderate medium angular blocky structure; common fine and many very fine pores; friable; no roots; gradual and smooth boundary;

IIBC1 (45) *125-155cm*; Red (2,5YR 4/6) clay; moderate medium angular blocky structure with few rounded burrows; many fine and abundant very fine pores; friable; no roots; gradual and smooth boundary; angular weathered rock fragments, some containing quartz;

IIBC2 (46) *155-245/275cm*; Red (2,5YR 5/6) clay loam; structure with many granular and fine granular elements; few rounded burrows; many fine and abundant very fine pores; friable; no roots; diffuse and wavy/oblique boundary; angular weathered rock fragments, some containing white and/or grey quartz;

C1 (47) *245/275-345/375cm*; Purple and white mixed silt loam with pockets of red (2,5YR 4/6) clay from overlying horizons; structureless; common very fine pores; friable; clear and oblique boundary; 40 to 60% of saprolite material showing schistosity;

C2 (48) *345/375-500+cm*; silt loam saprolite with pockets of weak red (10R 5/4) reworked material.

Profile P8

Profile identification: P8
Classification: Anionic Acrudox
Location: dirt road to Engenho da Barra, 7.6 km from the crossroads with road BR 265
Geological unit: Barbacena group (Archean)
Parent material: (graphitic) phyllites
Soil-landscape unit: SJR-sap
Topography: undulating to rolling
Elevation: 1012 m
Profile situation and position: roadcut, upper (convex) slope/crest
Landuse and/or vegetation: extensive grazing (native pasture); sparse savanna like vegetation (*campo cerrado/campo limpo)*
Erosion: none
Biological features: few termite mounds

Description:

A1 (495) *0-12cm*; Dark brown (7.5YR 4/4) clay; strong very fine granular structure; abundant fine and very fine pores; very friable; abundant fine and medium roots; clear and smooth boundary;

A2 (496) *12-40cm*; Dark brown (7.5YR 4/4) clay; strong coarse granular and fine subangular blocky structure; abundant fine pores; very friable; many fine roots; clear and smooth boundary;

AB (497) *40-55cm*; Reddish brown(5YR 4/4) clay; weak medium subangular blocky structure; many very fine pores; friable; common fine and very fine and few medium roots; gradual and smooth boundary; common burrows filled with material from overlying horizons;

Bw1 (498) *55-132cm*; Yellowish red (5YR 4/6) clay; weak medium subangular blocky breaking into fine medium granular structure; abundant very fine and common fine pores; friable; common fine roots; diffuse and smooth boundary

Bw2 (499) *132-280cm*; Red (25YR 4/6) clay; strong medium subangular blocky structure; many very fine and very few medium pores; firm; very few roots; abrupt and smooth boundary; very few quartz and phyllite gravels up to 5 mm randomly distributed in the horizon; the horizon has a granular aspect given by the presence of massive clay balls and/or cilinders (up to 1 cm) cemented by a more porous matrix;

st. line (500) *280-285cm*; quartz gravel layer; the quartz gravels have sizes up to 20 cm and are dominantly angular, with few subrounded larger ones;

BC1 (501) *285-310cm*; Red (10R 4/6) silty clay loam; weak medium subangular blocky structure; very few fine and very fine pores; firm; no roots; gradual and smooth boundary; 5% of phyllite gravelsrandomly distributed; silky shine on some ped surfaces;

BC2 (502) *310-385/395cm*; Red (10R 4/6) clay loam; weak coarse subangular blocky structure; very few fine and very fine pores; firm; no roots; clear to gradual and wavy boundary; silky shine on some ped surfaces;

C (503) *385/395-430/470cm*; Red (10R 4/6) to weak red (7.5R 4/4) loam; structureless; abrupt and wavy to irregular boundary; 20% of saprolite fragments with variegated colours from yellow to purple increasing towards the bottom;

rock (504) *430/470-500+cm*; laminated weathered phyllite with variegated colors.

VP sequence

Profile identification: VP
Classification: Anionic Acrudox
Location: dirt road to Catende, 2.8 km from the crossroads with road BR 265, São Sebastião da Vitória, Minas Gerais
Geological unit: Barbacena (Archean) and São João del Rei (Proterozoic) groups; Tertiary sediments
Parent material: saprolite of fine- and medium-textured metamorphic rocks
Soil-landscape unit: SJD-sed/ SJR-sap
Topography: undulating to rolling
Elevation: 1050 m
Profile situation and position: gully wall , upper slope
Landuse and/or vegetation: savana like vegetation (*cerrado/cerradão)*
Erosion: gully severe

Description:

AB (489) *0-10 cm*; Dark red (2.5YR 3/6) clay; strong fine granular structure; abundant fine and very fine pores (extremely porous); friable; abundant fine and very fine roots; clear and smooth boundary;

Bw1 (490) *10-85 cm*; Red (2.5YR 4/6) clay; moderate very fine granular structure; abundant fine and very fine pores (extremely porous); very friable; many fine and very fine roots; gradual and smooth boundary;

Bw2 (491) *85-150 cm*; Red (2.5YR 5/6) clay; moderate fine granular structure; many fine and very fine pores; friable; very few fine roots; diffuse and smooth boundary;

Bw3 (492) *150-320 cm*; Red (10R 4/6) clay; moderate fine granular structure; many fine and very fine pores; friable; very few fine roots; gradual and smooth boundary;

Bw4 (493) *320-530 cm*; Red (10R 4/6) clay; weak coarse subangular blocky to massive; many fine and very fine pores; firm; gradual and smooth boundary; presence of more massive elements (clay balls up to 1 cm), which have lighter colours than the matrix

Bw5 (65) *530-730 cm*; Red (10R 4/6) clay; weak coarse subangular blocky to massive structure; many very fine pores; firm; no roots; clear and irregular boundary; 1% of yellower slightly coarser material which appears looser than the matrix, and seems to be related to a crack;

BC1 (64) *730-800 cm*; Red (2.5YR 4/6) clay; massive; common very fine pores; hard; clear and wavy boundary; presence of slight stratification; colour becomes lighter to the bottom of the horizon;

BC2 (63) *800-860 cm*; Red (2.5YR 5/8) clay; massive with presence of channels (burrows up to 2 cm) with material of the overlying horizons and granular structure; very porous; at 840 cm a layer with yellowish red (5YR 5/8) massive clay balls appears; clear and wavy boundary;

C1 (62) *860-1020 cm*; Strong brown (7.5YR 5/8) to brownish yellow (10YR 6/8) clay with red (2.5YR 4/6) burrow channels filled with materials from overlying horizons; structureless to weak subangular blocky structure; common very fine pores; very friable to loose; abrupt and broken boundary; patches of yellowish brown (10YR 5/8) more massive clay units; few burrows up to 0.7 cm; slight stratification;

C2 (61) *1020-1110 cm*; Dark grayish brown (2.5Y 4/2) clay broken by gray massive clay banks with remnants of horizontal stratification; massive; hard; 40% of very fine light yellowish brown (2.5Y 6/4) to brown (10YR 5/3) clay fragments (burrows or pores); variegated yellow/gray horizon;

C3 (60) *1110-1180 cm*; Brownish yellow (10YR 6/6) clay loam; massive; few very fine channels filled with red material; remnants of horizontal stratification;

C4 (59) *1180-1325 cm*; Red (7.5R 4/6) clay; massive; hard; presence of brownish yellow (10YR 6/6) to strong brown (7.5YR 5/8) channels; clear and broken boundary;

V (56, 494) *1325-1380 cm*; predominantly red (2.5YR 4/6) clay loam; with abundant white (5YR 8/1) and gray to yellowish bleached channels and/or burrows;

IV (55) *1380-1480cm*; reddish clay matrix layer which bottom part is largely disrupted and obliterated by white channels, more abundant in the last 15 cm. In the upper part they disappear or occur along cracks. Rounded and subangular iron nodules and quartz pebbles occur occasionally at the bottom of the layer;

sap *1480-1560+cm;* Red (2.5YR 4/6) silt and sandy loam; massive saprolite strongly bleached at the top, with some Mn accumulations. (50-53, 57,58)

P6 sequence

Profille identification: P6
Classification: Petroferric Acrudox
Location: crossroads BR 265/BR383 to Madre de Deus de Minas, São João del Rei, Minas Gerais
Geological unit/parent material: Tertiary sediments
Soil-landscape unit: SJD-sed
Topography: undulating
Elevation: 1050 m
Profile situation and position: roadcut; middle slope
Landuse and/or vegetation: savana like vegetation (*cerrado)*/sparse savana like vegetation (*campo cerrado)*
Rock outcrops and/or surface coarse fragments: abundant gravels of petroplinthite and quartz
Erosion: sheet severe

Description

A/AB (486) *0-40cm*; Yellowish red (5YR 4/6) clay; strong fine granular structure; many fine and very fine pores; friable; many medium and fine roots; abrupt and smooth boundary which is partially lined with petroplinthite fragments up to 15 cm length and 2 cm thick; locally covered by strong brown (7.5YR 4/6) gravelly slope material;

Bw (485,39) *40-80cm*; Red (2.5YR 4/6; 10R 4/6) clay; strong very fine to fine granular structure; many very fine pores; friable; many medium and fine roots; abrupt and wavy boundary;

Bwm (488, 40) presence of many petroplinthite layers with thicknesses of 1 to 20 cm, red (10R 4/6) and dusky red (10R 3/2) in fresh surfaces; usually layered, wawy and discontinuous, sometimes cut by the present surface, sometimes nearly paralell to surface; at present, goethite is forming in crack surfaces and burrows;

Bwv (484, 483) *80-160cm*; Red (7.5R 4/6; 10R 4/6) clay, structureless to weak medium subangular blocky structure; many fine and very fine pores; hard to very hard and firm; very few roots in the not cemented part; abrupt and smooth boundary; presence of few gravels;

IV (38) *160-175/380cm*; Red (7.5R 4/6) clay; strong medium angular blocky to massive structure; few pores; firm; abrupt and wavy boundary; it consists of a 1.5 cm thick rather continuous petroplinthite; few to common rounded bleached root channels up to 2 cm diameter; few faint yellow mottles along root channels;

III (37,482) *175/380-550/800cm*; the top layer shows about 60-70% of yellow (2.5Y 7/6) to brownish yellow (10YR 6/6) burrows in a dark red (2.5YR 3/6) to red (10R 4/6) clay matrix and the bottom layer has about 30% of pale yellow (5Y 8/4) burrows in a red (10R 4/6) clay matrix; presence of common gravels (up to 2 cm, and larger) throughout the layer; presence of some discontinuous petroplinthite layers up to 3 cm; presence of a stone line at the lower boundary with thickness between 2 and 10 cm, consisting mostly of subrounded coarse (up to 7 cm) quartz fragments; it is more friable than the lower layers with a somewhat stronger red colour;

II (35,36, 481,480) *550/800-550/1290cm*; very homogeneous dark red (10R 3/6) to red (10R 4/6) clay with few burrows (up to 3 cm width) penetrating from overlying layer up to 1-2 m depth; burrows are red (2.5YR 5/8) in the inner part and yellow (10YR 7/8) to light gray (5Y 7/1) in the outer part; randomly distributed gravels, mostly of quartz (angular and subangular up to 3 cm)and some yellow 'ocre' nodules; presence of grayish and yellowish spots up to 0.5 cm; the layer is intensely fractured showing a cross pattern and common slickensides surfaces;

I (33,34, 477-479) *550/1290-2300+cm*; red (10R 4/6) to dark red (10R 3/6) and dusty red (10R 3/4) clay intensely burrowed; the burrows show a complex pattern without any preferential orientation; they are brownish yellow (10YR 6/6), yellow (10YR 7/6), and pale yellow (2.5Y 7/4) to light gray (5Y 7/1) in the outer part, and some are red (2.5YR 5/8) in the inner part; the gray colours are dominant, especially to the bottom of the layer; 60% of the material is matrix and the red burrows are superimposed on the gray ones; the burrowing increases

to the top of the layer (up to 90%); the red burrows dominating and obliterating almost all the yellow/gray ones; presence of some quartz in clusters.

II - SETE LAGOAS AREA

SL catena- Profiles C1 - C4

Profile identification: C1
Classification: Typic Haplustox
Location: road BR 040, km 419, right side in front of the entrance to Laginha farm, Paraopeba, Minas Gerais, Brazil
Geological unit: Bambuí group (Late Proterozoic)
Parent material: saprolite of fine-textured sedimentary and metasedimentary rocks
Soil-landscape unit: SL-sap
Topography: almost flat
Elevation: 760 m
Profile situation and position: wall from the road building, crest
Landuse and/or vegetation: secondary savanna like vegetation *(cerrado)*
Erosion: none
Drainage class: somewhat excessively drained

Description

A (66)	*0-0/40cm*; Dark reddish brown (2.5YR 3/4) clay; strong fine granular structure; very high porosity; very friable; abundant fine and very fine roots; clear and wavy boundary;
AB (67)	*0/40-46cm*; Dark red (10R 3/6) clay; weak medium subangular blocky breaking into strong fine granular structure; common fine and very fine pores; friable; common fine and very fine roots; gradual and smooth boundary;
Bw (68)	*46-100/130cm*; Red (10R 4/6) clay; moderate fine granular structure; abundant very fine, many fine and few medium pores; friable; common fine and very fine and few medium roots; clear and wavy boundary;
BC1 (69)	*100/130-165cm*; Red (2.5YR 4/8) clay; weak medium subangular blocky structure; many fine and very fine pores; firm; few fine and very fine roots; gradual and smooth boundary;
BC2 (70)	*165-195cm*; Red (10R 4/8) clay; moderate fine granular structure; many fine and very fine pores; friable; few medium roots; gradual and smooth boundary
BC3 (71)	*195-245cm*; Red (2.5 YR 4/8) clay; weak medium subangular blocky structure; many fine and very fine pores; friable; few fine roots; gradual and smooth boundary;
BC4 (72)	*245-375cm*; Red (10R 4/8) clay; weak medium subangular blocky breaking into moderate fine granular structure; many fine and very fine pores; very friable; few fine roots; gradual and smooth boundary;
BC5 (74)	*375-400+cm*; Red (10R 4/8) clay; weak medium subangular blocky structure; common fine and very fine pores; friable; few fine roots.

Profile identification: C2
Classification: Typic Haplustox
Location: road to Laginha farm, 4.0 km from road BR 040, km 419, Paraopeba, Minas Gerais, Brazil
Geological unit: Bambuí group (Late Proterozoic)
Parent material: saprolite of fine-textured sedimentary and metasedimentary rocks
Soil-landscape unit: SL-sap
Topography: almost flat to gently undulating

Elevation: 745 m
Profile situation and position: upper slope to crest (plan convex slope)
Landuse and/or vegetation: secondary savanna like vegetation *(cerrado)*
Erosion: none
Drainage class: well drained
Biological features: sparse termite mounds

Description

A (75) *0-20cm*; Red (10R 4/6) clay; weak medium to fine subangular blocky breaking into granular structure; abundant fine and very fine pores; very friable; common fine roots; clear and smooth boundary;

AB (76) *20-45cm*; Red (2.5 YR 4/6) clay; weak fine subangular blocky structure; abundant fine and very fine pores; friable; common fine and few medium roots; clear and wawy boundary;

Bw1 (77) *45-105cm*; Red (2.5 YR 4/8) clay; moderate fine granular structure, containing some non porous clayey nodules up to 2 cm; abundant fine and very fine pores; very friable, friable nodules; few medium, fine and very fine roots; gradual and smooth boundary;

Bw (78,79) *105-180cm*; Red (2.5 YR 4/8) clay; weak coarse subangular blocky breaking into strong fine granular structure, containing some non porous clayey nodules; abundant fine and very fine pores; very friable, friable nodules; few medium, and fine roots; gradual and wawy boundary;

BC (80) *180-210+cm*; Red (2.5 YR 5/8) clay; weak coarse subangular blocky, partially granular structure, with clay inclusions; common fine and abundant very fine pores; firm; very few roots; more biturbation and nodules.

Profile identification: C3
Classification: Typic Haplustox
Location: road BR 040, km 416, Paraopeba, Minas Gerais, Brazil
Geological unit: Bambuí group (Late Proterozoic)
Parent material: saprolite of fine-textured sedimentary and metasedimentary rocks
Soil-landscape unit: SL-sap
Topography: gently undulating
Elevation: 720 m
Profile situation and position: gully wall, lower to middle slope
Landuse and/or vegetation: secondary savanna like vegetation *(cerrado)*, forestry (*Eucaliptus sp*)
Erosion: sheet slight
Drainage class: well drained
Biological features: sparse termite mounds

Description:

AB (81) *0-40cm*; Red (2.5YR 5/8) clay; weak coarse subangular blocky structure; common fine and many very fine pores; firm; very few fine and very fine roots; clear and smooth boundary;

Bw (82) *40-125cm*; Red (2.5YR 5/8) clay; weak coarse subangular blocky to moderate very fine granular structure; many fine and abundant very fine pores; friable; few fine and medium roots; gradual and smooth boundary;

Bw (83) *125-195cm*; Red (2.5YR 5/8) clay; weak medium angular blocky breaking into strong very fine granular structure; common fine and abundant very fine pores; friable; very few fine roots; abrupt and smooth boundary; non porous weathered clayey rock fragments;

IIB (84) *195-210/230cm*; Red (10R 4/8) clay; strong very fine granular structure; very friable; gradual and wawy boundary; gravel layer with predominantly rounded brownish yellow (10YR 6/8) goethite concretions and some angular quartz;

IIIBC1 (85) *210/230-285cm*; Red (10R 5/8) clay; strong very fine granular structure; friable; very few fine roots; gradual and wawy boundary; presence of some non porous weathered rock fragments; 5% of gravel (up to

1.5cm) composed of rounded goethite concretions and angular quartz homogeneously distributed in the horizon;

IIIBC2 (86) *285-320cm*; Red (10R 5/8) silty clay loam; weak coarse subangular blocky structure; many fine and very fine pores; friable, no roots; gradual and smooth boundary; about 10% of non porous reddish yellow (7.5YR 7/8) weathered rock fragments up to 5 cm increasing with depth;

C (87) *320-470+cm*; Red (2.5YR 5/8) silty clay loam; weak coarse angular and subangular blocky structure; common fine and very fine pores; friable to firm; no roots; weathered rock fragments up to 5 cm; remnants of stratification.

Profile identification: C4
Classification: Inceptic Haplustox
Location: road to Laginha farm, 5 km from road BR 040, Paraopeba, Minas Gerais, Brazil
Geological unit: Bambuí group (Late Proterozoic)
Parent material: saprolite of fine-textured sedimentary and metasedimentary rocks
Soil-landscape unit: SL-sap
Topography: gently undulating to rolling
Elevation: 715/720 m
Profile situation and position: gully wall, lower to middle slope
Landuse and/or vegetation: savanna like (*cerrado*) to sparse savanna like vegetation (*campo cerrado*)
Rock outcrops and/or surface coarse fragments: weathered slate in the lower slope; many quartz pebbles (up to 10 cm) and concretions (up to 1.5 cm)
Erosion: sheet/gully severe
Drainage class: moderately to imperfectly drained
Biological features: few termite mounds

Description:

Crust *0-3cm*; Yellowish brown (10YR 5/6) silty clay; apedal; few medium pores; friable, dense; common fine and very fine roots; abrupt and wavy boundary; few angular quartz fragments;

Bw (88) *3-17/30cm*; Yellow (10YR 7/8) silty clay; strong medium subangular blocky structure; common fine and very fine pores; firm; common very fine roots; clear and wavy boundary; very few concentrations of quartz up to 1 cm at the bottom of the horizon; few reddish yellow (7.5YR 6/8) burrows filled with subsoil material;

BC1 (89) *17/30-65cm*; Red (2.5YR 5/8) silty clay; strong fine angular blocky structure; common fine and very fine pores; very firm; gradual and wavy boundary; few (occasional) concentrations of quartz and iron concretions; many fine yellow (10YR 8/8) channels;

BC2 (90) *65-142/160cm*; Red (10R 4/6) silty clay loam; strong medium to fine subangular blocky structure; many fine and very fine pores; friable to firm; very few fine roots; gradual and wavy boundary; very few concentrations of quartz, weathered rock fragments and iron concretions; presence of remnants of horizontal stratified layers; few channels;

C1 (91,92) *142/160-240/400cm*; Weak red (7.5R 5/4) silty clay loam; apedal (rock structure) strongly burrowed; few fine and very fine pores in the rock structured part, abundant fine and very fine pores in the burrowed part; friable; diffuse and wavy boundary; many very fine quartz fragments up to 1 mm; many burrows filled with upper material;

C2 (93-95) *240/400-540+cm*; Red (7.5R 5/6) to weak red (10R 5/6) silt loam saprolite with yellower burrowed zone (20%); many very fine pores; few yellow stratified horizontal bands up to 1 cm thick.

Profile C5

Profile identification: C5

Classification: Ustoxic Dystropept
Location: road BR 040, 18 km north from Sete Lagoas, Sete Lagoas, Minas Gerais, Brazil
Geological unit: Bambuí group (Late Proterozoic)
Parent material: yellow shale (weathered slate?)
Soil-Landscape unit: SL-sap
Topography: gently undulating to undulating
Elevation: 850 m
Profile situation and position: roadcut, upper slope to crest of a convex slope
Landuse and/or vegetation: sparse savanna like vegetation (*campo cerrado*)/ residential use
Rock outcrops and/or surface coarse fragments: weathered slate; many quartz pebbles (up to 10 cm) and concretions (up to 1.5 cm)
Erosion: sheet/gully severe
Drainage class: moderately to imperfectly drained
Biological features: few termite mounds

Description:

Ap	*0-20/30cm*; Yellowish brown (10YR 5/6) to brownish yellow (10YR 6/8) silty clay redeposited material; moderate medium to fine angular blocky structure; common medium, fine and very fine pores; hard; clear and wawy boundary; very mixed material with weathered rock fragments up to 10cm;
C1 (96)	*20/30-60cm*; Yellow (10YR 7/8) and reddish yellow (7.5YR 6/6) silty clay mixed with weathered rock fragments; massive; common fine and very fine pores; hard; clear and smooth boundary;
C2 (97)	*60-85cm*; Reddish yellow (5YR 6/8) burrows (50%) in a yellow (10YR 7/8) weathered silty clay loam bedrock; massive; many fine and very fine pores in the burrwed part, no pores in the bedrock; hard, no roots; abrupt and irregular boundary;
R (98-100)	*85-1070+cm*; mainly yellowish brown (10(Y?)R 5/4) and reddish yellow (5YR 6/6) silt loam weathered rock containing up to 10% of burrows, decreasing with depth; some bleaching along fracture plans; many small red (10R 5/8) infiltration rings of iron up to 3 mm; preserved stratification.

2. ROUTINE CHEMICAL ANALYSES

Table A2: Results of routine chemical analyses performed on the fine earth fractions of the studied materials (according to Buurman et al., 1996).

Prof.	samp. n.	horiz.	w [1] %	C [2] %	pH H_2O	pH KCl	ΔpH	Mg^{2+}	Ca^{2+}	Na^{+}	K^{+}	Al^{3+}	Sum Bas	ECEC [3]	CEC [4]	Base sat %	Free Fe %
								cmol(+)/kg									
	1	A	2.0	2.25	4.8	4.7	-0.0	0.3	0.4	0.0	0.1		0.8	0.8	5.6	15	6.2
	2	BA	7.0	1.07	5.0	5.8	0.8	0.0	0.0	0.0	0.0		0.0	0.0	5.9	0	6.5
	3	Bw1	5.3	0.86	5.2	6.2	1.0	0.0	0.0	0.0	0.0		0.0	0.0	6.0	0	6.4
	4	Bw2	5.1	0.58	5.4	6.5	1.1	0.0	0.0	0.0	0.0		0.0	0.0	5.7	0	6.9
P1	5	Bw3	8.8	0.44	5.6	6.6	1.0	0.0	0.0	0.0	0.0		0.0	0.0	5.2	0	7.3
	6	BC1	6.5	0.24	5.5	6.0	0.5	0.0	0.0	0.0	0.0		0.0	0.0	4.6	0	7.4
	7	BC2	2.9	0.32	5.5	5.0	-0.5	0.0	0.0	0.0	0.0		0.0	0.0	4.3	1	7.6
	8	BC3	3.4	0.20	5.5	4.8	-0.7	0.0	0.0	0.0	0.0		0.0	0.0	3.8	0	8.6
	9	C	1.0	0.04	5.3	4.6	-0.7	0.0	0.0	0.0	0.0		0.0	0.0	4.8	0	7.4
	11	A	1.4	2.41	4.6	4.5	-0.0	0.4	0.8	0.0	0.2	1.0	1.4	2.4	6.6	21	5.7
	12	AB	1.3	1.67	4.5	4.6	0.0	0.0	0.0	0.0	0.0		0.2	0.2	5.8	3	5.8
P2	13	Bw	1.2	1.03	5.0	5.2	0.2	0.0	0.0	0.0	0.0		0.1	0.1	5.8	2	5.5
	14	BC	1.0	0.54	5.1	5.2	0.1	0.0	0.0	0.0	0.0		0.0	0.0	4.8	0	6.4
	15	C	0.9	0.16	5.2	4.7	-0.5	0.0	0.0	0.0	0.0		0.0	0.0	4.2	0	7.1
	17	A	1.3	2.76	4.7	4.4	-0.3	0.0	0.0	0.0	0.1	1.4	0.2	1.6	5.1	4	4.4
	18	AB	1.3	2.40	4.7	4.5	-0.2	0.0	0.0	0.0	0.0	1.1	0.2	1.3	6.0	3	4.5
P3	19	Bw	1.2	1.65	4.9	4.7	-0.2	0.0	0.0	0.0	0.0		0.0	0.0	6.0	2	4.7
	20	BC1	1.1	0.94	5.4	5.2	-0.2	0.0	0.0	0.0	0.0		0.0	0.0	5.6	0	4.8
	21	BC2	1.1	0.53	5.2	5.0	-0.2	0.0	0.0	0.0	0.0		0.0	0.0	4.5	0	6.1
	22	C	0.7	0.41	5.4	4.7	-0.7	0.0	0.2	0.0	0.0		0.2	0.2	4.9	4	3.6
	23	A	1.6	2.87	4.3	4.3	0.0	0.0	0.2	0.0	0.1	1.4	0.4	1.8	7.0	6	5.2
	24	AB	1.5	2.42	4.6	4.4	-0.2	0.0	0.0	0.0	0.0	1.1	0.2	1.3	6.7	3	5.1
P4	25	Bw	1.5	2.19	4.7	4.6	-0.1	0.0	0.0	0.0	0.0		0.1	0.1	6.4	2	5.4
	26	BC1	1.3	0.88	5.2	5.6	0.4	0.0	0.4	0.0	0.0		0.4	0.4	6.4	7	5.9
	27	BC2	1.1	0.48	5.5	5.3	-0.2	0.0	0.2	0.0	0.0		0.2	0.2	3.7	6	6.4
	28	C	1.0	0.39	5.2	4.6	-0.6	0.0	0.2	0.0	0.0		0.2	0.2	5.1	4	6.0
	29	Bw	1.4	1.68	4.5	4.4	-0.0	0.0	0.0	0.0	0.0	1.2	0.0	1.3	6.7	0	5.7
P5	30	BC	1.0	0.32	4.9	4.5	-0.4	0.0	0.0	0.0	0.0	1.4	0.0	1.4	5.6	0	6.2
	31	C1	0.9	0.16	5.0	4.6	-0.4	0.0	0.0	0.0	0.0		0.0	0.0	5.3	0	6.9
	32	C2	0.9	0.09	5.1	4.6	-0.5	0.0	0.2	0.0	0.0		0.2	0.2	6.2	3	6.4
	41	Bw	2.2	2.01	4.6	4.4	-0.2	0.0	0.2	0.0	0.0	1.2	0.3	1.5	6.5	4.8	4.6
	42	BC1	1.9	1.47	4.5	4.7	0.2	0.0	0.2	0.0	0.0		0.3	0.3	5.9	5.1	4.6
	43	BC2	5.0	0.88	5.1	5.6	0.5	0.0	0.0	0.0	0.0		0.0	0.0	6.0	0.7	4.4
	44	IIBw	2.1	0.47	5.0	6.1	1.1	0.0	0.2	0.0	0.0		0.4	0.4	5.9	6.0	4.9
P7	45	IIBC1	2.2	0.39	5.1	5.5	0.4	0.0	0.2	0.0	0.0		0.4	0.4	6.2	5.6	4.9
	46	IIBC2	0.8	0.25	5.3	4.7	-0.6	0.0	0.0	0.0	0.0		0.0	0.0	6.5	0.9	4.8
	47	C1	0.8	0.24	5.4	4.7	-0.7	0.0	0.2	0.0	0.0		0.2	0.2	6.1	3.7	4.7
	48	C2	0.6	0.15	5.4	4.5	-0.9	0.0	0.0	0.0	0.0		0.0	0.0	5.6	1.7	0.8
	49	rock	0.0	0.13	6.5	4.9	-1.6	0.0	0.2	0.0	0.4		0.6	0.6	3.4	19.0	0.3
	495	A1	2.1	2.85	5.2	4.4	-0.8	0.2	0.4	0.1	0.2	0.8	2.0	2.8	6.3	14.3	5.0
	496	A2	2.1	2.57	4.9	4.4	-0.5	0.1	0.2	0.1	0.1	0.6	1.4	2.0	5.9	8.5	5.0
P8	497	AB	1.9	1.75	5.3	5.4	0.1	0.1	0.2	0.1	0.1		0.5	0.5	5.1	9.8	5.1
	498	Bw1	1.8	1.13	5.5	6.2	0.7	0.1	0.2	0.1	0.0		0.4	0.4	6.7	6.0	5.2
	499	Bw2	1.2	0.42	5.6	6.6	1.0	0.1	0.2	0.1	0.1		0.5	0.5	6.1	8.2	6.2

Table A2: Continued

Prof.	samp. n.	horiz.	w [1] %	C [2] %	pH H_2O	pH KCl	ΔpH	Mg^{2+} cmol(+)/kg	Ca^{2+} cmol(+)/kg	Na^{+} cmol(+)/kg	K^{+} cmol(+)/kg	Al^{3+} cmol(+)/kg	Sum Bas cmol(+)/kg	ECEC [3] cmol(+)/kg	CEC [4] cmol(+)/kg	Base sat %	Free Fe %
	500	sl	0.8	0.19	5.5	6.0	0.5	0.0	0.0	0.1	0.0		0.1	0.1	5.4	1.9	6.8
	501	BC1	0.7	0.13	5.5	5.4	-0.0	0.1	0.2	0.1	0.0		0.4	0.4	5.6	7.1	5.9
P8	502	BC2	0.5	0.08	5.6	4.6	-1.0	0.1	0.2	0.1	0.1		0.5	0.5	5.5	9.1	6.2
	503	C	0.3	0.04	5.6	4.9	-0.7	0.1	0.2	0.1	0.0		0.4	0.4	3.5	11.4	5.1
	504	rock	15.1		5.9	5.5	-0.4	0.0	0.5	0.1	0.0		0.6	0.6	3.5	17.1	6.7
	489	AB	2.0	2.44	5.2	4.5	-0.7	0.2	0.2	0.1	0.3	0.6	1.7	2.3	5.8	13.8	5.2
	490	Bw1	1.9	1.26	5.0	5.3	0.3	0.1	0.0	0.1	0.1		0.3	0.3	6.2	4.8	5.6
	491	Bw2	1.9	1.02	4.6	5.9	1.3	0.0	0.0	0.1	0.1		0.2	0.2	6.1	3.3	4.9
	492	Bw3	1.7	0.76	5.0	6.3	1.3	0.1	0.2	0.1	0.1		0.5	0.5	7.2	6.9	5.2
	493	Bw4	1.4	0.44	6.6	6.6	0.0	0.1	0.3	0.1	0.1		0.6	0.6	7.5	8.0	6.5
	65	Bw5	7.4	0.28	5.4	6.5	1.1	0.0	0.0	0.0	0.0		0.0	0.0	6.6	0.4	7.1
VP	64	BC1	7.1	0.18	5.3	6.5	1.2	0.0	0.0	0.0	0.0		0.0	0.0	7.1	0.0	7.2
sed	63	BC2	9.4	0.20	5.4	6.6	1.2	0.0	0.0	0.0	0.0		0.0	0.0	7.9	0.7	9.4
	62	C1	10.2	0.22	5.4	6.6	1.2	0.0	0.0	0.0	0.0		0.0	0.0	6.8	1.3	8.6
	61	C2	5.0	0.24	5.3	6.3	1.0	0.0	0.0	0.0	0.0		0.0	0.0	6.7	0.0	4.2
	60	C3	5.3	0.21	5.5	6.2	0.7	0.0	0.0	0.0	0.1		0.1	0.1	7.6	1.7	3.3
	59	C4	1.8	0.14	5.4	6.0	0.6	0.0	0.0	0.0	0.1		0.1	0.1	7.1	1.7	5.1
	494	V	1.8	-	5.5	5.6	0.0	0.1	0.0	0.1	0.1		0.3	0.3	6.5	4.6	7.7
	56	V	2.2	0.10	5.1	5.5	0.4	0.0	0.0	0.0	0.0		0.0	0.0	6.9	0.5	8.6
	55	IV	1.4	0.05	4.9	4.4	-0.5	0.0	0.0	0.0	0.0	2.7	0.0	2.7	90.	0.3	8.2
	58	sap	1.4	0.03	5.1	4.3	-0.8	0.0	0.0	0.0	0.0	4.7	0.1	4.8	9.0	1.2	4.3
	57	sap	1.8	0.04	5.0	4.3	-0.7	0.0	0.2	0.0	0.0	5.5	0.3	5.8	10.4	3.3	2.5
VP	53	sap	1.8	0.03	5.0	4.4	-0.6	0.0	0.2	0.0	0.0	3.6	0.3	3.9	9.6	3.1	5.7
sap	52	sap	2.4	0.02	5.1	4.3	-0.8	0.0	0.0	0.0	0.0	8.0	0.1	8.1	12.8	1.0	3.9
	51	sap	3.1	0.03	5.1	4.2	-0.9	0.0	0.0	0.0	0.0	10.3	0.1	10.4	14.4	1.0	3.3
	50	sap	3.5	0.05	5.3	4.2	-1.1	0.0	0.0	0.0	0.0	11.5	0.2	11.7	16.1	1.0	6.2
	240	rock	0.5	0.05	5.2	4.4	-0.8	0.6	0.0	0.0	0.0	1.7	0.6	2.3	5.7	10.9	5.1
	486	AB	1.6	2.11	4.6	4.2	-0.4	0.1	0.2	0.1	0.2	1.7	2.7	4.4	5.3	11.3	5.1
	39	Bw	7.8	0.87	4.7	5.2	0.5	0.0	0.4	0.0	0.0		0.5	0.5	5.6	8.1	6.3
	485	Bw	1.4	1.01	5.1	5.0	-0.0	0.1	0.2	0.1	0.0		0.4	0.4	4.9	8.2	6.0
	488	Bwm	16.5	-	5.5	5.2	-0.3	0.1	0.2	0.1	0.0		0.4	0.4	5.3	7.5	15.0
	40	Bwm	1.2	0.24	5.1	5.8	0.7	0.0	0.2	0.0	0.0		0.2	0.2	3.6	6.0	21.0
	484	Bwv	1.2	0.13	5.0	5.6	0.6	0.1	0.2	0.1	0.0		0.4	0.4	5.5	7.3	16.5
	483	Bwv	1.0	0.12	5.5	5.3	-0.2	0.1	0.2	0.1	0.0		0.4	0.4	5.4	7.4	12.2
	38	IV/b	5.8	0.22	5.0	5.0	0.0	0.0	0.2	0.0	0.0		0.3	0.3	5.6	4.6	9.0
	37	III/t	1.2	0.26	5.4	4.9	-0.5	0.0	0.0	0.0	0.0		0.0	0.0	5.6	0.3	8.8
P6	482	III/m	0.9	0.06	5.5	4.5	-1.0	0.1	0.2	0.1	0.0	0.6	1.1	1.7	5.3	7.5	7.3
	36	II/t	3.8	0.23	5.4	4.5	-0.9	0.0	0.0	0.0	0.0		0.0	0.0	5.3	0.3	8.9
	481	II/t	1.0	0.06	5.4	4.4	-1.0	0.1	0.2	0.1	0.1	1.1	1.8	2.9	5.0	10.0	6.4
	480	II/m	0.9	0.05	5.4	4.3	-1.1	0.1	0.2	0.1	0.1	1.1	1.9	3.0	4.9	10.2	6.3
	35	II/b	2.2	0.18	5.4	4.4	-1.0	0.0	0.0	0.0	0.0		0.0	0.0	6.0	0.9	5.5
	34	I/t	2.3	0.21	5.3	4.4	-0.9	0.0	0.2	0.0	0.0		0.2	0.2	5.5	3.9	6.8
	479	I/t	0.9	0.05	5.4	4.4	-1.0	0.1	0.2	0.1	0.2	0.8	1.6	2.4	5.2	11.5	7.1
	478	I/m	0.8	0.03	5.1	4.3	-0.8	0.1	0.2	0.1	0.1	1.1	1.8	2.9	5.2	9.6	6.3
	477	I/b	1.1	0.03	4.5	4.2	-0.3	0.1	0.2	0.1	0.0	1.1	1.7	2.8	4.0	10.0	5.0
	33	I/b	3.2	0.23	5.2	4.4	-0.8	0.0	0.2	0.0	0.0		0.2	0.2	5.5	4.5	7.4

Table A2: Continued

Prof.	samp. n.	horiz.	w [1] %	C [2] %	pH H_2O	pH KCl	ΔpH	Mg^{2+}	Ca^{2+}	Na^{+}	K^{+}	Al^{3+}	Sum Bas	ECEC [3]	CEC [4]	Base sat %	Free Fe %
								cmol(+)/kg									
	66	A	3.2	2.22	5.1	4.4	-0.7	0.5	0.8	0.0	0.1	1.5	1.4	2.9	6.7	20.9	5.1
	67	AB	2.5	1.21	4.6	4.3	-0.3	0.0	0.0	0.0	0.1	1.9	0.1	2.0	6.6	1.7	5.4
C1	68	Bw	2.5	0.41	4.6	4.5	-0.0	0.0	0.0	0.0	0.0	1.0	0.0	1.0	5.3	0.0	5.4
	69	BC1	2.6	0.63	5.0	4.7	-0.3	0.0	0.0	0.0	0.0		0.0	0.0	5.9	0.0	5.4
	70	BC2	1.8	0.60	5.1	4.8	-0.3	0.0	0.0	0.0	0.0		0.0	0.0	5.7	0.0	5.5
	71	BC3	4.9	0.54	5.0	5.3	0.3	0.0	0.0	0.1	0.0		0.1	0.1	6.2	2.4	5.3
	72	BC4	1.5	0.44	5.2	5.1	-0.1	0.0	0.0	0.0	0.0		0.0	0.0	5.9	0.5	5.7
	73	BC4	2.1	0.36	5.1	4.9	-0.2	0.0	0.0	0.0	0.0		0.0	0.0	3.9	0.8	6.5
	74	BC5	6.5	0.35	5.2	4.6	-0.6	0.0	0.0	0.0	0.0		0.0	0.0	5.3	0.0	6.2
	75	A	2.6	1.98	4.8	4.3	-0.5	0.0	0.2	0.0	0.0	1.9	0.3	2.2	5.6	6.1	4.6
	76	AB	2.8	1.59	4.8	4.4	-0.4	0.0	0.0	0.0	0.0	1.4	0.0	1.4	5.1	0.0	4.7
C2	77	Bw1	2.3	0.90	4.9	4.7	-0.2	0.0	0.0	0.0	0.0		0.0	0.0	5.2	0.0	4.7
	78	Bw2	2.3	0.78	4.8	4.9	0.1	0.0	0.0	0.0	0.0		0.0	0.0	5.4	0.0	4.7
	79	Bw2	4.6	0.63	5.1	5.1	0.0	0.0	0.0	0.0	0.0		0.0	0.0	5.2	0.2	4.7
	80	BC	5.6	0.51	5.2	5.3	0.0	0.0	0.0	0.0	0.0		0.0	0.0	5.0	0.0	4.9
	81	AB	5.0	0.73	4.5	4.8	0.3	0.0	0.2	0.0	0.0		0.3	0.3	6.0	5.3	4.4
	82	Bw1	3.2	0.62	4.8	5.0	0.2	0.0	0.0	0.0	0.0		0.0	0.0	6.4	1.1	4.5
	83	Bw2	6.0	0.40	5.1	4.9	-0.2	0.0	0.0	0.0	0.0		0.0	0.0	6.6	1.2	5.0
C3	84	IIBw	2.2	0.30	4.9	4.8	-0.1	0.0	0.0	0.0	0.0		0.0	0.0	6.0	0.3	6.4
	85	IIIBC1	2.4	0.21	5.3	4.4	-0.9	0.0	0.0	0.0	0.0	1.1	0.0	1.2	6.2	1.2	4.9
	86	IIIBC2	0.9	0.21	5.3	4.4	-0.9	0.0	0.0	0.0	0.0	1.7	0.0	1.7	5.9	0.4	3.6
	87	C	1.3	0.18	5.2	4.4	-0.8	0.0	0.0	0.0	0.0	1.9	0.0	2.0	6.2	1.4	4.6
	88	Bw	1.8	0.95	4.8	4.2	-0.6	0.0	0.0	0.0	0.0	1.8	0.0	1.9	5.1	1.3	2.4
	89	BC1	1.1	0.56	5.2	4.4	-0.8	0.0	0.0	0.0	0.0	1.6	0.0	1.6	6.3	0.1	3.0
	90	BC2	1.1	0.25	4.4	4.2	-0.2	0.0	0.0	0.0	0.0	2.9	0.0	2.9	7.2	0.8	3.0
C4	91	C1a	0.8	0.23	4.7	4.2	-0.5	0.0	0.0	0.0	0.0	2.6	0.0	2.6	7.6	0.9	2.7
	92	C1b	0.7	0.17	4.8	4.4	-0.4	0.0	0.2	0.0	0.1	2.1	0.3	2.4	7.3	4.8	2.4
	93	C2a	0.8	0.15	4.7	4.2	-0.5	0.0	0.2	0.1	0.0	2.2	0.3	2.6	7.3	4.7	3.3
	94	C2b	0.8	0.18	4.6	4.3	-0.3	0.0	0.2	0.0	0.0	2.4	0.3	2.7	7.2	4.1	3.1
	95	C2c	0.7	0.14	4.6	4.3	-0.3	0.0	0.0	0.0	0.0	2.1	0.0	2.2	6.4	1.2	3.0
	96	C1	1.2	0.74	4.9	4.3	-0.6	0.0	0.2	0.0	0.0	3.3	0.3	3.6	7.7	3.3	3.6
	97	C2	0.8	0.32	4.7	4.3	-0.4	0.0	0.2	0.0	0.0	3.8	0.3	4.0	8.6	2.9	3.5
C5	98	rock	0.6	0.16	5.1	4.5	-0.6	0.0	0.2	0.0	0.1	1.0	0.3	1.3	5.2	6.1	3.8
	99	rock	0.5	0.18	4.9	4.4	-0.5	0.0	0.4	0.0	0.1	1.6	0.7	2.3	6.4	10.2	3.8
	100	rock	0.5	0.14	4.8	4.4	-0.4	0.2	0.7	0.0	0.1	1.1	1.1	2.1	5.7	18.6	3.7

[1] moisture content; [2] total carbon; [3] effective cation exchange capacity; [4] cation exchange capacity.

3. XRF ANALYSES OF MAJOR OXIDES AND TRACE ELEMENTS

Table A3.1: Results of X-ray fluorescence analyses of major oxides in the fine earth fraction of the studied materials (according to Buurman et al., 1996)

Prof.	samp. n.	horiz.	SiO_2	TiO_2	Al_2O3	Fe_2O_3	MnO	MgO	CaO	K_2O	Na_2O	P_2O_5	SiO_2/Al_2O_3 [1]	SiO_2/R_2O_3 [1,2]
							%							
	1	A	30.62	3.05	41.58	23.83	0.09	0.00	0.02	0.11	0.52	0.17	1.25	0.92
	2	BA	30.62	2.92	42.33	23.86	0.07	0.00	0.00	0.07	0.00	0.13	1.23	0.90
	3	Bw1	28.11	2.86	43.70	25.04	0.08	0.00	0.00	0.08	0.00	0.14	1.09	0.80
	4	Bw2	27.07	2.83	44.62	25.21	0.07	0.00	0.00	0.07	0.00	0.14	1.03	0.76
P1	5	Bw3	27.75	2.75	44.17	25.00	0.07	0.00	0.00	0.09	0.05	0.12	1.07	0.78
	6	BC1	36.16	2.48	38.85	22.17	0.07	0.00	0.00	0.12	0.03	0.12	1.58	1.16
	7	BC2	40.75	2.12	36.29	20.39	0.23	0.00	0.00	0.12	0.03	0.08	1.91	1.40
	8	BC3	41.19	2.02	36.23	20.37	0.05	0.00	0.00	0.07	0.00	0.06	1.93	1.42
	9	C	44.11	1.90	33.82	19.80	0.09	0.00	0.00	0.15	0.08	0.06	2.22	1.61
	11	A	41.42	2.39	35.95	19.94	0.11	0.00	0.02	0.06	0.00	0.11	1.96	1.45
	12	AB	41.20	2.25	36.09	20.16	0.06	0.00	0.00	0.05	0.09	0.09	1.94	1.43
P2	13	Bw	38.65	2.24	38.25	20.25	0.06	0.00	0.00	0.08	0.37	0.09	1.72	1.28
	14	BC	40.49	1.99	37.23	19.87	0.07	0.03	0.00	0.07	0.17	0.07	1.85	1.38
	15	C	43.78	1.76	36.62	17.66	0.06	0.00	0.00	0.06	0.00	0.08	2.03	1.55
	17	A	47.41	2.15	32.62	17.31	0.08	0.05	0.02	0.10	0.14	0.13	2.47	1.84
	18	AB	46.56	2.14	33.46	17.58	0.06	0.00	0.00	0.08	0.00	0.12	2.37	1.77
P3	19	Bw	45.97	1.89	33.18	18.22	0.58	0.00	0.00	0.07	0.00	0.10	2.36	1.74
	20	BC1	44.93	1.91	35.47	17.47	0.05	0.00	0.00	0.07	0.00	0.10	2.15	1.64
	21	BC2	50.14	1.76	31.51	16.39	0.04	0.00	0.00	0.07	0.00	0.09	2.71	2.03
	22	C	44.99	2.36	34.11	18.19	0.08	0.00	0.00	0.10	0.06	0.11	2.24	1.67
	23	A	45.34	2.40	34.12	17.86	0.08	0.00	0.00	0.10	0.00	0.10	2.26	1.69
	24	AB	43.24	2.29	35.26	18.67	0.07	0.00	0.25	0.12	0.00	0.10	2.08	1.56
P4	25	Bw	43.04	2.24	35.63	18.79	0.09	0.00	0.00	0.10	0.00	0.10	2.05	1.54
	26	BC1	41.48	2.07	37.04	19.06	0.09	0.06	0.00	0.12	0.00	0.08	1.90	1.43
	27	BC2	43.96	1.85	35.77	18.12	0.07	0.00	0.00	0.14	0.00	0.08	2.09	1.58
	28	C	46.29	1.90	33.77	17.70	0.09	0.02	0.00	0.13	0.00	0.09	2.33	1.75
	29	Bw	46.88	2.11	33.37	17.33	0.06	0.05	0.00	0.11	0.00	0.10	2.39	1.79
P5	30	BC	50.00	1.57	32.61	15.38	0.06	0.12	0.00	0.17	0.00	0.09	2.61	2.00
	31	C1	50.03	1.60	31.98	15.75	0.13	0.19	0.00	0.15	0.09	0.09	2.66	2.02
	32	C2	47.00	1.79	32.88	17.64	0.21	0.13	0.00	0.13	0.00	0.22	2.43	1.81
	41	Bw	57.23	1.61	28.52	11.70	0.02	0.24	0.00	0.63	0.00	0.06	3.41	2.70
	42	BC1	57.12	1.58	28.77	11.65	0.00	0.14	0.00	0.68	0.00	0.06	3.38	2.68
	43	BC2	54.42	1.60	30.55	12.38	0.01	0.15	0.00	0.84	0.00	0.05	3.03	2.40
	44	IIBw	51.19	1.51	34.00	11.86	0.03	0.20	0.00	1.16	0.00	0.05	2.56	2.09
P7	45	IIBC1	52.90	1.37	32.80	11.30	0.02	0.13	0.00	1.44	0.00	0.05	2.74	2.25
	46	IIBC2	56.80	1.11	29.38	10.72	0.03	0.32	0.00	1.56	0.03	0.06	3.29	2.66
	47	C1	59.46	1.11	28.02	10.00	0.04	0.24	0.00	1.03	0.07	0.04	3.61	2.94
	48	C2	64.46	0.39	30.45	2.86	0.02	0.33	0.00	1.38	0.00	0.11	3.60	3.39
	49	rock	49.98	0.33	33.02	3.32	0.00	2.24	0.00	10.98	0.14	0.00	2.57	2.42
	495	A1	42.35	2.51	38.60	15.06	0.06	0.24	0.00	0.95	0.11	0.11	1.87	1.49
	496	A2	44.92	2.39	36.91	14.52	0.09	0.14	0.00	0.91	0.02	0.10	2.07	1.65
P8	497	AB	42.16	2.51	39.05	14.98	0.06	0.15	0.00	0.93	0.09	0.09	1.84	1.47
	498	Bw1	41.90	2.59	38.94	15.43	0.08	0.16	0.00	0.85	0.00	0.06	1.83	1.46
	499	Bw2	38.94	2.55	40.86	16.09	0.09	0.19	0.00	1.17	0.06	0.05	1.62	1.29

Table A3.1: Continued

Prof.	samp. n.	horiz.	SiO_2	TiO_2	Al_2O3	Fe_2O_3	MnO	MgO	CaO	K_2O	Na_2O	P_2O_5	SiO_2/Al_2O_3 [1]	SiO_2/R_2O_3 [1,2]
							%							
	500	sl	43.23	2.18	37.82	14.22	0.12	0.28	0.00	2.05	0.07	0.05	1.94	1.57
	501	BC1	48.18	1.78	34.71	12.68	0.25	0.27	0.00	1.95	0.14	0.05	2.36	1.91
P8	502	BC2	52.46	1.50	30.32	12.18	0.22	0.48	0.00	2.71	0.09	0.05	2.94	2.34
	503	C	58.48	1.20	25.15	9.32	0.30	0.87	0.00	4.46	0.13	0.09	3.95	3.19
	504	rock	53.45	1.24	31.26	10.74	0.12	0.40	0.00	2.62	0.09	0.08	2.91	2.38
	489	AB	39.56	3.07	37.76	19.34	0.06	0.00	0.00	0.07	0.00	0.14	1.78	1.34
	490	Bw1	39.28	2.97	38.43	19.04	0.06	0.00	0.00	0.04	0.06	0.12	1.74	1.32
	491	Bw2	38.70	3.01	38.92	19.19	0.05	0.00	0.00	0.04	0.00	0.10	1.69	1.29
	492	Bw3	39.77	2.94	38.42	18.68	0.06	0.00	0.00	0.04	0.00	0.10	1.76	1.34
	493	Bw4	38.31	2.88	39.33	19.29	0.07	0.00	0.00	0.04	0.00	0.08	1.66	1.26
	65	Bw5	41.14	2.66	37.68	18.21	0.06	0.00	0.00	0.03	0.11	0.11	1.86	1.42
VP	64	BC1	43.19	2.32	36.06	18.23	0.05	0.00	0.00	0.05	0.00	0.10	2.04	1.54
sed	63	BC2	40.59	2.41	35.42	21.34	0.05	0.00	0.00	0.03	0.07	0.09	1.95	1.41
	62	C1	37.45	2.74	37.89	21.74	0.05	0.00	0.00	0.04	0.00	0.09	1.68	1.23
	61	C2	41.53	2.95	40.90	14.43	0.05	0.00	0.00	0.04	0.00	0.11	1.73	1.41
	60	C3	42.05	2.95	41.40	13.34	0.04	0.00	0.00	0.04	0.00	0.19	1.73	1.43
	59	C4	45.27	2.74	35.66	16.04	0.04	0.00	0.00	0.04	0.00	0.22	2.16	1.68
	494	V	46.14	2.52	31.58	19.43	0.04	0.00	0.00	0.03	0.06	0.19	2.48	1.78
	56	V	45.41	2.47	31.24	20.58	0.05	0.00	0.00	0.02	0.00	0.22	2.47	1.74
	55	IV	48.62	1.67	29.48	19.81	0.03	0.06	0.00	0.03	0.10	0.20	2.80	1.96
	58	sap	61.31	1.02	26.75	10.53	0.06	0.11	0.00	0.14	0.00	0.08	3.90	3.11
	57	sap	68.96	0.76	22.87	7.03	0.00	0.15	0.00	0.14	0.03	0.05	5.12	4.28
VP	53	sap	58.58	0.80	28.46	11.95	0.04	0.05	0.00	0.03	0.00	0.09	3.50	2.76
sap	52	sap	63.79	0.97	25.67	8.91	0.39	0.16	0.00	0.03	0.00	0.07	4.22	3.46
	51	sap	63.21	1.00	26.47	8.78	0.12	0.31	0.00	0.03	0.00	0.09	4.06	3.35
	50	sap	52.87	1.34	27.39	17.52	0.39	0.27	0.00	0.02	0.00	0.19	3.28	2.33
	240	rock	61.16	1.03	27.03	10.51	0.07	0.10	0.00	0.04	0.00	0.06	3.85	3.08
	486	AB	48.26	2.66	33.01	15.45	0.05	0.04	0.00	0.40	0.06	0.08	2.49	1.91
	39	Bw	42.90	2.43	36.39	17.57	0.04	0.14	0.00	0.46	0.00	0.07	2.00	1.53
	485	Bw	41.57	2.67	37.40	17.69	0.04	0.16	0.00	0.40	0.00	0.07	1.89	1.45
	488	Bwm	37.31	1.50	27.94	32.89	0.02	0.00	0.00	0.30	0.00	0.04	2.27	1.29
	40	Bwm	21.83	1.00	17.08	59.89	0.00	0.00	0.00	0.16	0.00	0.03	2.17	0.67
	484	Bwv	37.77	1.64	26.03	34.16	0.02	0.00	0.00	0.33	0.00	0.05	2.47	1.34
	483	Bwv	43.05	1.83	29.79	24.76	0.03	0.02	0.00	0.37	0.09	0.06	2.46	1.60
	38	IV/b	44.57	1.81	33.73	19.38	0.03	0.05	0.00	0.36	0.00	0.06	2.25	1.64
	37	III/t	46.18	1.86	31.50	19.83	0.03	0.02	0.00	0.53	0.00	0.05	2.49	1.78
P6	482	III/m	52.92	1.80	30.23	14.15	0.05	0.10	0.05	0.59	0.06	0.06	2.98	2.29
	36	II/t	49.91	1.78	30.86	16.68	0.07	0.17	0.00	0.48	0.00	0.06	2.75	2.04
	481	II/t	55.12	1.76	30.25	12.18	0.07	0.02	0.00	0.49	0.06	0.06	3.10	2.46
	480	II/m	59.30	1.60	27.03	11.32	0.06	0.08	0.00	0.58	0.00	0.05	3.73	2.94
	35	II/b	57.89	1.66	29.03	10.82	0.05	0.00	0.00	0.51	0.00	0.04	3.39	2.74
	34	I/t	56.29	1.62	27.75	13.38	0.05	0.11	0.00	0.74	0.00	0.06	3.45	2.64
	479	I/t	54.02	1.83	29.36	13.75	0.05	0.11	0.00	0.78	0.04	0.05	3.13	2.41
	478	I/m	59.95	1.55	25.34	12.06	0.04	0.10	0.00	0.88	0.04	0.04	4.02	3.08
	477	I/b	66.79	1.19	21.18	9.16	0.03	0.29	0.16	0.96	0.20	0.04	5.36	4.20
	33	I/b	56.91	1.47	26.11	14.50	0.04	0.12	0.00	0.72	0.05	0.07	3.71	2.73

Table A3.1: Continued

Prof.	samp. n.	horiz.	SiO_2	TiO_2	Al_2O3	Fe_2O_3	MnO	MgO	CaO	K_2O	Na_2O	P_2O_5	SiO_2/Al_2O_3[1]	SiO_2/R_2O_3[1,2]
							%							
	66	A	53.26	2.03	31.40	11.92	0.03	0.29	0.00	0.94	0.04	0.09	2.88	2.32
	67	AB	51.91	2.10	32.37	12.56	0.02	0.28	0.00	0.69	0.00	0.07	2.73	2.18
C1	68	Bw	51.56	2.14	32.54	12.87	0.03	0.19	0.00	0.61	0.00	0.07	2.69	2.15
	69	BC1	51.41	2.14	32.98	12.63	0.02	0.23	0.00	0.53	0.00	0.05	2.65	2.13
	70	BC2	51.33	2.18	32.93	12.70	0.02	0.24	0.00	0.55	0.00	0.06	2.65	2.13
	71	BC3	49.92	2.26	33.90	13.14	0.02	0.28	0.00	0.44	0.00	0.05	2.50	2.01
	72	BC4	50.19	2.19	34.19	12.73	0.02	0.16	0.00	0.47	0.00	0.05	2.50	2.02
	73	BC4	48.54	2.27	34.96	13.33	0.03	0.17	0.00	0.48	0.17	0.05	2.36	1.90
	74	BC5	49.98	2.24	33.96	12.83	0.03	0.19	0.00	0.60	0.11	0.06	2.50	2.01
	75	A	52.14	2.19	32.65	11.69	0.07	0.30	0.00	0.85	0.00	0.11	2.71	2.21
	76	AB	51.54	2.22	33.09	11.84	0.07	0.31	0.00	0.83	0.00	0.10	2.65	2.15
C2	77	Bw1	51.60	2.23	32.98	11.86	0.05	0.33	0.00	0.86	0.00	0.10	2.66	2.16
	78	Bw2	51.56	2.27	33.08	11.86	0.05	0.28	0.00	0.82	0.00	0.08	2.65	2.16
	79	Bw2	51.27	2.25	33.38	11.90	0.06	0.32	0.00	0.75	0.00	0.08	2.61	2.13
	80	BC	50.38	2.32	33.84	12.25	0.10	0.32	0.00	0.72	0.00	0.07	2.53	2.06
	81	AB	50.27	1.99	30.61	15.79	0.01	0.28	0.00	1.01	0.00	0.05	2.79	2.10
	82	Bw1	51.90	2.11	32.17	12.70	0.00	0.20	0.00	0.79	0.09	0.06	2.74	2.19
	83	Bw2	51.61	2.15	32.44	12.60	0.01	0.35	0.00	0.76	0.03	0.05	2.70	2.17
C3	84	IIBw	51.88	2.11	32.46	12.33	0.03	0.24	0.00	0.90	0.00	0.05	2.72	2.19
	85	IIIBC1	56.32	1.87	28.88	11.07	0.01	0.41	0.00	1.40	0.00	0.03	3.32	2.66
	86	IIIBC2	63.34	1.57	24.88	8.11	0.00	0.50	0.00	1.56	0.00	0.03	4.33	3.58
	87	C	60.31	1.56	24.78	10.00	0.03	0.69	0.00	2.57	0.03	0.02	4.14	3.29
	88	Bw	72.39	1.49	17.82	6.51	0.03	0.39	0.00	1.19	0.13	0.04	6.91	5.60
	89	BC1	68.90	1.48	20.07	7.37	0.09	0.47	0.00	1.55	0.05	0.02	5.84	4.73
	90	BC2	70.13	1.32	19.42	6.74	0.03	0.52	0.00	1.72	0.10	0.03	6.14	5.02
C4	91	C1a	71.97	1.19	18.50	6.03	0.03	0.47	0.00	1.66	0.12	0.03	6.61	5.47
	92	C1b	74.85	0.99	16.83	5.19	0.02	0.39	0.00	1.36	0.33	0.03	7.56	6.31
	93	C2a	70.09	1.19	18.57	6.98	0.05	0.50	0.00	2.46	0.16	0.02	6.42	5.17
	94	C2b	70.20	1.17	18.84	6.52	0.03	0.63	0.00	2.44	0.13	0.03	6.33	5.19
	95	C2c	71.68	1.14	18.04	6.31	0.03	0.52	0.00	2.17	0.07	0.03	6.76	5.52
	96	C1	60.58	1.39	23.87	9.29	0.02	0.91	0.00	3.53	0.33	0.08	4.31	3.45
	97	C2	64.09	1.23	21.60	8.23	0.02	1.00	0.00	3.45	0.28	0.09	5.04	4.06
C5	98	rock	65.53	1.16	20.76	8.03	0.00	0.88	0.00	3.46	0.00	0.18	5.37	4.30
	99	rock	63.04	1.25	21.63	8.51	0.01	1.11	0.00	4.33	0.02	0.10	4.95	3.96
	100	rock	63.98	1.11	21.17	8.16	0.01	1.17	0.00	4.26	0.05	0.09	5.14	4.12

[1] molar ratios; [2] R_2O_3: (Al_2O_3 + Fe_2O_3)

Table A3.2: Results of X-ray fluorescence analyses of trace elements in the fine earth fraction of the studied materials (according to Buurman et al., 1996)

Prof.	samp n.	horiz.	Ba	Ce	Co	Cr	Cu	Ga	La	Nb	Nd	Ni	Pb	Rb	Sr	Th	V	Y	Zn	Zr
			ppm																	
	1	A	0	49	12	158	53	33	28	7	22	14	0	0	11	0	246	8	39	164
	2	BA	0	58	9	158	55	33	13	8	27	17	13	0	13	0	235	6	38	153
	3	Bw1	0	47	11	165	46	37	27	10	24	17	24	0	12	17	271	10	39	207
	4	Bw2	0	29	11	173	80	38	10	13	16	16	17	0	0	0	267	8	36	170
P1	5	Bw3	36	50	19	171	51	36	0	9	22	16	11	0	0	0	256	8	41	163
	6	BC1	0	54	20	150	64	33	19	0	24	17	12	0	0	0	217	7	48	130
	7	BC2	178	39	37	146	89	30	21	9	16	61	33	0	0	0	205	0	51	105
	8	BC3	0	32	14	202	87	28	0	9	9	15	13	0	0	0	209	6	41	69
	9	C	43	63	11	145	113	30	17	7	20	16	22	0	0	0	172	0	51	37
	11	A	74	56	7	141	73	30	26	11	26	15	20	0	0	0	215	8	52	148
	12	AB	0	76	11	163	62	31	0	12	33	13	16	0	0	0	245	6	42	170
P2	13	Bw	0	48	13	163	66	34	23	12	22	20	17	0	0	0	236	6	37	154
	14	BC	65	38	9	174	65	31	0	8	16	14	0	0	0	0	223	6	41	105
	15	C	91	214	6	150	76	28	0	7	72	15	18	0	0	0	256	0	40	73
	17	A	0	52	18	188	85	27	14	7	24	36	15	0	0	0	206	8	66	155
	18	AB	47	41	12	133	83	29	17	10	19	33	0	0	0	0	201	10	56	151
P3	19	Bw	1172	nd	34	181	110	28	14	16	nd	35	77	0	0	0	242	7	65	169
	20	BC1	0	70	10	134	87	29	23	7	32	30	12	0	0	0	212	5	65	218
	21	BC2	0	45	6	127	91	29	26	15	30	42	0	0	0	0	193	6	95	313
	22	C	26	109	13	135	169	29	17	9	38	36	25	0	0	0	247	7	81	105
	23	A	0	63	31	137	80	28	36	9	25	44	13	0	0	0	247	9	79	108
	24	AB	70	104	11	160	87	33	29	7	38	35	10	0	0	15	262	7	84	98
P4	25	Bw	0	65	16	140	82	31	41	10	25	52	15	0	0	0	232	6	90	92
	26	BC1	134	149	12	181	86	33	19	6	53	37	0	0	0	0	237	7	99	90
	27	BC2	77	51	9	139	162	32	0	7	21	38	19	0	0	0	222	5	98	77
	28	C	35	83	9	132	96	31	0	13	27	39	10	0	0	0	204	8	123	59
	29	Bw	66	35	14	121	73	28	0	0	17	27	0	0	0	0	200	7	78	104
P5	30	BC	49	73	9	87	93	32	46	6	28	37	0	0	12	0	123	6	107	85
	31	C1	135	34	22	79	91	31	0	6	12	42	30	0	0	0	127	10	104	53
	32	C2	87	57	28	86	126	33	24	6	21	62	0	0	0	0	144	0	153	39
	41	Bw	574	nd	6	175	38	26	0	22	nd	22	20	0	12	27	207	10	24	404
	42	BC1	506	357	0	192	58	28	0	20	134	27	14	0	10	21	197	12	24	447
	43	BC2	817	nd	9	192	39	31	0	23	nd	23	23	0	15	32	212	11	24	386
	44	IIBw	972	nd	9	200	64	28	0	25	nd	29	37	0	17	24	173	10	23	426
P7	45	IIBC1	1075	nd	23	185	47	31	21	23	nd	39	26	0	17	24	188	10	25	351
	46	IIBC2	1127	240	11	215	67	28	0	10	86	40	44	0	14	22	149	10	24	250
	47	C1	864	nd	11	236	57	27	0	20	nd	36	70	0	0	0	151	6	24	242
	48	C2	1347	62	14	84	69	28	nd	8	28	29	279	0	60	0	39	13	22	149
	49	rock	nd	0	12	65	16	40	22	19	0	19	22	209	59	24	120	11	36	171
	495	A1	257	67	0	188	15	30	0	28	33	12	22	23	18	16	232	39	31	443
	496	A2	202	93	6	188	13	31	0	28	38	12	22	23	18	18	242	41	31	453
P8	497	AB	211	75	6	197	15	32	11	31	35	12	17	22	16	21	251	42	27	467
	498	Bw1	235	60	7	197	16	33	0	31	34	13	15	21	17	21	247	39	29	472
	499	Bw2	272	158	8	211	11	35	10	30	61	13	21	22	20	17	254	41	32	464

Table A3.2: Continued

Prof.	samp n.	horiz.	Ba	Ce	Co	Cr	Cu	Ga	La	Nb	Nd	Ni	Pb	Rb	Sr	Th	V	Y	Zn	Zr
			ppm																	
	500	sl	479	425	7	193	18	33	0	27	134	17	34	42	26	20	245	36	33	413
	501	BC1	888	244	8	212	19	29	16	22	82	19	43	40	44	15	217	28	31	385
P8	502	BC2	1235	293	7	192	12	26	17	21	95	21	60	51	65	16	185	26	26	352
	503	C	1961	209	8	164	85	24	0	16	68	22	108	80	57	0	219	20	26	267
	504	rock	1180	63	0	177	16	24	0	16	29	18	44	52	37	0	158	18	27	321
	489	AB	41	31	0	176	19	31	0	19	23	16	0	0	0	0	249	17	34	454
	490	Bw1	46	28	6	179	16	30	28	22	24	20	0	0	0	0	253	15	31	446
	491	Bw2	73	26	0	187	18	30	19	21	22	16	0	0	0	0	270	16	29	447
	492	Bw3	55	30	0	180	18	32	0	19	21	20	12	0	0	0	264	14	31	417
	493	Bw4	87	24	0	188	21	32	0	17	20	23	0	0	0	0	277	14	34	419
	65	Bw5	0	0	18	189	37	32	0	27	19	28	15	0	11	0	272	11	44	419
VP	64	BC1	0	0	12	210	50	32	34	22	15	32	18	0	0	0	247	9	50	295
sed	63	BC2	0	0	25	214	45	31	12	25	21	30	10	0	0	0	258	13	40	367
	62	C1	0	68	32	229	41	34	27	23	35	33	17	0	0	0	305	13	39	326
	61	C2	0	34	12	166	67	35	14	19	27	38	0	0	11	0	343	10	49	378
	60	C3	0	30	12	158	67	36	21	27	25	47	18	0	11	0	228	12	58	365
	59	C4	29	98	187	204	77	39	83	37	56	78	18	0	29	0	255	12	0	467
	494	V	60	30	0	219	39	30	29	17	24	36	18	0	0	0	353	12	63	338
	56	V	0	64	9	207	59	33	31	19	33	41	15	0	13	0	355	10	64	314
	55	IV	93	53	11	188	68	28	61	11	28	36	19	0	25	0	337	14	61	179
	58	sap	89	63	23	48	48	27	0	10	21	59	18	0	0	0	120	6	85	64
	57	sap	75	43	86	34	71	24	0	16	25	59	0	0	0	0	49	9	29	316
VP	53	sap	46	49	19	55	104	19	16	9	23	123	16	0	0	0	135	10	78	145
sap	52	sap	488	nd	119	29	116	20	35	15	nd	68	16	0	0	0	121	13	73	187
	51	sap	138	259	51	26	92	20	23	11	93	41	20	0	0	0	99	15	61	156
	50	sap	754	141	40	109	74	21	0	6	52	37	37	0	0	0	270	15	53	92
	240	rock	82	51	12	89	42	27	57	8	23	35	0	0	0	0	146	31	53	168
	486	AB	144	46	6	168	15	31	14	29	33	17	15	16	24	16	258	29	59	504
	39	Bw	29	49	39	192	48	38	36	36	35	35	24	0	34	24	287	27	71	468
	485	Bw	114	44	6	195	16	35	17	26	33	23	17	16	31	19	292	31	66	513
	488	Bwm	107	44	6	165	0	29	29	17	29	21	20	14	20	0	247	23	68	323
	40	Bwm	98	57	14	125	0	18	42	10	30	17	15	0	22	0	172	15	47	216
	484	Bwv	138	39	0	154	0	26	23	21	29	21	20	14	23	0	225	26	64	345
	483	Bwv	96	58	8	171	0	31	21	20	33	23	16	17	26	0	263	23	65	402
	38	IV/b	79	62	13	175	21	37	28	26	35	26	18	0	34	15	246	21	80	350
	37	III/t	146	27	6	174	26	33	43	29	26	28	25	0	33	21	261	23	81	388
P6	482	III/m	97	35	6	151	17	30	29	23	27	27	25	28	34	0	212	28	73	434
	36	II/t	49	58	14	144	58	30	42	27	34	36	28	15	38	16	216	25	86	368
	481	II/t	131	62	11	164	18	30	19	22	33	29	29	34	40	0	193	28	75	404
	480	II/m	162	53	0	148	18	28	17	23	31	24	24	39	39	19	193	26	77	408
	35	II/b	80	78	6	133	34	28	30	28	39	28	21	16	40	21	199	20	81	351
	34	I/t	235	37	7	162	66	30	13	27	28	31	26	27	38	15	242	19	92	354
	479	I/t	203	62	0	170	24	31	43	24	33	29	28	41	36	15	250	30	94	415
	478	I/m	222	39	6	165	26	25	30	22	23	28	28	48	39	0	245	28	84	366
	477	I/b	268	42	6	127	30	23	27	14	24	22	27	43	39	16	183	22	73	279
	33	I/b	84	65	10	169	30	31	40	23	34	31	39	27	34	19	273	24	89	345

Table A3.2: Continued

Prof.	samp n.	horiz.	Ba	Ce	Co	Cr	Cu	Ga	La	Nb	Nd	Ni	Pb	Rb	Sr	Th	V	Y	Zn	Zr
			ppm																	
	66	A	158	129	11	158	52	29	39	36	67	45	29	55	20	24	203	35	52	563
	67	AB	82	115	9	220	45	29	23	40	64	39	32	36	21	28	206	31	48	588
C1	68	Bw	120	133	5	214	30	31	23	42	70	40	21	29	18	22	222	31	52	584
	69	BC1	106	132	7	186	32	31	36	36	68	38	20	23	15	26	226	31	49	599
	70	BC2	39	141	14	188	36	29	19	44	73	46	15	23	17	20	213	31	49	606
	71	BC3	0	131	7	248	32	32	33	39	71	39	25	15	14	24	230	27	49	618
	72	BC4	0	136	12	191	36	31	0	42	71	43	31	16	18	22	220	29	45	635
	73	BC4	43	134	12	232	68	31	51	46	72	45	24	24	17	27	227	26	45	663
	74	BC5	104	156	19	190	40	32	48	37	79	47	20	24	20	23	216	31	49	622
	75	A	211	238	10	148	27	27	35	33	105	25	29	32	55	25	199	42	48	577
	76	AB	299	218	10	152	26	29	71	36	100	26	18	32	56	22	189	42	49	584
C2	77	Bw1	236	250	13	150	27	30	76	36	108	24	26	32	57	21	209	42	49	595
	78	Bw2	257	218	11	149	31	29	36	37	98	24	21	28	59	22	192	42	49	601
	79	Bw2	216	239	15	148	31	30	65	40	108	26	25	26	56	24	200	43	50	614
	80	BC	315	241	15	150	32	30	57	43	107	25	32	23	60	22	212	46	63	631
	81	AB	93	71	8	389	21	30	40	41	54	18	21	33	11	19	229	29	41	654
	82	Bw1	94	105	10	180	23	30	28	41	63	20	21	27	0	24	188	24	37	680
	83	Bw2	64	126	7	211	25	30	17	40	70	21	23	25	11	21	202	28	38	696
C3	84	IIBw	172	244	15	153	24	29	0	40	106	23	27	32	12	25	212	28	35	686
	85	IIIBC1	218	66	11	202	34	26	28	38	48	20	21	51	11	25	188	28	46	635
	86	IIIBC2	141	56	9	122	26	22	26	37	45	20	22	55	0	17	139	24	40	564
	87	C1	405	96	23	138	29	26	20	21	48	23	27	96	13	19	154	26	51	429
	88	Bw	175	149	14	101	22	17	58	28	77	22	25	43	23	18	109	66	51	543
	89	BC1	378	214	21	131	28	22	67	28	99	29	45	60	23	19	142	68	55	504
	90	BC2	216	86	13	101	26	19	83	22	55	25	16	60	17	21	133	78	56	405
C4	91	C1a	151	77	10	93	22	18	68	25	52	23	14	56	13	15	119	96	52	378
	92	C1b	178	54	18	76	23	16	95	16	39	22	16	41	12	21	89	99	63	309
	93	C2a	281	39	11	100	13	20	40	20	36	19	16	93	13	15	125	99	50	359
	94	C2b	262	40	13	107	18	20	60	24	38	20	18	95	18	17	114	98	40	334
	95	C2c	255	31	18	111	16	18	67	19	35	21	16	83	15	0	120	98	47	357
	96	C1	409	61	11	124	28	26	93	26	40	36	23	139	19	21	160	52	58	283
	97	C2	399	77	26	113	23	23	124	20	46	39	14	129	16	15	138	73	61	281
C5	98	rock	965	176	28	177	33	21	182	15	84	198	41	128	55	0	143	85	94	277
	99	rock	449	19	12	133	29	23	45	18	16	33	15	162	17	20	154	60	59	227
	100	rock	459	29	8	133	27	22	44	17	23	29	10	165	19	0	137	53	67	215

SUMMARY

In geologically old landscapes of the humid tropics, soils usually have a very complex history. Because of extremely long periods of soil formation and different soil formation circumstances such soils are polygenetic. The state of Minas Gerais, Brazil, has large areas of polygenetic soils developed on surfaces that have been exposed since the Tertiary or longer. Erosional reprises caused either by climatic changes or tectonic movements promoted the rejuvenation of the landscapes and triggered new soil formation cycles.

A significant part of these long-time exposed landscapes is related to areas of fine- and medium-textured sedimentary and metamorphic rocks, which comprise about 30% of the state's area. The soils found in these areas are under growing pressure from various forms of use and are very susceptible to erosion. These soils are mainly Oxisols that are not well known, especially with regard to their (poly)genesis. Unraveling the genesis of such polygenetic soils is a complex task because of the overprinting of various phases of soil formation. The combination of continuously exposed (stable) landscapes with sedimentary deposits in graben zones offers the possibility of interpreting the history of the soils found at the present day surface. In continuously exposed surfaces, various phases of soil formation are superimposed, and thus very difficult to separate. Soil genetic studies may be able to identify many different phases of soil formation, but not their relative time frame. In adjacent graben zones, sedimentation alternated with soil formation. Sediments were deposited during periods of tectonic activity, while soil formation on these sediments took place during periods of landscape stability. Although overprinting may still be present in some buried soils, the fact that various phases of soil formation are separated by sediments, enables the study and sequencing of the separate phases and comparison with the polygenetic soils of the stable areas.

This research aimed to understand the main aspects of soil genesis in relation to landscape development in this kind of tropical environment. Soil processes were reconstructed by studying differences in physical, chemical, mineralogical, and micromorphological properties of soils developed on continuously exposed surfaces and on sedimentary layers from graben zones. This was achieved by the study of soil sequences on landscapes affected and not affected by neotectonism. The study areas are situated in the state of Minas Gerais, near the towns of Sete Lagoas (SL) and São João del Rei (SJR). Geographical coordinates are 19-20°S and 44-45°W for the SL area, and 21-22°S and 44-45°W for the SJR area.

The main types of parent materials recognized in the field were rock-saprolites and Tertiary sediments. Rock-saprolites are found in the remnants of the Tertiary *Sulamericana* surface, on sedimentary (SL) and metamorphic (SJR) rocks of pre-Cambrian age. The difference in rock type influenced some mineralogical and chemical characteristics, but the soil evolution trend is similar, thus comparable. Tertiary sediments consist of reworked soils and sediments deposited in grabens zones formed by neo-Cenozoic tectonic activity.

The combination of various parent materials and landscape type enabled the distinction of three main soil-landscape units. The first two units consist of red and/or yellow soils (mainly Oxisols) developed on rock-saprolites. These soils developed on continuously exposed surfaces, which may have been eroded in response to (sub)recent overall rejuvenation of the landscape, or to neotectonic activity. Red soils occur in the more stable parts of the landscape, while yellow soils occur on the slopes, where the original red Oxisols were eroded. The third unit consists of red soils developed on Tertiary sediments that occur in the SJR area.

Polygenesis of the soils

Polygenesis of the soils is indicated by the presence of a large diversity of relict features inherited from previous soil formation phases. Micromorphology proved to be a very suitable tool to recognize and interpret this kind of features. Ferruginous pedorelicts, such as iron nodules and concretions, are typical relict features found in all soils. The red colouring of the groundmass is also a relict feature, since it is not observed in the younger soils forming after (sub)recent landscape dissection. Compact yellowish clay nodules found in the red soils from the SJR area show that these soils underwent more than one evolutionary phase. The nature of all relicts suggests that the soils and saprolites from which they were derived were already strongly weathered. The ferralitic character of the yellow soils found on (sub)recently eroded slopes is inherited from their parent material, which was already ferralitized. This corroborates the idea that ferralitic characteristics are the most important relict features of most tropical soils, since the present pedogenic conditions would hardly result in the formation of this type of weathered materials. Also, the large variation observed in goethite properties within the same horizon in soils on rock-saprolites and on sediments reflects the polygenetic nature of the soils.

Weathering, soil formation, and paleoenvironments

The micromorphological aspects that point to increasing weathering and soil formation towards the surface are: (a) clay formation; (b) increase of individualized structural elements (with decrease of their size) and porosity; (c) weakening of the b-fabric from crystallitic towards random striated and undifferentiated; and (d) uniform reddish or yellowish colouring of the materials. Biological mixing appears to be the main process acting on the materials. Mixing is obviously most intense in top horizons, regardless of composition and weathering stage, but burrowing and rooting are also observed in saprolites. Micromorphology of the sequences developed on Tertiary sediments showed iron accumulation features and formation of plinthite related to surface- and groundwater saturation phenomena. Such accumulations are no longer visible in the B horizons, where they disappeared through pedoturbation.

Clay formation in the studied soil sequences encompasses mineral comminution and/or dissolution, and (neo)formation of clay minerals. Laser diffraction grain-size studies showed

clearly the strong increase in clay contents and disappearance of silt fractions towards the soil surface, as a result of weathering and soil formation. Clay accumulation features are abundant in buried soils developed on sediments. The clay accumulation features consist of coatings and infillings, which result either from precipitation or illuviation. The fact that clay illuviation and precipitation are associated indicates strong weathering, and probably, a climate with contrasting dry and wet seasons. Both processes occurred over long periods of soil formation alternating with large erosional reprises. This is indicated by the fact that clay formation and accumulation features are found in various buried layers in soil-sediment sequences, and as relicts in the red soils on stable parts of the landscape in the SJR area.

The mineralogical composition of all materials indicates a high degree of weathering and homogenization. Kaolinite is the main component of the clay fraction in the soils and of the silt fraction in the saprolites. The occurrence of two types of kaolinite in the sequences on rock-saprolites indicates different environments of formation during the evolution of the soils. The coarser kaolinites from the saprolites are transformed into clay-sized particles either by comminution due to pedoplasmation or by dissolution and neoformation. Kaolinites in the sediments were inherited as submicron-sized particles from eroded older soils.

Apart from kaolinite, iron oxides are ubiquitous in all materials, and are usually accompanied by gibbsite in *sola*, and by micas in saprolites. The high degree of weathering is further illustrated by dissolution of quartz and weathering of ilmenite in all materials from the SJR area. Factor analysis indicated that 32% of the total variance of the chemical composition is explained by the weathering status, as also reflected by the contents and proportions of major oxides. Soils and saprolites from the SL area show a lower degree of weathering than those from the SJR group, apart from the fact that their parent materials are slightly different. Differences in parent material and associated differences in weathering explain another 57% of the total variance of the chemical elements in the studied materials.

Hematite and goethite are the only iron oxides found in the clay and silt fractions. Micromorphology suggests that during rock weathering, hematite forms in the saprolites as 'droplets' (spherical aggregates), which have a discrete size of about 2 μm. The droplets diminish in size through pedoturbation and dissolution, and eventually disappear in younger, yellow topsoils, or occur in fractions smaller than 1 μm, thus invisible under the optical microscope. In the sediments from the graben zones, hematite was either inherited or precipitated as (hypo)coatings as a result of periodic water saturation. Goethite is less commonly formed in the rock saprolites and is, therefore, mostly a 'secondary' product that more closely reflects the soil forming environment. Recent pedogenesis causes the transformation of hematite to goethite (xanthization). Xanthization reaches its maximum in topsoils formed on saprolites of eroded Oxisols in the stable parts of the landscape. It also affects the red soils, as shown by the yellowing of topsoils compared to B horizons, in the less eroded Oxisols.

Laser diffraction grain-size investigation showed that different iron forms have different influence on aggregation. Oxisols developed on rock-saprolites do not have strong aggregation

due to iron oxides alone. This suggests that hematite droplets formed in the saprolite do not have an effect on aggregation. Conversely, aggregation by iron is evident in the Oxisols on sediments, which have secondary iron accumulations related to remobilization of iron during periodic water saturation. This indicates that, apparently, iron needs to be remobilized during soil formation to play a major role in aggregation.

Unraveling the evolutionary history of the soils

Soils from group SL-sap have undergone a rather continuous evolution without evident major erosional and depositional events, indicating a minimal polycyclicity of the landscape, as also suggested by the few types of relicts found in these soils. With limited erosion, climatic changes cannot change much deep Oxisol profiles, because their chemistry, clay contents, and aggregation are not easily altered from the status they reached. Conversely, the SJR area underwent a more complex evolution caused by the greater polycyclicity of the landscape resulting in higher polygenesis of the soils. Here, the stabilized surface was disrupted by neotectonic activity which caused major erosion in both tectonically uplifted parts and proximal areas. As a result, grabens and tectonically controlled basins were filled with colluvium and sediments derived from soils in the surroundings.

A number of evolution phases were recognized in both continuously exposed surfaces (5 phases) and graben fillings (10 phases). They were linked in a relative time frame in order to recognize the main evolutionary phases undergone by the studied soils. The masking effect caused by the superposition of erosion and soil formation phases on a sole profile is well illustrated in this procedure. Seven distinct phases recognized in the various sedimentary layers from the graben fillings are hidden in two coupled phases in the soils formed on continuously exposed landscapes. These coupled phases encompass at least three soil formation and subsequent erosional phases. Formation of yellow soils and xanthization of the red ones is the most recent phase. The stripping of both the saprolites and subsoil layers and the petroplinthite layers belong to the same erosional event, previous to (sub)recent pedogenesis. Also, the last Oxisol formation common to the whole landscape is recognized in both types of sequences. The geological time frame encompassing this evolution extends from the Middle Tertiary (Late Paleogene) up to the Holocene (Quaternary), representing some 40 million years.

This study showed that a fairly detailed history of polygenetic soils can be supplied by genetic studies of soils developed on continuously exposed landscape compartments, in combination with such a study of buried soils in adjacent, contemporaneous sedimentary deposits.

SAMENVATTING

Bodems van geologisch oude landschappen in de humide tropen hebben meestal een complexe geschiedenis. Door extreem lange perioden van bodemvorming en verschillende bodemvormende omstandigheden zijn zulke bodems polygenetisch. In de staat Minas Gerais in Brazilië bevinden zich grote gebieden met polygenetische bodems, die ontwikkeld zijn op oppervlakken die sinds het Tertiair of langer aan verwering zijn blootgesteld geweest. Erosie, als gevolg van klimaatveranderingen of door tektonische activiteit, of beide, veroorzaakte landschapsverjonging en gaven aanleiding tot nieuwe cycli van bodemvorming.

Een aanzienlijk deel van deze langdurig blootgestelde landschappen, die ongeveer 30% van de oppervlakte van de staat beslaan, wordt gevonden op sedimentaire en metamorfe gesteenten van fijne en middelfijne korrelgrootte. De bodems in dit gebied staan onder toenemende druk van verschillende vormen van gebruik en zijn zeer erosiegevoelig. Het zijn voornamelijk Oxisols waarvan vooral de polygenetische aspecten weinig bestudeerd zijn. Het ontrafelen van de ontstaanswijze van deze polygenetische bodems is ingewikkeld, vanwege de superpositie van de verschillende fasen van bodemvorming. De vergelijking van bodems op continu blootgestelde oppervlakten, met die voorkomend in en op sedimentaire afzettingen in tectonische slenken, biedt de mogelijkheid om de geschiedenis van de bodems aan het huidige oppervlak te interpreteren. Op voortdurend blootgestelde oppervlakken zijn opeenvolgende bodemvormende fasen gesuperponeerd en daardoor zeer moeilijk te onderscheiden. Bodemgenetische studies maken het mogelijk verschillende fasen van bodemvorming te herkennen, maar niet het relatieve tijdskader te reconstruëren waarbinnen deze plaatsvonden. In nabijgelegen slenk werd sedimentatie afgewisseld door bodemvorming. Tijdens perioden van tektonische activiteit werden sedimenten afgezet terwijl bodemvorming plaatsvond gedurende perioden waarin het landschap stabiel was. Hoewel superpositie van vormingsfasen nog steeds mogelijk is in sommige begraven bodems, maakt het feit dat verschillende bodemvormingsfasen gescheiden zijn door sediment het mogelijk de afzonderlijke fasen in de tijd te plaatsen en de vergelijking met de polygenetische bodems van de stabiele gebieden te bestuderen.

Dit onderzoek heeft als doel de belangrijkste aspecten van bodemvorming in relatie tot landschapsontwikkeling in dit type tropische omgeving te begrijpen. Bodemprocessen zijn gereconstrueerd door het bestuderen van verschillen in fysische, chemische, mineralogische en micromorfologische eigenschappen van bodems die ontwikkeld zijn, enerzijds op continu blootgestelde oppervlakken, en anderzijds in sedimentlagen in slenk zones. Dit is bereikt door het onderzoeken van bodemsequenties in door neotektoniek aangetaste en niet door neotektoniek aangetaste landschappen. De bestudeerde gebieden liggen in de staat Minas Gerais, dichtbij de steden Sete Lagoas (SL) en São João del Rei (SJR). De geografische coördinaten van het SL gebied zijn 19-20° ZB en 44-45° WL, en van het SJR gebied 21-22° ZB en 44-45° WL.

De belangrijkste typen moedermateriaal die in het veld onderscheiden zijn, zijn saprolieten en Tertiaire sedimenten. Saprolieten werden aangetroffen op de overblijfselen van het Tertiaire *Sulamericana* oppervlak, op sedimentaire (SL) en metamorfe (SJR) gesteenten van Precambrische ouderdom. Het verschil in gesteente-type heeft sommige mineralogische en chemische eigenschappen beïnvloed, maar de trend in bodemevolutie is verwant en daardoor vergelijkbaar. De Tertiaire sedimenten bestaan uit omgewerkte bodems en sedimenten die afgezet zijn in de slenk zones, welke gevormd zijn door tektonische activiteit in het jong-Tertiair. Drie grote bodem/landschaps-eenheden kunnen worden onderscheiden op basis van de combinatie van moedermateriaal en landschapstype. De eerste twee eenheden bestaan uit (1) rode en (2) gele in saproliet ontwikkelde bodems, die voornamelijk geclassificeerd zijn als Oxisolen. Deze bodems zijn ontwikkeld op continu blootgestelde oppervlakken, waar erosie kan zijn opgetreden als gevolg van een (sub)recente landschapsverjonging en/of in relatie tot neotektonische activiteit. De rode bodems komen voor in de stabielere delen van het landschap terwijl de gele bodems zich bevinden op de hellingen waar de oorspronkelijke rode Oxisolen zijn geërodeerd. De derde eenheid bestaat uit rode bodems ontwikkeld in Tertiaire sedimenten in het SJR gebied.

Polygenese van de bodems

Aanwijzingen voor de polygenese van de bodems worden gevonden in de aanwezigheid van een breed scala van fossiele kenmerken die geërfd zijn van eerdere bodemvormingsfasen. Micromorfologie bleek een zeer geschikt middel om dit soort kenmerken te herkennen en interpreteren. Ferrugineuze pedorelicten, zoals ijzernodules en -concreties zijn typische fossiele kenmerken die in alle bodems gevonden zijn. De roodkleuring van de grondmassa is ook een fossiel kenmerk, aangezien deze niet wordt waargenomen in de jongere bodems die gevormd zijn na (sub)recente landschapsversnijding. Compacte, geelachtige kleinodules, gevonden in de rode bodems in het SJR gebied, tonen aan dat deze bodems meer dan één evolutionaire fase hebben ondergaan. De aard van alle relicten suggereert dat de bodems en saprolieten waarvan ze afkomstig zijn reeds sterk verweerd waren. Het ferralitische karakter van de gele bodems, die gevonden worden op (sub)recent geërodeerde hellingen, is geërfd van het al eerder geferralitiseerde moedermateriaal. Dit ondersteunt het idee dat ferralitische kenmerken de belangrijkste fossiele kenmerken zijn van de meeste tropische bodems, aangezien de huidige bodemvormende omstandigheden nauwelijks zouden kunnen leiden tot de vorming van dit type verweerd materiaal. Ook de grote variatie in de eigenschappen van goethiet binnen eenzelfde horizont in bodems op saproliet en sediment illustreert de polygenetische aard van de bodems.

Verwering, bodemvorming en paleomilieu

De micromorfologische aspecten die duiden op toenemende verwering en bodemvorming in de richting van het bodemoppervlak zijn (a) kleivorming; (b) een toename van de hoeveelheid granulaire elementen (met een afname van de grootte) en de porositeit; vergezeld door een afzwakking van de b-fabric van *crystallitic* naar *random striated* en *undifferentiated*; (d) een egale rood- of geelachtige kleuring van het materiaal. Biologische menging lijkt het belangrijkste proces dat invloed heeft uitgeoefend op het materiaal. Menging is duidelijk het meest intens in de bovenste horizonten, ongeacht de samenstelling en verweringsgraad, maar graaf- en wortelgangen zijn ook in saprolieten waargenomen. In de in Tertiaire sedimenten ontwikkelde bodems werden, met behulp van de micromorfologie, kenmerken van ijzeraccumulatie en plintietvorming, veroorzaakt door verzadiging met oppervlakte- dan wel grondwater, aangetoond. Deze accumulaties zijn niet meer zichtbaar in de B horizonten, doordat ze door pedoturbatie verdwenen zijn. De kleivorming in de bestudeerde bodemsequenties is een gevolg van verkleining en/of oplossing van mineralen, en nieuwvorming van kleimineralen. Korrelgroottestudies van de bodems met behulp van laser diffractie lieten duidelijk de sterke toename in het kleigehalte en de verdwijning van de siltfractie in de richting van het bodemoppervlak zien, als een gevolg van verwering en bodemvorming.

Kenmerken van klei-accumulatie zijn overvloedig aanwezig in de in sediment ontwikkelde begraven bodems. Ze bestaan uit coatings en opvullingen, die óf door neerslag (precipitatie) óf door inspoeling (illuviatie) ontstaan zijn. Het feit dat de klei-inspoeling en -neerslag samen voorkomen wijst op een sterke verwering en waarschijnlijk een klimaat met afwisselend droge en natte seizoenen.Beide processen vonden plaats gedurende lange perioden van bodemvorming afgewisseld door intense erosiefasen. Aanwijzingen hiervoor zijn de kleivorming en -accumulatie die gevonden worden in verschillende begraven bodems in de sedimentsequenties en die optreden als relicten in de rode bodems op de stabiele landschapsdelen in het SJR gebied.

De mineralogische samenstelling van al het materiaal duidt op een hoge mate van verwering en homogenisatie. Kaoliniet is het hoofdbestanddeel van de kleifractie in de bodems en van de siltfractie in de saprolieten. Het vóórkomen van twee soorten kaoliniet in de saprolietsequenties duidt op verschillende vormingsmilieus gedurende de evolutie van de bodems. De grovere saproliet-kaolinieten werden omgevormd tot deeltjes van kleigrootte hetzij door verkleining als gevolg van pedoplasmatie, hetzij door oplossing en nieuwvorming. De sediment-kaolinieten zijn overgeërfd als deeltjes van sub-microngrootte van oudere geërodeerde bodems. Naast kaoliniet zijn ijzeroxiden alom aanwezig in al het materiaal, meestal vergezeld door gibbsiet in de sola en door mica's in de saprolieten. De hoge verweringsgraad wordt verder geïllustreerd door oplossing van kwarts en de verwering van ilmeniet in al het materiaal van het SJR gebied. Factoranalyse duidde aan dat 32 % van de

totale variantie van de chemische samenstelling verklaard wordt door de verweringsstatus, die tevens weergegeven wordt door de gehalten van en verhoudingen tussen de belangrijkste oxiden. De bodems en saprolieten uit het SL gebied hebben een lagere verweringsgraad dan die uit het SJR gebied, terwijl ook het moedermateriaal enigszins verschillend is. Verschillen in moedermateriaal en daaraan gekoppelde verschillen in verwering verklaren nog eens 57 % van de totale variantie in de chemische samenstelling van het bestudeerde materiaal.

Hematiet en goethiet zijn de enige ijzeroxiden die gevonden zijn in de klei- en siltfracties. Micromorfologie duidt aan dat, tijdens de verwering van het vaste gesteente, hematiet in de saprolieten gevormd wordt als *droplets* (afgeronde korreltjes) die een discrete grootte hebben van ongeveer 2 micron. De droplets nemen in grootte af door pedoturbatie en oplossing, en verdwijnen uiteindelijk in de jongere gele bovenste bodemhorizonten, of komen voor in de fracties kleiner dan 1 micron en zijn daardoor onzichtbaar onder de optische microscoop. In de sedimenten in de slenk is de hematiet ofwel overgeërfd, of neergeslagen als (hypo) coating door periodieke waterverzadiging. Goethiet wordt minder vaak gevormd in saprolieten en is daardoor voornamelijk een 'secundair' product dat het bodemvormend milieu in detail weergeeft. Recente bodemvorming veroorzaakt de omzetting van hematiet naar goethiet (xanthisatie of vergeling). Deze xanthisatie is maximaal ontwikkeld in de toplagen van bodems gevormd in saprolieten van geërodeerde Oxisols in de stabiele delen van het landschap. Vergeling tast ook de rode bodems aan zoals te zien is aan de sterkere geelkleuring van de toplagen van de bodems in vergelijking tot de B horizonten in de minder geërodeerde Oxisols.

Korrelgrootte-onderzoek van de bodems met behulp van laser diffractie toont aan dat verschillende ijzervormen een verschillende invloed hebben op de bodemaggregatie. Oxisols die ontwikkeld zijn in saproliet hebben geen sterke aggregatie door ijzerbestanddelen alleen. Dit suggereert dat de in de saproliet gevormde hematiet-droplets geen aggregerend effect hebben. Daarentegen is aggregatie door ijzer duidelijk aanwezig in de in sediment ontwikkelde Oxisolen, die secundaire ijzeraccumulaties hebben die veroorzaakt zijn door remobilisatie tijdens periodieke waterverzadiging. Dit duidt aan dat ijzer klaarblijkelijk geremobiliseerd moet worden tijdens bodemvorming om een belangrijke rol te spelen in aggregatie.

Het ontrafelen van de ontstaansgeschiedenis van bodems

Bodems ontstaan uit saprolieten in het SL gebied hebben een tamelijk continue ontwikkeling doorlopen zonder duidelijk optreden van sterke erosie- of depositie-fasen, hetgeen duidt op een minimale polycycliciteit van het landschap. Dit wordt ook gesuggereerd door het geringe vóórkomen van fossiele kenmerken in deze bodems. Bij een beperkte erosie kunnen veranderingen in bodemvormende processen als gevolg van klimaatsveranderingen nauwelijks veranderingen veroorzaken in sterk ontwikkelde, diepe Oxisolprofielen, omdat de chemie, het kleigehalte en de aggregatie niet makkelijk veranderd worden vanuit de bereikte toestand.

Het SJR gebied daarentegen heeft een veel complexere ontwikkeling doorgemaakt door de grotere polycycliciteit van het landschap, die, door verwijdering van de sterk verweerde bovengrond, leidde tot een duidelijk effect van de opeenvolgende fasen van bodemvorming. Hier is het gestabiliseerde oppervlak verstoord door neotektonische activiteit dat grote erosie in zowel de tektonisch opgeheven- als in de nabije gebieden veroorzaakte. Dit resulteerde in de opvulling met colluvium en sedimenten, afkomstig van de omliggende bodems, van de slenken en de door tektoniek beheerste bekkens.

Een aantal ontwikkelingsfasen kon worden onderscheiden in zowel de voortdurend blootgestelde oppervlakken (5 fasen) als in de slenken (10 fasen). Deze zijn in een relatief tijdkader aan elkaar gekoppeld om de belangrijkste fasen in de bodemontwikkeling te kunnen onderscheiden. Het maskeringseffect, veroorzaakt door de superpositie van erosie en bodemvormende fasen binnen één enkel profiel, wordt door deze procedure goed geïllustreerd. Zeven verschillende fasen, onderscheiden in de verschillende sedimentaire lagen van de opvulling van de slenk, zijn verborgen in twee gekoppelde fasen in de bodems die gevormd zijn in het continu blootgestelde landschap. Deze gekoppelde fasen omvatten tenminste drie bodemvormende- en daaropvolgende erosieve fasen. Hiervan is de vorming van gele bodems en de xanthinizatie van de rode bodems de meest recente fase. De erosie van de saprolieten en de diepere horizonten van de bodems, en van de petroplintietlagen horen bij eenzelfde erosieve gebeurtenis die vooraf ging aan (sub)recente bodemvorming. Ook de laatste Oxisolvorming, die algemeen is in het gehele landschap, is in beide sequenties onderscheiden. Het geologische tijdkader waarbinnen deze ontwikkeling heeft plaatsgevonden strekt zich uit vanaf het Midden Tertiair (Laat-Paleogeen) tot aan het Holoceen (Kwartair), en vertegenwoordigt dus meer dan 40 miljoen jaar.

Deze studie heeft aangetoond dat een behoorlijk gedetailleerde reconstructie van de geschiedenis van polygenetische bodems kan worden bereikt door genetische studies van bodems ontwikkeld op voortdurend blootgestelde landschapsdelen in combinatie met een vergelijkende studie van begraven bodems in aangrenzende, en contemporane, sedimentaire afzettingen.

RESUMO

Os solos encontrados em superfícies geologicamente antigas nas regiões tropicais úmidas apresentam em geral uma história bastante complexa. Esses solos são considerados poligenéticos devido às diferentes condições a que foram expostos durante a sua evolução. O Estado de Minas Gerais, Brasil, apresenta extensas áreas de solos poligenéticos formados em superfícies expostas desde o Terciário ou mais antigas. Retomadas erosivas causadas tanto por mudanças climáticas como por movimentos tectônicos causaram o rejuvenescimento destas superfícies, dando origem a novos ciclos de formação de solos. Uma parte significativa destas superfícies antigas corresponde a áreas de rochas sedimentares e metamórficas de textura fina e média, que ocupam aproximadamente 30% da área do estado. Os solos destas áreas apresentam elevada susceptibilidade a erosão e, atualmente, encontram-se sob crescente pressão de uso. Estes solos, *Oxisols*[1] em sua maior parte, são pouco conhecidos, especialmente no que se refere a sua (poli)gênese.

O entendimento da gênese de solos poligenéticos é uma tarefa complexa, uma vez que várias fases de formação de solos se encontram superpostas, e são assim difíceis de serem separadas. A combinação de superfícies continuamente expostas (estáveis) com depósitos sedimentares em áreas de *graben* torna possível o entendimento da história de solos poligenéticos que ocupam a presente superfície. Em superfícies continuamente expostas, estudos de gênese são capazes de identificar as diferentes fases de formação de solos, mas não a sua distribuição relativa no tempo. Já em áreas de deposição, tais como zonas de *graben*, episódios de sedimentação encontram-se alternados com episódios de formação de solos, relacionados respectivamente a períodos de atividade tectônica e a períodos de estabilidade. Embora a superposição de várias fases possa ainda ocorrer, o fato das várias fases de formação de solos estarem separadas por depósitos sedimentares viabiliza o estudo de cada fase individualmente. Isso torna possível o estabelecimento da cronologia relativa das diferentes fases e a comparação com os solos poligenéticos das superfícies estáveis.

A presente pesquisa teve como objetivo entender os principais aspectos da gênese dos solos em conexão com a evolução da paisagem nesse tipo de ambiente tropical. Processos pedogenéticos foram interpretados através do estudo comparativo de propriedades físicas, químicas, mineralógicas e micromorfológicas de solos desenvolvidos em superfícies continuamente expostas e de solos desenvolvidos sobre depósitos sedimentares em zonas de *graben*. Sequências de solos em superfícies afetadas e não afetadas por neotectonismo foram selecionadas para estudo. As áreas estão situadas no Centro-Sul do Estado de Minas Gerais, próximo as cidades de Sete Lagoas (SL) e São João del Rei (SJR), entre as latititudes de 19-20° (SL) e 21-22° Sul (SJR) e longitudes de 44-45° Oeste.

Os principais materiais de origem identificados no campo foram saprolitos de rochas e

[1] Incluem Latossolos e Cambissolos

sedimentos Terciários. Saprolitos são encontrados nos remanescentes da superfície *Sulamericana*, de idade Terciária, sobre rochas sedimentares (SL) e metamórficas (SJR) do pré-Cambriano. Apesar da diferença em tipo de rochas influenciar algumas características mineralógicas e químicas dos solos, a evolução pedogenética é similar, portanto comparável. Sedimentos Terciários consistem de solos retrabalhados e sedimentos correlativos depositados em zonas de *graben* formadas por atividade tectônica neo-Cenozóica.

A combinação de vários materiais de origem e tipos de paisagem resultou na distinção de três grupos principais de unidades solo-paisagem. As duas primeiras unidades consistem de solos vermelhos e/ou amarelos (principalmente *Oxisols*) desenvolvidos sobre saprolitos de rocha. Estes solos se desenvolveram em superfícies continuamente expostas, e podem ter sido erodidos, em resposta a um rejuvenescimento geral (sub)recente da paisagem ou à atividade tectônica. Os solos vermelhos ocorrem nas partes mais estáveis da paisagem, enquanto os solos amarelos ocorrem nas encostas, onde os *Oxisols* vermelhos originais sofreram erosão. A terceira unidade engloba solos vermelhos desenvolvidos sobre sedimentos Terciários que ocorrem na área SJR.

Poligênese dos solos

O caráter poligenético dos solos estudados é corroborado pela grande variedade de feições reliquiais herdadas de fases pedogenéticas anteriores. Nesse estudo, a micromorfologia demonstrou ser uma técnica bastante adequada para o reconhecimento e interpretação deste tipo de feições. Pedorelíquias ferruginosas, tais como nódulos e concreções ferruginosas, são feições reliquiais típicas encontradas em todos os solos estudados. A coloração avermelhada da matriz é também uma feição reliquial, visto que não é observada nos solos mais jovens, formados após a dissecação (sub)recente da paisagem. Nódulos argilosos amarelados e compactos, encontrados nos solos vermelhos da área SJR mostram que estes solos são resultado de mais de uma fase de pedogênese. A natureza das relíquias observadas indica que os solos e saprolitos dos quais elas são derivadas já se encontravam intensamente intemperizados. Da mesma forma, o caráter ferralítico dos solos amarelos das encostas rejuvenescidas é herdado do seu material de origem. Isso corrobora a idéia de que características ferralíticas são as feições reliquiais mais importantes da maioria dos solos tropicais, uma vez que as condições pedogenéticas atualmente existentes dificilmente resultariam na formação deste tipo de materiais. A variabilidade observada entre goethitas de um mesmo horizonte, em solos desenvolvidos sobre saprolitos e sobre sedimentos, também reflete a natureza poligenética desses solos.

Intemperismo, pedogênese e paleoambientes

Os aspectos micromorfológicos que indicaram intemperismo e pedogênese crescentes em direção à superfície são: (a) formação de argila; (b) aumento de unidades estruturais individualizadas (com decréscimo de seu tamanho) e porosidade; (c) enfraquecimento da b-fábrica, de cristalítica para aleatóriamente orientada e indiferenciada; e (d) uniformização da coloração vermelha ou amarela dos materiais. Atividade biológica é o principal processo pedogenético atuante sobre os materiais estudados, indicado pelas marcas de bioturbação presente e passada. Bioturbação é obviamente mais intensa nos horizontes superficiais, independente da composição ou estágio de intemperismo, embora marcas de escavações e de raízes sejam também observados nos saprolitos. Feições relacionadas a processos hidromórficos, tais como acumulação de ferro e formação de plintita, foram observadas nas sequências de solos desenvolvidos sobre sedimentos Terciários. Estas feições tendem a desaparecer nos horizontes B, devido a pedo(bio)turbação.

A formação de argila nas pedosequências estudadas se dá por cominuição e/ou dissolução de minerais de frações mais grosseiras e por neoformação de minerais de argila. Estudos de distribuição granulométrica por meio de difração a laser mostram o marcante aumento em conteúdo de argila e diminuição de silte em direção à superfície do solo, como resultado de intemperismo e pedogênese. Acumulação de argila consiste de cutãs e preenchimentos que resultam tanto de precipitação como de iluviação. A associação de iluviação e precipitação indica elevado grau de intemperismo e, provavelmente, um clima com estações seca e úmida contrastantes. Ambos processos ocorreram ao longo de extensos períodos de formação de solos, alternados com retomadas erosivas. Isto é indicado pelo fato de que feições resultantes de formação e acumulação de argila são encontradas em várias das camadas enterradas das sequências pedosedimentares, e também como relíquias nos solos vermelhos nas partes estáveis da paisagem na área SJR.

A composição mineralógica de todos os materiais indica um elevado grau de intemperismo e homogeneização. Caulinita é o principal componente da fração argila dos solos e da fração silte dos saprolitos. A ocorrência de dois tipos de caulinita nos perfis sobre saprolitos indica distintos ambientes de formação durante a evolução dos solos. A caulinita dos saprolitos, de maior tamanho e melhor cristalinidade, é transformada em partículas de argila nos solos, por cominuição e por dissolução e neoformação. Nas sequências pedosedimentares a caulinita é herdada de solos préviamente existentes, consistindo de partículas submicrométricas.

Além da caulinita, óxidos de ferro estão presentes em todos os materiais, usualmente acompanhados por gibbsita nos solos e por mica nos saprolitos. Nos perfis da área SJR, o elevado grau de intemperismo é também ilustrado pela alteração de quartzo e ilmenita. Análises fatoriais indicaram que 32% da variância total da composição química são explicadas pelo estágio de intemperismo dos materiais. Solos e saprolitos da área SL mostraram um

menor grau de intemperismo em comparação aos solos da área SJR. As diferenças existentes entre materiais de origem das duas áreas e a influência destas sobre o intemperismo explicam outros 57% da variância total dos elementos químicos.

Hematita e goethita são os únicos óxidos de ferro encontrados nas frações argila e silte dos materiais estudados. Análises micromorfológicas sugerem que a hematita se forma inicialmente durante o intemperismo das rochas e saprolitos. Nesse estágio, a hematita apresenta uma morfologia característica de *droplets* consistindo em agregados esferoidais com dimensões médias de 2 μm. Os *droplets* diminuem em tamanho e frequência em direção à superfície do solo devido à pedoturbação e/ou dissolução. Nos solos amarelos rejuvenescidos, os *droplets* desaparecem ou ocorrem em frações menores do que 1 μm, invisíveis ao microscópio ótico. Nas sequências pedosedimentares a hematita apresenta duas origens: (i) herdada e, (ii) precipitada em ferrãs, como resultado de saturação periódica por água. A goethita não é comumente formada nos saprolitos, sendo portanto um produto 'secundário' que reflete mais diretamente os vários pedoambientes de formação. A transformação de hematita em goethita (xantização) é resultado de pedogênese (sub)recente: ela atinge o seu máximo em horizontes superficiais de solos formados sobre saprolitos de *Oxisols* que foram expostos pela erosão. Solos vermelhos tambem são afetados por xantização, como mostra o amarelamento de horizontes A em comparação aos horizontes B dos *Oxisols* menos erodidos.

A investigação da distribuição granulométrica por meio de difração a laser nos perfis e sequências estudados, mostrou que formas diferentes de ferro tem influência distinta na agregação dos solos. Óxidos de ferro tem pouca influência na agregação de *Oxisols* desenvolvidos sobre saprolitos, sugerindo que *droplets* de hematita formados nos saprolitos não tem efeito na agregação. Ao contrário, agregação por óxidos de ferro é evidente em *Oxisols* sobre sedimentos, os quais apresentam acumulações secundárias de óxidos de ferro relacionadas à remobilização de ferro durante saturação periódica por água. Isto indica que aparentemente o ferro necessita ser remobilizado durante a pedogênese para influenciar efetivamente a agregação do solo.

Revelando a história evolutiva dos solos

Os solos da área SL são resultado de uma evolução relativamente contínua sem maiores eventos erosivos e deposicionais. Isso é evidenciado pelos poucos tipos de pedorelíquias encontradas nestes solos. Em condições de erosão limitada, mudanças climáticas não são capazes de imprimir modificações consideráveis em *Oxisols* profundos, uma vez que a sua composição química, conteúdos de argila e agregação já atingiram um estágio evolutivo muito avançado.

A área SJR, ao contrário, apresenta uma história geomorfológica mais complexa, resultando em maior poligênese dos solos. Nesta área, a estabilidade da paisagem foi rompida por atividade neotectônica, resultando em maior erosão, tanto nas partes que foram elevadas

tectonicamente, como nas áreas proximais. Em seguida, *grabens* e bacias tectonicamente controladas foram preenchidas com sedimentos e colúvio derivados de solos das áreas vizinhas. O estudo genético dos solos dessa área possibilitou a identificação de várias fases evolutivas tanto nas sequências continuamente expostas, em partes estáveis da paisagem (5 fases), como nas sequências em depósitos sedimentares adjacentes (10 fases). Essas fases foram combinadas em um contexto temporal relativo de modo a permitir o reconhecimento das principais fases de evolução dos solos. O efeito mascarador causado pela superposição de fases de erosão e pedogênese em um mesmo perfil é claramente ilustrado através desse procedimento. Sete fases distintas identificadas nas várias camadas sedimentares em zonas de *graben* estão diluídas em duas fases conjugadas que incluem pelo menos três fases erosivas subsequentes, nos solos das superfícies continuamente expostas. Formação de solos amarelos e xantização de solos vermelhos é a fase evolutiva mais recente. Um mesmo evento erosivo anterior à pedogênese (sub)recente é responsável pela remoção de solos e saprolitos, e de camadas de petroplintita. Da mesma forma, o último episódio de formação de *Oxisols* é reconhecido nos dois tipos de sequências. Essa evolução se estende do Terciário até o Holoceno (Quaternário), compreendendo cerca de 40 milhões de anos.

A presente pesquisa mostrou que uma história relativamente detalhada de solos poligenéticos pode ser obtida pela combinação de estudos de gênese de solos desenvolvidos sobre superfícies continuamente expostas e de solos enterrados presentes em depósitos sedimentares adjacentes contemporâneos.

CONDENSED PERSONAL HISTORY

Cristine Carole Muggler was born on May 2nd 1960, in Belo Horizonte, Brazil, daughter of Swiss immigrants. She is married to Celso Marcatto and has one son, Pedro, and two stepdaughters, Francisca and Marisa.

Her primary and secondary education was done in Belo Horizonte, Minas Gerais. In 1978, she started her university studies at the Federal University of Ouro Preto. During her study she undertook a teaching assistantship for courses in Mineralogy and Petrology. In the last year, she had practical periods at three mining companies. She graduated as a geological engineer in December/1982.

In 1983, she was admitted, through public examination to the Soil Science Department of the Federal University of Viçosa, Viçosa, Minas Gerais. Until 1987, she was fully involved in undergraduate teaching. She taught courses in soils, geology, mineralogy, and paleontology.

In 1988, she started a M.Sc. Course in Soil and Plant Nutrition at the School of Agriculture of Lavras, Minas Gerais (presently Federal University of Lavras), under the supervision of Professor Dr. Nilton Curi. She graduated in December/1989, defending a thesis entitled "Relações geopedológicas em área dos Chapadões do rio Corrente, sudoeste da Bahia" (Geopedologic relationships in the area of the Corrente river Plateau, southwest of Bahia, Brazil).

Returning to the Federal University of Viçosa in 1990, she started her activities in graduate courses and participation in M.Sc. committees. Also, she was involved in the development of extension courses in subjects related to soils for professional upgrading and complementary training of school teachers. She was appointed the person in charge of the assets and assemblage of the Alexis Dorofeff Museum, Reference Centre of Minerals, Rocks and Soils for the *Zona da Mata* region. The museum opened its doors in December/1993 (shortly after Pedro was born, thus was like a "second son").

From 1990 to 1992, she was a member of the board of the faculty teacher's union, a period of intensive activity next to the Brazilian National Congress and general public, with the purpose of upholding the quality and vigor of the Brazilian Federal Universities.

In March 1994, she started her Ph.D. training at the Laboratory of Soil Science and Geology at the Wageningen Agricultural University. Her research was supported by the Federal University of Viçosa and was funded by CAPES/Ministry of Education of Brazil.